



HAL
open science

Modelling Microbial Methane Processes in Marine Environments: from Source to Seep. Insights from Basin Analysis

Martina Torelli

► **To cite this version:**

Martina Torelli. Modelling Microbial Methane Processes in Marine Environments: from Source to Seep. Insights from Basin Analysis. Earth Sciences. Sorbonne Université, 2021. English. NNT: 2021SORUS270 . tel-03547072

HAL Id: tel-03547072

<https://theses.hal.science/tel-03547072>

Submitted on 28 Jan 2022

HAL is a multi-disciplinary open access archive for the deposit and dissemination of scientific research documents, whether they are published or not. The documents may come from teaching and research institutions in France or abroad, or from public or private research centers.

L'archive ouverte pluridisciplinaire **HAL**, est destinée au dépôt et à la diffusion de documents scientifiques de niveau recherche, publiés ou non, émanant des établissements d'enseignement et de recherche français ou étrangers, des laboratoires publics ou privés.



Sorbonne Université

Ecole doctorale

ED398 / IFPEN / TOTAL

**Modelling Microbial Methane Processes in Marine
Environments: from Source to Seep**
Insights from Basin Analysis

Martina Torelli

Doctoral Thesis in Geoscience

Director Eric Deville (IFPEN), co-director Stéphanie Dupré (Ifremer)

Advisors: Isabelle Kowalewski (IFPEN), Claude Gout (TOTAL), Johannes
Wendebourg (TOTAL)

Présentée et soutenue publiquement le 27 avril 2021

Devant un jury composé de :

Mme. Isabelle MORETTI, Chercheur Associé – E2S UPPA, (Presidente du Jury)

M. Marcelo KETZER, Professeur - Linnaeus University, (Rapporteur)

M. François GUYOT, Professeur – Muséum National d’Histoire Naturelle, (Rapporteur)

M. Pieter VAN RENSBERGEN, Chercheur Ingenieur – Shell, (Examineur)

Mme. Swanne GONTHARET, Maître de conférence – Sorbonne Université (Examinatrice)

M. Eric DEVILLE, Professeur - IFP School (Directeur de thèse)

Mme. Stéphanie DUPRE, Chercheur – Ifremer (Co-Directrice de thèse)

Torelli Martina – Thèse de doctorat – 2021

M. Johannes WENDEBOURG, Expert pour le système pétrolier – Total (Invite)

Mme Isabelle KOWALEWSKI, Chercheur Ingénieur – IFPEN (Invitée)

Acknowledgements

Firstly, I would like to thank TOTAL, IFP Energies Nouvelles and IFREMER to have co-funded my PhD as part of the PAMELA research project (Passive Margin Exploration Laboratories). Thanks also to the OROGEN Project funded by Total, BRGM, CNRS & INSU for providing data used in this PhD thesis. I also would like to thank Beicip-Franlab for providing a license of the TemisFlow simulator.

I express my gratitude to my supervisors Isabelle Kowalewski and Claude Gout for their help and support, and to my director, Eric Deville, and my co-director, Stéphanie Dupré, for their encouragement and guidance. Sylvie Wolf and Veronique Gervais are acknowledged for providing me fundamental tools of numerical modelling and statistics. Special thanks to all who contributed to my research on recent organic matter: Anne Battani, Daniel Pillot, Eric Kohler, Joel Lopes De Azevedo, Lucie Pastor, Christophe Brandily, Sabine Schmidt and Gwenael Jouet. Renaud Traby and Didier Granjeon are also thanked for helping me with the basin model construction. A special thank goes to Sylvie Pegas for providing me support during numerical modelling experiments. I am also grateful to all my colleagues who were available to discuss and exchange with me on scientific questions: Benoit Chauveau, Arnaud Pujol, Frederic Schneider, Matthieu Dubille, Jean-Philippe Mathieu and Mathieu Ducros.

I am particularly grateful to Johannes Wendebourg for his invaluable help that improved significantly the results of my research, and for his support, enthusiasm and inspiration that enabled me to develop confidence and to persevere during my PhD thesis. Our discussions taught me the importance of being consistent, disciplined and always trying to exploit new avenues.

At last but not least, un grazie speciale alla mia famiglia, ad Andrea e ai miei amici più cari perchè su di voi posso sempre contare.

Table of Contents

Acknowledgements	3
Table of Contents	4
List of abbreviation.....	7
1. Introduction to biogenic methane	9
1.1 The global methane budget and the organic carbon cycle	9
1.2 Biogenic methane processes	14
1.2.1 Shallow fluid systems.....	14
1.2.2 Methanogenesis.....	17
1.3 Evidence of fluid systems at the seafloor.....	21
1.3.1 Pockmarks and gas seepages	21
1.3.2 Methane-Derived Authigenic Carbonate (MDAC).....	23
1.3.3 Gas Hydrates.....	24
1.4 PhD thesis objectives as part of the PAMELA Research Project.....	26
1.4.1 The Mozambique Channel natural laboratory	28
1.4.2 The Offshore Aquitaine natural laboratory	31
1.4.3 PhD thesis outline	35
2. Natural sources of microbial gas	36
2.1 Biogenic source rock potential	36
2.2 Organic matter production	38
2.3 Organic matter composition	39

2.4 Preservation and burial of organic matter in marine settings	41
3. A case study from the Mozambique Basin (manuscript in submission process)	44
4. Modelling microbial gas processes at the basin scale	75
4.1 The OM reactivity model	78
4.1.1 The discrete model	79
4.1.2 The continuum model	80
4.1.3 Conceptual approach for biogenic CH ₄ processes at the basin scale	82
4.2 The TemisFlow basin model	87
4.3 Modelling biogenic gas migration	89
4.3.1 Modelling adsorption of biogenic gas	91
4.3.2 Modelling dissolution of methane in pore water	93
4.3.3 Modelling migration as a free gas phase	93
4.4 Trapping and sinks of biogenic gas	94
4.5 Critical parameters for biogenic gas generation and migration	95
5. A case study from the Offshore Aquitaine (Paper in Marine and Petroleum Geology, 2021)	97
6. Issues with the analytical procedure to characterize recent terrestrial OM	130
7. Conclusions	135
8. Future research on biogenic gas generation and migration	139
8.1 Hydrate stability zones as paleo-gas migration indicators	139
8.2 Additional research questions	148
9. References	153

10. Figures Table	174
11. Tables Table	179
12. Appendices	180
12.1 Publications	180
12.2 International Conferences	180
12.3 Internal PAMELA seminars	184
12.4 PhD thesis pitch	191
12.5 International Training and School	192
13. Summary	194
14. Résumé.....	196

List of abbreviations

A

AA: Amino Acids

AMB: Aircraft Mass Balance

AOM: Anaerobic Oxidation of Methane

B

BH: Beira High

BHT: Bottom Hole Temperature

BRGM : Bureau de Recherches
Géologiques et Minières

BSE: Back Scattered Electron

BSR: Bottom Simulating Reflector

BU: Bottom-Up

C

CH: Carbohydrates

CNRS: Centre National de la Recherche
Scientifique

CSTJF: Centre Scientifique et Technique
Jean Féger

D

DIC: Dissolved Inorganic Carbon

DSDP: Deep Sea Drilling Project

E

EA: Elemental Analysis

EDS-SEM: Energy Dispersive X-Ray
Spectroscopy – Scanning Electron
Microscopy

EoS: Equation of State

EPA: United States Environmental
Protection Agency

F

FA: Fatty Acids

FID: Flame Ionization Detector

FTIS: Fourier Transform Infrared
Spectroscopy

G

GWP: Global Warming Potential

GSA: Global Sensitivity Analysis

GHSZ: Gas Hydrate Stability Zone

H

HC: Hydrocarbon

HI: Hydrogen Index

HSZ: Hydrate Stability Zone

I

IFPEN: Institut Français du Pétrole et
Energies Nouvelles

IFREMERMER : Institut Français de Recherche
et de l'Exploitation de la MER

INSU: Institut National des Sciences de
l'Univers

IODP: International Ocean Discovery
Program

IPCC: Intergovernmental Panel on Climate
Change

L

LAB: Lithosphere-Asthenosphere
Boundary

LI: Lignin

M

MDAC: Methane-Derived Authigenic
Carbonate

MDT: Modular Dynamic Formation Tester

MINC: Mineral Carbon

MTB: interface multi-corer

N

NMR: Nuclear Magnetic Resonance spectroscopy

O

OC: Organic Carbon

OET: Oxygen Exposure Time

ODP: Ocean Drilling Program

OI: Oxygen Index

OM: Organic Matter

OPD: Oxygen Penetration Depth

P

PAMELA: Passive Margin Exploration Laboratories

PETM: Paleocene-Eocene Thermal Maximum

POM: Particulate Organic Carbon

PVT: Pressure-Volume-Temperature

R

RE: Rock-Eval

RCM: Reactive Continuum Model

S

SAR: Sediment Accumulation Rate

SE: Secondary Electron

SOM: Sedimentary Organic Matter

SMTZ: Sulphate-Methane Transition Zone

SQG: Total Generated Gas

T

TC: Total Carbon

TCF: Trillion Cubic Feet

TD: Top-Down

Tg: Teragram

TOC: Total Organic Carbon

TOCZlab: Total Organic Carbon Thermo-Labile

TOClab: Total Organic Carbon Labile

TOCref or TOCbio-ref: Total Organic Carbon Refractory

U

UNFCCC: United Nation Framework Convention on Climate Change

UOM: Uncharacterized Organic Matter

X

XRF: X-Ray Fluorescence

1. Introduction to biogenic methane

1.1 The global methane budget and the organic carbon cycle

Estimates of the total methane (CH₄) budget emitted annually in the atmosphere either from anthropogenic or natural sources are required for advising achievable pathways to mitigate climate change (Nisbet et al. 2019). CH₄ represents a powerful green-house gas with a stronger Global Warming Potential (GWP) than carbon dioxide (CO₂). According to the United Nation Framework Convention on Climate Change (UNFCCC – Kyoto protocol), 1 kg of methane contribute 28 times more to the greenhouse effect than 1 kg of carbon dioxide over a 100-year timescale (IPCC 2013). As presented by the United States Environmental Protection Agency (EPA), methane can have even a greater greenhouse impact, up to 36 times more than CO₂ over the same timescale. However, it has a shorter atmosphere lifetime (8 - 10 years in 2010) compared to CO₂ (Prather et al. 2012), therefore a stabilization or reduction of its emissions could rapidly reduce CH₄ atmospheric concentration and its radiative forcing (Saunois et al. 2020). Hence, a better understanding of methane processes, from production to emissions, can help to reduce, control or predict the amount of methane emitted in the atmosphere, and represents a first realistic pathway to rapidly mitigate climate change (Nisbet et al. 2019; Saunois 2020).

Atmospheric methane is originated by two main sources: anthropogenic and natural (Kirschke et al. 2013; Saunois et al. 2016; Ganesan et al. 2019; Jackson et al. 2020). Latest estimates of the relative impact of each source is given in Saunois et al. (2020) based on both Bottom-Up (BU) and Top-Down (TD) approaches to assess the global methane budget in the framework of the Global Carbon Project. BU estimates, are determined by multiplying average emission factors (g/y/km²) by the activity factor (number of emission points or areal distribution) for each known CH₄ source category to estimate the annual emissions from an establishment or emission source (*e.g.* for specific regions, industry segments, facilities). In contrast, TD approaches at the regional scale measure the atmospheric methane concentrations which are then used in numerical models to determine emission rates (*e.g.* aircraft mass balance methods – AMB) (Vaughn et al. 2018 and reference therein). Estimates of methane emissions and sinks from BU and TD methods should reconcile.

From 2008 to 2017 the global methane emissions have been estimated by TD inversion methods to be $576 \text{ Tg CH}_4 \text{ yr}^{-1}$ (Saunois et al. 2020; Table 1). About 62% of these estimates correspond to anthropogenic sources (*e.g.* agriculture, waste management and fossil-fuel-related activities) while the remaining 38% corresponds to natural sources (*e.g.* wetlands, geological sources including hydrates melting). Global methane emissions estimated from BU approach correspond to $735 \text{ Tg CH}_4 \text{ yr}^{-1}$ equal to almost 30% larger emission than TD estimates (Saunois et al. 2020; Table 1). According to BU estimates, natural and anthropogenic contributions are approximately equal. As discussed in Saunois et al. (2020) the discrepancy between BU and TD estimates suggests that BU emissions are probably overestimated and the main source of uncertainty are natural methane emissions. According to Etiope et al. (2019), currently natural source estimates present uncertainties especially concerning the global methane estimates from geo- CH_4 sources only (Etiope et al. 2019). Indeed, current estimates (Saunois et al. 2016; Etiope and Schwietzke 2019, Etiope et al. 2019; Saunois et al. 2020) consider that methane fluxes from the Earth to the atmosphere are constant. As discussed in Etiope et al. (2019), seepages may vary annually and spatially as a function of geological (endogenous) or atmospheric (exogenous) factors. These factors may include pressure variations in the subsurface, tectonic stresses, seismicity or meteorological and climatic changes (*e.g.* decreasing of the bacterial activity during wintertime) (Etiope 2005; Etiope and Klusman 2010; Etiope et al. 2019). Specific studies on temporal variability of biogenic methane emissions from natural geo-sources are still missing, therefore all these estimates must be interpreted as an average of present-day degassing (Etiope et al. 2019).

There are also several methane reduction mechanisms representing the major sink of methane which need to be considered in order to assess the global methane budget (Table 1). They include natural sinks such as methane degradation in the atmosphere (*e.g.* tropospheric OH oxidation), methane dissolution in water, and oxidation of methane in soils by bacterial degradation (Saunois et al. 2016, Saunois et al. 2020). As shown in Table 1, natural methane sinks are estimated by TD inversion methods to be $556 \text{ Tg CH}_4 \text{ yr}^{-1}$ corresponding to an annual CH_4 growth of $20 \text{ Tg CH}_4 \text{ yr}^{-1}$. Global methane sink estimated from BU technique correspond to $625 \text{ Tg CH}_4 \text{ yr}^{-1}$ equal to an annual methane growth of almost $110 \text{ Tg CH}_4 \text{ yr}^{-1}$.

Table 1. Global CH₄ emissions and sinks by main source type summarized after Saunio et al. (2020) (left column) for bottom-up and top-down approaches in Tg CH₄ yr⁻¹ (second and third column respectively) and the relative fraction of BU and TP approaches (fourth and fifth column respectively). The difference between emissions and sinks result in a negative methane budget mainly due to anthropogenic emissions. Here, we are giving only the average estimate for each methane source and sink. Range of values associated with uncertainties and presented in this thesis, are given in Saunio et al. (2020).

Global Carbon Project 2008-2017 (Saunio et al. 2020)	Bottom Up (Tg CH ₄ yr ⁻¹)	Top Down (Tg CH ₄ yr ⁻¹)	Bottom Up (%)	Top Down (%)
Fossil Fuel Production and Use	128	111	17	19
Agriculture	206	217	28	38
Biomass	30	30	4	5
Total Anthropogenic Emissions	364	358	50	62
Wetlands	149	181	20	31
Other Natural Sources	222	37	30	6
Total Natural Emissions	371	218	50	38
Atmospheric Sinks	595	518	95	93
Soil Sinks	30	38	5	7
Total Natural Sinks	625	556	100	100
Total Emissions	735	576		
Total Sinks	625	556		
Annual Methane Growth	110	20		

Studies of gas seeps or gas provinces at the regional scale are required to better assess present-day methane emission, as well as in the geologic past. Basin modelling can help to better understand microbial gas generation processes at longer time scales, and to identify and predict the distribution of biogenic gas in the subsurface. Numerical model experiments can be a key tool to assess the spatial distribution of gas seeps which is required to quantify the methane budget from geo-sources. However, in order to better understand natural microbial gas processes (production, emissions, sink) it is required to assess the geo-sources from which methane can be generate.

Microbial methane generation is a complex process which implies redox biochemical reactions that are heterogeneous laterally and vertically as function of the Organic Matter (OM) availability and environmental conditions. Therefore, to assess the OM distribution in time and space and its impact on methane generation is essential to understand the carbon cycle. In particular, it is required to analyse and characterise the type of the original biomass (*e.g.* lacustrine, marine or terrestrial) from which the organic compounds (*e.g.* aminoacids, carbohydrates, lipids, vitrinite) are generated and used by microorganism. Photosynthesis is at the base of the OM production on earth (Tissot and Welte 1984). The carbon cycle starts with

the photosynthesis of terrestrial plants and algae which are capable of converting the atmospheric CO₂ into carbon and oxygen through the energy from sunlight.

The total organic carbon on earth is estimated to be around $6.4 \cdot 10^{15}$ t (Welte 1970). The majority of the total carbon ($5 \cdot 10^{15}$ t) is concentrated in sedimentary rocks either as organic or inorganic carbon, with a relationship between these two endmembers. In the hydrosphere CO₂-reservoir, carbonates may precipitate from organisms in form of skeletons or shells, resulting in the deposition of carbonate sediments. On the other hand, carbonate rocks may dissolve to participate at the CO₃²⁻, HCO₃⁻ and CO₂ equilibrium in seawater (Tissot and Welte 1984). The main processes and pathways involving the elemental carbon and its exchanges in the biosphere are summarized in Figure 1. Plant and animal respiration, bacterial decay, natural oxidation of OM and hydrocarbon combustion (naturally or by human activity) represent the most important process to recycle carbon dioxide back to the atmospheric CO₂-reservoir.

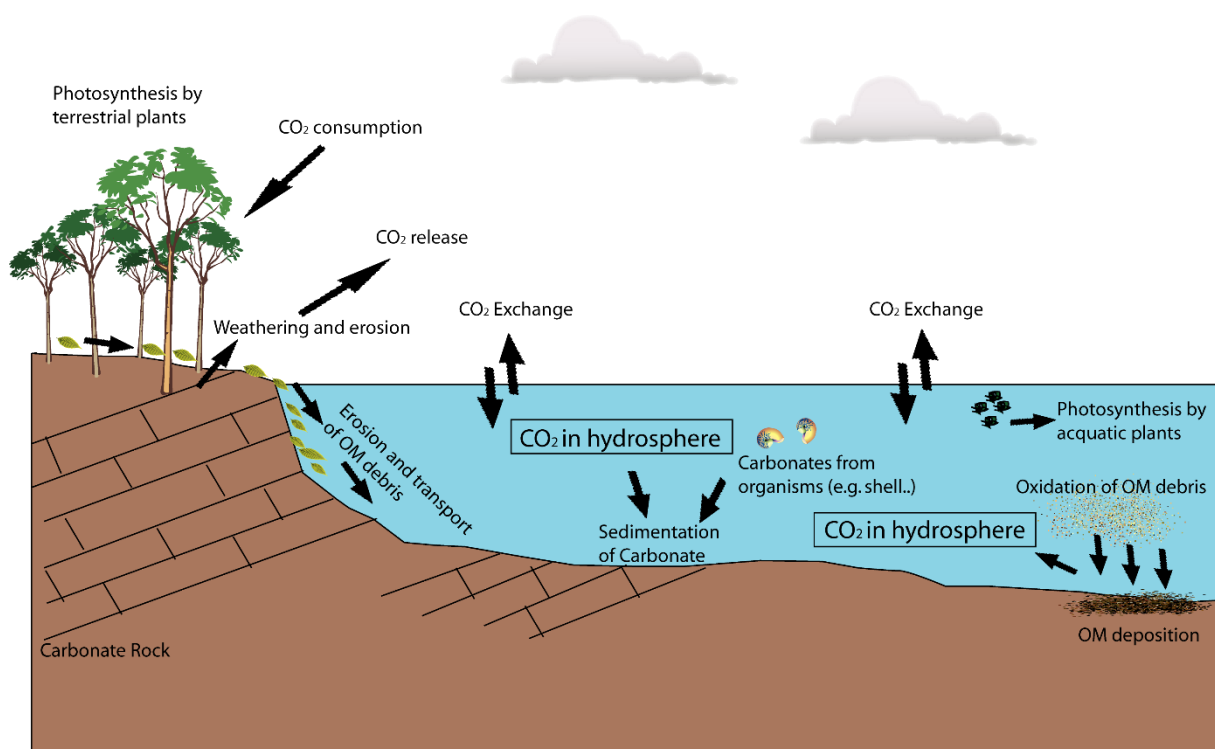


Figure 1. Main elements of carbon circulation in the biosphere (modified after Tissot and Welte 1984). Most of the carbon is fixed in sediments (82% and 18% of the total inorganic and organic carbon in sedimentary rocks respectively). The organic carbon produced by living organism is rapidly oxidized in CO₂ and recycled in the biosphere. A small amount of carbon can escape the carbon cycle through burial in sediments which subsequently generate hydrocarbons (Allen and Allen 2013).

It is possible to identify two major Organic Carbon (OC) cycles (Fig. 2) (Tissot and Welte 1984). There is a primary or small cycle, called the “biological cycle” that starts with the photosynthesis of living plants and bacterial. It continues in the biosphere through several trophic levels (dead plants/animals and OM accumulation in soil and recent sediments) until the oxidation of the OM into carbon dioxide back to the atmospheric CO₂-reservoir. The small cycle is characterized by an organic carbon turnover of about 2.7 to 3 *10¹² t, with a half-life of days to tens of the years according to the age of the organism (Tissot and Welte 1984; Schulz and Zabel 2006).

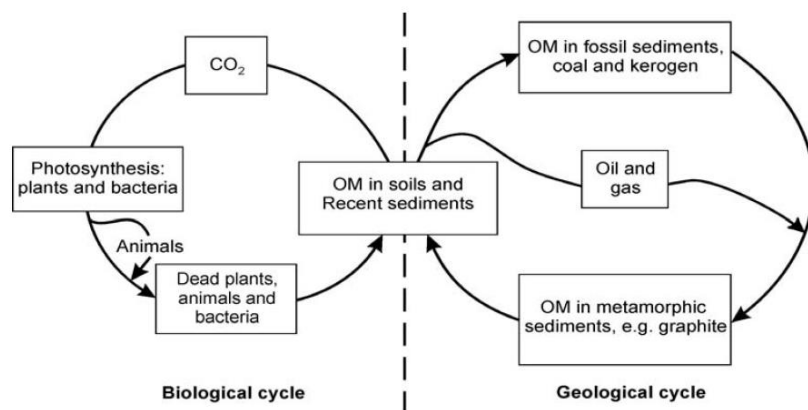


Figure 2. The two main organic carbon cycles on earth (Schulz and Zabel 2006; Tissot and Welte 1984).

The secondary or large cycle, called the “geological cycle” begins with the deposition of the OM in soil or sediments and continues with the generation of natural gas, oil or coal until the metamorphic transformation of the organic carbon in deeply buried sediments (*e.g.* graphite) (Fig. 2). The erosion of sedimentary rocks as well the combustion of fossil fuels results in the re-oxidation of the organic carbon into CO₂ which goes back into the atmosphere. The organic carbon turnover of the large cycle is estimated to be around 6.4*10¹⁵ t, with a half-life of several million years (Tissot and Welte 1984).

The transition between the biosphere and the geosphere is not perfectly defined (Schulz and Zabel 2006). There is a small gap of about 0.01% - 0.1% of the Total Organic Carbon (TOC) between the two cycles which is represented by the deposition of OM in buried sediments. The process of the OM transformation starts right after the degradation of the living organisms during transport (*e.g.* sinking in the water column) and alteration at the sediment interface (*e.g.* bacterial activity). This process extends in the buried sediments where bacterial

can be active for example at several hundred meters of depth in layers deposited up to ~15 Ma ago (Wellsburry et al. 2002).

Exploration geologists are interested in the small portion of OC which is deposited in sediments under anoxia. Since anoxia is commonly associated with specific geological conditions (*e.g.* high primary productivity, relatively high sedimentation rate and lower geothermal gradient) there are preferential environments in which the accumulation of this portion of OC can lead to the development of source rock layers that can generate large quantities of hydrocarbons (HCs). In the framework of this PhD thesis, a special regard is given to the characterization and description of source rock layers that are responsible for methane generation at low temperature (less than 80°C).

1.2 Biogenic methane processes

1.2.1 Shallow fluid systems

Shallow fluid systems are widespread natural processes that result from the interaction of geological, biological and chemical processes. They are identified from characteristic geological features that are widely distributed along near-shore, continental slope and deep oceanic environments and include shallow gas accumulations, pockmarks, seeps, mud-volcanoes, authigenic carbonate precipitations and gas hydrates (Jensen 1992; Römer et al. 2012; Skarke et al. 2014; Dupré et al. 2007; Pierre et al. 2017; Hovland et al. 2002; Judd et al. 2002).

Such shallow fluid systems represent both a benefit and a hazard for human activity. They may contain shallow energy resources but they also play an important role in shaping and stability of the seabed and therefore may present a risk for infrastructure installed at the seabed. They also affect marine biological processes as they can alter locally the composition of the ocean water.

A major component of such fluids is methane which is associated with water or other gases such as carbon dioxide (CO₂) or heavier gaseous (ethane, propane) or liquid hydrocarbons (HCs). Methane (CH₄) is the smallest HC component and can have different origins:

- Methane can derive from the decomposition of Sedimentary Organic Matter (SOM) during the early stages of diagenesis through bacterial activity (Whiticar et al. 1986;

Schulz et al. 2015). Such methane is called **primary biogenic gas**. In the framework of this PhD thesis, we are interested in the analysis of this type of gas and we refer to it as **microbial gas** or **biogenic gas**.

- Methane and other HC components can also have **thermogenic** origins as the product of thermal cracking of the organic matter during catagenesis (Tissot and Welte 1984; Jones et al. 2008).
- Methane can also be the result of the bacterial degradation of oil accumulated in reservoirs (Milkov 2011) which is called **secondary biogenic gas**.
- A different type of methane is represented by **abiotic methane** (resulting from an abiotic source of carbon). It is generally interpreted as related to reaction of H₂ with CO₂. In marine environments, abiotic methane is the result of reactions at high-temperatures along mid-oceanic ridges (Welhan and Craig 1979, Charlou et al. 2002; Proskurowski et al. 2008). Onshore, it has been found in different settings, like ophiolitic massifs, intracontinental cratons or volcanic/hydrothermal gas systems (Etiopie et al. 2011). It is found much more rarely compared to thermogenic or biogenic gas.

The scientific community has always been interested in methane in the subsurface (Rice and Claypool 1981; Rice 1992; Whiticar 1994) as it is ubiquitous (from continental margins to mid-oceanic ridges) and represents a major energy source that has a lower carbon footprint than liquid HC or coal. In addition, the quantification of natural methane sources and sinks, both at present day and in the geological past, are of interest to the scientific community working on present and future global climate change (Regnier et al. 2011; Saunois et al. 2016). Despite this increasing interest, methane generation and biological degradation mechanisms are still not well understood.

In addition to the OM composition, methane generation is controlled by several other factors such as surface temperature, eustatic sea level variation and temperature changes at the sea bottom (Judd et al. 2002), as well as the type of microorganisms that mediate the reactions of gas generation (Boetius et al. 2000). Therefore, an accurate characterization of the microbial gas generation process is necessary in order to understand the evolution and the importance of this potential energy source.

Microbial methanogenesis is the result of complex degradation processes of the OM that take place at different stages of diagenesis (Whiticar et al. 1986; Floodgate and Judd 1992;

Whiticar 1999; Schulz and Zabel 2006). Degradation can be assimilated to an anaerobic respiration resulting first in methane (CH_4) and subsequently, in moderate quantities, in ethane (C_2H_6) production. The efficiency of this process is determined by the quality and quantity of the OM and the temperature conditions (Schulz and Zabel 2006). Poor-OM layers ($\text{TOC} < 0.5\%$) can however generate important volumes of microbial gas (Clayton 1992). Therefore, large accumulations of biogenic gas can be found in offshore environments when conditions at the seafloor are compatible with an anaerobic respiration. For instance, in deltaic settings such as the Amazon cone (Arning et al. 2013) or the Carupano Basin (Schneider et al. 2012), generation and accumulation of biogenic gas is occurring because the dispersed OM is transported and deposited with relative high sedimentation rates at low geothermal gradients which are key conditions for biogenic gas generation (Clayton 1992). With increasing burial and temperature, the activity of the micro-organisms decreases (Clayton and Hay 1994). Above 60 to 80°C, the generation of microbial gas slows down considerably, and progressively thermal cracking of the OM takes place (Zeikus and Winfrey 1976; Zeikus 1997; Whiticar et al. 1986; Whiticar et al. 1999).

Pathways of OM degradation by microbial activity are linked to the type of microorganisms, their metabolic pathways, and to the type of carbon source. Metabolisms of methanogens include three main pathways: methylotrophy, hydrogenotrophy and acetotrophy. As methyl compounds are easily degraded, methyl fermentation is restricted to the uppermost part of the sediments (*i.e.* first meters). The main mechanisms are carbon dioxide reduction and acetate fermentation (Whiticar et al.; 1986). These different pathways may coexist but the reduction of H_2 and CO_2 from microbial activity is still considered the most efficient process to produce large methane quantities in marine environments. Indeed, notably in the framework of the PAMELA (Passive Margin Exploration Laboratories) project, it has been shown that acetotrophs are absent in marine environments suggesting a competition with sulfate reducing bacterias (Odobel 2017).

The biodegradation of OM depends on its reactivity to microbial activity. The OM is usually subdivided into a refractory part and a biodegradable part (Burdige 2007, 2006). A part of the biodegradable fraction (called “labile” such as proteins or carbohydrates) is rapidly degraded into methane whereas a more refractory part (called “thermo-labile” such as vitrinite and lipids) is remobilized as temperature increases and only then becomes available for micro-organisms to produce additional methane (Burdige 2011; Kamga 2016). Whereas the refractory

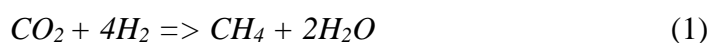
TOC content is easily defined through geochemical analysis (*e.g.* Rock-Eval technique or LECO) (Espitalié et al. 1977, 1984; Lafargue et al. 1998; Behar et al. 2001), it is not the same when we try to reconstruct the biodegradable compounds of the initial TOC content. It is still challenging to characterize the biodegradable OC as it is linked to OM preservation and mineralization processes (Burdige 2007). Different types of OM have different reactivities and, depending on their quality, they can also undergo different selective preservation and/or remineralization processes (Burdige 2007, 2011). Therefore, it is important to consider the effect of the quality and quantity of the OM on methane production, especially with regards to the effect of its initial labile and thermo-labile fractions. This study therefore aims to understand the effect of the OM quality on CH₄ production, using geochemical analysis that is integrated with basin modelling.

1.2.2 Methanogenesis

Microbial gas, or primary biogenic methane, can be distinguished from thermogenic gas based on composition and isotopic signature. Biogenic gas is usually extremely dry ($C1/(C2+C3) > 100$) and characterized by a light isotopic signature ($\delta^{13}C\text{-CH}_4$ between -90‰ and -50‰) (Bernard et al. 1976; Milkov and Etiope, 2018). In contrast, secondary biogenic gas displays a more variable isotopic signature, sometimes close to the signature of thermogenic gas ($\delta^{13}C > -55‰$) (Katz, 2011).

Microbial gas is the result of the respiration by micro-organisms. This process first tends to use molecular oxygen as long as oxygen is available in the environment. When O₂ is depleted, microbial respiration proceeds consuming electron acceptors in the order NO₃⁻, Mg²⁺, Fe²⁺, then SO₄²⁻ (Archer, 2007; Clayton and Hay, 1994). Once the sulfate reduction ends, methanogenesis starts (Fig. 3).

Methanogenesis requires anoxic conditions, low sulfate content, low temperatures, presence of OM, and sufficient pore space to host micro-organisms (Rice 1992). Depending on the amount of available SO₄²⁻, methanogenesis follows different generation pathways (Whiticar and Schoell, 1986) (Fig. 4). As mentioned before, in seawater the preferential pathway is reduction of CO₂ by molecular hydrogen (Eq. 1) (Archer 2007). In contrast, in fresh water environment, the preferential pathway is fermentation of acetate (Eq. 2) (Hoehler et al. 1999).



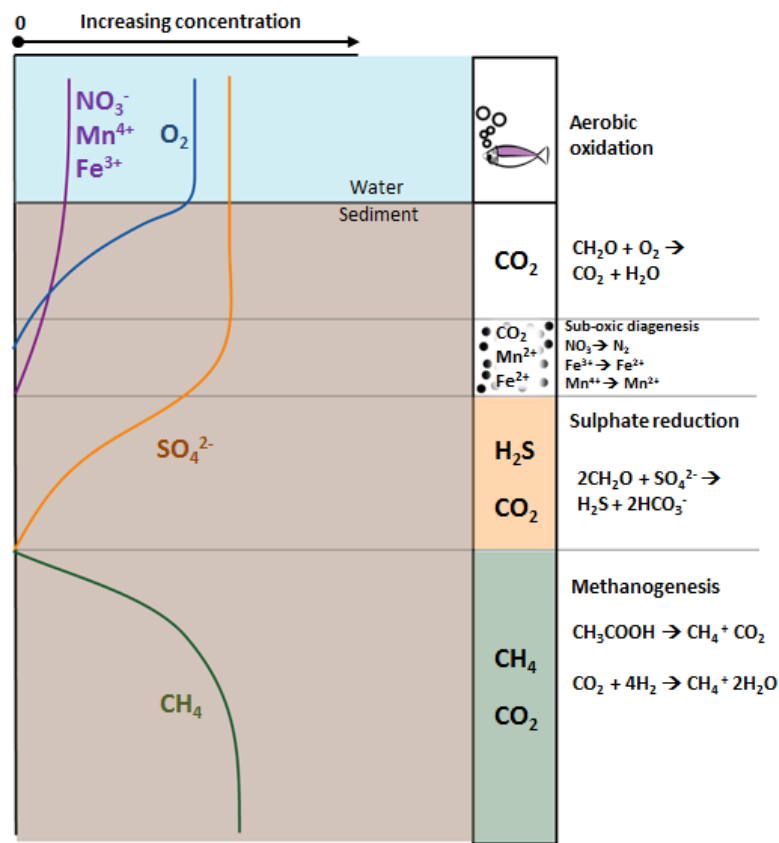
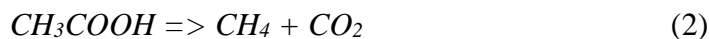


Figure 3. Distribution of the main elements along the sedimentary column (modified after Clayton and Hay 1994).

Despite the fact that methane can be generated either in fresh or marine environment, the relative proportion of each pathway and the final amount of generated CH_4 , are strongly controlled by the availability of substrate and hydrogen for the methanogens, which can be limited by the competition with sulfate reducing bacteria (Whiticar et al. 1986). The rate of methane generation is influenced by several parameters where temperature (Belyaev et al. 1983) represents one of the main controlling factor. The microbial activity is classified by increasing temperature resistance: Psychrophiles, Mesophiles, Thermophiles and Hyperthermophiles (Fig. 5). The peak of CH_4 generation is around $\sim 40^\circ C$ corresponding to the mesophiles level, whereas neither psychrophiles nor thermophiles are capable of generating important microbial gas volumes (Katz 2011).

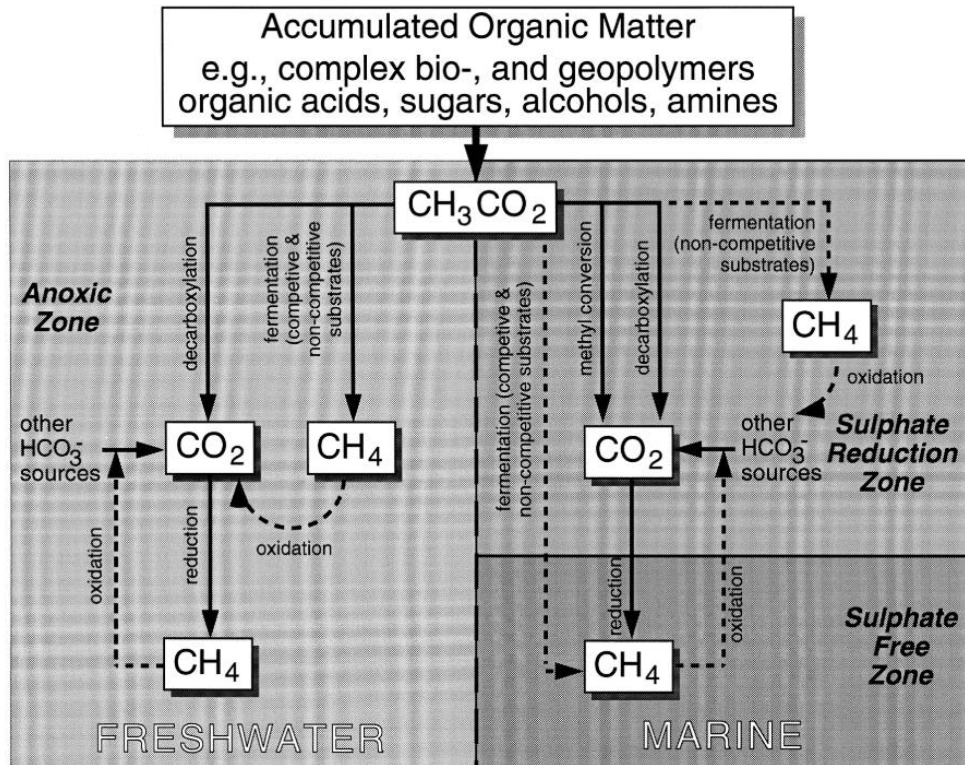


Figure 4. OM degradation pathways (acetate fermentation vs CO_2 reduction) in freshwater and marine settings (Whiticar *et al.*;1986; Whiticar 1999).

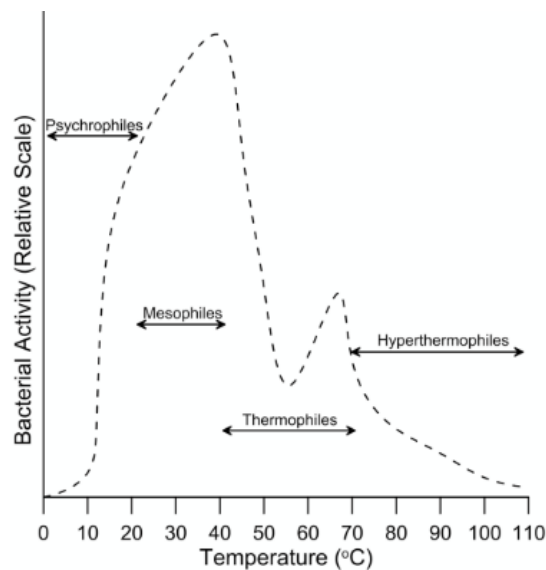


Figure 5. Evolution of the bacterial activity levels as a function of increasing temperature (Katz 2011).

Methanogenesis is linked also to the salinity of pore water (Waldron *et al.* 2007) since microbial activity may be inhibited when salinity is too high (Zindler 1993; Schoell 1980). Sufficient pore space is also required to allow growth of microbial population (Chapelle and Lovley 1990). However, as observed by Chapelle and Lovley (1990), the abundance of

substrate can impact the overall amount of methane but it doesn't seem to be a controlling factor of the rate of methane generation.

Clayton (1992) determined that the key controlling factors of microbial gas generation and accumulation are thermal gradient and burial rate of the source rock. If the sedimentation rate is too low, the metabolizable organic carbon may be consumed in the aerobic or sulphate reduction zone and only a small fraction can reach the methanogenesis zone, resulting in a dispersion of the generated methane to the surface. If sedimentation is too fast, the sedimentary organic matter (SOM) may by-pass the methanogenesis window too quickly to generate large amounts of gas. Figure 6 shows the optimum heating rate (the product of geothermal gradient and sedimentation rate) for microbial gas production (Clayton 1992). This diagram was constructed with data from geological settings where extensive methanogenesis is observed such as in California, Po Valley, Offshore Peru and Offshore Louisiana (Clayton 1992 and references therein). The upper boundary of the diagram is equivalent to a heating rate of 18°C/My while the lower boundary is equivalent to a heating rate of 7°C/My (Clayton 1992). The optimum balance between production and accumulation with normal thermal gradients (20-40 °C/km) occurs at burial rates of 200-1000 m/My and yields heating rates located between 7 and 18 C/My.

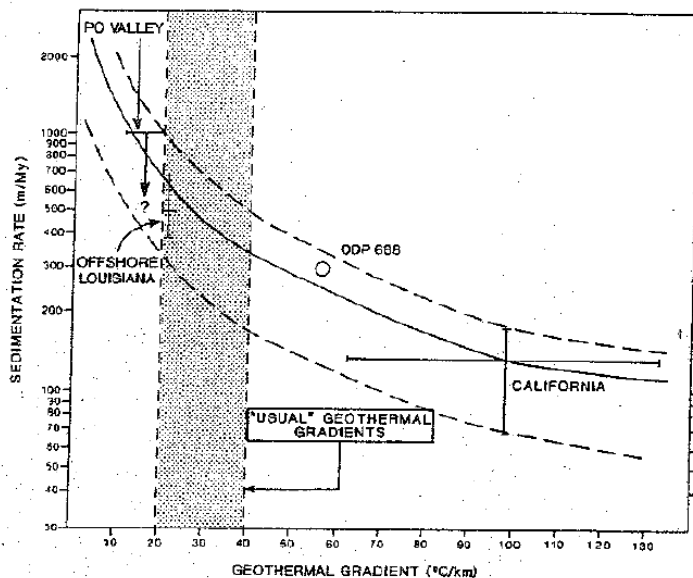


Figure 6. Sedimentation rate vs geothermal gradient converted to heating rate for methanogenesis (Clayton 1992). The microbial gas production is likely when the curve is comprised between 18°C/Ma and 7°C/ Ma.

1.3 Evidence of fluid systems at the seafloor

When CH₄ generation occurs at shallow depths and hydrostatic pressures, in unconsolidated sediments (Fig. 7) (Verweij et al. 2018) there may be no conditions for trapping of gas. Potential seals cannot hold even moderate gas columns as they easily exceed the low capillary entry pressures at these shallow depths (Fig. 7). This lack of effective sealing results in continuous fluid emanations at the ocean floor. These continuous emanations contrast with features of focused fluid escape structures such as pockmarks which are commonly associated with physico-chemical manifestations such as mineral precipitations of authigenic carbonates or hydrates formation.

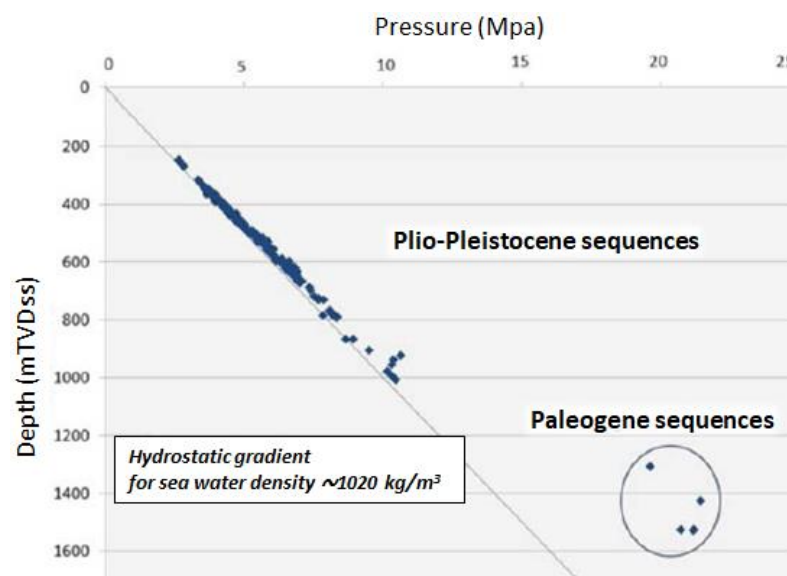


Figure 7. Pore-fluid pressures vs depth for Plio-Pleistocene and Paleogene sequences in the Southern North Sea delta (modified after Verweij et al. 2018). Pore-fluid pressures are hydrostatic or close to hydrostatic in the first 1000 m of depth.

1.3.1 Pockmarks and gas seepages

Pockmarks are morphological depressions in the soft seabed formed by fluid expulsions including gas (Hovland 1989). They can be cone- or saucer-shaped depressions with generally a size varying from 1 to more than a few 100 meters and height between 1 to more than 10 meters (Dimitrov and Woodside 2003). Pockmarks have been observed and described for the first time in the Nova Scotia continental shelf by King and McLean (1970) and, then, they have been recognized along many continental margins (Hovland and Judd 1988). These features are found widely distributed in the deep-water domain and in shallow environment (such as in the

Lower Congo Basin or in the Norwegian offshore) (Gay et al. 2006; Rise et al. 2014) as the result of interactive processes between fluids and sediments.

It is now well accepted that pockmarks are the expressions related to fluid seepage at the seafloor (Hovland et al. 1984, Hovland et al. 2005) or of gas hydrate dissolution (Sultan et al. 2014), which can be originated by either thermogenic and biogenic gas emissions (Hovland and Judd 1988). They can be present as a cluster or as a string reflecting subsurface structures (e.g. fractures or faults) (Hovland et al. 2010; Pilcher and Argent 2007; Gay et al. 2007). Several studies (Sultan et al. 2010; Davy et al. 2010) tried to classify and differentiate pockmarks between classical fluid escapes with a conical shape (Type-I) and hydrate-bearing depressions developed over several kilometers (Type-II) (Fig. 8). Type-I pockmarks are characterized by a sub-circular shape whose diameters vary between 10 to 900 m, with a depth of 0.1 to 50 m (Riboulot et al. 2016). They are usually associated with a gas chimney or acoustic pipes and are commonly observed on continental margins. Type-II pockmarks show irregular morphology with diameters varying between 50 – 800 m and depths of about 10 m, and they are not associated to vertical chimneys (Riboulot et al. 2016).

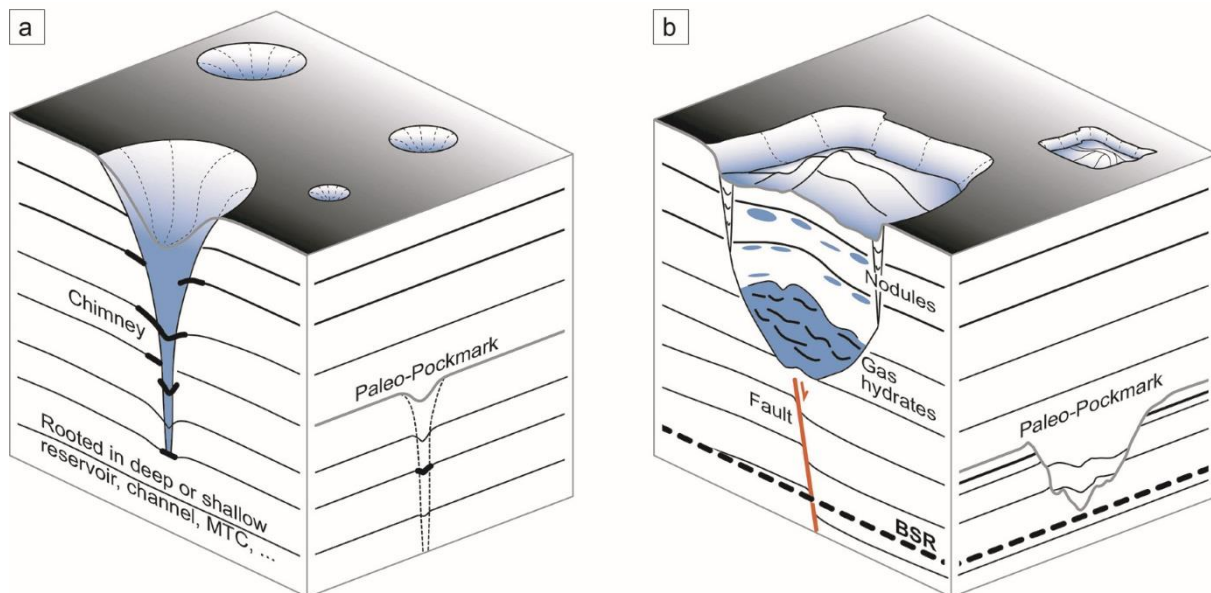


Figure 8. Morphological and geometrical characterization of the two different types of pockmarks (Riboulot et al. 2016). a) Type-I pockmark with gas chimney association; b) Type-II pockmark with an irregular shape associated to hydrates occurrence.

According to Etiope et al. (2019), seepages can be classified into (1) onshore seeps in sedimentary basins (e.g. CH₄ seeps and mud volcanoes), (2) offshore seeps where methane is

usually released at shallow depths (200 to 400 mbsl) and CH₄ can likely reach the atmosphere as a function of the amount of emitted gas and the water depth, (3) deep-sea seeps, (4) geothermal and volcanic manifestations, where CH₄ and CO₂ are usually associated.

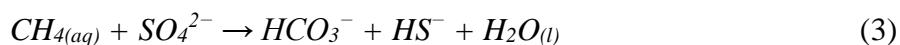
The interest regarding these features is growing since they can be a key for understanding fluid flow in sedimentary basins (Chenrai and Huuse 2017). Pockmarks and paleo-pockmarks (Andresen et al. 2008) can be used as first indicators of active or paleo-fluid escapes to the seafloor, giving information on hydrocarbon and hydrate occurrences as well as on the paleo-fluid flow history. They can also contribute to the emissions of large quantities of gas directly into the ocean, with a possible transfer to the atmosphere, resulting in a negative impact on climate and environment.

Distributions of pockmarks and seeps have been identified and mapped along the areas studied in this PhD thesis, both in the Offshore Zambezi (Deville et al. 2020) and in the offshore Aquitaine (Dupré et al. 2014, 2020; Michel et al. 2017).

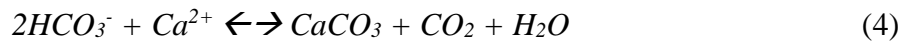
1.3.2 Methane-Derived Authigenic Carbonate (MDAC)

Methane-Derived Authigenic Carbonates (MDACs) are sedimentary features resulting from the Anaerobic Oxidation of Methane (AOM) (Jørgensen 1976, Boetius et al. 2000, Judd et al. 2007). MDAC precipitation takes place within the Sulphate-Methane Transition Zone (SMTZ) which corresponds to a boundary located mostly below the seafloor at variable depths (Boetius et al. 2000). MDACs are characterized by variable precipitation rates of several cm/ky to m/ky (ky = 1000 years) (Luff and Wallmann 2003).

During upward migration, the generated methane meets the SO₄²⁻ of the downward diffusing seawater in the Sulphate-Methane Transition Zone (STMZ) where it is consumed by the activity of methanotrophic microorganisms with Sulfate Reducing Bacteria (SRB) in anoxic conditions (Boetius 2000; Conrad 2005; Thauer 2010; Lash 2015). The AOM redox reaction can be described as the net reaction between seawater sulfate and methane (Eq. 3):



The dissolved inorganic carbon (bicarbonate) generated in the STMZ under anaerobic conditions increases alkalinity which promotes carbonate precipitation resulting in the formation of authigenic carbonates (Eq. 4) (Boetius 2000; Regnier et al. 2011; Lash 2015).



This process is a widespread diagenetic reaction along modern continental margins (Reeburgh 2007, Lash 2015). MDACs have an important role in climate control (Noble-James et al. 2020). Indeed, they represent a major sink for methane, with a consumption varying from 10 to 80% of the total up-ward migrating methane before it is released at the seafloor (Conrad 2009, Regnier et al. 2001).

MDAC can precipitate either in the form of isolated crystals dispersed in sediments, or chimneys or areal massive distributions when fluid emissions are important and sustained over time (Paull and Ussler, 2008). MDAC precipitation requires anoxic conditions which implies in most cases that these features precipitate in the sediments below the seafloor (Paull and Ussler, 2008). Therefore, according to the authors, the presence of MDAC at the sediment/water interface is usually the result of erosional processes which removed the uppermost sedimentary cover. Examples of such features are found along the Offshore Aquitaine (Dupré et al. 2014; Pierre et al. 2017; Dupré et al. 2020) and in the Offshore Zambezi (Deville et al. 2020) (Fig. 9).

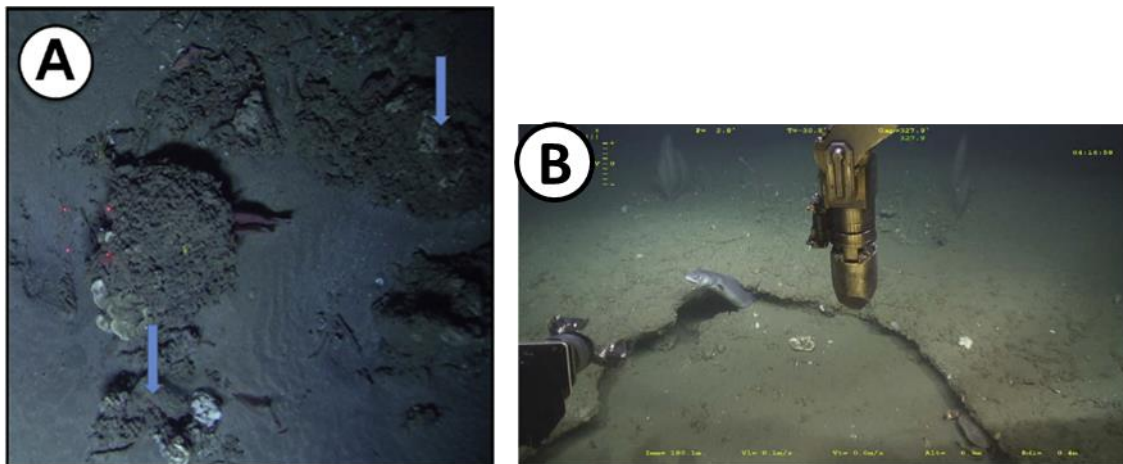


Figure 9. Examples of methane-derived authigenic carbonate structures Offshore Zambezi (A) (Deville et al. 2020) and Offshore Aquitaine (B) (Pierre et al. 2017).

1.3.3 Gas Hydrates

Gas hydrates are solids formed by cages of water molecules within which different type of gases such as methane, ethane, propane and carbon dioxide can be trapped (Kvenvolden 1988). When the stored natural gas is mainly methane (> 99%), they are called methane hydrates. Hydrates are found at specific pressure-temperature conditions (Fig. 10) which principally occur in permafrost both onshore and offshore (e.g. Western Siberia), or along the

continental shelf when water depths exceed 300-500 m (e.g. Gulf of Mexico) (Kvenvolden 1993). Usually, saturated methane hydrates present a methane to water weight ratio of 1:6 that is equal to a volumetric ratio of ~164:1 (Davidson et al. 1978; Kvenvolden 1988, Sun and Duan 2005) which represents an enormous storage of methane. Kvenvolden (1998) published a first methane hydrate quantification based on the worldwide distribution of the Hydrate Stability Zone (HSZ) yielding 10^{13} and $20 \cdot 10^{15}$ m³ of gas, onshore and offshore respectively. However, these estimates are probably excessive especially for offshore methane hydrates due to the lack of information concerning the type and permeability of sediments (Grauls 2001).

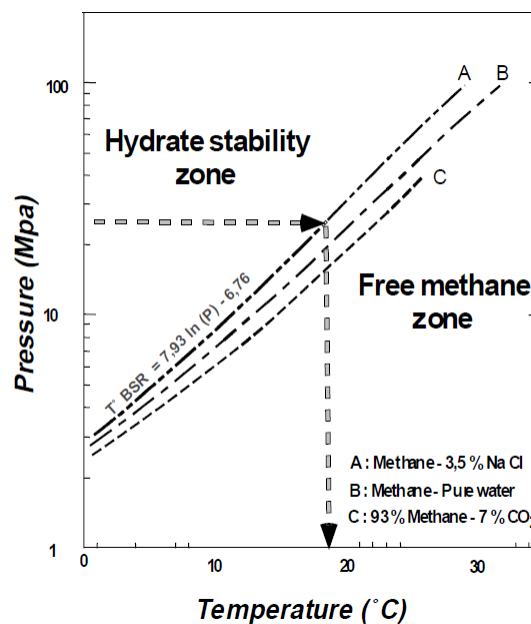


Figure 10. Pressure-temperature equilibrium diagram for hydrate stability (Grauls 2001).

Hydrates can be identified by direct observation, from well log interpretation or on seismic reflection profiles whenever a free gas saturation occurs (Kvenvolden 1988; Grauls 2001; Hovland and Svensen 2006). Under these conditions, the contact between the solid phase (hydrates) and the vapor phase (free gas) consists of an acoustic impedance contrast that is identified by a characteristic Bottom Simulating Reflector (BSR). BSRs represent the base of the hydrate stability zone and, as the name suggests, are usually sub-parallel to the seafloor topography, with a negative phase polarity in seismic data (Shipley et al. 1979; Kvenvolden 1988).

Hydrates are an interesting subject for the scientific and industrial communities as they can be:

- (1) a drilling and production hazard for the industry,
- (2) an efficient seal and a direct index of hydrocarbon accumulations below the HSZ,
- (3) a direct heat flow indicator as the BSR are stable under specific thermodynamic conditions

In addition, hydrate resources can account for twice the conventional fossil energy (Grauls 2001) or for 50% of the organic carbon in the Earth (Kvenvolden 1988). However, they can be subjected to melting linked to anthropogenic ocean warming (Ketzner et al. 2020), representing both a potentially important future hydrocarbon resource but equally a risk for climate and environment.

1.4 PhD thesis objectives as part of the PAMELA Research Project

The PAMELA (PASSive Margin Exploration Laboratories) project is a collaborative research project between TOTAL, Ifremer, IFPEN, the Sorbonne University, University of Rennes, University of Brest and CNRS. The overall objective of PAMELA is to better understand the evolution of transform and passive continental margins. PAMELA integrates the study of geodynamics, sedimentary systems, slope instabilities, fluid systems and ecosystems of these depositional environments. The project started in 2013 and was closed in 2019. During these 7 years, a great quantity of scientific results has been gathered, especially in two natural laboratories: the Aquitaine Basin (Bay of Biscay) and the Mozambique Channel. This PhD thesis is part of the working group dedicated to the analysis of fluid systems and ecosystems which involved mainly Ifremer, IFPEN and TOTAL.

Previous results concerning the gas systems in the Bay of Biscay and in the Mozambique Channel (GAZCOGNE-1 and 2; MOZ-01; MOZ-02; MOZ-04) (Zambezi and Madagascar offshore) focused on $\delta^{13}\text{C}\text{-CH}_4$ and molar gas composition and confirmed that fluids are linked to microbial activity in both areas (Ruffine et al. 2017a; Deville et al. 2020), with pure methane (about 100% C1) and depleted isotope values of $\delta^{13}\text{C} < -60 \text{‰}$ (Fig. 11).

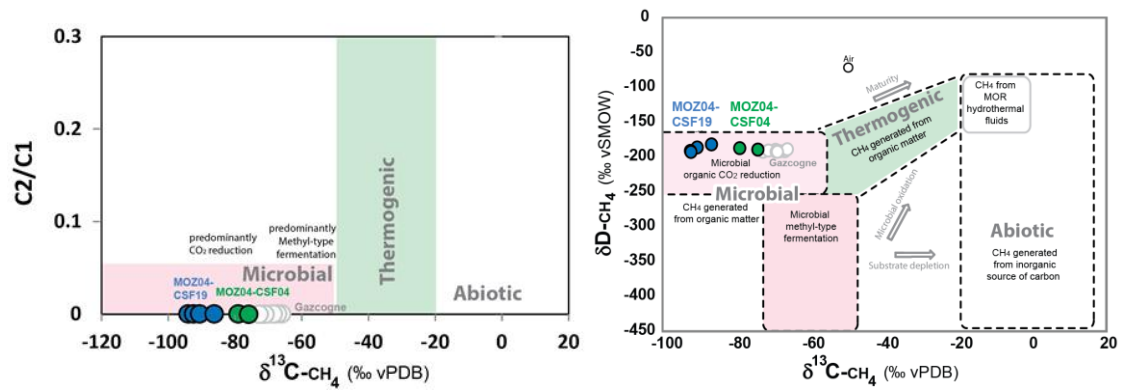


Figure 11. Geochemical results on gas samples collected in the offshore Mozambique (MOZ04 – CSF19 and CSF04) and in the Bay of Biscay (Gazcogne2 Pegaz samples) (Deville et al. 2018 Internal Report IFPEN; Ruffine et al. 2017). The isotopic composition of the collected gas shows that for all the studied areas the gas is purely of biogenic origin. However, the comparison between the two study sites highlighted differences in terms of $\delta^{13}\text{C-CH}_4$ signature. It could be related to the presence of different OM sources, as well as different geodynamic conditions or differences in terms of microbial activities.

The isotopic signature of the collected gas showed differences in terms of $\delta^{13}\text{C-CH}_4$ (Fig. 11). The geochemical results linked to local estimations of emitted gas from gas seeps (Ruffine et al. 2017) and to the analysis of authigenic carbonates resulting from degassing processes (Pierre et al. 2017) brought up the following questions:

1. Could differences in isotopic signature be related to different initial OM sources or to different geodynamic conditions for the same biogenic gas production process?
2. What are the main factors controlling biogenic gas generation and accumulation at the basin scale?
3. Are these systems continuously sourced by an active system at the present-day or are they old systems slowly degassing?
4. Can we determine the beginning of the biogenic gas generation process and the amount of emitted gas over time at the basin scale?
5. Can we propose a workflow to estimate the methane budget (generated, trapped, consumed and emitted) in continental shelf environments?

The main objective of this PhD study is therefore to characterize the OM in shallow depositional system and its impact on biogenic gas, from its generation to emission at the water/sediments interface, including main methane sinks (*e.g.* MDACs). Starting from the dataset collected in the framework of the PAMELA research project, we show how recent active shallow fluid systems are impacted by biogenic gas production and how, by means of two case

studies, findings can be generalized to any shallow fluid system with a large biogenic gas component.

In the first case study, we performed a large-scale screening of the OM evolution in the Mozambique Channel. This was done using Rock-Eval analysis on suspended sediments and on seafloor sediments in order to understand the spatial and vertical evolution of the OM. Pyrolysis was coupled with EDS-SEM analysis to assess the impact of the mineralogical composition of sediments on OM preservation. In addition, we compared sediment accumulation rates and oxygen exposure times in the main physiographic provinces of the Mozambique Channel to better understand the evolution of the deposited OM in a regional context.

In a second case study, we analyzed the shallow fluid system of the offshore Aquitaine with basin modelling, using a recent model of microbial processes developed by IFPEN (modified after Pujol et al. 2016). Our approach includes a sensitivity analysis on the critical parameters impacting biogenic gas generation which allows us to identify a reasonable geological scenario that has been calibrated to gas flux data (Dupré et al. 2020). We also analyzed the role of geochemical reactions affecting methane migrating upward in the shallow system. These reactions such as oxidation to CO₂ represent the main CH₄ sinks. Our work therefore represents a significant contribution to the understanding of biogenic gas generation and migration/expulsion processes at the basin scale which is useful for the E&P industry to identify the occurrence and estimate the size of biogenic gas accumulations. Our work is also useful to the scientific community working on global warming issues (IPCC, 2013).

1.4.1 The Mozambique Channel natural laboratory

The Mozambique Channel presents the typical features of an active cold fluid system, such as pockmarks (King and MacLean, 1970; Hovland and Judd, 1988), authigenic carbonates (Boetius 2000; Regnier et al. 2011; Lash 2015) and seeps (Dupré et al. 2007). Indeed, the offshore Zambezi is characterized by slope destabilization processes which may trigger fluid seeps (Deville et al. 2020). These seepages are found associated with pockmarks, authigenic carbonate crusts and acoustic anomalies within the water column which are interpreted as the result of bubbling activity mostly located outside the destabilization zone (Fig. 11). Results from geochemical analysis on gases in the sediments confirmed that the fluid system is sourced by CH₄ of microbial origin, generated by hydrogenotrophic methanogenesis from a substrate

of organic origin with no link to a deeper thermogenic gas source (Fig.12) (Deville et al. 2018; 2020). Some pockmarks are active while others are inactive in terms of fluid seepage at present. They are associated with chimneys of authigenic carbonate buildups.

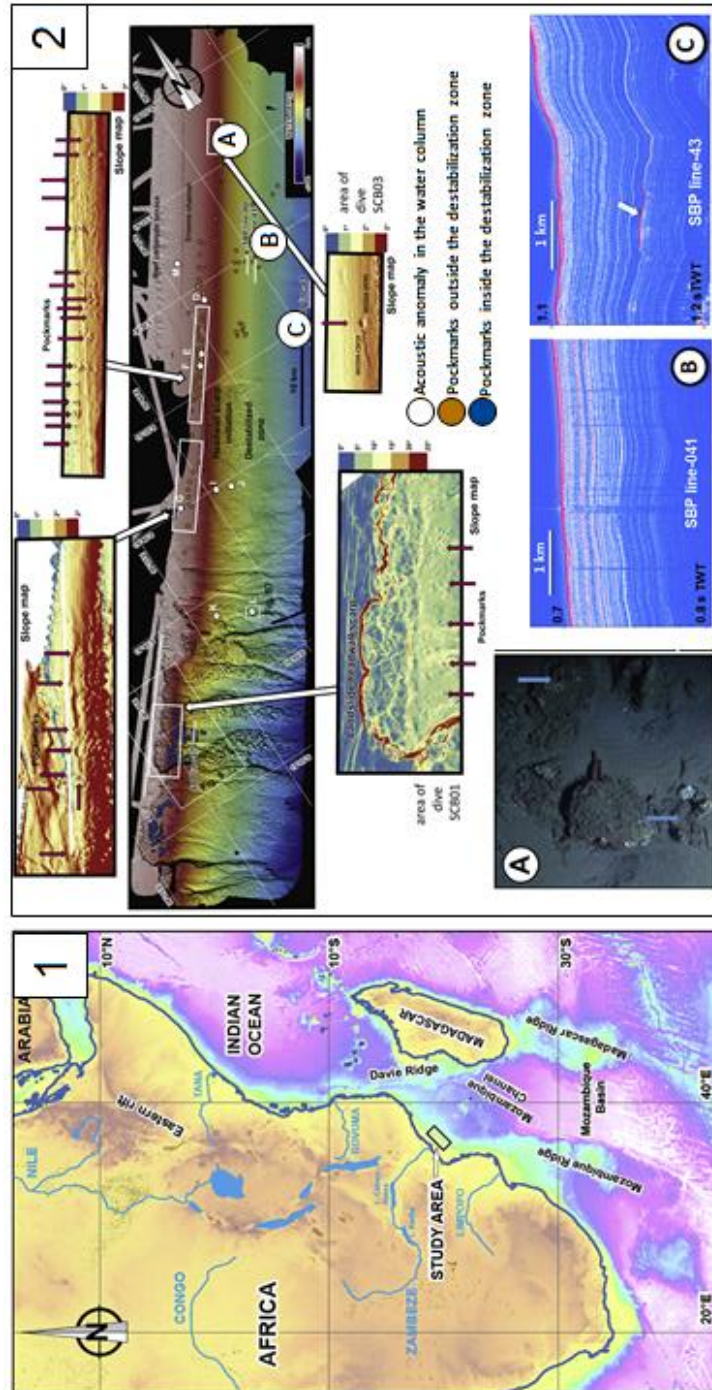


Figure 12. (1) Location of the study area offshore Zambezi. (2) Location of the pockmarks in the study area: (A) authigenic carbonates occurrences; (B,C) vertical seismic anomalies interpreted as gas escape pathway (modified after Deville et al. 2020).

Samples have been collected with sediment traps in moorings located 47 m above seabed (before the deposition), with a multicorer at the water/sediment interface (MTB up to 40 cm of depth) and with corers in the first few meters of sediments (up to 12 – 33 m of depth). Rock-Eval analysis of these samples indicated that the organic matter (OM) is heterogeneous in terms of quality and quantity (Deville et al. 2018 - IFPEN Internal Report).

The first part of this PhD thesis is dedicated to the integration of new Rock-Eval (RE) analyses, Scanning Electron Microscopy (SEM) analyses, Sediment Accumulation Rates (SAR) and oxygen exposure times using the large PAMELA dataset (Deville et al. 2018 - IFPEN internal report) to investigate transport and preservation conditions of the OM over the entire area (Fig. 13). This work helps to better assess the fate of the organic carbon once it reaches the ocean, as a good understanding of its evolution is key to the quantification of the processes linked to the carbon cycle and global warming processes.

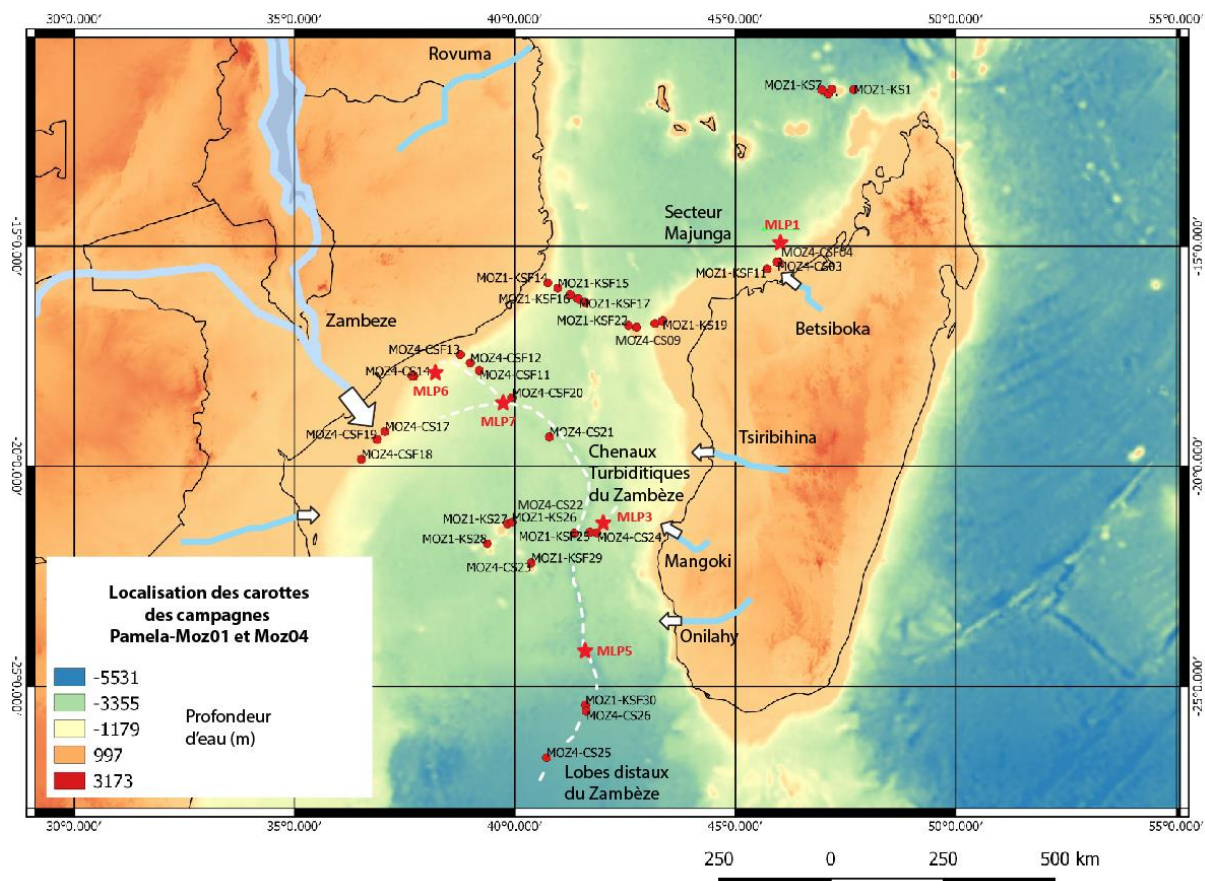


Figure 13. Location map of the collected cores during the PAMELA missions (MOZ01 and MOZ-04) (Deville et al. 2018, IFPEN Internal Report). The red stars represent the position of the particle traps installed during the MOZ-01 mission (December 2014) and the red dots represent the positions of the collected cores during the missions MOZ-01 and MOZ-04.

1.4.2 The Offshore Aquitaine natural laboratory

A first quantification of the emitted gas from the seafloor along the Aquitaine shelf was published by Ruffine et al. (2017) yielding values between 35 to 368 mLn·min⁻¹ (volume normalized to atmospheric pressure) from 9 *in situ* bubbling sites. These estimates were integrated over the entire area of interest using acoustic signatures from bubbling sites (about 2612 seeps) (Dupré et al. 2014; 2020) (Fig. 14) which yield 144 MgCH₄/y of emitted gas from the sea bottom. Associated with these gas escapes are authigenic carbonate pavements that represent a major sink of methane and that occur widely above and below the sub-seafloor over 375 km² (Pierre et al. 2017; Dupré et al. 2020). The bubbling sites as well the authigenic carbonates are located at the shelf break of the Offshore Aquitaine (Fig. 14) and no such activities were observed along the slope or inside the erosional canyon where the uppermost Pleistocene layers were removed (Michel et al. 2017; Dupre et al., 2020). Emission sites are mainly located along a narrow N-S oriented line parallel to the Aquitaine Shelf, with a more intense fluid activity in the southern part of the basin compared with the northern part. Similar differences are observed for the MDAC deposits which are widely distributed in the south and more localized in the northern area (Dupre et al. 2020). These local variations could be the result of variable OM provenance but also of the temperature distribution along the sea bottom, or the result of a heterogeneous sedimentation rate. In order to better understand the evolution of the biogenic gas system and the role of the MDACs in gas migration in the Offshore Aquitaine, we investigated the area with a 3D basin model.

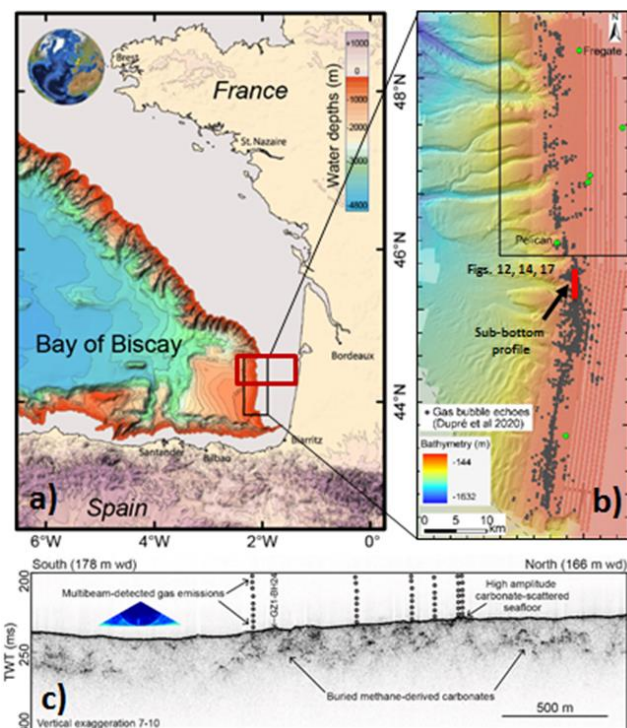


Figure 14. a) Bathymetric map of the Bay of Biscay (Southwestern France) and modelled area (red rectangle) of Fig. 3 modified after Sibuet et al. (2004) and Dupré et al. (2020); b) Detailed shaded bathymetric map offshore Aquitaine (Loubrieu 2013, Gazcogne1) with gas emission site distribution and localization of the sub-bottom profile (red line) shown in Fig. 1c and the modelled offshore area in Fig. 1b (black rectangle) (modified after Dupré et al. 2020); c) Sub-bottom profile acquired in the emission site showing the presence of sub-cropping MDACs from Dupré et al. (2020).

A previous PhD project (Michel 2017) within the PAMELA research project was focused on a better understanding of this fluid system based on the observed geometries and the authigenic carbonate pavements, the OM source distribution and the migration paths. Michel (2017) proposed three possible scenarios for the generation, migration and expulsion of the microbial gas in the Offshore Aquitaine (Fig. 15).

In the **first scenario**, the OM is in Cretaceous sediments, with a TOC content between 0.5-1% in the central part of the basin. The seepages could be the result of:

1. Generation of the gas in the western side of the plateau with lateral migration eastwards from the deeper part of the shelf break through the Plio-Pleistocene clinoforms;
2. Generation of the gas at the shelf break and vertical migration of the gas from the Cretaceous layers through the sedimentary column;
3. Generation of the gas in the eastern side of the system and migration westwards, constrained by the presence of the aquifer.

In the **second scenario**, the OM is in the Paleogene series, with a TOC content between 0.2-1% where the gas migrates upslope along the sedimentary drains. The migration pathways are similar to the first scenario. However, the lateral migration proposed in the 2.1 and 2.3 sub-scenarios are not consistent with the extension of the OM-rich horizon (Michel 2017).

In the **third scenario**, the OM source rock is represented by the Miocene layers that have a thickness between 200 and 600 m. The Miocene contains a TOC between 0.3-0.7% of a continental-derived OM. The gas founded in the Miocene-Pliocene series shows a pure biogenic origin, not linked to a thermogenic source. The proposed migration pathways are the same presented in the second scenario.

Finally, based on regional horizon geometry, Rock-Eval analysis and potential migration pathways, the author suggests that the microbial gas system is mainly sourced by the Plio-Pleistocene progradational system (Michel 2017). However, given the regional geothermal gradient (Biteau et al. 2006) and temperatures of peak microbial activity for methanogenesis (Katz 2011), we cannot exclude a possible contribution from a Miocene source (Dupre et al. 2020).

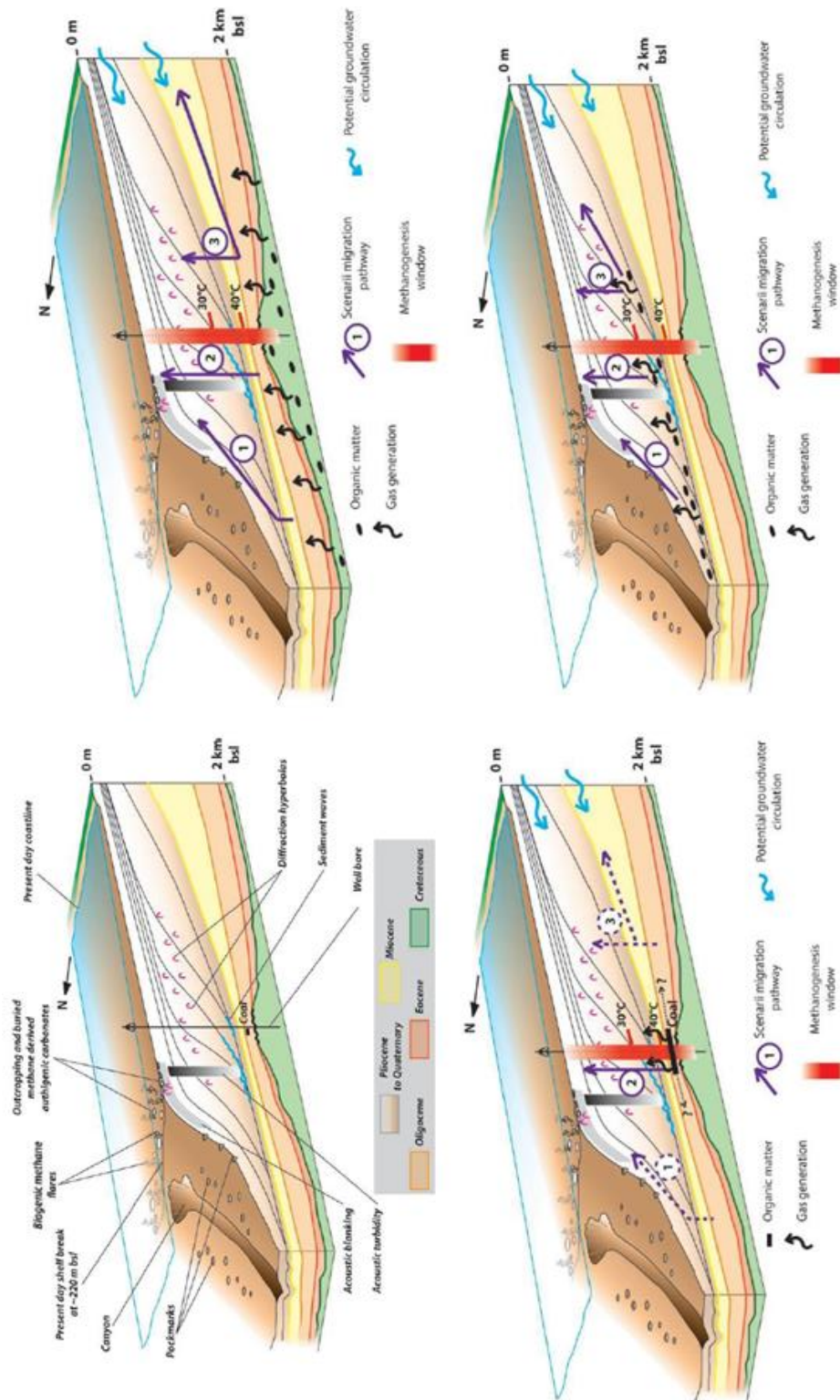


Figure 15. Upper left: synthetic 3D block of the central part of the Parentis basin representing the main geometry and stratigraphy (Michel 2017). In the first scenario (upper right), methane is generated from a deep source located in the Cretaceous. In the second scenario (lower left), the methane is generated from a Paleogene source. In the third scenario (lower right), methane is generated from a Miocene source. In all three scenarios, methane can migrate 1) from the bottom of the shelf break through the Plio-Pleistocene clinoforms; 2) vertically through the sedimentary column; 3) from the eastern side to the shelf break with a westward migration imposed by the presence of the aquifer.

In this PhD study, we use a 3D model in order to take into account and analyze the main mechanisms that play a crucial role during the CH₄ generation process. We apply a new modelling approach for biogenic methane generation developed by IFPEN (modified after Pujol et al. 2016). In this model, the degradation law is taken from a marine OM that is based on published data of the quantification of biodegradable vs more refractory TOC (Burdige 2007, 2011, Ravin et al. 2013; Pujol et al. 2016). A key part of our project is dedicated to a sensitivity analysis to rank and optimize the main geochemical parameters that are critical for biogenic gas generation from terrestrial OM. Using evidence from Rock-Eval data and the results of this sensitivity analysis, we propose a degradation model for terrestrial OM where reactivity and degradation laws are calibrated to a real case study. This work allows us to quantify for the first-time natural microbial methane emissions in the Offshore Aquitaine by a basin modelling approach.

Modelling of geological processes is widely used in the geoscience community as it involves conceptualization and simplification of complex interactions between various interdependent processes such as those involved in the generation and migration of biogenic gas. Modelling can provide an important platform for interdisciplinary knowledge synthesis, with which the meaning and the role of multiple mechanisms and parameters can be analyzed and discussed (Arndt et al. 2013).

1.4.3 PhD thesis outline

The PhD thesis is organized as follows. In chapter 2, we describe the role and composition of the Organic Matter (OM) for biogenic gas generation. The main results concerning the transportation, accumulation and degradation of OM at large scale in the Mozambique Channel are presented in chapter 3 which consists of a manuscript currently in the submission process to Marine Geology. In chapter 4, we describe our workflow to quantify biogenic gas processes at the basin scale with a modelling approach. It includes the description of our OM reactivity model and our analysis of biogenic gas systems at the basin scale. An application of our workflow to the offshore Aquitaine is presented in chapter 5 which consists of a published paper in Marine and Petroleum Geology (2021). Issues of OM analysis and characterization encountered in this PhD thesis are discussed in chapter 6. Finally, chapters 7 and 8 give conclusions and perspectives of our work, including a discussion of paleo-fluid systems and paleo-pockmark hydrates with an application to the offshore Zambezi.

2. Natural sources of microbial gas

2.1 Biogenic source rock potential

Analytical geochemistry is oftentimes used to describe and map potential source rock distribution which are needed for hydrocarbon exploration. Source rock richness, type and maturity are key elements to identify the potential of a petroleum system in terms of oil and gas generation. Different depositional environments result in different source rock quality. Independently from OM origin, an efficient OM preservation is required to accumulate such potential source rocks. Peters (1994) categorizes a source rock based on its Total Organic Carbon (TOC) content as (1) poor ($\text{TOC}\% < 0.5\%$), (2) fair ($0.5 < \text{TOC}\% < 1$), (3) good ($1 < \text{TOC}\% < 2$), (4) very good ($2 < \text{TOC}\% < 4$), and (5) excellent ($\text{TOC}\% > 4$). This classification can be applied to active thermogenic systems that require an oil- or gas-prone source rock with TOC content values at least in the range of good or very good. Can this classification also be applied to biogenic gas systems?

Primary biogenic gas can be generated from very small amounts of TOC. There are examples of such activity all over the world. In the Great Australian Bight, analyses from ODP (Ocean Drilling Program) samples have shown that methanogenesis is affected by low TOC but not inhibited (Mitterer 2010). The author discusses how low organic carbon content ($< 0.4\%$) results in low-methane accumulations compared to high-gas sites where TOC content is in the range of 1%. This statement demonstrates that methanogenesis can occur even in sediments with low-TOC, less than 0.4%. Another example is the Woodlark Extensional Basin east of Papua New Guinea where methanogens are active in deep sediments with very low organic carbon content (less than 0.4%) (Wellsbury et al. 2002). The Pleistocene turbidite sequences of the Daini-Atsumi area, eastern Nankai Trough, Japan, show active biogenic systems in sediments with TOC less than 0.5% (Fujii et al. 2016). Another example of primary biogenic gas generated from very low amounts of continental OM ($0.32\% < \text{TOC}\% < 0.52\%$) is represented by the late Quaternary sediments in the modern Changjiang delta, eastern China (Zhang and Lin 2017). All these examples demonstrate that low-OM content in Cenozoic sediments can be effective for methanogenesis, even if in small amounts. When this dispersed OM is deposited at relatively high sedimentation rates and/or distributed over a large area in a basin, large amounts of methane can be generated if the conditions in the subsurface are compatible with an anaerobic microbial activity. This process is already described by Clayton

(1992) who states that 0.2% TOC can already generate amounts of biogenic gas as a function of the sedimentation rate and thermal gradient (Fig. 6). Therefore, important biogenic gas occurrences are observed in deltas where large amounts of sediment are deposited in a short time, containing low dispersed continental OM, *e.g.* in the Amazon Delta (TOC ~ 0.8%) (Arning et al. 2013) or in the Carupano Basin (TOC ~ 1%) (Schneider et al. 2012).

Note that TOC measured at present day corresponds to an OM that is already altered and degraded during transport at the seabed. This is due to a more refractory component of the initial OM where methanogens have already consumed the labile and thermo-labile fractions to produce methane. It is then necessary to reconstruct the original OM composition since these fractions are preferentially degraded (Cowie and Hedges, 1994; Ravin et al. 2013). Thus, not only the TOC but also the SOM type is critical for the gas generation potential of a biogenic source rock.

Biogenic gas is firstly generated from the decomposition of the most labile compounds of the SOM and subsequently, higher activation energies are required to decompose the thermo-labile compounds with increasing temperatures. Based on the H/C and O/C molar ratios (Tissot and Welte 1984 and reference therein), the SOM can be categorized into three main types. Type I and type II or IIS (*i.e.* rich in Sulphur) OM are defined by relatively high atomic H : C ratio and low atomic O : C ratio. In contrast, type III OM is characterized by low H/C and high O/C. These differences in molar ratio are related to variable initial OM input (*e.g.* aquatic plants and/or phytoplankton *vs* terrestrial plants) with variable labile and thermo-labile fractions. For instance, type II OM is composed of 30-40% labile and 8-15% thermo-labile fractions (Burdige 2007, 2011). Various analytical procedures (*e.g.* Rock-Eval, Elemental Analysis, Solid-state ¹³C NMR, Fourier Transform Infrared Spectroscopy) have been applied to determine the initial composition of organic-rich sediments that were sampled in the offshore Namibia as part of the Ocean Drilling Program and which have been characterized as type II OM (Ravin et al. 2013). In this study, the authors quantify the atomic ratios (C, H, O, N, S and Fe) and the distribution of carbon among the various functional groups which allows them to determine the respective labile/thermolabile and refractory portions of the initial OM (Ravin et al. 2013; Hatcher et al. 2014). In contrast, there are no such reference cases or studies applied to a type III OM or mixed Type II/III to our knowledge. Type III OM is more resistant to degradation than type II OM, especially at low temperatures, since it is characterized by higher amount of plant debris and is general also composed of reworked material already oxidized due to transport conditions

(Kamga 2016). Further analytical analyses are necessary to characterize the labile/thermo-labile character of a type III OM since this is also the most likely OM feeding biogenic gas systems as they are usually found in depositional environments with high terrigenous input.

A new concept of a biogenic source rock is required since microbial activity is already active at low temperatures (no catagenesis is required to generate dry gas) in sediments with dispersed-OM (the OM does not have to be concentrated in TOC-rich horizons). In this PhD thesis, we studied the evolution of the OM from transport to deposition at large scale and we propose a new geochemical description of dispersed type III OM in Cenozoic sediments. However, the analytical procedure encountered several issues which did not enable us to molecularly characterize the initial OM and to determine the degradation rate of the initial repartition in labile and thermo-labile fractions (chapter 7). More advanced analytical procedures are required to address this point. In the following chapters, we discuss the main processes of OM production, composition and preservation in recent sediments and their impact on biogenic gas generation.

2.2 Organic matter production

The nature and production of the OM is quite different between marine and continental ecosystems. The marine environment is characterized by primary organic carbon producers in the hydrosphere which are represented by phytoplankton responsible for over the 90% of the total OM supply (Tissot and Welte 1984; Romankevich et al. 2009). It results in large accumulations of OM that are observed along continental shelf where different factors control the organic activity such as, among others, *sunlight* (water depth < 200 m), *nutrient supply* (e.g. large river input or freshwater circulation), *salinity*, and *temperature*. Hence it is possible to recognize various spatial organic productivity trends:

- (1) decreasing from coastal/marine shelf to deep ocean;
- (2) decreasing from humid and equatorial to polar latitudes (Romankevich 1984).

In contrast, OM supply in continental ecosystems is dominated by land plants and freshwater algae and requires an equilibrium between transport and accumulation rates of dead continental plants. An equilibrium between subsidence rate and anoxic conditions is required to prevent bacterial decay. Note that primary productivity is one of the factors controlling the accumulation of marine OM in buried sediments. However, the critical factors to develop a source rock layer are deposition and preservation conditions (Allen and Allen 2013).

It is important to underline that carbon production and OM degradation are not constant in time (Arthur et al. 1985) or space (Blair and Aller 2012). Different factors have to be considered to explain their spatial and temporal variability (Arndt et al. 2013). These factors can be divided into those that have a direct impact on the OM degradation efficiency, such as the OM composition (Westrich and Berner 1984; Hedges et al. 1988), availability of electron acceptors (Emerson et al. 1985), microbial community composition, physical protection in the mineral matrix (Keil et al. 1994); and those that have an indirect effect, such as the sedimentation rate (Muller and Suess 1979; Calvert and Pedersen 1992). Moreover, few data are available about the factors controlling the variation of OM degradability during burial (Arndt et al. 2013). We know that some OM compounds are preferentially degraded compared to others resulting in a decrease of OM bulk reactivity with depth and time (Cowie and Hedges, 1994; Middelburg, 1989).

2.3 Organic matter composition

The OM in marine sediment is derived from marine and continental sources. The end-members of these two groups are respectively phytoplankton debris and terrestrial plant (Burdige 2007). Despite the differences in the OM initial composition and the processes of fractionation and degradation, the OM is composed by (Allen and Allen 2013 and references therein):

- Carbohydrates: main source of energy as sugar, cellulose (supporting tissue of terrestrial plants) and chitin.
- Proteins: derived from amino acids that characterize most of the OM in shells and substances as hair or nails.
- Lipids: animal fats, vegetables oils and waxes which are insoluble in the water column (*e.g.* cutin).
- Lignin: substance providing strength to plant tissue (common in higher plants)

Living organisms present variable percentages of these organic compounds which result in a variable reactivity to oxygen exposure or bacterial decay. Generally, it is accepted that some bio-molecules are particularly sensitive to biodegradation (*e.g.* proteins, nucleic acids) because they present weak molecular bonds and they represent nutrients for microbes, compared with other bio macromolecules (*e.g.* algae, cutan) that are characterized by aliphatic

fractions and non-reactive bonds (Tegelaar et al. 1989). Between the two endmembers there are relatively labile compounds (*e.g.* carbohydrates, cellulose ...) (Fig. 16).

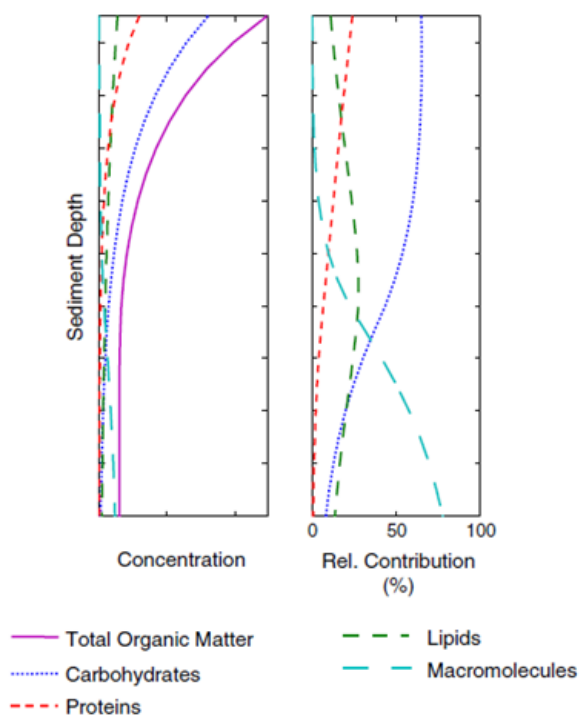


Figure 16. Evolution of the OM and different OM compounds with depth (Arndt et al. 2013). The OM degradability evolves in accordance with the degradability of its different components. The depth profiles of the relative contributions of each compound shows a dominance of the refractory compounds at depth.

Burdige (2007) identified two end-member sources, marine OM and vascular plant material, considering the whole OM (100%). Marine OM can be characterized by 20-40% of carbohydrates, 50-60% of amino acids and 5-30% of lipids; vascular plant material contains 1-2% of carbohydrates, ~70% of amino acids, ~30% of lignin and ~1-2% lipids. The biochemical composition of soils and marine coastal sediments is also presented in Hedges and Oades (1997 and references therein). The authors estimate an average composition of 10-20% of carbohydrates, 10% of amino acids and 15% of lipids (mainly fatty acids) for soils and 5-10% of carbohydrates, 10-15% of amino acids, 3-5% lignin (Cowie and Hedges 1992) and 5% lipid (Tissot and Welte 1984) for marine coastal sediments. The remaining fraction is composed mainly of Uncharacterized Organic Matter (UOM) (Burdige 2007) which are molecular complexes that are more resistant to biological degradation.

The different composition of terrestrial- and marine-derived OM results in different reactivity to degradation during sediment burial. Terrestrial OM is mainly composed of higher plants characterized by lower hydrogenated and higher oxygenated functional groups than

marine OM (Burdige 2011; Kamga 2016). Degradation tends towards an increasingly refractory nature in its molecular composition and in association with the mineral matrix. As a result, terrestrial-derived OM is less reactive and more thermally resistant than marine organic matter, especially at low temperatures (Cowie et al. 1992; Burdige 2007, Kamga 2016).

2.4 Preservation and burial of organic matter in marine settings

The preservation of the OM in marine sediments is a complex task and the main controlling factors, among others, are (1) the initial organic carbon flux through the water column and bulk sedimentation rate, (2) the chemical and physical properties of the OM itself (which are different depending on OM origin), and (3) the OM alteration during diagenesis (*e.g.* polycondensation, sulfurization or its incorporation on mineral surfaces that are particularly effective on clay) (Müller and Suess 1979; Suess 1980; Schulz and Zabel 2006). Therefore, the degradability or preservation of the OM is not only an intrinsic property of the OM itself, but it is the result of the interaction between the OM and its depositional environment (Mayer 1995) which is linked to the quality of the OM. One of the main factors impacting the preservation of the OM during transport is the residence time of the OM in the water column as a function of the oxygen conditions of the water. Studies on particles sampled in the water column have demonstrated that the OM flux decreases with depth (Suess 1980), therefore preservation is favorable when large OM particles are deposited in shallow depth environments. The sediment grain size has also a major control on OM preservation. Fine-grained sediments have low permeabilities and therefore are less oxygenated and oxidants are slow to diffuse from water into sediments. Coarse-grained sediments are characteristic of high-energy environments that are likely to be well oxygenated (Allen and Allen 2013). Another factor is the sedimentation rate as the OM can be diluted and protected in the sediments (Burdige 2007). High sedimentation rates favor OM preservation but if the OM is too diluted, potential source layers have a low organic carbon content and are incapable of generating and expel HCs at greater depth. However, such poor-organic carbon layers represent the main source for anaerobic bacteria and methane production during the first phase of burial.

Once the OM is deposited, it is subject to chemical transformation which is controlled by biological activity, as well as temperature and pressure conditions of the sedimentary basin (Tissot and Welte 1984). The interaction between the mineral matrix and the organic compounds occurs at different stages of burial and is strongly correlated with the original

composition and abundance of the OM itself. The evolution of the OM with depth from deposition to the metamorphic stage is summarized in Figure 17. During burial, the main stages of the OM evolution are diagenesis, catagenesis and metagenesis, and at the end the remaining organic carbon is subject to metamorphism (*e.g.* graphite).

Diagenesis is the first stage affecting the SOM. The system tends to equilibrium during the early stage of burial when sediments become increasingly consolidated at low temperature and pressure conditions. This stage may affect sediments in the first several kilometers of depth (Tissot and Welte 1984). During low T-P conditions, the chemical transformations of the OM are mainly the result of bacterial activity. Part of the initial terrestrial-OM is associated with mineral, adsorbed and free OM fragments. If the most refractory part of the initial OM composition is unreactive at this stage (Fig. 17), these free OM fragments contain labile and labilizable fractions which are remobilized when temperature increases, and exposed to bacterial decay. Firstly, the most labile fractions of the SOM (such as amino acids and carbohydrates) are degraded leading to the generation of biogenic methane (Kamga 2016) which represents the most important hydrocarbon formed during this stage (Fig. 17). Although diagenesis represents the key to biogenic gas generation, little information is available in the literature concerning the reactivity of the SOM during this stage.

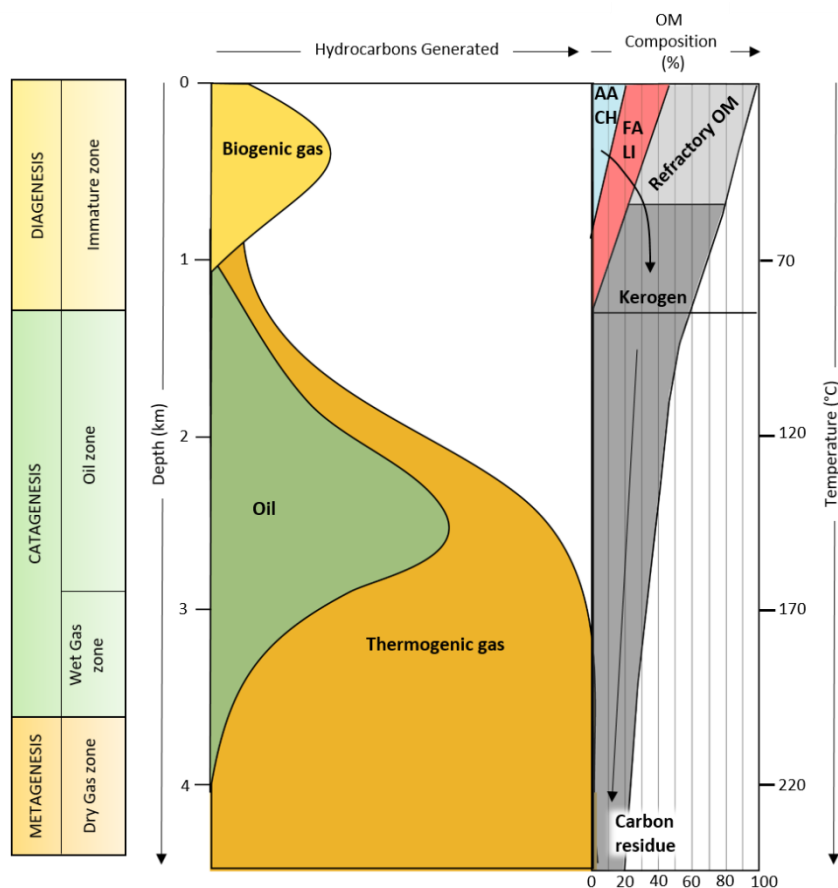


Figure 17. General scheme of the main stages of the evolution of the OM and the relative hydrocarbon generated (modified after Tissot and Welte 1984). The composition of the fresh OM is based on published data for general coastal sediments (Tissot and Welte 1984; Cowie and Hedges 1992; Hedges and Oades 1997; Burdige 2007). AA – Amino Acids; CH – Carbohydrates; FA – Fatty Acids (Lipids); LI - Lignin.

Therefore, with increasing burial, the OM tends towards a more refractory nature forming new poly-condensed structures (“geopolymers”) before being transformed into *kerogen*. Once sediments are buried deep enough, they undergo *catagenesis* which implies a strong increase of temperature and pressure (> 150 °C and 1000 bar respectively) (Tissot and Welte 1984). Sediments become fully compacted, and the cracking of the kerogen results in oil and subsequently in gas formation. The last stage of the OM evolution is the metagenesis. In the framework of this PhD thesis, we are mainly interested in the transformation of the OM during diagenesis, resulting in biogenic methane production.

3. A case study from the Mozambique Basin (manuscript in submission process)

The following chapter is a major synthesis of the first part of this PhD thesis and concerns the large-scale evolution of organic matter from its origin to deposition in the Mozambique Channel. **It is a manuscript that is still in the submission process which will be subjected to changes and revisions.**

The main purpose of this study is the characterization of the OM and its degradation-preservation process in recent sediments, from shallow water to deep-water turbidite systems. We performed a general Rock-Eval survey with a dual approach, analyzing the organic matter in the settling particles within the water column and in the shallow sediments. A complementary study using EDS-SEM analysis has been conducted to analyze the impact of the mineralogical composition and the lithofacies of the sediments on the preservation of the organic matter. Finally, we analyzed the evolution of the deposited organic matter in a regional context, comparing sediment accumulation rates and oxygen exposure times in the main physiographic provinces of the Mozambique Channel. Our results indicate that the organic matter is transported by turbidite and/or contour currents and deposited in the turbidite system of the deep-water area of the Mozambique Basin, preserving relatively poorly oxidized organic matter. However, in the sediments near the water-sediment interface, the OM is largely oxidized. We propose a scenario in which the combined effects of lower sedimentation rate, higher porosity of the sand-rich material and the activity of important marine currents are responsible for the remobilization of the OM particles at the sea bottom, leading to oxic conditions and higher oxygen exposure time in the uppermost centimeters of the sediments.

Organic matter distribution in modern sediments of the Mozambique Channel: Evidence for widespread oxidation processes in the deep-water domains

To be submitted to Marine Geology

Martina Torelli¹, Anne Battani¹, Daniel Pillot¹, Eric Kohler¹, Joel Lopes De Azevedo¹, Isabelle Kowalewski¹, Lucie Pastor², Christophe Brandily², Sabine Schmidt³, Gwenael Jouet⁴, Eric Deville¹

1 IFP Energies Nouvelles, 1-4 Av. de Bois-Préau, 92852 Rueil-Malmaison Cedex, France

2 IFREMER, Centre de Bretagne, REM/EEP, Laboratoire Environnement Profond, F-29280 Plouzané, France

3 UMR5805 EPOC, CNRS, OASU, Université de Bordeaux, 33615 Pessac, France

4 IFREMER, Centre de Bretagne, REM/GM, Laboratoire Cycles Géochimiques et ressources, F-29280 Plouzané, France

ABSTRACT

The Mozambique channel is fed by several sourcing rivers issued from the African continent and from Madagascar and therefore represents a favorable area to study the evolution of the detrital organic matter (OM) in deep-water depositional systems. The OM collected from Quaternary sediments shows heterogeneities in terms of quality and quantity. Rock-Eval analysis on long piston core samples collected to a maximum depth between 12 to 33 m, revealed that the Majunga (Madagascar NW margin) and the Zambezi (Mozambique margin) continental slopes contain the highest Total Organic Carbon (TOC) fractions (between 1 and 2%). Results from Scanning Electron Microscopy analysis reveal a different composition of the mineral matrix between the two depositional systems. Sediments from the offshore Zambezi River present a mineral matrix which includes iron oxides typical of higher oxic conditions compared with the Majunga margin. Away from the margin areas, within the deep-water areas of the Mozambique Basin, the analysis of samples collected with particle traps at 47 m above the seabed, has shown that the OM is transported by shallow and deep (turbidite and/or contour) currents and deposited while preserving relatively good TOC between 1.5 and 3%. However, the sedimentary OM is largely oxidized close to the water-sediment interface (Oxygen Index > 300 mg CO₂/g TOC). Only a small amount of TOC (< 0.5%) is preserved within the recent sediments of the distal area of the Zambezi turbidite system at water depths below 2500 m. Interface sediments sampled to a maximum depth of 40 cm, show intermediate TOC values between those collected in the particle traps and those from long piston cores suggesting that the degradation of the OM is mainly active at the water-sediment interface. This OM oxidation and degradation process in the deep-water domains of the Mozambique Basin is probably due to the conjugate effects of low sediment accumulation rate (SAR) and high permeability of the coarse-grained sediments but also to important bottom currents that promote the remobilization and the rearrangement of fine grained sediments.

Key words: organic matter, transport, preservation, oxidation, Mozambique Channel, Rock-Eval, Scanning Electron Microscopy

INTRODUCTION

The organic carbon (OC) available in continental settings is a product of the breakdown of biomolecules such as cellulose, lignin, polysaccharides, carbohydrates, proteins and lipids

(Wang et al., 1998; Wakeham et al., 1997). In terrestrial environments, the major organic matter (OM) sources are higher plants while animal biomass and plankton are negligible. The continental organic carbon is transported mainly by rivers to the ocean with a mean flux which has been estimated to about 0.4×10^{15} g C/year (Hedges et al., 1997). More than 80% of OM particles are buried on continental and insular margins (Hedges and Keil, 1995), however the fate of the OC reaching the oceans remains a questionable matter. The burial of continental organic carbon in marine sediments is a sink for CO₂ possibly greater than the one resulting of the alteration of silicates (Galy et al., 2015). A good understanding of its evolution is key for a quantification of the processes linked to the carbon cycle and global warming processes.

Most of the sedimentary OM is rapidly re-mineralized once it reaches the continental margins but a part of it can be preserved and reaches the deep-water domains. The main conditions controlling the OM sedimentation and preservation processes are the primary productivity (Pedersen and Calvert, 1990) and the combination of several factors such as distance to the coast, water depth, oxygen condition in the water column and in the first centimeters of the sediments, as well as the sediment accumulation rate (SAR) which controls the dilution of the OM in the sediments (Burdige, 2007). Studies on particles sampled in the water column have shown that the OM flux provided by marine phytoplankton decreases significantly with depth (Suess, 1980). Thus, conventional hypotheses concerning the OM preservation did not consider scenarios with large accumulations of organic matter in deep-water areas. However, deep depositional environments can be characterized by important OM accumulations, as shown by Stow et al. (2001) in the Makassar Strait (Indonesia). The OM associated to the continental sediments transported through the Mahakam Delta Province and deposited during the Last Glacial Maximum presents relatively high TOC values (around 5%). Another example of such depositional environment is the Congo system in which the OM is transported 760 km offshore through the canyon until the distal fan (Vangriesheim et al., 2009). The characterization of the OM transported in the channel and the distal lobe of the Congo system highlighted that the deposited OM is mainly composed of a type III kerogen (70-80%) (Baudin et al., 2010; Baudin et al., 2017). Within the distal lobes, the TOC values range between 3.5% and 4%, due to an efficient OM preservation process. The high sedimentation rate of the Congo system favored the preservation and thus the accumulation of important amount of OM in the deep-water environment. Active upwelling zones are also favorable places for OM accumulations of planktonic origin (Henrichs and Farrington, 1984; Pelegrí et al., 2005; Ahuva et al., 1993; Nieto-Cid et al., 2006). In these areas, the TOC content reaches up to 25% within the shelf,

close to the hydrodynamic cells that feed the upwelling zone, and 3% in the deep-sea areas composed mainly of pelagic sediments at several thousand m of water depth. In this case, the OM is mainly transported from the shelf by turbidity currents which lead to the re-deposition of OM-rich levels in deep-water domains (Stow et al., 2001).

The study presented in this paper provides a global screening of the distribution of the OM at a wide scale in the Mozambique Channel. The purpose of this work is to characterize the OM in recent sediments and its degradation-preservation process during deposition, from shallow to deep-water turbidite systems (between 500 and 4400 m of water depth). The study is mainly based on a general Rock-Eval survey with a dual approach by analyzing the OM content in the settling particles within the water column before deposition and in the recent sediments. A complementary study using EDS-SEM analysis has been conducted to explore the nature of the mineralogical composition and the lithofacies of the sediments which has an important impact on the OM preservation. Finally, the evolution of the deposited OM is compared between the main physiographic provinces of the Mozambique Channel regarding their sediment accumulation rates and oxygen exposure times.

GEOLOGICAL FRAMEWORK

The Mozambique channel corresponds to a wide straight between Africa and Madagascar (Fig. 1). It was formed progressively, during more than 140 Ma, since the breakup of Gondwana (Rabinowitz et al., 1983) and the formation of the oceanic lithosphere of the Mozambique Basin during Jurassic-Cretaceous times (Mueller and Jokat, 2019; Thompson et al., 2019). The central part of the Mozambique Channel is still tectonically active today in the southern prolongation of the eastern branch of East African Rift System, and this tectonic activity has controlled the development of volcanic systems and related seamounts emerging locally in Europa and Bassas da India (Deville et al., 2018). These active tectonics is associated with a zone of uplift which has influenced the sedimentary pattern, notably the Zambezi turbidite system (Fierens et al., 2019). The continental margins of the Mozambique Channel are mostly steep transform or transtensive margins. The Mozambique Basin is largely invaded by the turbidite system issued from the Zambezi River, the main river along the east African coast, and partly by turbidite flows issued from Madagascar, mainly focused in the Tsiribihina submarine valley which is sourced mainly by the Tsiribihina and Mangoki Rivers (Fierens et al., 2019; Fig. 1). The Betsiboka and Mahavavy Rivers, in the north-western part of Madagascar, are responsible for large sedimentary accumulations on the continental shelf (Berthois and Crosnier, 1966; Wiles

et al., 2009; Pastor et al., 2020; Fig. 1). These rivers coming either from Africa or Madagascar are providing large detrital OM input toward the Mozambique Channel. In the Mozambique Basin, strong bottom currents have been described even in the very deep-water areas (Miramontes et al., 2019). These bottom currents are responsible for the development of eddies which partly block the Mozambique undercurrents, enhancing southward flow along the Zambezi Channel. Measured bottom currents in the Zambezi and Tsiribihina submarine valleys reach more than 50 cm.s^{-1} , and these strong bottom currents are responsible for high erosion processes along the Zambezi deep sea valley (Miramontes et al., 2019).

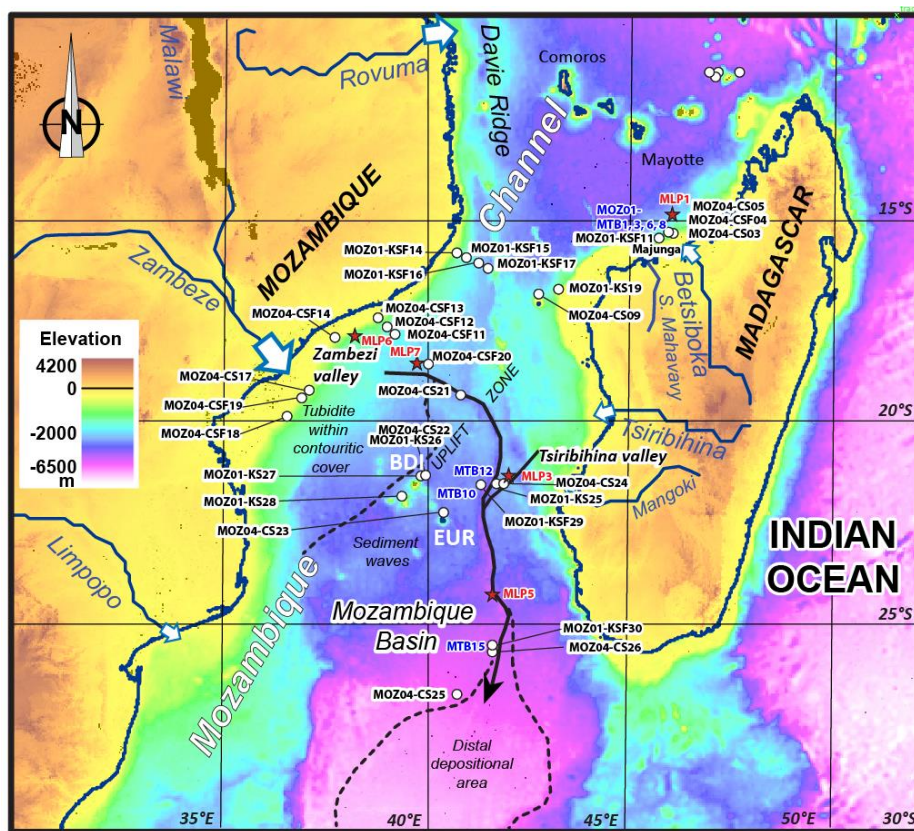


Fig. 1. Location map of the samples collected in the Mozambique Channel. The geological context presented in this figure is issued from Fierens et al. (2019). BDI: Bassas da India Island. EUR: Europa Island.

MATERIAL AND METHODS

This study was conducted in the framework of the PAMELA (PASSIVE Margin Exploration Laboratory) research project (Bourillet et al., 2013). Samples were collected during several oceanographic exploration surveys in the Mozambique Channel, Pamela-Moz01 (Olu, 2014), Pamela-Moz04 (Jouet and Deville, 2015) and Pamela-Moz08 (Khripounoff, 2016) with the objective to better understand the evolution of the OM in the Quaternary sediments along the

Eastern Margin of Africa (Fig. 1). Samples were collected along the continental slope and distal part of the Zambezi and Tsiribihina turbidite systems, as well as along the continental slope off the Betsiboka and South-Mahavavy Rivers (the largest rivers NW of Madagascar Island; Fig. 1). Geochemical analyses on the sedimentary OM have been performed with Rock-Eval 6 (RE6). On selected cores, Total Carbon (TC) contents (%) obtained with Rock-Eval method have been compared with TC contents obtained by LECO elemental analyzer (Fig. 2A). Also, calcite contents (%) obtained with Rock-Eval (Pillot et al., 2015) have been compared with XRF (X-Ray Fluorescence) results with a scanner XRF Avaatech (Fig. 2B). In addition, Rock-Eval TC results on all the core samples collected have been cross-checked with results obtained by elemental analyses (Fig. 2C).

394 RE6 analyses were performed on samples collected (1) with the Küllenberg corer (KS or KSF, recovered core length up to 12 m) of the R/V *Atalante* (Pamela-Moz01 survey) and the Calypso corer (CS or CSF, recovered core length up to 33 m) of the R/V *Pourquoi Pas?* (Pamela-Moz04 survey), 11 RE6 analyses on samples collected (2) with an interface multicorer (MTB, 30-40 cm maximum penetration), and 101 analyses on samples collected with (3) sediment traps in moorings located 47 m above seabed (sampling systems with gravity/piston cores, interface cores and sediment traps are described in Supplementary Material; Fig. S1, Appendix A). Furthermore, selected samples have been characterized by Energy Dispersive X-Ray Spectroscopy – Scanning Electron Microscopy (EDS-SEM) to discuss the role of the mineral matrix and of the oxidizing/reducing conditions controlling the OM preservation. Finally, sedimentary accumulation rates (SARs) and O₂ micro-profiles were determined on interface cores (MTBs) in the first centimeters of sediments.

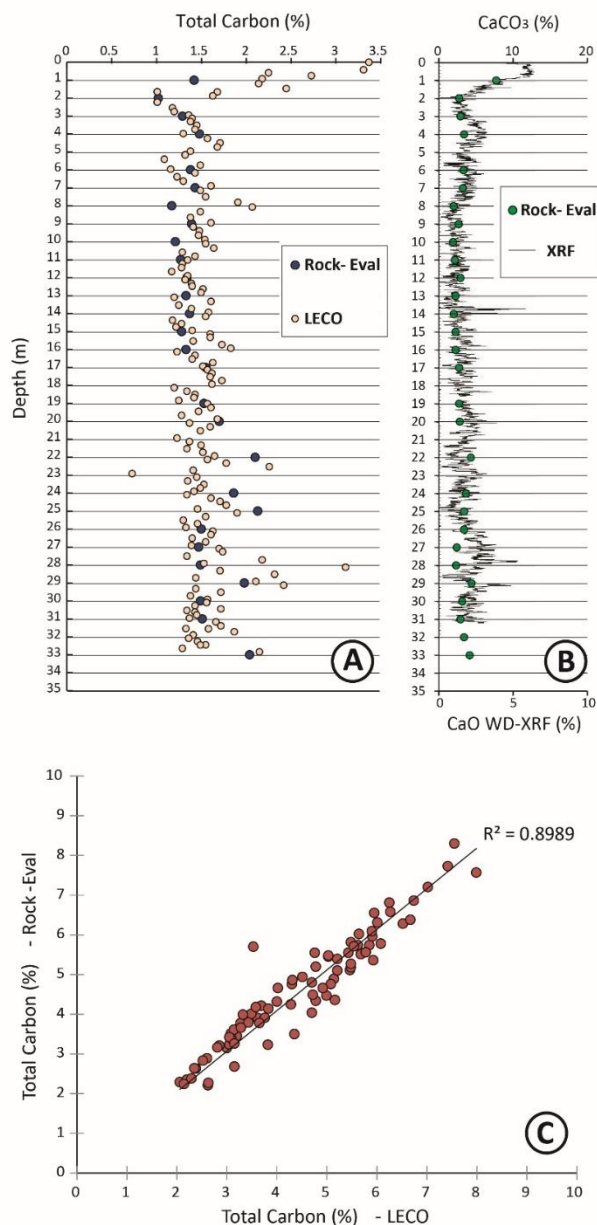


Fig. 2. (A) Comparison of the Total Carbon content (%) obtained by Rock-Eval and LECO elemental analyzer in core Pamela-MOZ04-CS17 in the Zambezi. (B) Comparison of calcite content (%) obtained by Rock-Eval method (Pillot et al., 2015) and Ca content deduced from XRF analysis (also core Pamela-MOZ04-CS17). (C) Cross-plot between Total Carbon contents determined by Rock-Eval and LECO elemental analyzer.

Rock-Eval

Rock-Eval pyrolysis is a classic standard method for the study of organic-rich rocks originally developed for petroleum purposes which provides a rapid determination of the content, type and maturity of organic matter (Espitalié et al., 1977, 1984; Lafargue et al., 1998; Behar et al.,

2001), as well as the type and amount of carbonates within sedimentary rocks (Pillot et al., 2014). The analysis can be performed either on the bulk rock (Espitalie et al., 1977) or on concentrated organic matter samples (Behar et al., 2001). The principles of Rock-Eval 6 analysis (Lafargue et al., 1998) consists of calculating the petroleum potential of sedimentary rocks through pyrolysis during which samples are heated in a pyrolysis furnace under inert gas, and then in a combustion furnace using air. The hydrocarbons liberated during the progressive heating are measured by means of a FID detector (Flame Ionization Detector) and form the peak S1 representing the free thermo-vaporized hydrocarbons, and the peak S2 corresponding to the liquid effluents released during cracking of organic matter. The residual rock is then subjected to a progressive combustion (oxidation under air). CO and CO₂ released during pyrolysis and combustion are measured continuously using Infra-Red cells. The peak S3 corresponds to the CO₂ content released during pyrolysis of the insoluble organic matter (kerogen). These measurements enable determining the mineral carbon (MINC) and the TOC of the analyzed samples. The amount of rock required for the analyses ranges from 50 to 70 mg of bulk rocks. In this study, we applied a method classically used at IFPEN adapted for recent sediments (Deroo et al., 1983; Deville et al., 2015) applying a lower heating program than the one used for the more classical study of consolidated sediments with an initial plateau at 200°C (procedure adapted for immature sediments), instead of 300°C for the classical procedure. In addition, since the analyzed samples correspond to poorly compacted sediments rich in seawater, they were firstly rinsed with fresh water, centrifuged and then dried before analysis. This was done to overcome the problem related to the presence of sodium chloride which can generate HCl inducing an early destabilization of carbonate during pyrolysis and subsequent damage the analyzing device. A similar method has also been used by Baudin et al. (2017).

EDS-SEM analysis

Results on two unconsolidated samples are presented in this paper, the first one was collected along the Zambezi continental slope at 78 cm bsf from the top of core MOZ04-CS17 (602 m of water depth), and the other one in the Majunga continental slope at 54 cm bsf from the top of the core MOZ01-KSF12 (735 m of water depth). EDS-SEM techniques are used to determine the microscopic structures of minerals and organic matter assemblages producing a surface map of the chemical composition of the sample. This latter is afterwards converted into a mineralogical map of the total matrix. The samples selected for this analysis were not consolidated and characterized by very low permeability. In order to remove all the water, they

were first dried 1 week at 60°C and after frozen at -80°C and then lyophilized. Lyophilization is a process that removes the water from low permeability material with limited damage to the micro-structure of the sample. Because of their low permeability, samples have been impregnated with a depressurization cup at -0.8 Bar to enable injection of the resin in the small sample pores. The impregnated samples were then sawed and polished for the SEM analyses. The microscopic observations were performed with a “high vacuum” conventional SEM (EVO MA10, Zeiss SMT) in IFPEN laboratories. A motorized five axis stage provided a first visualization of the samples. The electron microscope is characterized by a tungsten filament at 15 kV and 100 mA and a probe current at 700 to 750 pA for EDS analysis (mineral identification). It is also used with a probe current at 150 pA for secondary electron (SE) imaging at high spatial resolution to observe the surface topography, and with a back scattered electron detector (BSE) to obtain images with atomic number contrast. The calibration of the silicon drift detector of EDS is done on pure cobalt for quantitative analysis during 10 s at 10 to 15 kcps (kilo-counts per second), with a dead time of about 15%. In some cases, XRD is not enough to identify minerals. In this case, SEM micrography coupled with EDS analysis can be used to identify and define mineral phases through their chemical composition revelation. Chemical micro-analysis is standardized on various minerals with a well-known chemical composition and controlled by electron microprobe (Reference standards for X-ray microanalysis n° 7610 from Micro-Analysis Consultant Limited, UK).

Sediment accumulation rates

Sediment accumulation rates (SARs) are determined with different methods depending on the available samples. SARs were calculated from depth profiles of excess ^{210}Pb ($^{210}\text{Pb}_{\text{xs}}$; $T_{1/2} = 22.3$ years) of interface cores of Madagascar and Mozambique Margins: MOZ1-MTB6 (Fontanier et al., 2018), MOZ1-MTB3, MOZ4-MTB2 and MOZ4-MTB3 (Pastor et al., 2020) and MOZ4-MTB4 and MOZ4-5 (this work). Activities of ^{210}Pb and ^{226}Ra were determined on sediment samples by gamma spectrometry using a well-type, high-efficiency gamma detector “Canberra” (Schmidt and De Deckker, 2015). The detector was calibrated using IAEA reference material. Activities are expressed in mBq g^{-1} and errors are based on one standard deviation counting statistics. Excess ^{210}Pb was calculated by subtracting the activity supported by its parent isotope, ^{226}Ra from the total ^{210}Pb activity in the sediment. Sediment layers were measured downcore until reaching rather negligible excess values. Mean SARs were calculated from the profiles of $^{210}\text{Pb}_{\text{xs}}$ assuming constant flux and constant sedimentation (referred to as

the CF:CS model). SAR along the Zambezi deep sea valley has been deduced from one radiocarbon dating performed on foraminifera on the interface core MOZ1-MTB10 at 35 cm below seafloor. As these data were not available in the Tsiribihina valley, minimum SAR was estimated by converting the mean annual mass flux measured by a moored sediment trap placed 47 m above the sea floor over a period of 13 months (Miramontes et al., 2019) and assuming a density of 1.5 g cm^{-3} (average gamma density measured on piston cores).

O₂ microprofiling

The O₂ profiles were measured on interface cores kept in a refrigerated box to reproduce a temperature close to the *in-situ* conditions. For each station, the oxygen concentration in the bottom water was determined by the Winkler titration technique adapted by Aminot and K erouel (2004). The surface water was gently bubbled to avoid any stratification during the profiling. A microsensor multimeter (Unisense S/A, Denmark) with one to two Clark type oxygen probes Ox-50 (Revsbech, 1989) with a motor controller were used to record depth microprofiles inside the sediment with a 50 to 500 μm resolution depending on the oxygen penetration depth. A linear calibration was performed between the oxygen concentration measured in the overlying water and an oxygen free solution. Between 1 and 12 profiles were performed in each core. For each profile, the oxygen penetration depth (OPD) was estimated. Oxygen exposure times (OET) were calculated as the ratio between OPD and SAR (Hedges and Keil, 1995). They provide an estimate of the time duration during which accumulating uppermost sediments are exposed to molecular oxygen.

RESULTS

Rock-Eval analyses

Full results are attached in Supplementary Material in Table S1, Appendix B and RE6 analyses are presented as average values by piston core, interface core and mooring in Table 1. The location of the sampling sites is presented in Fig. 1 and detailed locations are indicated in Table 1. The TC (total carbon) contents obtained by Rock-Eval and LECO show a good correlation ($R^2 = 0.8989$; Fig. 2A,C). Also, there is a good fit between CaCO₃ contents determined with Rock-Eval method and Ca contents determined by XRF (Fig. 2B). Note that samples presented in Figure 2 were selected in the same levels but the analysed material is not exactly the same

which explains the moderate differences. Therefore, the validation of both (1) the Total Carbon measured by Rock-Eval method with LECO and (2) the Mineral Carbon with XRF, reflects that the TOC determined from Rock-Eval is reliable and calibrated for the analysed samples in this study.

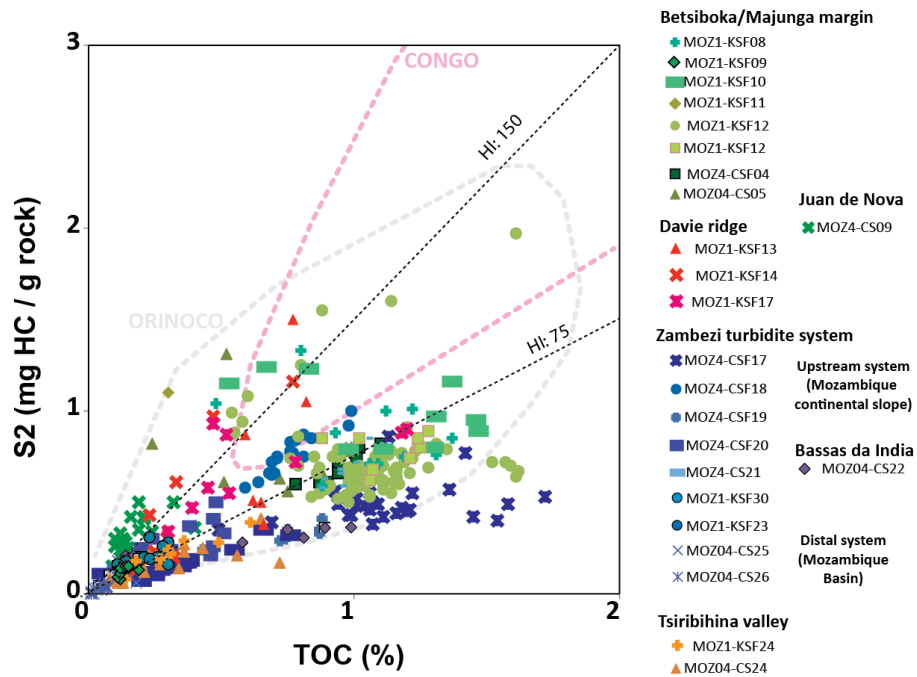


Fig 3. Rock-Eval results obtained on the sedimentary organic matter from the cores collected in the Mozambique channel (Comparison with Orinoco from Deville et al., 2015 and Congo from Baudin et al., 2017).

	latitude °S	longitude °E	Water depth m	Mean S2 mg HC/g rock	Mean S3 mg CO ₂ /g rock	Mean TOC %Wt	TOCmin %Wt	TOCmax %Wt	Mean Tmax °C	Mean HI mg HC/g TOC	Mean OI mg CO ₂ /g TOC	nb. Meas.
MOZ1-KSF8	15.36752	45.98712	528	0.88	4.72	1.06	0.8	1.37	410	79.9	441.2	12
MOZ1-KSF9	15.36143	45.95630	760	0.69	4.6	0.98	0.87	1.09	391	70.8	472.8	10
MOZ1-KSF10	15.51918	45.71581	773	1	3.99	1.29	0.83	1.47	409	80.9	348	10
MOZ1-KSF11	15.51590	45.71387	806	2.46	3.56	1.44	0.3	2.08	404	156	272	3
MOZ1-KSF12	15.36352	45.96047	735	0.75	4.73	1.06	0.87	1.62	399	71.6	464	96
MOZ1-KSF13	16.18514	41.40799	2618	1.02	5.58	0.79	0.29	1.94	402	120.3	771.7	8
MOZ1-KSF14	15.83619	40.74369	1552	0.53	3.94	0.36	0.15	0.77	395	151	709	7
MOZ1-KSF17	16.20568	41.44814	2730	0.69	3.39	0.66	0.3	1.2	417	102.2	437	9
MOZ1-KSF23	21.53033	41.34588	3206	0.2	3.43	0.21	0.11	0.28	357	64	554	12
MOZ1-KSF24	21.51834	41.86120	3084	0.22	2.78	0.31	0.13	0.61	381	64	554	9
MOZ1-KSF30	25.42679	41.59536	4076	0.12	2.28	0.13	0.11	0.19	364	78	501	9
MOZ4-CSF04	15.37050	45.95183	757	0.77	4.87	0.98	0.58	0.87	392	122	752	11
MOZ4-CS05	15.36513	45.93953	898	0.76	4.83	0.78	0.24	1.11	378	78	501	11
MOZ4-CS09	16.84670	42.75748	1909	0.43	3.17	0.2	0.1	0.44	398	45	314	26
MOZ4-CS17	19.21335	37.04798	602	0.5	3.46	1.13	0.49	1.72	344	45	314	28
MOZ4-CS18	19.84385	36.51310	410	0.76	3.43	0.76	0.7	0.99	379	100	451	18
MOZ4-CSF19	19.38998	36.87213	315	0.28	2.48	0.62	0.5	0.79	369	42	375	10
MOZ4-CSF20	18.44643	39.93160	2501	0.31	4.36	0.37	0.19	0.47	367	42	375	10
MOZ4-CS21	19.33855	40.77837	3036	0.17	1.49	0.34	0.2	0.76	366	46	424	21
MOZ4-CS22	21.27402	39.93130	3099	0.2	2.87	0.31	0.04	0.99	344	42	364	20
MOZ4-CS24	21.51845	41.86132	3089	0.16	2.6	0.25	0.05	0.56	364	42	361	30
MOZ4-CS25	26.62197	40.71247	4388	0.03	1.39	0.06	0.01	0.18	259	10	10	10
MOZ4-CS26	25.56643	41.61643	4130	0.05	1.42	0.06	0.01	0.15	339	10	10	14
MPL1	15.51933	45.71572	781	4.72	5.22	2.25	1.94	3.3	400	207	232	20
MPL3	21.52106	41.83437	3415	5.73	6.03	2.49	2.2	2.73	414	229	243	22
MPL5	23.97512	41.47293	4054	4.31	4.63	2.1	1.52	2.67	409	224	245	18
MPL7	18.6898	39.71093	2833	5.74	8.83	2.43	1.63	3.36	414	233	373	23
MPL8	22.22217	41.2715	3450	4.69	8.01	1.88	1.22	2.83	415	248	451	18
MOZ1_MTB6	15.51913	45.71551	789	1.78	4.03	1.24	1.05	1.43	386	141	311	2
MOZ1_MTB8	15.36358	45.96081	740	1.99	5.27	0.9	0.25	0.31	409	1	1	1
MOZ1_MTB10	21.53058	41.34562	3205	0.455	3.56	0.28	0.17	0.24	371	2	2	2
MOZ1_MTB12	21.51842	41.8613	3082	0.31	3.03	0.21	0.17	0.24	369	2	2	2
MOZ1_MTB15	25.42687	41.59557	4074	0.25	1.22	0.15	0.1	0.2	345	4	4	4

Table 1. Rock Eval results for the core samples collected in the Mozambique channel.

Recent sediments from piston cores in the Mozambique Channel collected at a maximum variable depth of 12 to 33 m, show moderate total OM contents (TOC < 1.8%), S₂ peaks < 2 mg HC/g of rock and T_{max} values characteristic of completely immature sediments (< 420°C) (Table 1). The higher OM content is observed in the northwestern part of Madagascar (Majunga margin), off the mouth of the Betsiboka and South-Mahavavy rivers, as well as in the Davie Ridge area and along the Zambezi continental slope (Fig. 3). All the samples also show a low Hydrogen Index (HI: S₂/TOC × 100 mg HC/g TOC) values around 300 mg HC/g TOC and a higher Oxygen Index (OI: S₃/TOC × 100 mg CO₂/g TOC) with a mean value of 300 mg CO₂/g TOC (Table 1). Note that HI and OI values were not taken into account in this study for TOC values < 0.5% because they were considered as not reliable. These results are characteristic of a continental OM composed mainly of higher plants (Type III kerogen; van Krevelen, 1950). However, a process of oxidation of marine organic matter (Type II kerogen) can also produce an increase of the OI associated with a decrease of the HI. In this case, the Rock-Eval HI and OI values appear as similar to a type III organic material even if the original OM is derived from marine organic materials (Type II OM). Considering an HI value of 400 mg HC/g TOC and 100 mg HC/g TOC for a type II and a type III kerogen respectively (Espitalie et al., 1985), it is possible that the OM analyzed from core samples is composed of a mixture of the two sources. This question arises especially for certain samples of the sector of Majunga and the Davie Ridge in the northern part of the Mozambique Channel (Fig. 3). Debris of higher plants is present in some samples (leaf and wood fragments easily recognizable especially in the Majunga slope area samples). The samples of the sector of Majunga and the Davie Ridge, which are relatively rich in OM, show two characteristic trends in terms of HI (Fig.3). The first trend shows HI values between 50 and 100 mg HC/g TOC with a mean value of 75 mg HC/g TOC. The second trend is characterized by a mean HI value of 150 mg HC/g TOC. Sediments from the Zambezi continental slope contain typical type III OM, with S₂ values around 1 mg HC/g rock and a TOC content of up to 1.8%. Sediments collected from the Zambezi turbidite system (upstream and distal systems) are characterized by low S₂ below 0.5 mg HC/g rock and TOC lower than 0.8% (Fig.3). Sediments from Tsiribihina turbidite system (issued from Madagascar) show even lower TOC values between 0.13 and 0.61%. Finally, samples collected in the distal area of the Mozambique basin show the lowest S₂ (< 0.3 mg HC/g rock) and TOC values (< 0.2%; Fig.3). As such, a strong OM decrease is observed from the Zambezi continental slope to the distal valley of the Zambezi turbidite system (Fig. 4).

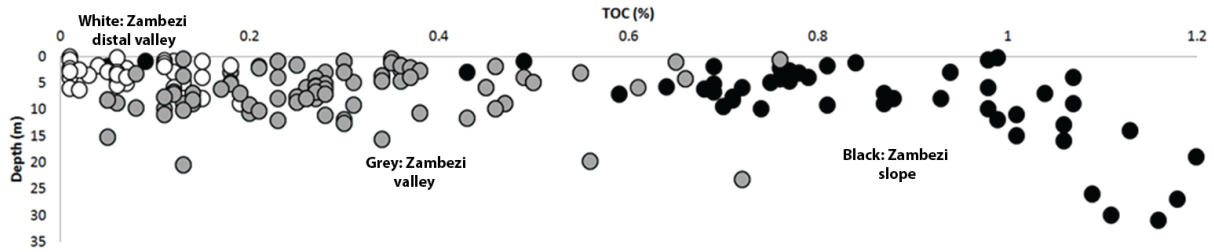


Fig 4. TOC (%) diagram variations (RE6 analyses) *versus* depth (m) in the sediment for the cores sampled in the Zambezi turbidite system. Note the strong TOC decrease towards the terminal distal channel.

Results obtained on interface core samples at a maximum depth of 30 – 40 cm (MTB) show much higher values in terms of TOC (1 to 3.5%), S2 (2.5 to 10 mg HC/g rock), and HI (180 to 320 mg HC/ g TOC), while OI are lower than 300 mg CO₂/g TOC in the Majunga area, in the Tsiribihina channel area and in the distal channel of the Zambezi turbidite system. OI values are higher than 300 and up to 600 mg CO₂/g TOC along the Zambezi slope (Table 1 and Supplementary material, Table S1, Appendix B). From a general point of view, relatively high T_{max} for completely immature OM can be regarded as a record of an advanced state of OM degradation of humic substances (Hare et al., 2014). According to RE6 results during the oxidation phase and following the method of Pillot et al. (2015), the mineral carbon is present in all the samples mainly in the form of calcium carbonate. Fig. 5 and Fig. 6 compare the content of organic carbon (TOC %) and mineral carbon (MINC %) in the analyzed core samples as a function of depth. Depending on the core location, the organic matter evolution is either correlated (CS17, CS21, CS25, CS26) or anti-correlated (CS22; Fig. 6) with the mineral carbon content. In the latter case, the dilution of the MO is related to contributions of carbonate turbidites issued from Bassas da India Island (Fig. 1).

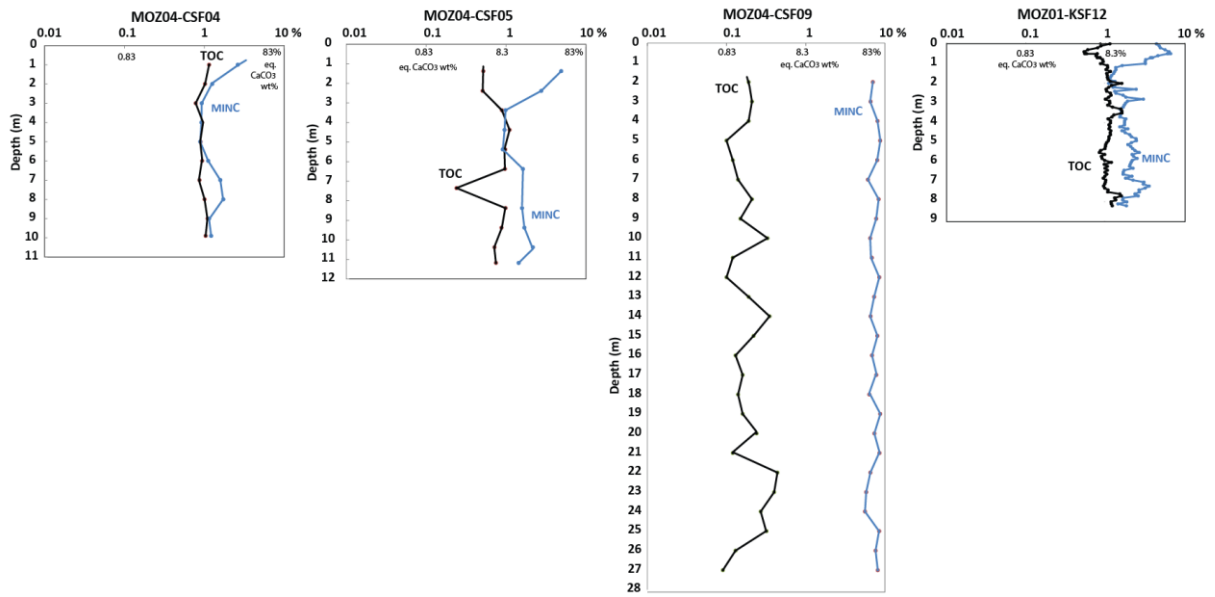
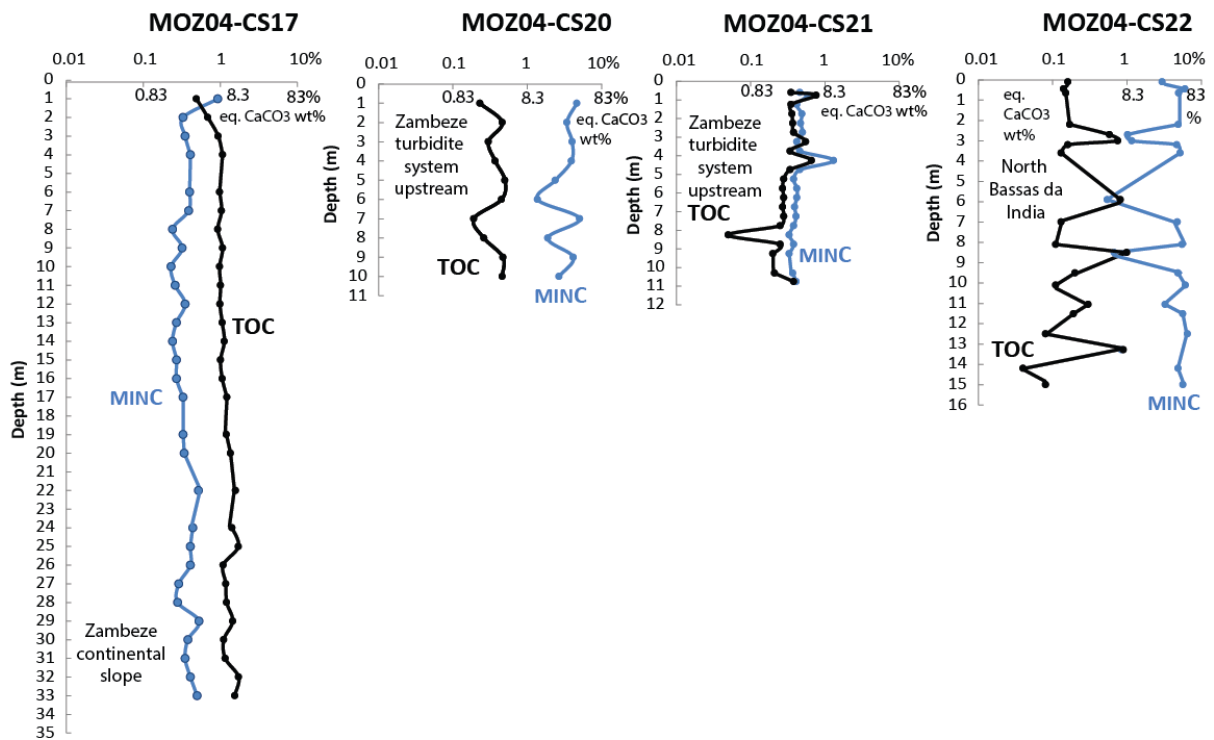


Fig. 5. TOC and $_{MINC}$ profiles *versus* depth from core samples in the Majunga margin.



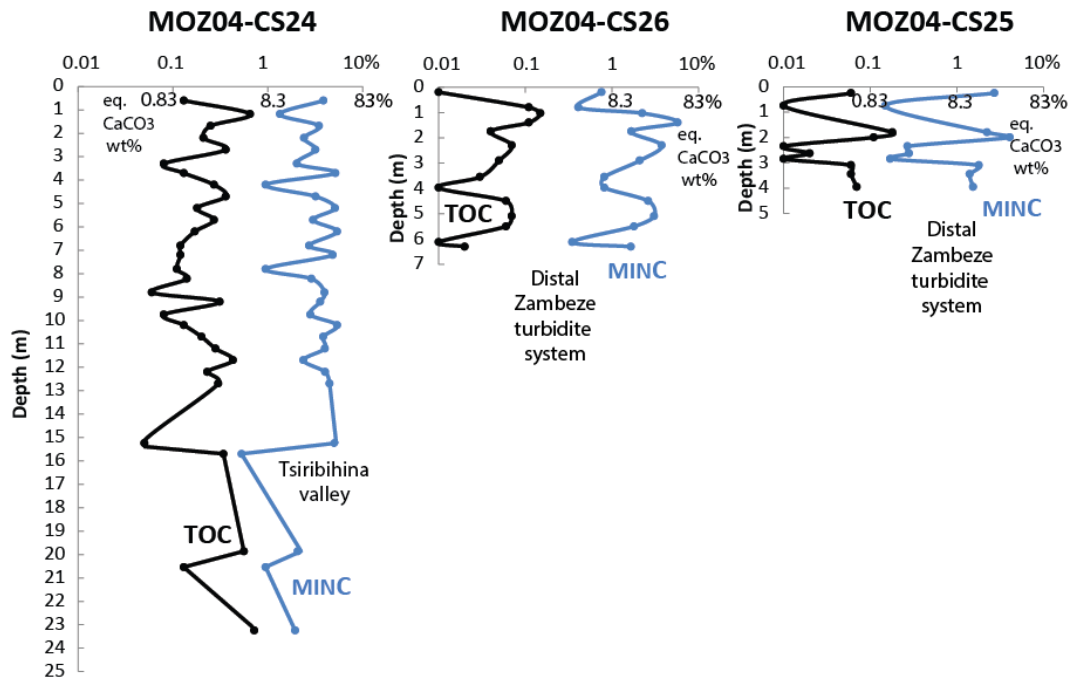


Fig. 6. TOC and $_{\text{MINC}}$ profiles *versus* depth along the Zambezi turbidite system (Mozambique continental slope and deep basin).

The particles collected by moored sediment traps before deposition (at 47 m above the seabed) are richer in OM compared to the core samples. They show TOC values between 1.5% and 3.5%, S₂ peaks between 2.3 and 10 mg HC/g of rock, with HI between 180 and 300 mg HC/g TOC and OI between 150 and 300 mg CO₂/g TOC (Fig. 7a). These values are characteristic of a predominantly continental organic material (*i.e.* Type III kerogen which is less oxidized than the kerogen collected from cores). These results demonstrate that continental-derived OM is transiting along continental slopes while preserving relatively good TOC and HI values, and is transported down to the distal area of the Zambezi turbidite system.

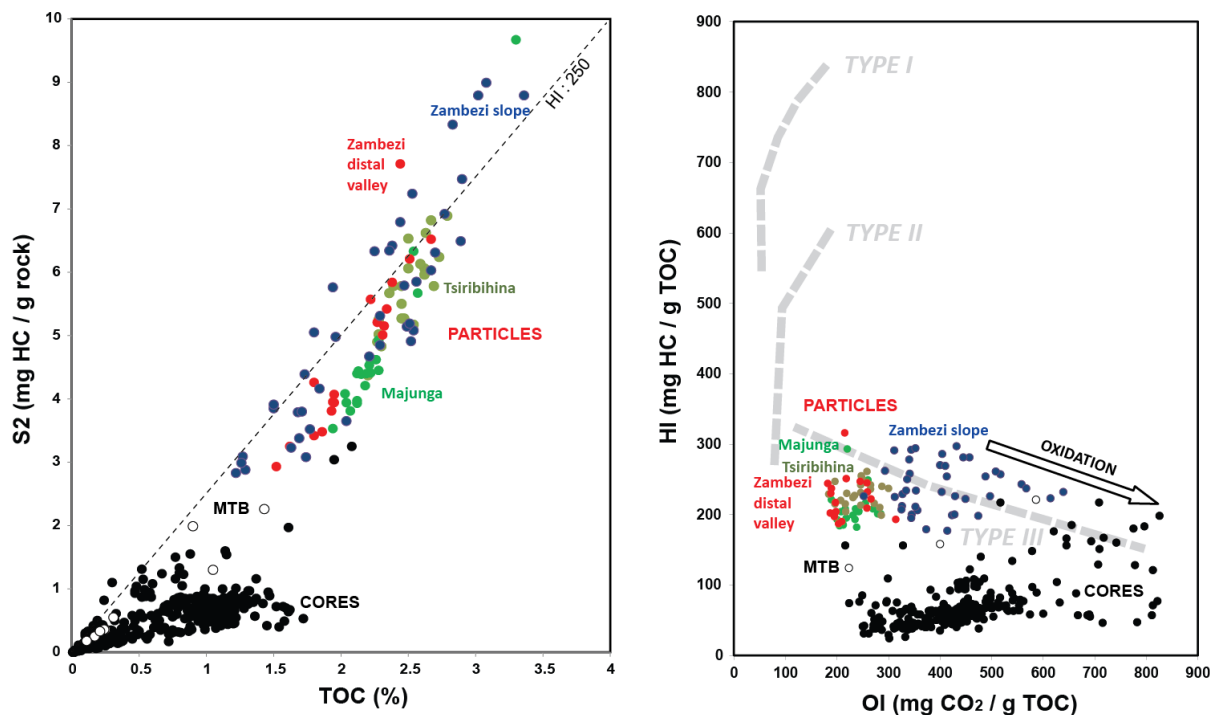


Fig. 7. S2 versus TOC (a) and HI versus OI (b) diagrams comparing the sediment (black) and the settling particles (Zambezi slope: blue; Zambezi distal valley: red; Majunga slope: dark green; Tsiribihina valley: light green).

The RE6 results indicate that particulate sediments collected on the upstream Zambezi system before deposition are characterized by higher OI values (300 to 700 mg CO₂/g TOC) compared to particle sediments from the deep-water distal channel (150 to 300 mg CO₂/g TOC) (Fig. 7b). This result suggests higher oxidation conditions along the upstream Zambezi and that in this area the OM has already been largely oxidized before its deposition. On the other hand, a different trend is observed for the distal area where the collected particulates are less oxidized (Fig. 7b). Oxidation of OM can be regarded as an irreversible process and particles from the deep-water show more affinity in terms of S2, TOC, HI and OI values with particles collected in the Tsiribihina submarine valley or even in the Majunga margin (Fig. 7a,b). This directly suggests that the Zambezi distal system would be preferentially fed by the Madagascar river system rather than from the Mozambique system.

EDS-SEM analyses

EDS-SEM analyses have shown that sediments collected along the Zambezi continental slope and in the Majunga margin (respectively samples MOZ04-CS17-S1-78 and MOZ01-KSF12-S1-54) are mainly characterized by a matrix composed of very fine minerals and shell debris

principally made of calcite with a mean size around 100 μm dispersed in the matrix (Fig. 8; table 2).

Table 2. Qualitative study of the mineralogical composition of samples MOZ01-KSF12-S1-54 Madagascar NW slope and MOZ04-CS17-S1-78 Zambezi slope (in normalized %).

	Quartz	Calcite	Halite	Feldspars	Kaolinite	Dolomite	Mica	Aragonite	Pyrite
KSF12-S1-54	9.2	28.4	2.1	3.5	22.6	tr	8.7	24.1	tr
CS17-S1-78	19.9	2.1	1.1	16.7	39.2	tr	20.1	-	tr

All the samples show quartz, calcite and feldspars and the minerals are usually well preserved and not altered. However, a drastic textural difference appears between the sediments collected in the Zambezi slope and those from the Majunga slope. Indeed, the samples from the Majunga slope show a better preservation compared to those from the Zambezi slope which appears largely mechanically damaged (Fig. 8). Also, the repartition and quantities of chemical elements are very different between these two areas (Table 2). EDS-SEM highlighted that CS17-S1-78 is composed mainly of K-feldspar and phyllosilicates such as mica (Biotite and Muscovite; Fig. 9).

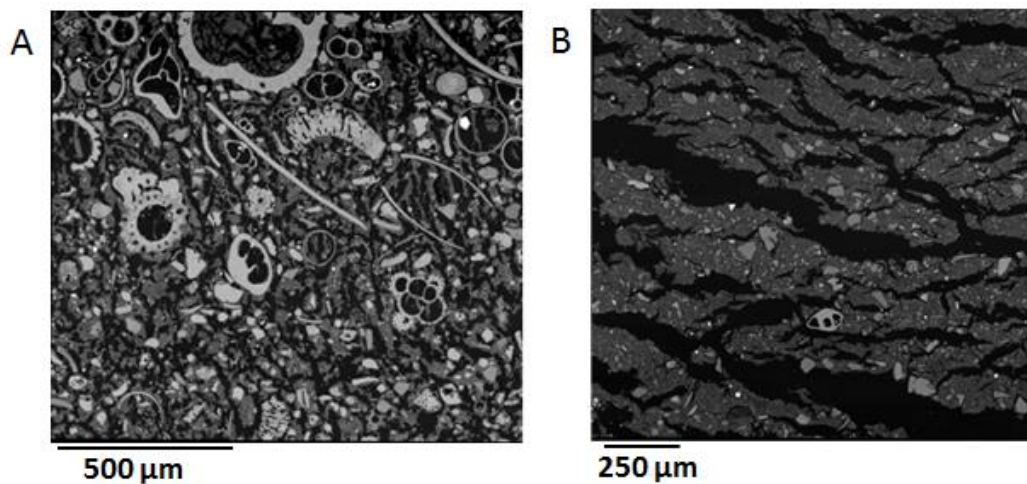


Fig. 8. SEM results illustrating the textural differences in the modern sediments from the Majunga slope, north-west of Madagascar (A) and the modern sediments from the Zambezi slope (B).

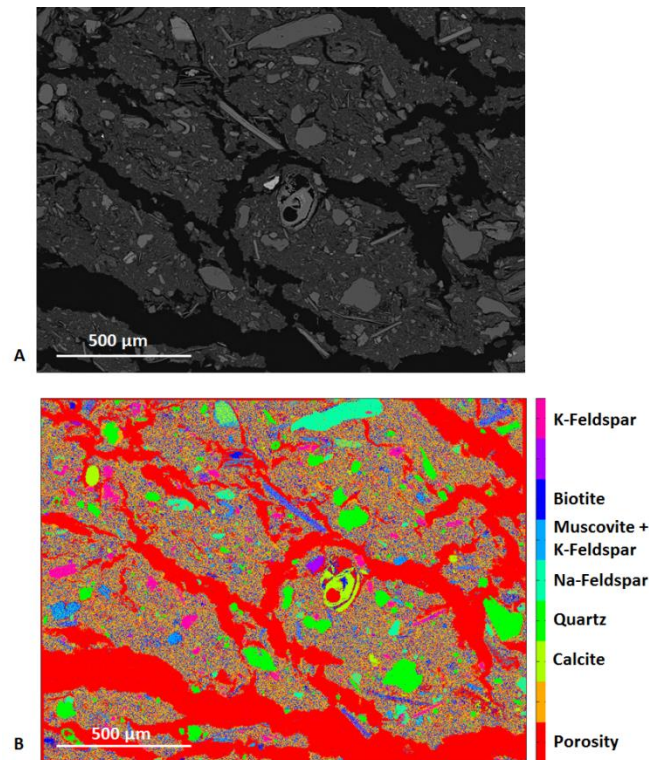


Fig. 9. EDS-SEM mineralogical mapping obtained by a statistical calculation (k-means clustering) on a sample of core Pamela-MOZ04-CS17 (depth 78 cm bsf), Zambezi slope.

Aggregates of iron oxides are found inside bioclasts and inside OM which is also partly calcified with accumulation of silica (Fig. 10). On the other hand, the MOZ01-KSF12-S1-54 sample (offshore Majunga) is composed mainly of calcite and aragonite with small amount of K-feldspar and mica. These sediments are very rich in bioclasts but they do not show accumulation of iron oxides (Fig. 11).

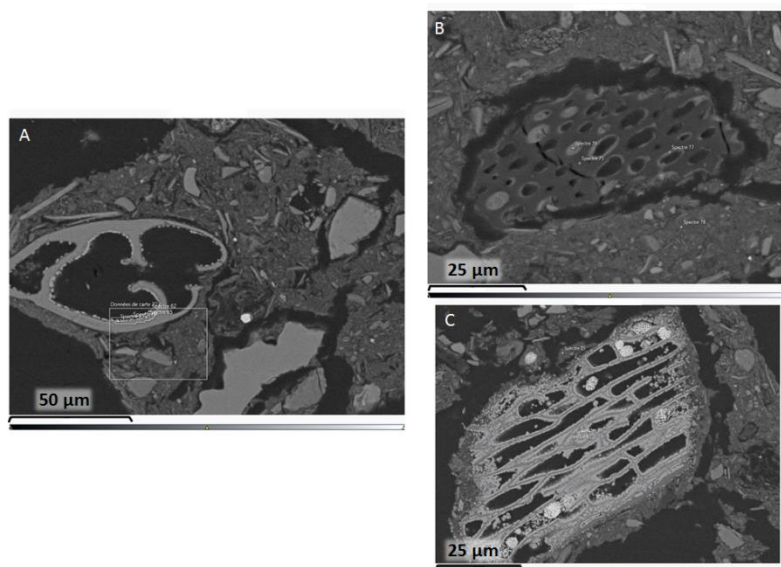


Fig. 10. SEM results illustrating in (A) the presence of neo-formed iron oxides inside foraminifera test, in (B) the presence of silica in OM, and in (C) calcified OM, samples from core Pamela-MOZ04-CS17, Zambezi slope.

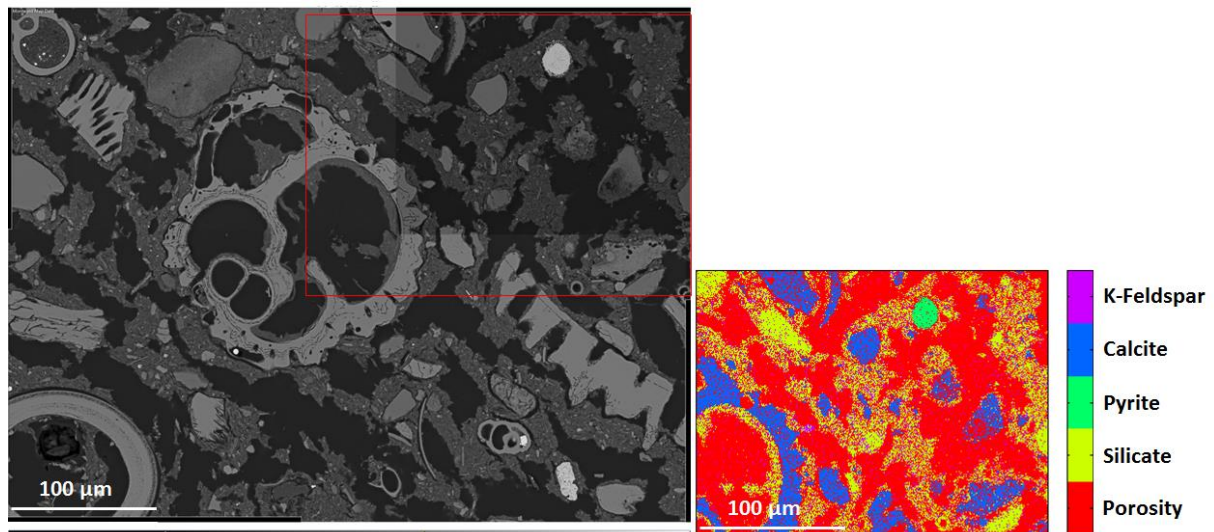


Fig. 11. Mineralogical mapping of a sample of core Pamela-MOZ01-KSF12 (depth 54 cm bsf), Majunga slope, north-west of Madagascar.

Sediment accumulation rates

^{210}Pb -derived SARs range between 0.4 and 2.49 cm yr^{-1} in the Madagascar margin (Fontanier et al., 2018; Pastor et al., 2020) and between 0.064 and 1.43 cm yr^{-1} on the Mozambique margin (this study; Table 3; Fig. S2, Appendix A). In the Zambezi channel, radiocarbon dating gave a calibrated age of 7090 ± 150 Cal yrs BP (calibrated years before the present) (6580 ± 30 ^{14}C yrs BP) and thus a minimum SAR of approximately 0.005 cm yr^{-1} . In the Tsiribihina valley, mass accumulation rate in a sediment trap gave a value of 8 $\text{mg cm}^{-2} \text{yr}^{-1}$. This is equivalent to a sediment accumulation rate of 0.012 cm yr^{-1} in the sediments (assuming a density of 1.5 g cm^{-3} of the sediments; Table 3). Note that this SAR value is regarded as a minimum estimate of the sedimentation rate because it does not integrate the sediment supply which occurs laterally between the sediment traps (47 m above seabed) and the seabed, notably coarse clastic material transported by turbidite/contourite currents.

Table 3. OPD: Oxygen penetration depths measured on interface cores; SAR: sediment accumulation rates based mainly on ^{210}Pb profiles in interface cores (NW Madagascar slope and Mozambique slope), on ^{14}C dating (Zambezi valley) and from an estimation made from mass accumulation rates in a moored sediment trap (Tsihiribihina valley; see explanation in the text); OET: oxygen exposure times calculated in interface cores; a. From Fontanier et al., 2016; b. From Pastor et al., 2020; c. This study (^{210}Pb profiles are plotted in the supplementary Fig. S2, Appendix A).

Area	Interface core	Lat (°S)	Long (°E)	Water depth (m)	OPD (mm)	SAR (cm yr^{-1})	OET (yr)
NW Madagascar margin	MOZ1-MTB3	15°21.695	45°57.3886	757	34 ^c	0.52 ^b	65
	MOZ1-MTB8	15°21.815	45°57.6485	740	10 ^c	0.45 ^c	22
	MOZ1-MTB6	15°31.148	45°42.9309	789	17.5 ^a	2.49 ^a	7
	MOZ4-MTB1	15°21.812	45°57.628	735	5 ± 2 ^c	0.45 ^c	11
	MOZ4-MTB2	15°21.685	45°57.378	754	28 ± 4 ^c	0.39 ^b	72
	MOZ4-MTB3	15°22.230	45°57.110	762	5 ± 1 ^c	0.59 ^b	8
Mozambique margin	MOZ4-MTB4	19°50.650	36°30.765	412	24 ± 4 ^c	1.43 ^c	17
	MOZ4-MTB5	19°23.330	36°52.390	316	11 ± 2 ^c	0.064 ^c	172
Zambezi channel	MOZ1-MTB10	21°31.835	41°20.7374	3205	83 ^a	0.005 ^c	16600
Tsihiribihina channel	MOZ1-MTB12	21°31.105	41°51.6780	3082	110 ^a	0.012 ^c	9167
Zambezi distal channel	MOZ1-MTB15	25°25.612	41°35.7334	4074	120 ^c		

Oxygen penetration depths

At all sites of the study area, the oxygen concentrations reach zero within the upper 3 cm of sediment, except in the deep-water area of the Mozambique Basin in the Tsihiribihina valley (MOZ1-MTB12) and the Zambezi valley (MOZ1-MTB10 and MOZ1-MTB15; Fig. 12). The lowest measured OPD gave values of 5 mm (Table 3). They were found in the Madagascar margin in reduced sediments from areas with methane upward diffusion (MOZ4-MTB1 and MOZ4-MTB3; Pastor et al., 2020). The highest OPD were found in the Tsihiribihina valley (> 9 cm at MOZ1-MTB12) and the Zambezi valley (8.3 cm at MOZ1-MTB10; > 9 cm at MOZ1-MTB15). In the deepest site which has been studied in the distal part of Zambezi valley (4070 m at MOZ1-MTB15), concentrations were still above 25 μM at 8 cm (Fig.12). Assuming a continual decrease in oxygen concentrations with depth, the OPD in the Tsihiribihina valley and the Zambezi distal channel could be estimated to 11 and 12 cm respectively (Table 3).

OET values are low in the margin areas (below 200 years) whereas they reach several thousands of years in the deep-water area of the Mozambique basin (Table 3).

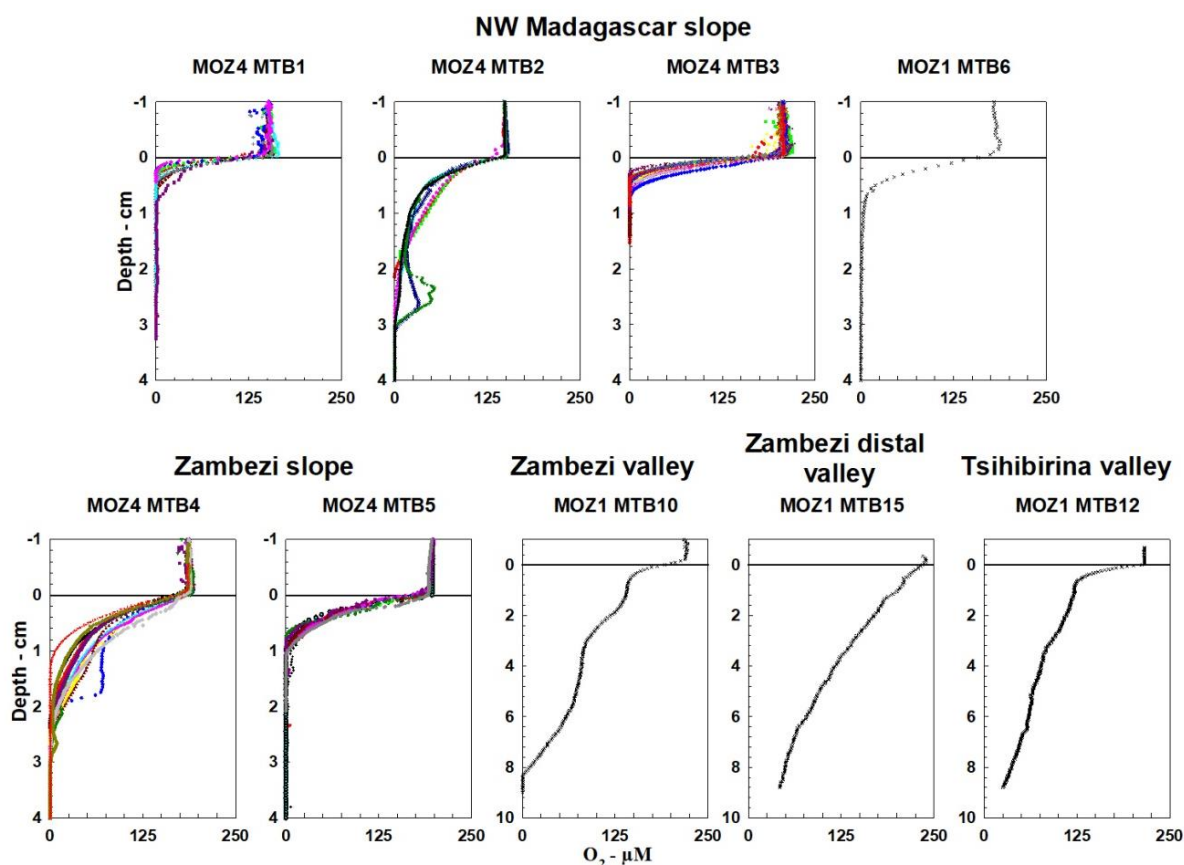


Fig. 12. Oxygen profiles measured on interface cores collected in the Mozambique Channel.

DISCUSSION

A prevailing hypothesis assumes that the carbon flux strongly decreases with water depth related to degradation processes that occur in the water column before OM reaches the seabed (Suess, 1980). If this process is indeed largely active concerning the marine planktonic pelagic OM flux (type II OM), this is not the case for the more refractory detrital OM fluxes issued from the continents (type III OM). Indeed, as mentioned in introduction, several studies have shown that OM can be preserved in deep-water domains (Stow et al., 2001; Baudin et al., 2017). In this work, we present the analysis of the organic matter evolution at a wide scale from shallow areas to deep-water domains. Results on the OM collected from sediments traps located at 47 m above the seabed (before deposition), at the water/sediments interface and in the first meters of the sedimentary pile (< 33 m of depth) led to better assess the transport and preservation conditions characterizing the recent sediments in the Mozambique Channel.

RE6 results on core samples collected north-west of Madagascar and in the Davie Ridge area show that the OM is characterized by two HI groups: a first group with average HI values

around 150 mg HC/g TOC and second group with average HI values around 75 mg HC/g TOC (Fig. 3). As mentioned above, these two groups could result from two different OM sources, a main source of terrestrial material and eventually a second source with marine OM material that became eventually diluted where the higher HI values may correspond to less oxidized continental OM. However, microscopic studies did not show evidence for marine OM and the higher HI values follow the same trend than HI values of particles sampled in moorings which have been less affected by oxidation processes but show typical type III OM characteristics (Fig. 7). It is also worth noting that particulate organic matter (POM) sampled along the upstream zone of the Zambezi turbidite system is more oxidized ($OI > 300 \text{ mg CO}_2/\text{g TOC}$) than POM sampled in the distal area of the Zambezi turbidite system ($OI < 300 \text{ mg CO}_2/\text{g TOC}$). POM from the distal valley of the Zambezi turbidite system is better correlated with the signature of POM from the Majunga slope and the Tsibihirina valley (Fig. 7). Oxidation being an irreversible process and based on the geochemical affinity of the POM sampled in the deep-water with POM collected in the Tsiribihina submarine valley or even in the Majunga margin (Fig. 7a,b), we can assume that the OM which reaches the distal depositional area is preferentially issued from Madagascar rather than from Mozambique. This interpretation is consistent with the fact that the recent uplift associated with active tectonics across the Mozambique Channel (Deville et al., 2018) is responsible for a partial abandonment of the main Zambezi turbidite channel toward places located west of the Bassas da India-Europa area (Fierens et al., 2019). This interpretation should be confirmed by additional studies concerning the nature of the associated terrigenous material.

In terms of transport and preservation, particles collected in the water column before deposition contain the highest OM contents (TOC values between 1.5 and 3%) both in the shallow water domains and the deep-water domains (Fig. 7a). Based on Rock-Eval results on POM, the organic matter is transported over large distances, being minimally affected by degradation processes (Fig. 7). Indeed, especially along the Zambezi deep turbidite system, the material collected in sediment traps has shown that the OM transported by turbidite and/or bottom currents towards the deep-water domains is preserved with higher TOC values and $HI > 200 \text{ mg HC/g TOC}$ and $OI < 300 \text{ mg CO}_2/\text{g TOC}$ (Fig. 7). In the deep-water area of the Mozambique Basin (below 2500 m of water depth), the OM content preserved in the sediments after deposition is low, as shown by a strong decrease of TOC values, especially in the distal depositional area (Fig. 4, 13). This decrease of TOC in the deep-water domain is notably important compared to other turbidite systems which are comparable by their size and their OM

supply, such as the Orinoco river (Deville et al., 2015), or the Congo river (Baudin et al., 2017; Fig. 3).

The EDS-SEM study of selected representative samples from the Zambezi slope and from Majunga slope has shown that the mineralogical differences are characteristic of two different depositional environments which may affect preservation conditions (Table 2). The studied samples from the uppermost sediments of the Mozambique slope present mainly K-feldspar and micas but no aragonite and only small amounts of calcite typical of a high depositional rate and elevated terrigenous supply (Fig. 9; Table 2). This result is characteristic of a well oxygenated environment which is consistent with the presence of iron oxides in both, the mineral matrix and the calcified OM (Fig. 10). In contrast, the samples from the uppermost sediments of northwestern Madagascar are rich in aragonite, calcite and shell residues with no or limited iron oxide (Fig. 11, Table 2). This is representative of a less-oxygenated depositional environment in the uppermost first centimeters of sediments. These results are compatible with RE6 data that show that along the Zambezi slope, the terrestrial particulate OM carried by the Zambezi River and the coastal alongshore currents, is largely oxidized (Fig. 7 b). S2 *versus* TOC and HI *versus* OI diagrams on settling particles show that oxidation largely occurred before deposition (Fig. 7b). The presence of iron oxides precipitations inside microfossil shells along the Zambezi slope (cf. EDS-SEM results) can be the result of higher oxygenation conditions of this area compared to the Majunga slope (Fig. 11). These oxic conditions combined with the mechanical damage of the microfossil shells, which has been observed along the Zambezi slope (Fig. 8), suggest a major role of the currents along the slope (Miramontes et al. 2019b). However, even though of more oxic conditions, the presence of iron oxides is prone to contribute to the preservation of the OM after sediment is deposited (Barber et al., 2017).

The comparison of the analytical results obtained in moorings, interface cores and piston cores suggests that OM was largely degraded in the first centimeters of the water-sediment interface in areas below 2500 m of water depth (Fig. 12 and 13), which correspond to areas where oxygen was measured at least down to 8 cm in the sediments and where OET reaches several thousand years (Table 3, Fig. 12). Indeed, in the deep-water area of the Mozambique Basin, important oxidation processes occurred in the uppermost sediments as confirmed by the decrease of the S2 peak (< 0.5 mg HC/g rock) and of the TOC content (< 0.5%), coupled with an increase of the OI (> 300 mg CO₂/g TOC) (Fig. 7a,b). This is very probably correlated with more oxidizing conditions, as shown by thicker O₂-bearing zones in the uppermost sediments of the deep-water

area of the Mozambique Basin along the distal Zambezi and Tsirihibina valleys (Fig. 12). These higher oxidizing conditions are interpreted by the conjugated effects of lower sedimentation rate (Table 3) and higher porosity of the sand-rich material present in the Zambezi distal system (Fierens et al., 2019). This is also probably due to the activity of important bottom currents (Miramontes et al., 2019) which is prone to maintain oxidizing conditions by the remobilization of both the uppermost sediments and the organic matter within. This interpretation is in good agreement with the fact that current velocities reach up to 50 cm.s^{-1} in the Zambezi valley at MPL2 (Fig. 1), 38 cm.s^{-1} in the Tsirihibina valley at MPL3 (Fig. 1) and 36 cm.s^{-1} in the Zambezi distal valley at MPL5 (Miramontes et al., 2019; Fig. 1). Overall, these processes are responsible for higher oxygen exposure times ranging from a few years (7 to 172 yrs in the Mozambique and Madagascar margins) to thousands of years (up to 16,600 yrs in the Zambezi distal valley; Table 3). The longest oxygen exposure times can thus be regarded as responsible for higher oxidation of OM.

CONCLUSION

The Mozambique Channel receives large amount of continental-derived organic matter issued from both Madagascar and Mozambique margins. The highest levels of OM quantity from piston cores are found in the Majunga area, NW of Madagascar and in the continental slope of the Zambezi (offshore Mozambique). Particle samples collected in the water column from the distal lobes of the Zambezi turbidite system show relatively high content of poorly oxidized OM compared to the Zambezi slope where the OM is already largely oxidized before deposition. Rock-Eval results suggest that in the distal area, the continental-derived OM is preferentially issued from Madagascar rather than from Mozambique. Our findings lead to the hypothesis that in the deeper parts of the Channel, the OM is efficiently transported by turbidite and/or contour currents and deposited in the turbidite system down to the deep-water area of the Mozambique Basin while preserving relatively poorly oxidized OM. However, once it is deposited the OM is largely oxidized in the sediments near to the water-sediment interface. This process is probably related to the conjugated effects of lower sedimentation rate and higher porosity of the sand-rich material present in the Zambezi distal system. In this area, the activity of important marine currents is also responsible for the remobilization of the OM particles at the sea bottom leading to oxic conditions and higher oxygen exposure time in the uppermost centimeters of the sediments.

Acknowledgements

This work has been conducted within the framework of the PAMELA (PAssive Margin Exploration Laboratories) project sponsored by IFREMER and TOTAL in collaboration with IFP Energies Nouvelles, Université de Bretagne Occidentale, Université de Rennes 1, Sorbonne Université and CNRS (Bourillet al., 2013). Data acquisition was performed in 2014 during the PAMELA-MOZ01 campaign (Olu, 2014) onboard the R/V *L'Atalante*, in 2015 during the PAMELA-MOZ04 campaign (Jouet and Deville, 2015) onboard the R/V *Pourquoi Pas?*, and during the PAMELA-MOZ08 campaign (Khripounoff, 2017) onboard the R/V *Antea*. We thank captains, officers, crew members and the scientific teams of these cruises for their technical support.

APPENDIX A. SUPPLEMENTARY MATERIAL

1. Piston cores



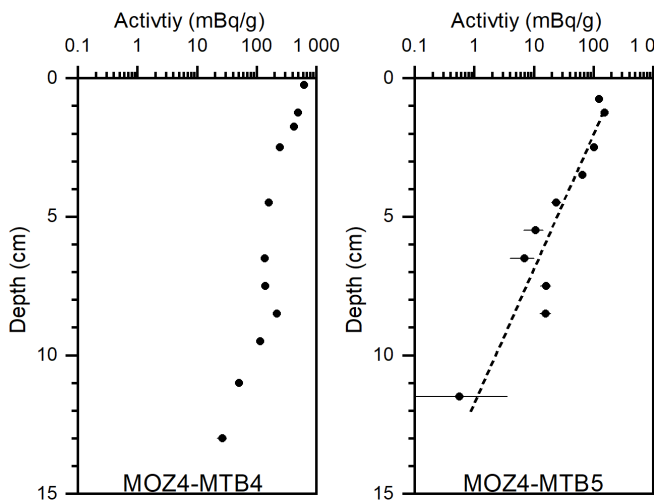
2. Interface sampler (multitubes)



3. Moorings (particle trap)



Supplementary Fig. S1. The three different types of sampling devices.



Supplementary Fig. S2. $^{210}\text{Pb}_{\text{xs}}$ profiles measured on cores MOZ4-MTB4 and MOZ4-MTB5. Error bar on radionuclide profiles correspond to 1 SD. Dashed lines show the regression line used to calculate mean sediment accumulation rates.

Appendix B. Supplementary data

Supplementary data to this article (Table S1. Full result of RE6 analyses) can be found at <http://www.seanoe.org/data/> (License: Creative Commons Attribution, no commercial usage, sharing under the same conditions).

REFERENCES

- Ahuva, A.L., Amos, B., Sass, E., 1993. Late Cretaceous upwelling system along the Southern Tethys Margin Israel Interrelationship between productivity, bottom water environments, and organic matter preservation. *Paleoceanography* 8, 5, 671–690.
- Aminot, A., K erouel, R., 2004. Hydrologie des  cosyst mes marins. Param tres et analyses. 335 p.
- Barber, A., Brandes, J., Leri, A., Lalonde, K., Balind, K., Wirick, S., Wang, J., G linas, Y., 2017. Preservation of organic matter in marine sediments by inner-sphere interactions with reactive iron. *Scientific Reports* 7, 366, <https://DOI:10.1038/s41598-017-00494-0>.
- Baudin, F., Disnar, J-R., Martinez, P., Dennielou, B., 2010. Distribution of the organic matter in the channel-levees systems of the Congo mud-rich deep-sea fan (West Africa). Implication for deep offshore petroleum source rocks and global carbon cycle. *Marine and Petroleum Geology* 27, 5, 995–1010. <https://DOI:10.1016/j.marpetgeo.2010.02.006>.
- Baudin, F., Stetten, E., Schnyder, J., Charlier, K., Martinez, P., Dennielou, B., Droz, L., 2017. Origin and distribution of the organic matter in the distal lobe of the Congo deep-sea fan – A Rock-Eval survey. *Deep Sea Research Part II: Topical Studies in Oceanography* 142, 75–90. <https://DOI:10.1016/j.dsr2.2017.01.008>.
- Behar, F., Beaumont, V., B. Penteado, H. L. de, 2001. Rock-Eval 6 Technology. Performances and Developments. *Oil & Gas Science and Technology* 56 2, 111–134. <https://DOI:10.2516/ogst:2001013>.
- Berthois, L., Crosnier A., 1966. Etude dynamique de la s dimentation au large de l'estuaire de la Betsiboka. *Cahiers O.R.S.T.O.M., s r. Oc anogr.* IV, 2.
- Bourillet, J.F., Ferry, J.N., Bourges, P., 2013. PAMELA, Passive Margins Exploration Laboratories. <https://dx.doi.org/10.18142/236>.
- Burdige, D.J., 2007. Preservation of Organic Matter in Marine Sediments: Controls, Mechanisms, and an Imbalance in Sediment Organic Carbon Budgets? *Chemical Reviews* 107, 467-458. <https://doi.org/10.1021/cr050347q>.
- Deroo, G., Herbin, J. P., Roucach , J., 1983. Organic geochemistry of upper Jurassic Cretaceous sediments from site-511, leg-71, Western South-Atlantic. *Initial Reports of the Deep Sea Drilling Project*, 71, 1001–1013.
- Deville, E., Mascle, A., Callec, Y., Huyghe, P., Lallemand, S., Lerat, O., Mathieu, X., Padron de Carillo, C., Patriat, M., Pichot, T., Loubrieux, B., Granjeon, D. 2015. Tectonics and sedimentation interactions in the east Caribbean subduction zone. An overview from the Orinoco delta and the Barbados accretionary prism. *Marine and Petroleum Geology* 64, 76–103. <https://DOI:10.1016/j.marpetgeo.2014.12.015>.
- Deville,  ., Guerlais, S-H., Callec, Y., Griboulard, R., Huyghe, P., Lallemand, S., Mascle, A., Noble, M., Schmitz, J. and the CARAMBA research team, 2006. Liquefied vs Stratified Sedimentation Mobilization Processes: Insight from the South of the Barbados Accretionary Prism. *Tectonophysics*, 428, 33-47. <https://DOI:10.1016/j.tecto.2006.08.011>.
- Espitalie, J., Laporte, J.L., Madec, M., Marquis, F., Leplat, P., Paulet, J., 1977. M thode rapide de caract risation des roches m res, de leur potentiel p trolier et de leur degr  d' volution. *Rev. Inst. fr. petr.*, 32, 1, 23-42. <https://doi.org/10.2516/ogst:1977002>

- Espitalié, J., Madec, M., Tissot, B., Mennig, J. J., Leplat, P., 1977. Source Rock Characterization Method for Petroleum Exploration. In. Offshore Technology Conference. OTC, 1977/1/1, Offshore Technology Conference, p. 6.
- Espitalié, J., Senga Makadi, K., Trichet, J., 1984. Role of the mineral matrix during kerogen pyrolysis. *Organic Geochemistry* 6, 365–382. [https://doi.org/10.1016/0146-6380\(84\)90059-7](https://doi.org/10.1016/0146-6380(84)90059-7).
- Espitalie, J., Deroo, G., Marquis, F., 1985. Rock-Eval pyrolysis and its applications. *I Rev. Inst. fr. petr.* 40, 5, 563–579.
- Fierens, R., Droz, L., Toucanne, S., Raisson, F., Jouet, G., Babonneau, N., Miramontes, E., Landurain, S., Jorry, S., 2019. Late Quaternary geomorphology and sedimentary processes in the Zambezi turbidite system (Mozambique Channel). *Geomorphology* 334, 1–28. <https://DOI:10.1016/j.geomorph.2019.02.033>.
- Fontanier, C., Mamo, B., Toucanne, S., Bayon, G., Schmidt, S., Deflandre, B., Dennielou, B., Jouet, G., Garnier, E., Sakai, S., Lamas, R.M., Duros, P., Toyofuku, T., Salé, A., Belleney, D., Bichon, S., Boissier, A., Chéron, S., Pitel, M., Roubi, A., Rovere, M., Grémare, A., Dupré, S., Jorry, S.J., 2018. Are deep-sea ecosystems surrounding Madagascar threatened by land-use or climate change? *Deep Sea Research Part I, Oceanographic Research Papers* 131, 93-100. <https://doi.org/10.1016/j.dsr.2017.11.011>.
- Galy, V., Peucker-Ehrenbrink, B., Eglinton, T., 2015. Global carbon export from the terrestrial biosphere controlled by erosion. *Nature* 521, 204. <https://DOI:10.1038/nature14400>.
- Hare, A.A., Kuzyk, Z.Z.A., Macdonald, R.W., Sanei, H., Barber, D., 2014. Characterization of sedimentary organic matter in recent marine sediments from Hudson Bay, Canada, by Rock-Eval pyrolysis. *Organic Geochemistry* 68, 52–60. <https://doi.org/10.1016/j.orggeochem.2014.01.007>.
- Hartnett, H. E., Keil, R.G., Hedges, J.I., Devol, A.H., 1998. Influence on oxygen exposure time on organic carbon preservation in continental margin sediments. *Nature* 391, 372-374.
- Hedges, J. I., Keil, R.G., 1995. Sedimentary organic matter preservation: an assessment and speculative synthesis. *Marine Chemistry* 49, 81-115.
- Hedges, J.I., Keil, R.G., Benner, R., 1997. What Happens to Terrestrial Organic Matter in the Ocean? *Organic Geochemistry* 27, 5/6, 195–212. [https://doi.org/10.1016/S0146-6380\(97\)00066-1](https://doi.org/10.1016/S0146-6380(97)00066-1).
- Henrichs, S. M., Farrington, J. W., 1984. Peru upwelling region sediments near 15S. Remineralization and accumulation of organic matter. *Limnology and Oceanography* 29, 1–19.
- Jouet, G., Deville, E., 2015. PAMELA-MOZ04 cruise, R/V Pourquoi Pas? <https://doi.org/10.17600/15000700>.
- Khripounoff, A., 2017. PAMELA-MOZ08 cruise, R/V Antea. <https://doi.org/10.17600/17003900>.
- Lafargue, E., Marquis, F., Pillot, D., 1998. Rock-Eval 6 Applications in Hydrocarbon Exploration, Production, and Soil Contamination Studies. *Rev. Inst. Fr. Pét.* 53, 4, 421–437. <https://DOI:10.2516/ogst:1998036>.
- Miramontes, E., Penven, P., Fierens, R., Droz, L., Toucanne, S., Jorry, S.J., 2019. The influence of bottom currents on the Zambezi Valley morphology (Mozambique Channel, SW Indian

- Ocean). In situ current observations and hydrodynamic modelling. *Marine Geology* 410, 42–55. <https://DOI:10.1016/j.margeo.2019.01.002>.
- Mueller, C. O., Jokat, W., 2019. The initial Gondwana break-up: A synthesis based on new potential field data of the Africa-Antarctica Corridor. *Tectonophysics*, 750, 301–328. <https://doi.org/10.1016/j.tecto.2018.11.008>.
- Nieto-Cid, M., Alvarez-Salgado, A., Pérez, F.F., 2006. Microbial and Photochemical reactivity of fluorescent dissolved organic matter in a coastal upwelling system. *Limnology and Oceanography* 51, 3, 1391–1400. <https://DOI:10.2307/3841185>
- Olu, K., 2014. PAMELA-MOZ01 cruise, R/V L'Atalante, .
- Pastor, L., Brandily, C., Schmidt, S., Miramontes, E., Péron, M., Appéré, D., Besson, S., Boissier, A., Jouet, G., 2020. Modern sedimentation and geochemical imprints in sediments from the NW Madagascar margin. *Marine Geology* (in press).
- Pedersen, T.F., Calvert, S.E., 1990. Anoxia vs. Productivity. What Controls the Formation of Organic-Carbon-Rich Sediments and Sedimentary Rocks?. *AAPG Bulletin* 74, 4, 454–466. <https://doi.org/10.1306/0C9B282B-1710-11D7-8645000102C1865D>.
- Pelegrí, J.L., Arístegui, J., Cana, L., González-Dávila, M., Hernández-Guerra, A., Hernández-León, S., 2005. Coupling between the open ocean and the coastal upwelling region off northwest Africa. Water recirculation and offshore pumping of organic matter. *Journal of Marine Systems* 54, 1-4, 3–37. <https://DOI:10.1016/j.jmarsys.2004.07.003>.
- Pillot, D., Deville, E., Prinzhofer, A., 2014. Identification and Quantification of Carbonate Species Using Rock-Eval Pyrolysis. *Oil & Gas Science and Technology* 69, 2, 341–349. <https://DOI:10.2516/ogst/2012036>.
- Rabinowitz, P.D., Coffin, M.F., Falvey, D., 1983. The Separation of Madagascar and Africa. *Science* 220, 4592, 67–69. <https://DOI:10.1126/science.220.4592.67>.
- Revsbech, N.P., 1989. An oxygen microsensor with a guard cathode. *Limnology and Oceanography* 34, 2, 474-478. <https://doi.org/10.4319/lo.1989.34.2.0474>
- Schmidt, S., De Deckker, P., 2015. Present-day sedimentation rates on the southern and southeastern Australian continental margins. *Australian Journal of Earth Sciences* 62, 143-150. <https://DOI:10.1080/08120099.2015.1014846>.
- Stow, D.A.V., Huc, A. Y., Bertrand, P., 2001. Depositional Processes of Black Shales in Deep Water. *Marine and Petroleum Geology* 18, 491–498. [https://doi.org/10.1016/S0264-8172\(01\)00012-5](https://doi.org/10.1016/S0264-8172(01)00012-5).
- Suess, E., 1980. Particulate organic carbon flux in the oceans—surface productivity and oxygen utilization. *Nature* 288, 5788, 260. <https://DOI:10.1038/288260a0>.
- Thompson, J.O., Moulin, M., Aslanian, D., de Clarens, P., Guillocheau, F., 2019. New starting point for the Indian Ocean : Second phase of breakup for Gondwana. *Earth-Science Reviews*, 191, 26–56. <https://doi.org/10.1016/j.earscirev.2019.01.018>.
- Vangriesheim, A., Khripounoff, A., Crassous, P., 2009. Turbidity events observed in situ along the Congo submarine channel. *Deep-Sea Research Part II-Topical Studies in Oceanography* 56, 23, 2208-2222. <https://10.1016/j.dsr2.2009.04.004>.
- Van Krevelen, D. W., 1950. Graphical-statistical method for the study of structure and reaction processes of coal. *Fuel* 29, 269–284.

- Wakeham, S.G., Lee, C., Hedges, J.I., Hernes, P.J., Peterson, M.J., 1997. Molecular indicators of diagenetic status in marine organic matter. *Geochimica et Cosmochimica Acta* 61, 24, 5363–5369. [https://DOI:10.1016/S0016-7037\(97\)00312-8](https://DOI:10.1016/S0016-7037(97)00312-8).
- Wang, X. C., Druffel, E.R.M., Griffin, S., Lee, C., Kashgarian, M., 1998. Radiocarbon Studies of Organic Compound Classes in Plankton and Sediment of the Northeastern Pacific Ocean. *Geochimica et Cosmochimica Acta* 62, 8, 1365–1378. [https://doi.org/10.1016/S0016-7037\(98\)00074-X](https://doi.org/10.1016/S0016-7037(98)00074-X).
- Wiles, E., Green, A., Watkeys, M., Botes, R., Jokat, W., 2019. Submarine canyons of NW Madagascar: A first geomorphological insight. *Deep Sea Research Part II: Topical Studies in Oceanography* 161, 5-15. <https://doi.org/10.1016/j.dsr2.2018.06.003>.

4. Modelling microbial gas processes at the basin scale

Sedimentary basins can contain valuable resources such as minerals, hydrocarbons and geothermal fluids. They also offer the possibility to store fluids and energy such as heat, carbon dioxide and methane. The potential of a sedimentary basin to contain hydrocarbon resources can be assessed by regional basin models which is a widely accepted approach in the oil and gas industry as part of hydrocarbon exploration studies (Ungerer et al. 1990; Doré et al. 1993). A basin model is a dynamic model of a sedimentary basin with its processes of compaction, thermal maturation and fluid movements that may lead to hydrocarbon accumulations. The main modules of basin models perform temperature and pressure modelling through geologic time, and generation and migration of HCs. However, basin modelling encompasses a wide range of geological disciplines to define the evolution of a sedimentary basin. It is not only used in petroleum exploration, but it can also be applied to studies of geothermal energy (*e.g.* Omodeo-Salé et al. 2020) or CO₂ capture and storage (*e.g.* Teles et al. 2014). Even though basin modelling can be applied in multiple scientific contexts, to our knowledge there are no such studies concerning the analysis of the biogenic methane budget from generation to emission at the basin scale (from source to seep). To better estimate the biogenic gas volume generated from biological activity, it is necessary to accurately account for the complexity of biogenic gas processes.

Biogenic gas production is a process that occurs at the microscopic scale and varies laterally and vertically as a function of OM availability. Therefore, it is challenging to simulate the genesis of biogenic CH₄ at geological time and basin-wide space scales. Published OM degradation models are the result of experimental laboratory studies, based on short time scales (human scale) under specific and fully controlled thermal conditions suitable for microbes. In contrast, a basin model accounts for the entire geological history of a basin and its thermal evolution at a geological time scale. It is therefore necessary to find a general modelling procedure that accounts for the main biogenic gas production processes and that can be applied in different geological contexts. Published OM degradation processes are calibrated on initial TOC values, on final generated products (CH₄, Dissolved Inorganic Carbon - DIC, acetate), on substrates and nutrients (acetate, DIC, NH₄⁺, SO₄²⁻), and on the microbial activity. A synthesis of the approaches that quantify the OM degradation rate and the mathematical laws is presented in Arndt et al. (2013). In addition, degradation models account also for the different classes of OM that are characterized by different reactivities (Westrich and Berner 1984). It is therefore

possible to account for all of these processes at the micro-scale, but it is not always possible to do this at the basin scale (macroscopic scale). What can be adapted at the basin scale are the descriptions of the biogenic gas generation processes and of the OM in terms of its origin, specifically:

- (1) the type of OM (*e.g.* type I, II/IIIS, III),
- (2) the TOC fractions (labile *vs* refractory)
- (3) the degradation law.

A model that describes OM degradation from microbial activity resulting in biogenic gas has been published by Middelburg (1989) which was subsequently modified by Wallman et al. (2006). Another model used to reproduce biogenic gas processes is the Clayton model (Clayton 1992).

The Wallman model is an optimization of the Middelburg model which mainly focuses on the microbial activity at shallow depths. Both models involve an exponential decrease of the OM concentration with depth and time which leads to a strong degradation of the OM in the first meters of the sedimentary section. Dealing with such a high vertical resolution is not appropriate since the vertical resolution of a basin model is usually in the order of 10s to 100s meters. Moreover, in the TemisFlow basin simulator, all HCs generated from the youngest layer are lost to the surface due to lack of capillary pressure. If we consider a strong reactivity in the first meters as proposed by Middelburg (1989), we could not generate biogenic gas at greater depth since all the biodegradable OM would have been already consumed at the deposition time and all the generated gas would be lost. However, a long-lasting methanogenesis is required to generate observed biogenic gas volumes that are sometimes even large enough to be of commercial interest.

The Clayton (1992) model requires to define two parameters:

- (1) the area which can produce HCs
- (2) the total TOC from which a volume of biogenic gas can be generated.

The author estimates that 10% of the total TOC can generate biogenic gas, without describing any boundary conditions for bacterial activity or the initial composition of the OM. In the Clayton model, microbial activity is considered constant everywhere in the defined area

which is however unlikely considering the dependency of bacterial activity notably on temperature.

The published models cannot accurately reproduce methanogenesis at the basin scale because they are unable to account for the conditions associated with bacterial activity, and OM reaction rates and degradation laws which are a function of the original OM composition. Here, we propose a new model which accounts for the geological evolution of the basin and the OM composition and its degradation by bacterial activity through time and in space. In order to account for methanogenesis in the deeper parts of the basin, a “thermally-induced” source of methane (called here TOCzlab or thermo-labile TOC) is introduced which is degraded following a first order kinetic equation (Burdige et al. 2007). This formalism applied in our model does not correspond to the classical thermal cracking used for the conversion of kerogen into oil. Our model consists in generating a new pool of biodegradable OM with temperatures at a basin scale during early diagenesis where part of this process can be described by a first order kinetic law (*i.e.* the thermal evolution of the TOCzlab).

Very little is known about the reactivity of such compounds. Previous studies tried to quantify the OM decomposition pathways during early diagenesis. Mackin and Swider (1989) analysed the anaerobic respiration reactions in nearshore sediments from the Flax Pond muds in Long Island (USA), yielding activation energy values comprised between 71 and 109 kJ/mol. Canuel and Martens (1996) determined the degradation rate of lipid components in coastal sediments from Cape Lookout Bight, North Carolina (USA). In their work, the authors proposed an activation energy for fatty acids in the range of 50 kJ/mol, varying from fatty acids derived from phytoplankton (rapidly degraded) to fatty acids derived from higher plants (more resistant to biodegradation). The evolution of the organic carbon content in coastal sediments from the Iberia Peninsula is presented in Forja et al. (2004). The authors estimate activation energy values in the range of 33 to 53 kJ/mol based on temperature dependent DIC (Dissolved Inorganic Carbon) and O₂ fluxes. However, the type of reaction/decomposition (*e.g.* bond scission) associated with these activation energies is still not well understood. Other studies tried to better describe the evolution of microbial activity with temperature through laboratory experiments (Wellsburry et al. 1997; Parkes et al. 2007; Burdige, 2011). Major observations have been made based on parameters such as sulphate disappearance (*i.e.* bacterial sulfato-reduction activity), methane production (*i.e.* bacterial methanogenesis activity) and also hydrogen production (Parkes et al, 2007). Based on all these results, it is possible to propose a

general range of reactivities for recent OM during early diagenesis between 50 and 130 kJ/mol (Burdige 2011). However, such a large range is too wide and requires further analysis. For instance, specific studies on the type of reaction and decomposition associated with different activation energies can help to improve our understanding of OM reactivity during early diagenesis. Note that different types of SOM present different labile/thermolabile characters (e.g. amount of carbohydrates, protein, lipids, and vitrinite) (Cowie and Hedges 1992; Hedges and Oades 1997; Burdige 2011) resulting in different reactivities to biodegradation during early diagenesis.

In our approach, we mainly focus on the description of the reactivity of a Type III OM during early diagenesis. Terrestrial OM is mainly composed of aliphatic fractions as long-chain saturated fatty acids and diacids derived mainly from waxes of higher plants (Largeau and Vanderbroucke 2007; Kamga 2016). Therefore, we can assume that methane generation at low temperatures is mainly the result of the degradation of these aliphatic fractions (Kamga 2016) which present the most thermo-labile compounds with low activation energies.

Our new approach allows to model the biogenic gas system which in turn allows to identify biogenic kitchens and locations of biogenic gas accumulations in order to assess and estimate the size of such accumulations. Our approach can also be used to identify conditions for shallow gas accumulations that may present a drilling hazard in form of sudden gas kicks. Other interesting applications of our approach are global warming studies, as compared to satellite data or ocean expeditions, it can be used to evaluate basins (up to 1000 x 1000 km scale) with important and more or less continuous gas emissions from the past to present-day.

This chapter focuses on the modelling of biogenic gas processes at the basin scale. It gives first a general overview of the reactivity models for OM degradation during early diagenesis which is followed by a description of the concepts used in our basin model. A case study is then presented in chapter 5 as a major application and calibration of our approach.

4.1 The OM reactivity model

The SOM fractionation and alteration/degradation processes are the result of diagenesis which is the transformation of both the organic and the mineral fractions (Ishiwatari 1992). Different models have been published in the last decades with the aim to understand and constrain the carbon cycle and its fate at the geological time scale (Arndt et al. 2013 and

references within). These models account for diagenesis processes (which include sediment compaction, water advection and diffusion of solutes), microbial growth and reactivities of the various SOM compounds. Reactivities and in particular the initial composition are difficult to determine and not well understood.

The degradation of SOM follows a first-order kinetic law (Eq. 5):

$$R = dG/dt = k * G \quad (5)$$

where R = degradation rate, G = mass of SOM and k = reactivity of SOM. In accordance with Middelburg (1989), k can be determined from the evolution of G over a time interval Δt (Eq.6):

$$k = \frac{1}{\Delta t} * \ln \frac{G(t)}{G(t+\Delta t)} \quad (6)$$

Therefore, **degradation rate (R)** is a function of the **reactivity (k)** and the amount of **SOM (G)**. In order to account for the decrease in OM degradability with time and depth, G and k are expressed as a function of time ($G(t)$; $k(t)$) (Arndt et al. 2013). These time dependencies can be described by two models: the *discrete model* and the *continuum model*.

4.1.1 The discrete model

In the discrete model (Westrich and Berner 1984), the sedimentary organic biomass (G) is described as composed by different biomass classes $G_i(t)$ with reactivities k_i . In this way, it is possible to account (1) for the heterogeneity of the SOM and (2) its degradability during the early stages of diagenesis. Therefore, at each moment in time, the total biomass G_T can be defined as the sum of all biomass classes ($G_T = \sum_i G_i$) and the total degradation rate R_T as the sum of all degradation rates (Eq. 7):

$$R_T(t) = dG_T/dt = \sum_i -k_i * G_i(t) \quad (7)$$

The reactivity k_i of each biomass G_i is defined by a kinetic model of first order. If the SOM is composed by different G_i with different k_i , then a biomass characterized by a stronger reactivity will be degraded earlier than a biomass with a weaker reactivity. We need also to keep in mind that the global reactivity R_T is continuously decreasing with depth and time as it is proportional to G_T . The main limitation of this approach is the difficulty to obtain the relative mass and reactivity of each G_i (Middelburg 1989; Boudreau and Ruddick 1991). However, results from

DSDP and ODP site samples have shown that the SOM is reactive at all depths (Robinson and Brink 2005 and references within) and therefore it is possible to consider the OM as a whole (Middelburg 1989). For this reason, the continuum model (described in the following section) is more appropriate. In addition, the continuum model allows to consider a much higher number of OM compounds as it is given, as the name suggests, by a continuous distribution of OM fractions compared to the discrete model that considers a subdivision of OM into a limited number of OM fractions.

4.1.2 The continuum model

In the continuum model, SOM is represented by a continuous distribution of OM of reactive types $g(k,t)$ that is mathematically represented by the Reactive Continuum Model (RCM) (Boudreau and Ruddick 1991). In the RCM, the reactivity k is considered a continuous variable resulting in the following integral rate R (Eq. 8):

$$R = \int_0^t k * g(k,t) * dk \quad (8)$$

In Eq 8, $g(k,t)$ represents a SOM with a reactivity between $k(t)$ and $k(t+dt)$ (Boudreau and Ruddick 1991). If we consider the degradation as a function of time, then we can approximate the degradation rate with a first order kinetics (Eq. 9):

$$R(t) = k(t) * G(t) = v (a + t)^{-1} * G(t) \quad (9)$$

where a is the initial age of the SOM and v is a shape parameter of the initial OM compound distribution (Arndt et al. 2013). High v values correspond to an OM mixture mainly composed by labile fractions which are easily degraded; low v values represent an OM mixture that is more refractory and less reactive to degradation.

Westrich and Berner (1984) computed k values for oxic plankton decomposition derived from laboratory experiments. Their results have been plotted versus time by Middelburg (1989) as shown in Figure 18.

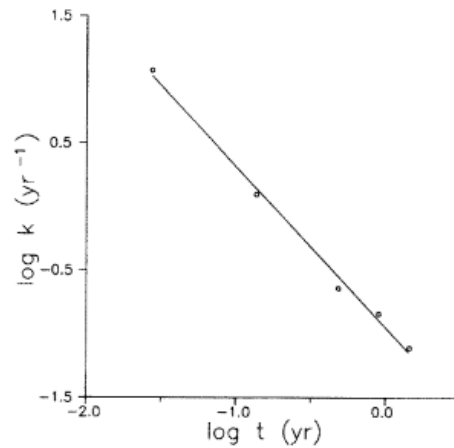


Figure 18. Reactivity (k) of Organic Carbon as function of time (t) in oxic plankton decomposition experiment presented by Westrich and Berner (1984).

At the time scale of laboratory experiments, the reactivity k of the OM decreases while being degraded. The experimental data can be fitted with a log-log linear correlation between k and time (Fig. 18, Eq 10) which has a correlation coefficient of 0.997:

$$\text{Log } k = -1.26 (\pm 0.05) * \log t - 0.95 (\pm 0.04) \quad (10)$$

In order to understand the evolution of the reactivity of SOM at the geological time scale, Middelburg (1989) derived a degradation rate from a large dataset of both, published laboratory experiments and field data (Middelburg 1989 and reference therein). The author converted the evolution of the OC with depth in cores to age with well-constrained sedimentation rates and plotted them on a diagram together with laboratory data (Fig. 19). For this plot, the author used depth intervals between each sample as Δt , and depths of the midpoint of each sample as t . Middelburg (1989) shows field and experimental data in a log-log linear correlation of reactivity with time (Figure 19) which can be expressed by Equation (11a) that has a correlation coefficient of 0.987:

$$\text{Log } k = -0.95(\pm 0.01) * \log t - 0.81(\pm 0.04) \quad (11a)$$

which can be simplified to yield:

$$k = 0.16 t^{-0.95} \quad (11b)$$

In this plot, Middelburg (1989) observed a continuous decrease of OM reactivity which is valid for field and laboratory data, as well as for anoxic and oxic environments.

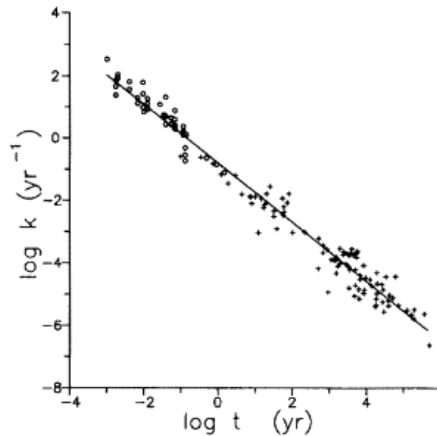


Figure 19. Reactivity of OC vs time (Middelburg 1989 and reference within). First order degradation parameters are calculated starting from Equation 6. The compilation of field work results and laboratory data covers a large range of natural environment.

In figure 19, all data samples follow the same reactivity decrease even when their initial starting point is different. In order to account for the “apparent initial age”, we can come back to Equation 9 (Janssen 1984; Middelburg 1989; Boudreau and Ruddick 1991) and describe the reactivity k as follows (12):

$$k = 0.16(a + t)^{-b} \quad (12)$$

where a is the initial age of the SOM, t is the time since the beginning of the decomposition process and $b = 0.95$. In order to account for different initial reactivities in different sedimentary environments, the degradation rate can now be described with the following power law (Middelburg 1989):

$$R(t) = 0.16 * (a + t)^{-0.95} * G(t) \quad (13)$$

The IFPEN approach for biogenic gas production at the basin scale follows the theoretical model of Middelburg (1989) for the evolution of the labile OM which is integrated with a temperature dependency function for bacterial activity (*e.g.* Fig. 5) (Ducros and Wolf 2014 – IFPEN internal report).

4.1.3 Conceptual approach for biogenic CH₄ processes at the basin scale

The chemical composition of the OM evolves with depth, reflecting the evolution of the generation of biogenic gas. In fact, as presented in figure 3, above the sulfate reduction zone, no methane is produced. Below the sulfate reduction zone, methane and CO₂ are generated by

microbial consumption of the biodegradable part of the initial OM. Therefore, the biogenic potential of a given SOM is strongly linked to the reactivity of the biodegradable TOC. As we have shown in the previous section, it is appropriate to model the evolution of the OM degradation with a continuum model such as the one published by Middelburg (1989).

In our model, the total initial TOC is composed of a refractory and a biodegradable TOC fraction. The refractory TOC represents the part of the initial TOC which can turn into HCs by thermogenic reactions. This organic part does not undergo any biodegradation and is constant during the entire simulation for biogenic production. This refractory part of the TOC is usually quantified by Rock-Eval analysis. In contrast, the biodegradable TOC is prone to biodegradation and results in the generation of biogenic gas. The biodegradable TOC is subdivided into two components: a labile fraction, corresponding to 30-40% of the initial TOC for a type II OM, and a thermo-labile fraction, corresponding to 8-15% of the initial TOC for a type II OM (Burdige, 2007, 2011, Pujol et al. 2016). The labile TOC represents the carbon fraction of the OM which is directly consumed by bacteria during the very early diagenesis phase from which biogenic gas generation is calculated. The thermo-labile TOC represents the fraction of the OM which can be trapped in the mineral matrix and therefore is protected from the microbial activity during the first diagenesis stages. Therefore, this fraction can be considered as a more refractory OM. However, it can turn into a labile OM with increasing temperature and will therefore enrich the labile pool. This process allows the release of new labile component resulting in an additional generation of biogenic gas. The transformation of the thermo-labile TOC is modeled by a first-order kinetic scheme.

The main conceptual approach for the biogenic gas generation at the basin scale is summarized in Figure 20.

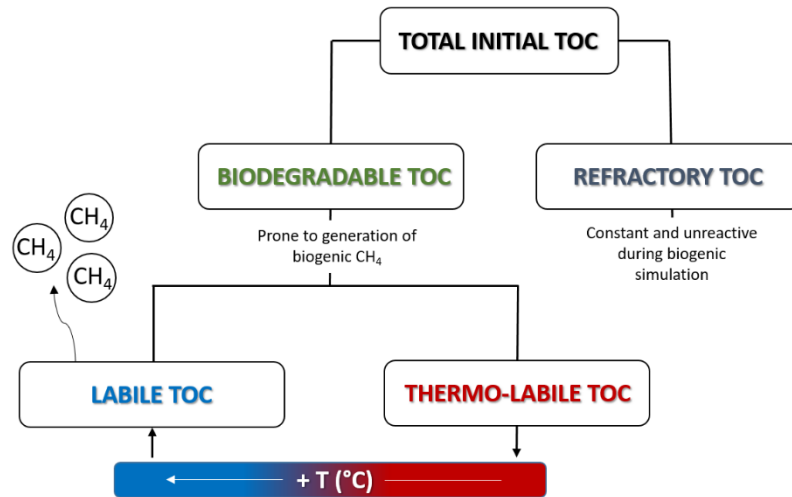


Figure 20. The main concept accounted in the biogenic gas simulator. The Total Initial Organic Carbon is composed by a refractory TOC and a biodegradable TOC which is prone to generation of CH₄. Only this last one is accounted by the simulator during biogenic CH₄ generation.

In summary, our model for the biogenic CH₄ production at the basin scale accounts for:

- The different fractions of the initial TOC: refractory, labile and thermo-labile;
- The decrease of the OM reactivity with time;
- The varying temperature during the generation of the biogenic gas;
- A kinetic thermal source of labile organic fractions evolving as function of temperature;
- The preservation of the refractory fraction (constant during the degradation process).

Therefore, a labile TOC fraction is generated twice in our model and transformed into methane through bacterial decay:

1. Right after deposition.
2. By later transformation of the thermo-labile TOC (TOCzlab) fraction.

Thus, the total labile fraction conversion is expressed as (Eq. 14):

$$\frac{\delta TOClab}{\delta t} = \frac{\delta TOClab}{\delta t} - \frac{\delta TOCzlab}{\delta t} \quad (14)$$

A detailed description of the physical laws used to represent biogenic gas processes at the basin scale is given in Chapter 5.

There are several important assumptions made in our model to simulate biogenic gas processes at the basin scale.

1. Thermogenic processes and biogenic processes are completely decoupled. The refractory TOC is considered as constant during the biogenic gas generation and it cannot produce biogenic gas. However, in nature these two processes are continuous and directly linked by the OM evolution with the increasing burial. The decreasing degradability of the OM with depth is the result of the selective preservation of the refractory part at the expense of the labile part (Arndt et al. 2013).
2. The OM degrades into methane with a ratio of 0.5 which means that for 1 mole of organic carbon (OC) we produce 0.5 mole of CH₄ and 0.5 mole of CO₂ (Fig. 21). This ratio is optimistic and not necessarily true. Indeed, this process is much more complicated, with multiple chemical reactions mainly linked to the microbial activity and the different type of methanogens. In order to better address this point in our case study, we performed a sensitivity analysis on the main input parameters of the simulator including the OM degradation ratio which is from now on considered as a variable called “*S_{bio}*”.
3. The Anaerobic Oxidation of Methane (AOM) is not accounted for in our model but actually more than 50% of the produced methane can be consumed through it (Regnier et al. 2001) (chapter 1.3.2). The geochemical transformations affecting the methane migrating upwards are not modeled. For instance, neither the methane oxidation through the sulphate transition zone nor the subsequent potential CO₂ precipitation to authigenic carbonates are computed in the simulator. However, as presented in Chapter 5, it is possible to estimate an average AOM efficiency as a function of the volume of the authigenic carbonates.

Based on these assumptions, we propose a regional basin modelling approach which helps to better understand microbial gas generation processes at geological time and space scales. It also helps to identify the distribution of biogenic gas in the subsurface and to quantify the budget of methane from the past to the present day. These calculations are important for resource estimations but also for the quantification of atmospheric emissions.

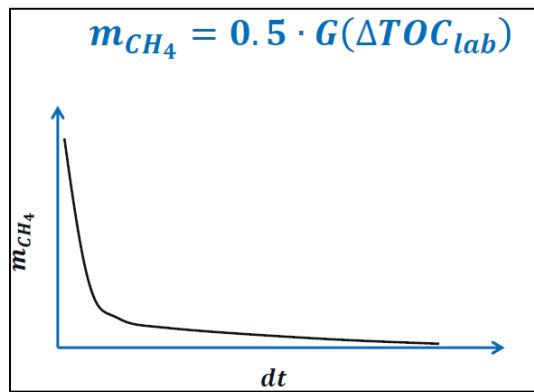


Figure 21. Example of methane mass production evolution over time (Pujol et al. 2016).

Our model requires to set up the following input parameters:

- Three types of TOC: TOC_{ref} , TOC_{lab} and TOC_{zlab} (in wt%);
- The type of the generated methane, thermogenic and/or biogenic (in our case study purely biogenic);
- The reactivity of the labile fractions;
- The activation energy for the thermo-labile fractions;
- The bacterial activity;

HC generation can be modeled using single component or multi-component kinetics. In our case it is only a single component: pure biogenic CH_4 . The main outputs are:

- the mass of CH_4 generated from biogenic production (kg/m^2),
- the total mass of CH_4 in the porous media, adsorbed and dissolved (kg/m^2)
- the total mass of CH_4 (kg/m^2) in the system.

Once biogenic gas is generated, it can migrate in the basin. As function of the basin geometry, sediment permeability, pressure and temperature conditions, the generated gas is either adsorbed to the OM or dissolved in the formation water but it can also move as a free gas phase in the sediments where it will eventually be trapped in the sediments (e.g. below a sealing formation or in form of gas hydrates), or otherwise emitted at the seafloor.

The dissolved CH_4 migrates in the water phase by advection. Depending on temperature and pressure conditions when water becomes saturated with methane, CH_4 can be instantaneously released and lost to the sea floor. This CH_4 mass is not calculated in the current version of the simulator but can be calculated as follows:

$$\text{Mass of CH}_4 \text{ lost} = \text{Mass of generated CH}_4 - \text{Total Mass of CH}_4$$

Where Total Mass of CH₄ = adsorbed CH₄ + dissolved CH₄ + free CH₄.

4.2 The TemisFlow basin model

In TemisFlow (Ungerer et al. 1990; Schneider et al. 2000; Teles et al. 2014; Torelli et al. 2020), as in other similar basin modelling tools, a sedimentary basin model is constructed with a sequence of stratigraphic layers defined by depth maps (horizons) and their corresponding geological age. Each stratigraphic layer includes a single or multiple sedimentary facies. Each facies is defined by a lithology type with its associated physical properties such as thermal conductivity, permeability, radiogenic heat production and compaction parameters. In order to reconstruct the subsidence history of the basin, geological events such as erosions or hiatuses, expressed as layers of missing section or non-deposition need to be estimated, as well as maps of paleo-bathymetry at each geological age to account for the paleo-geometry of the basin. In addition, faults need to be mapped, including their geometry and properties such as the permeability along the fault plan. Source rocks are defined by their organic facies including kerogen type and TOC content (Schneider et al. 2000) (Fig. 22).

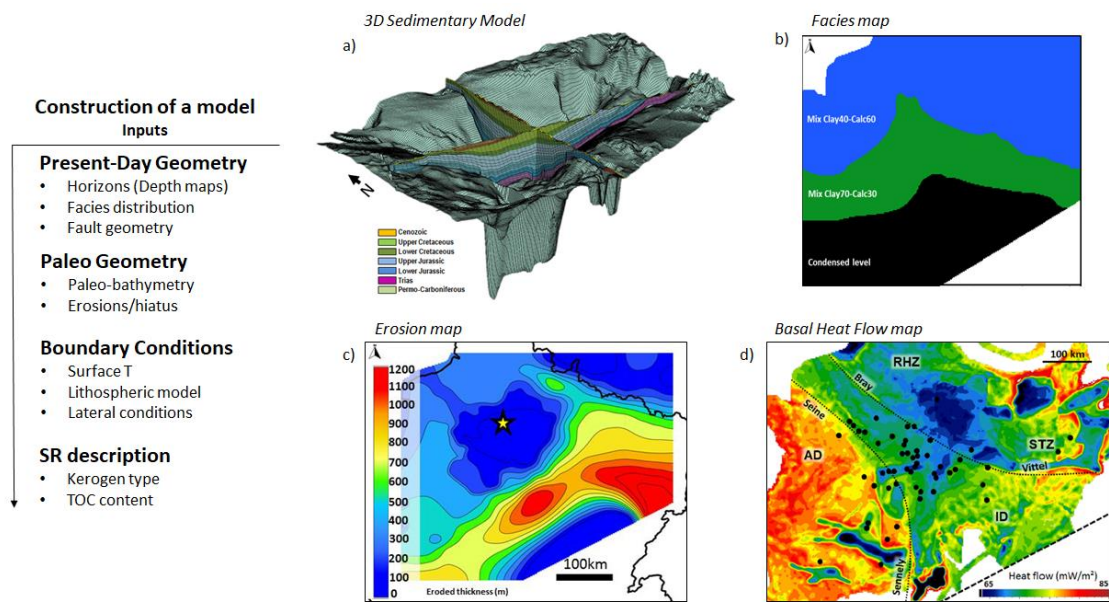


Figure 22. Main steps required to construct a basin model and examples from the Paris Basin case study (modified after Torelli et al. 2020). a) 3D sedimentary model of the Paris Basin; b) Facies map distribution including facies variations in the same horizon; c) erosion event map for the main Cretaceous erosion event; d) Basal Heat Flow carried out through a lithospheric model of the Paris Basin.

As a first calculation step, the evolution of the geometry of the basin is reconstructed backward in time using back-stripping, an automatic restauration based on vertical decompaction. In the TemisFlow software, the compaction processes are described with a double exponential porosity-effective stress law as explained in Schneider et al. (1994). Back-stripping is performed one layer at a time while correcting for compaction and possible uplift.

The second and main calculation step is a forward simulation of the poro-elastic, thermal and fluid-flow evolution of the basin, using the ages and sedimentation rates that have been determined from the back-stripping procedure. Temperature evolution is calculated according to Fourier's law while pressure and fluid flow are calculated using Darcy's law coupled with Terzaghi's law of vertical effective stress. A detailed description of the equations and physical concepts used in TemisFlow is given in Schneider et al. (2000). In order to solve this coupled system of partial differential equations numerically, maps are discretized as regular grids, and thermal and hydraulic boundary conditions are defined for each geological time step. Thermal boundaries are imposed for each geological time step at the top of the model by a map of surface temperature, and at the bottom of the model by a basal heat flow map or a lithospheric model. The hydraulic boundaries are hydrostatic at the top of the model and no-flow at the bottom of the sedimentary section. Lateral boundaries are either open or closed to flow. The spatial discretization yields a grid of cells for which the equations are solved numerically using the

method of finite volumes by mass conversation (Schneider et al. 2000). Each cell is defined by a single, effective and average value of physical or geological properties such as conductivity, porosity, permeability, compressibility etc... from which temperatures, pressures, and fluid saturations and compositions are calculated through time that vary continuously from cell to cell.

Model outputs include spatial and temporal distributions of thermal properties (thermal gradients, heat flow, source rock maturity, transformation ratio, composition of generated HCs) and flow related properties (pressure, porosity and permeability, hydrocarbon migration paths, hydrocarbon volumes and their distribution) in the basin. In order to validate the model, it needs to be calibrated. Calibration includes all relevant data from geophysical measurements (*e.g.* gravity and seismic data), from wells (*e.g.* temperature, pressure, fluids) or from geochemical or petrophysical procedures on outcrop samples, cuttings and core material (*e.g.* OM maturity, porosity, capillary pressures).

4.3 Modelling biogenic gas migration

Pressure and temperature conditions have a major control on the equilibrium phase of a gas. The gas phase stability can be determined through an equation of state which is generally defined as function of absolute pressure (P), temperature (T) and molar volume of the gas (V_m) expressed as $f(P, T, V_m) = 0$. The general equation for an ideal gas is represented by the Clapeyron equation which assumes that:

- the product PV is constant at constant temperature and low-pressure conditions
- all gases have the same V_m at the same P-T conditions.

The Clapeyron equation of state is expressed as:

$$PV_m = RT \quad (15)$$

where R as the universal gas constant ($0.08314472 \text{ bar} \cdot \text{mol}^{-1} \cdot \text{K}^{-1}$).

The ratio RT/PV_m defines the compressibility factor (Z) of a gas. Z varies with pressure and temperature. The more Z varies, the further the gas behavior is from that of an ideal gas. Therefore, the general gas equation is valid only under very limited pressure and temperature ranges (*e.g.* at atmospheric conditions). Methane does not behave as an ideal gas as it is highly

compressible. At a temperature of 290 K (~16 °C), methane can be approximated to an ideal gas only in the range of pressures lower than 15 bars (1,5 MPa) (Fig. 23) (de Almeida et al. 2014). At pressures over 15 bars, the ideal gas law is inadequate for methane.

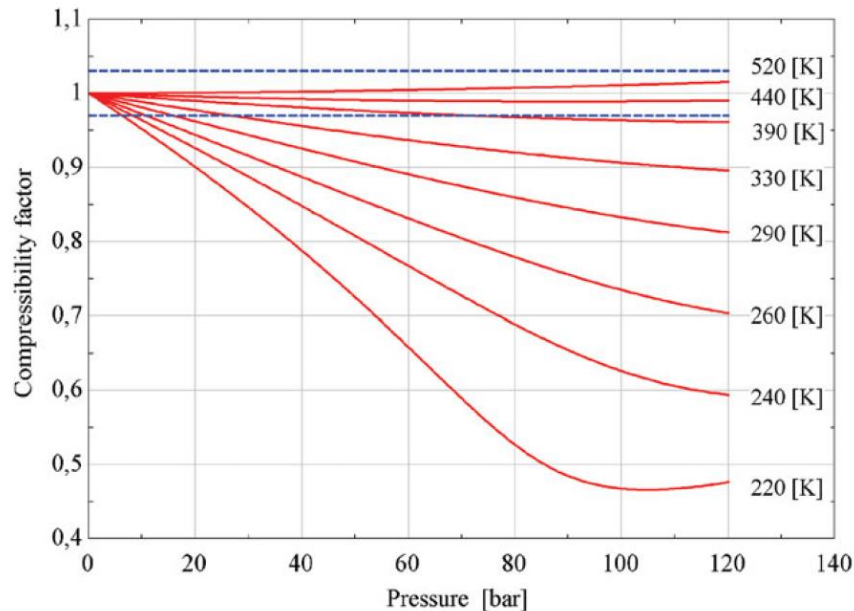


Figure 23. Compressibility factor for methane as function of temperature (K) and pressure (bar) (de Almeida et al. 2014). The ideal gas model could be used to represent the behavior of methane assuming values highlighted between the blue lines.

In a sedimentary basin, pressure and temperature increase with depth and vary over time. Once methane is generated in a source rock, other processes start to kick in as a function of the amount of generated gas and depending on pressure and temperature conditions and on salinity. The main processes controlling the fate of the generated methane in the sedimentary system are

- adsorption
- dissolution in water
- transport as a separate vapor phase.

At the pore scale, biogenic gas generation occurs at the interface of the solid OM and the pore water. First, the gas is adsorbed to the OM and, once adsorption capacity is reached, methane goes into solution in the water. Once water is saturated with methane, the gas can be present in a vapor phase. Therefore, in our approach, the gas is modeled sequentially as follows (Fig. 24):

1. Adsorbed to the OM according to the Langmuir mechanism.

2. Dissolved in the water following the model published by Duan et al. (1992).
3. Free in the vapor phase following multi-phase Darcy's flow.

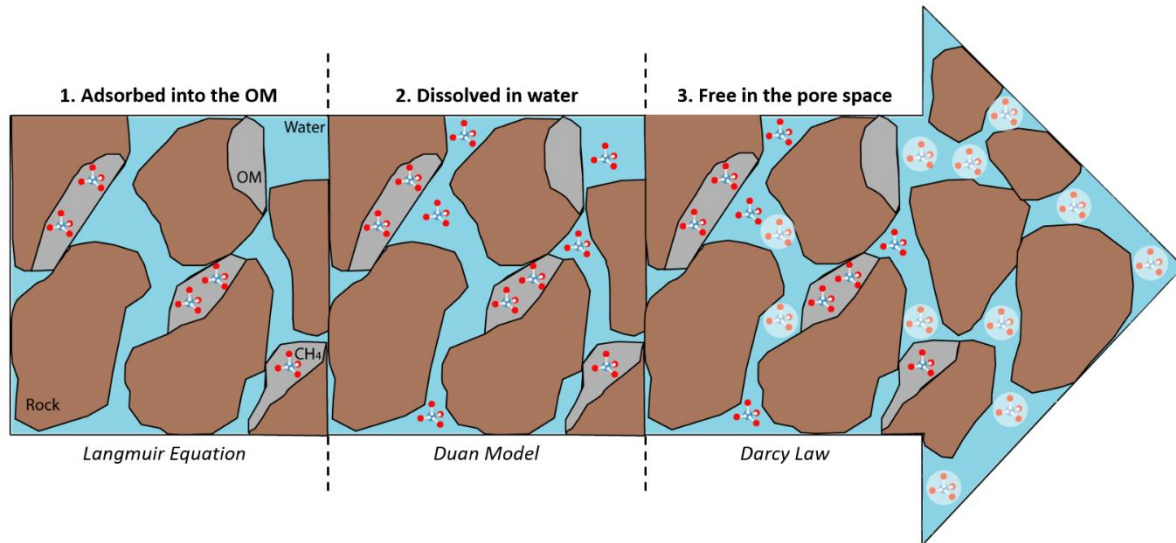


Figure 24. Evolution of the generated biogenic CH₄ in TemisFlow. 1) The generated biogenic methane is firstly adsorbed onto the OM. 2) Once the sorption capacity is reached, the biogenic methane is dissolved in the water. 3) Once the water is saturated in gas, the biogenic methane can migrate in the vapor phase.

4.3.1 Modelling adsorption of biogenic gas

Adsorption is a physical process through which the solute or adsorbate (here the biogenic gas) penetrates within the solid or adsorbent (here the OM) *via* diffusion. The adsorption capacity varies as function of the adsorbent type and surface, and pressure and temperature conditions (Young and Crowell 1962). The first methane molecules of the biogenic gas that are generated by the source rock are adsorbed to the OM itself. Adsorption is the first process affecting the generated biogenic gas. Pressure and temperature have opposite effects on the sorption capacity. An increase in pressure favors adsorption. In contrast, as temperature increases, the sorption capacity decreases.

As adsorption evolves with increasing temperature (T) and pressure (P), the amount of adsorbate (n) can be described with isotherms that are empirically defined (Eq. 16):

$$n = f(P)_T \quad (16)$$

In our model, the adsorption capacity is defined in accordance with the Langmuir isotherm. The Langmuir model is based on the following assumptions:

- adsorption is localized and only allows the formation of a monolayer of adsorbate;
- adsorption sites are equivalent, and the adsorbent surface is homogeneous;
- one site can host only one adsorbate molecule;
- no interaction exists between the molecules in different sites.

This model implies a limited number of available adsorbent sites (Eq. 17).

$$m_a = \frac{m_{a,max} K_L c}{1 + K_L c} \quad (17)$$

where $m_{a,max}$ = maximum mass of solute which can be adsorbed in one monolayer of the adsorbent surface, K_L = ratio between the reaction rate constants for adsorption (k_a) and desorption (k_d), c = molar concentration of the adsorbate in the solution.

The Langmuir isotherms that describe the adsorption of methane on the OM in TemisFlow are shown in Figure 25. The same isotherms are used for the adsorption of methane on the source rock during methanogenesis. Pressure has a major impact on the adsorption capacity where higher pressures are favorable for adsorption for a given temperature (Young and Crowell 1962).

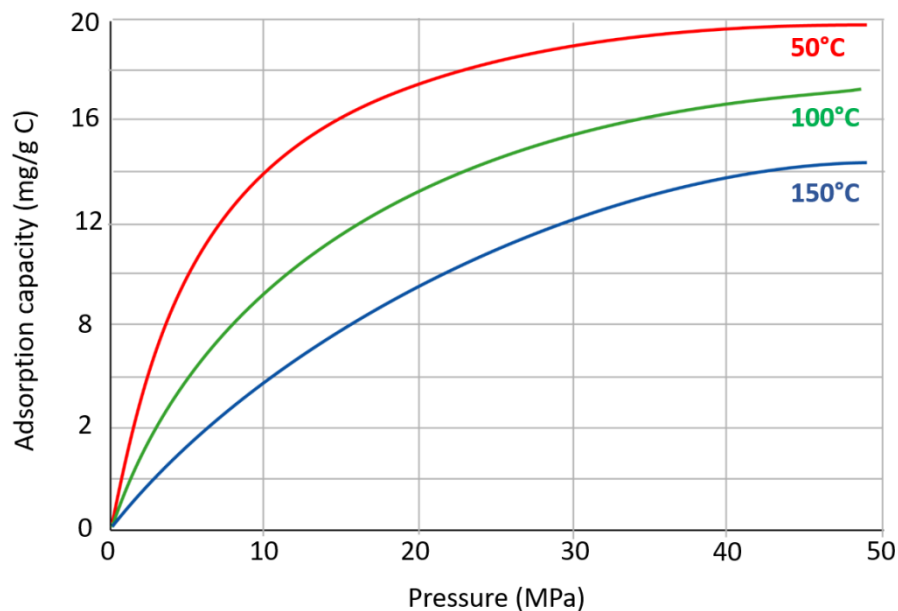


Figure 25. Langmuir isotherms defined in TemisFlow to account for the gas adsorption on the OM during methanogenesis.

4.3.2 Modelling dissolution of methane in pore water

To better assess the migration of biogenic methane after generation and adsorption, methane can dissolve in the formation water (pure or brine) and be transported by advection. Methane solubility is determined based on the thermo-dynamic properties of the H₂O-CH₄-NaCl system. Different empirical laws (Price et al. 1981; McGee et al. 1981; Spivey et al. 2004) and equations of state (Duan et al. 1992, Part I; II) have been tested for basin simulators to describe the methane solubility (Guichet 2015, Internal IFPEN Report). In TemisFlow, methane solubility is described according to the equation of state published by Duan et al. (1992). We consider that only one component (CH₄) can be dissolved in water as a function of salinity which is constant over time and space.

The Duan Equation of State

A cubic equation of state (EoS) has been published by Duan et al. (1992, I) for pure systems (CH₄, CO₂, H₂O) from zero to 1000 °C and from zero to 8000 bar. This EoS has been extended for mixture systems from 50 to 1000 °C and zero to 1000 bar (Duan et al. 1992, II). Duan et al. (1992) published also an algorithm to predict methane solubility in natural waters from zero to 250 °C and from zero to 1600 bar. Methane concentration in brines is described as a function of methane content, methane fugacity in the vapor phase, its chemical potential in the liquid phase, water salinity and temperature. The previously published EoS is used to calculate the fugacity coefficient of methane (at fixed T, P and salinity) and a Pitzer formalism is used to determine the coefficient of activity of the dissolved methane. Chemical potential and interaction coefficients are polynomial functions of temperature and pressure. For further details, the reader is referred to Duan et al. (1992).

4.3.3 Modelling migration as a free gas phase

Methane is in a free gas phase whenever methane saturation is reached in the water phase. Migration in the vapor phase follows Darcy's law for a diphasic model of water and HC. The hydrocarbon phase is composed of a single component which can migrate in the basin over time (Schneider et al. 2000).

The migration process is described by two different phase velocities for gas and water which are each composed of a pressure term and a gravity term where the difference between the two pressures is given by the capillary pressure (Eq. 18, 19):

$$\vec{V}_g = - \frac{k k_{rg}}{\mu_g} (\overrightarrow{grad} (P - P_c) - \rho_g \vec{g}) \quad (18)$$

$$\vec{V}_w = - \frac{k k_{rw}}{\mu_w} (\overrightarrow{grad} (P) - \rho_w \vec{g}) \quad (19)$$

Where:

- \vec{V}_g, \vec{V}_w = gas and water velocities;
- k = sediment permeability (m²);
- k_{rg}, k_{rw} = the relative permeabilities of gas and water (dimensionless);
- μ_g, μ_w = dynamic viscosities of gas and water (Pa s);
- P = water pressure (Pa);
- P_c = capillary pressure (Pa);
- ρ_g, ρ_w = gas and water densities (kg/m³);
- \vec{g} = acceleration of gravity (m.s⁻²).

4.4 Trapping and sinks of biogenic gas

Once the biogenic gas migrates in the vapor phase, it can be trapped either in structural traps, or in stratigraphic traps in the sediments, or as a solid phase, *i.e.* as gas hydrate. In the TemisFlow simulator, gas hydrate is not modeled explicitly but the probability of the presence of hydrates can be calculated using post-processing that does not need any calculation of biogenic methane production in the basin. The stability of hydrates is calculated as a function of pressure and temperature during the geological history of a basin. This “Hydrate risk” is expressed in time (My) corresponding to a residence time in the hydrate stability zone (favorable P-T conditions).

For one of the case studies, the Aquitaine Shelf, the absence of hydrates (Ruffine et al. 2017; Dupré et al. 2020) is confirmed by the 3D basin model, given present-day temperature and pressures condition (Fig. 26). Small areas of the basin are characterized by temperature, pressure and depth conditions that are consistent with a high probability of hydrates occurrence. In our model, these favorable conditions are most probably related to boundary effects. In addition, the distribution, thickness and depth of such small areas of the basin are not sufficiently large to store any gas in a solid phase. Pressure and temperature values from wells

confirm that the Aquitaine Shelf falls outside the methane hydrates window, as shown by the hydrate stability plot (Fig. 26).

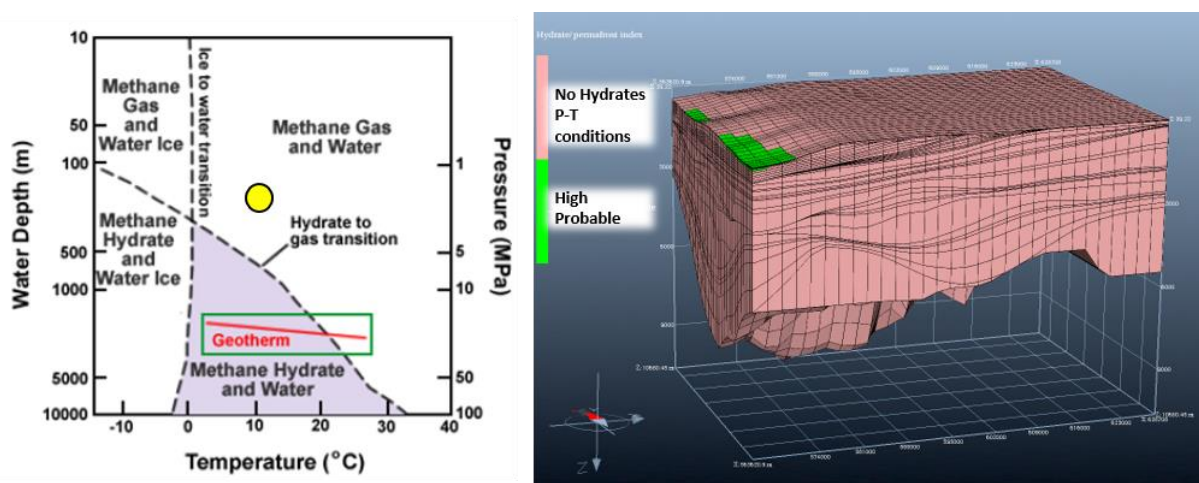


Figure 26. The presence of gas hydrates is linked to pressure and temperature conditions at given depths shown in the diagram on the left (modified after Kearns 2018). In the diagram, the Aquitaine Shelf (yellow dot) falls outside the methane hydrate window (temperature of 12°C at 150 m of water depth) (Marié et al. 2019; Dupré et al. 2020). When the property of hydrate formation in the TemisFlow simulator is activated (right figure), there are no P-T conditions to accumulate methane in the solid phase.

4.5 Critical parameters for biogenic gas generation and migration

One of the main issues related to basin modelling is insufficient data availability and quality. It is rarely possible to have access to sufficient data that are required to fully construct and constrain a basin model, or sometimes available data are of poor quality. In that case, the available dataset is characterized by large uncertainties. In addition, basin models are forward models and therefore fundamentally deterministic. Given the uncertainties and limited amount of data to constrain input parameters, different modelling results may fit the same data (so called model non-uniqueness). In that case, sensitivity analysis is a commonly used procedure to determine the impact of input parameters on the modelling results and the interaction between such input parameters and multiple interrelated processes. If an input parameter only has an insignificant impact on the simulation result, it may be discarded from the sensitivity analysis. Therefore, sensitivity analysis can discriminate, prioritize and optimize the main uncertain input parameters. Once important input parameters have been identified, they can be adjusted in such a way to minimize the difference between calibration data and model output. For example, modeled temperatures (model output or results) are compared with measured temperatures in wells. Input parameters that have been identified in the sensitivity analysis as critical to model temperatures can be adjusted to minimize the difference between modeled and observed

temperatures. As temperature measurements have themselves uncertainties stemming from the way how they have been measured in wells (e.g. Modular Dynamic Formation Tester (MDT) temperatures have a higher accuracy compared to Bottom Hole Temperature (BHT) that need to be corrected for cooling due to drilling mud and circulation time), a reasonable fit requires to fall within the range of such temperature measurements. The larger the uncertainty of the observed data, the less constrained will be the model result (e.g. MDT temperatures represent better constraints to the model as they are more accurate than uncorrected BHT temperatures). This procedure is also called “inversion” and automatized inversion methods can be applied also to basin modelling.

Simulating the biogenic gas generation at the basin scale involves parameters that are highly interrelated such as TOC partitioning, OM degradation rates, activation energies for the thermo-labile component and the microbial activity curve. However, also less obvious factors could have an impact on the generation of biogenic gas such as, among others, water salinity, sediment porosity or type of microbes residing in the system. In order to improve our understanding of biogenic gas at the basin scale, we performed a sensitivity analysis on the main processes involved during the biogenic gas generation and migration.

The approach presented here is based on the Global Sensitivity Analysis (GSA) methodology published by Gervais et al. (2018). It consists of analytical functions (metamodels or response surfaces) that are computationally fast to create (Wendebourg 2003). This statistical approach gives an idea of the relation between input parameters and model output properties that is based on a limited set of input parameters generated by Latin hypercube sampling (Gervais et al. 2018; Bruneau et al. 2018). This method quantifies in each location of the basin the influence of those input parameters that can help to rank the influence of each process of biogenic gas generation and gas distribution in the basin. Model input parameters are considered independent random variables with associated probability distributions (Gervais et al. 2018).

5. A case study from the Offshore Aquitaine (Paper in Marine and Petroleum Geology, 2021)

The following paper focuses on a basin-scale application of all concepts of biogenic gas generation and migration discussed in the previous chapters. The purpose of this study is a better understanding of biogenic methane through numerical modelling of the generation and migration processes which can help estimate the total methane emitted naturally from shallow-water shelf areas. It proposes a new workflow to assess and predict biogenic gas occurrences in offshore environments where gas is sourced from recent continental-derived OM. It accounts for different OM compounds (presented in section 4.1.3) which are partially degraded by microorganisms during the early diagenesis stage resulting in methane production. It also accounts for a major sink of methane in form of MDACs. The application area is the offshore Aquitaine where a basin model is constructed as described in section 4.2. The main model input parameters are identified and ranked with a sensitivity analysis as described in section 4.5.

Quantification of natural microbial methane from generation to emission in the offshore Aquitaine: A basin modelling approach Published in Journal of Marine and Petroleum Geology

Martina Torelli¹, Isabelle Kowalewski¹, Veronique Gervais¹, Johannes Wendebourg², Stéphanie Dupré³, Sylvie Wolf¹, Claude Gout⁴, Eric Deville¹

¹IFP Energies Nouvelles, 92852 Rueil-Malmaison Cedex, France

²Total Exploration Americas, Houston, TX, 77027, USA

³Ifremer, Géosciences Marines, 29280 Plouzané Cedex, France

⁴Total, Exploration and Production, Pau Cedex, France

DOI: <https://doi.org/10.1016/j.marpetgeo.2021.104949>

ABSTRACT

Marine sediments near continental margins contain sedimentary organic matter (SOM) which is subject to the metabolic activity of micro-organisms during early diagenesis resulting in production of biogenic methane. This process occurs at microscopic scale and anaerobic conditions. Here, we apply a new numerical approach to simulate biogenic methane production offshore Aquitaine (Bay of Biscay) where gas seeps have been recently observed as the result of microbial activity. This new approach accounts for: (1) degradation of a labile-SOM fraction to methane, (2) first order kinetics of the thermal degradation of a thermo-labile-SOM fraction into labile fraction at greater burial and (3) decrease of SOM reactivity with time. First, the organic matter is characterized through pyrolysis using Rock-Eval performed on cuttings

collected from two wells located within the methane seepage area. The microbial system is fed from a type III continental-derived SOM which is immature (average $T_{max} < 425^{\circ}\text{C}$). The basin model is built and calibrated on seismic and well data. It accounts for the consumption of methane required to precipitate methane-derived authigenic carbonates which are found widely distributed on the seafloor as the result of the anaerobic oxidation of methane during upward migration. A sensitivity analysis is performed on the main model input parameters to quantify their impact on the biogenic gas production and expulsion/migration processes. Results led to a reference scenario for microbial gas production in offshore Aquitaine. With this model the generated methane is predominantly dissolved in water and transported by advective processes. Migration is mainly vertical from the source rock layers to the seafloor and controlled by sediment porosity and strata geometry. Modelling can reproduce natural processes such as gas migration at emission points (gas seeps) which have been previously mapped in the offshore Aquitaine Basin. Our results suggest that the biogenic methane is sourced by a present-day active system with a mean flow rate of 27 Mg/y which is relatively lower than flux modelled during the early Pleistocene reaching up to 41 Mg/y. Calculated total methane lost to the seafloor along the Aquitaine Shelf is in accordance with methane flow rate estimated from in situ measurements and acoustic signatures of bubbling sites, and ranges between 0.87 Tcf/My and 1.48 Tcf/My. Here we propose a new workflow to assess and predict biogenic gas occurrences in offshore environment at the basin scale where gas is sourced by recent continental-derived organic matter. This new approach can help to better assess the total biogenic methane budget emitted naturally in the shelf area of oceans that may reach the atmosphere with a negative impact on climate and environment.

Key words: Biogenic Methane, Basin Modelling, Methane-Derived Authigenic Carbonates (MDAC), Anaerobic Oxidation of Methane (AOM), Sensitivity Analysis, Sedimentary Organic Matter (SOM), Aquitaine Shelf

1. INTRODUCTION

Over the last few decades, natural gas has received increasing attention concerning its application as a major and cleaner energy source compared with coal and liquid fossil fuel (Rice and Claypool 1981; Rice 1992; Whiticar 1994; Kvenvolden 1993; Katz 2011). It is estimated that the annual methane emission from geo-sources only (onshore mud-volcanoes, onshore gas-oil seep, submarine seepage, micro-seepage, geothermal-volcanic manifestations) directly in the atmosphere yields between 27 – 63 Megatons (Etiopie and Schwietzke, 2019), with a negative impact on the global climate (IPCC, 2013; Khalil et al. 1993; Judd et al. 2002; Dickens 2004). Even though several estimates have been published over the past years (Hornafius et al. 1999; Judd et al. 2002; Judd et al. 2004; Kvenvolden et al. 2001; Etiopie et

al. 2008; Etiopie and Klusman 2010) our understanding of the methane budget is still uncertain (Etiopie and Klusman 2002; Saunio et al. 2016; Schwietzke et al. 2016; Etiopie and Schwietzke 2019) especially concerning the potential of natural methane sources from sedimentary basins resulting from microbial activity and/or thermal cracking of buried sedimentary organic matter (Klusman et al. 2000; Etiopie and Klusman 2002). It is well accepted that fluid emanations through the ocean floor are ongoing processes represented by characteristic geological features that are widely distributed along near-shore, continental slope and in deep ocean. They include shallow gas accumulations, pockmarks, seeps, mud-volcanoes, authigenic carbonate precipitations and gas hydrates (Jensen

1992; Römer et al. 2012; Skarke et al. 2014; Dupré et al. 2007; Pierre et al. 2017a; Hovland et al. 2002; Judd et al. 2002).

Methane generation is the result of Sedimentary Organic Matter (SOM) degradation which takes place at different diagenesis stages (Whiticar et al. 1986; Floodgate and Judd 1992; Whiticar 1999; Schulz and Zabel 2006). In addition to the degradation process of SOM, methane production is controlled by other factors such as temperature, primary productivity, sedimentation rate (Clayton 1992; Judd et al. 2002) and the microorganisms mediating the reaction (Boetius et al. 2000). Biogenic systems can be sourced by poorly-OM layers (TOC < 0.5%) (Clayton 1992). This process is usually observed in deltas where large amounts of sediment are deposited in a short time, containing low continental-OM dispersed in sediments such as the Amazon Delta (TOC ~ 0.8%) (Arning et al. 2013) or in the Japanese Pleistocene turbidite sequences of the eastern Nankai Trough (TOC ~ 0.5%) (Fujii et al. 2016). Methanogenesis in low organic matter sediments is also observed in the Great Australian Bight (TOC < 0.4%) (Mitterer 2010) and in the Woodlark Basin (TOC < 0.4%) (Wellsbury et al. 2002). Therefore, a better understanding of the microbial gas generation process at a large scale is necessary to identify the distribution of methane in the subsurface. In addition, quantifications of natural methane sources and sinks, both at the present day and in the geological past, are of interest to the scientific community working on present and future global climate change (Regnier et al. 2011; Saunois et al. 2016).

Numerical modelling is a way to study the interactions of the various geological processes leading to biogenic gas generation, accumulation and migration as these interactions cannot be reproduced in the laboratory given the large spatial dimensions and the slow natural reaction and migration rates. Modelling can be used to critically evaluate and discuss the significance and the role of the main parameters that lead to biogenic gas accumulations. However, it is a challenge to integrate the microscopic processes

of methane production at the basin scale. In this paper, we present a quantitative model of the total methane volume generated from microbial activity and emitted offshore Aquitaine (Bay of Biscay, SW France) that is compared with an estimation of emitted methane based on both in situ measurements and acoustic records of a few thousand bubbling sites (Dupré et al. 2020) (Fig. 1). Our approach consists in simulating the biogenic gas generation and migration with a 3D basin model of the study area using a recent numerical implementation for microbial processes modified after Pujol et al. (2016).

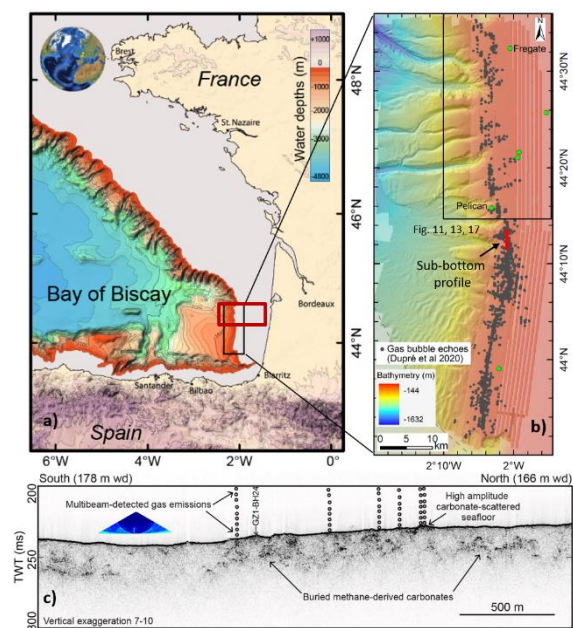


Figure 1. a) Bathymetric map of the Bay of Biscay (Southwestern France) and modelled area (red rectangle) of Fig. 3 modified after Sibuet et al. (2004) and Dupré et al. (2020); b) Detailed shaded bathymetric map offshore Aquitaine (Loubrieu 2013, Gazcogne1) with gas emission site distribution and localization of the sub-bottom profile (red line) shown in Fig. 1c and the modelled offshore area in Fig. 1b (black rectangle) (modified after Dupré et al. 2020); c) Sub-bottom profile acquired in the emission site showing the presence of sub-cropping methane-derived authigenic carbonates from Dupré et al. (2020).

For biogenic gas generation, our model considers that the initial Total Organic Carbon (TOC) can be partitioned into three different fractions (Fig. 2). A labile fraction called TOClab is composed by the OM that is sensitive to biodegradation from the

beginning of deposition (Wallman et al. 2006). A thermo-labile fraction called TOC_{zlab} is composed by the OM that is less reactive and therefore can be preserved in the mineral matrix (Burdige et al. 2007, 2011). The third bio-refractory fraction called TOC_{bio-ref} represents the part of the OM which is later converted to hydrocarbons by thermal cracking when the temperature increases above 80°C (Fig. 2). In our model, this temperature corresponds also to the pasteurization temperature of the micro-organisms (Rice and Claypool 1981; Clayton 1992). Average percentage of TOC_{bio-reactive} for a typical Type II marine OM are: TOC_{lab} = 30-40% (Burdige 2007; Wallmann et al. 2006) and TOC_{zlab} = 8-15% (Burdige 2011). Unfortunately, such fractions have not been described for continent-derived terrestrial type III-OM such as found in the Offshore Aquitaine (Michel 2017). It is well known that terrestrial organic matter is mainly composed by higher plants characterized by lower hydrogen and higher oxygenated functional groups contents than marine OM (Burdige 2011; Kamga 2016). When entering in the marine environment, the terrestrial OM is probably already highly altered (Zonneveld et al. 2010). Then, the degradation of OM is followed by an evolution of its molecular composition and its association with the mineral matrix, which tends towards an increasingly refractory nature. As a result, type-III OM dispersed in sediments is less reactive and more thermally-resistant than type II organic matter specially at low temperature (Cowie et al. 1992; Burdige 2007, Kamga 2016). Here, we described the OM based on data available in the literature concerning the geochemical characterization and degradation rate of recent continental-OM (Cowie et al. 1992; Martens and Canuel 1996; Hedges and Oades 1997; Burdige 2007, 2011). However, the fraction of the terrestrial organic carbon preserved in marine sediments is still poorly constrained.

The offshore Aquitaine is a unique case study as (1) methane is purely of microbial origin and not related to a thermogenic petroleum system or gas hydrates, (2) there is evidence of persisting methane circulation over time in the form of

Methane-Derived Authigenic Carbonates (MDAC) pavements and (3) the quantity of released methane along the shelf at the present day is rather widespread and important (144 Mg/y) (Dupré et al. 2014; 2020; Pierre et al. 2017a; Ruffine et al. 2017). In this study, we build a 3D sedimentary model of the offshore Aquitaine that includes a lithospheric model allowing to account for the thermal history of the basin. The model is calibrated with eleven wells that are regionally distributed over the study area (Fig. 3). It also takes into account the MDAC deposits. However, as mentioned above, some parameters related to biogenic gas generation are still uncertain. Thus, we performed a sensitivity analysis to study the impact of these parameters on biogenic gas generation. More precisely, we sampled the parameter space and simulated gas generation and migration for the corresponding set of models to estimate sensitivity indices. Finally, we used the available gas flow rate data to identify a realistic scenario among the sample. The biogenic CH₄ budget for the offshore Aquitaine was calculated for this model, taking the presence of MDAC into account, and compared with locations and quantities of observed natural emissions. According to our results, a gas system originating from only microbial activity can be active over millions of years and can generate important volumes of methane which may either be trapped in the sediments or directly escape to the seafloor, depending on the specific geological settings.

The paper outline is as follows. First, the geological setting of the case study is introduced, followed by a description of the data set used to build the 3D basin model. The workflow used to quantify the generated biogenic gas is described in section 4. It encompasses the definition of the 3D sedimentary model, the modelling of the processes of biogenic gas production and migration, and the sensitivity analysis on the uncertain parameters. The application of this workflow to the Aquitaine Basin is described in section 5, followed by some discussions of the results in section 6.

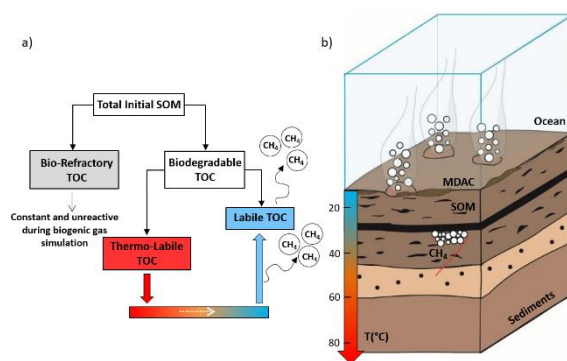


Figure 2. a) Schematic diagram of the microbial gas generation concept. The gas is generated during the early diagenesis stage by the labile TOC. At greater burial and depth, the transformation of the thermo-labile TOC allows to produce new labile fraction that generate new gas. The bio-refractory TOC is non-reactive and constant during biogenic gas simulation but it can be transformed into hydrocarbons by thermogenic cracking at greater temperature ($> 80^{\circ}\text{C}$). b) Schematic block diagram offshore Aquitaine.

2. GEOLOGICAL SETTING

Geodynamic Evolution of the Bay of Biscay

The study area is located in the Bay of Biscay which is bordered by the Armorican Shelf in the North and by the narrow and shallow Basque plateau in the South (Ferrer et al. 2008; Roca et al. 2011; Tugend et al. 2015). The opening of the Bay of Biscay was influenced by the structuration of the Variscan orogeny and is the result of different extensional and compressional cycles (Tugend et al. 2014), and notably two rift systems (Ferrer et al. 2008; Tugend et al. 2014): a first North Atlantic rifting phase at the beginning of the Triassic, followed by a second rifting phase during late Triassic to early Jurassic which induced crustal thinning (Boillot et al. 1979) and the formation of intracontinental basins such as the Aquitaine Basin. During the Santonian, the opening of the Atlantic Margin induced a compressional deformation in the southern Bay of Biscay and a weak compressive reactivation in the northern area (Thinon et al. 2001; Tugend et al. 2014). This compressional movement led to the inversion and reactivation of extensional structures which initiated the Pyrenean orogenesis. The major compressional phase was reached during the

Eocene and lasted until the end of the Oligocene. It resulted in the accretion of the Pyrenean chain and the formation of the foreland Aquitaine Basin (Tugend et al. 2014). The main target area of our study is the Aquitaine Shelf (Fig. 1) which is part of the offshore Parentis Basin and also represents the main hydrocarbon province of France (Biteau et al. 2006). It is filled-up with 15 km of sedimentary cover over a relatively thin crust (Biteau et al. 2006; Bois et al. 1997; Ferrer et al. 2008).

Stratigraphic Framework

This section presents an overview of the Aquitaine Basin stratigraphy. For a more detailed stratigraphic description, readers can refer to Biteau et al. (2006).

The sedimentary column is composed at the bottom of a thick evaporitic sequence (anhydrite and salt) deposited in the Triassic during a period of high subsidence.

During the Jurassic, deposition was mainly characterized by the development of a westward carbonate shelf: limestones and shale during the Lias, limestones and dolomites during the Dogger. In Oxfordian time, extensional tectonics accelerated which led to the differentiation of the Bay of Biscay into various structural units such as the Parentis Basin where limestone deposition continued, with locally condensed sections until the Kimmeridgian (Biteau et al. 2006). During the late Jurassic the depositional environment became increasingly marine followed by the deposition of the “Mano Dolomite”.

The Early Cretaceous corresponds to the deposition of undifferentiated marly sediments representative of a shelf environment. During the Aptian, sediments in the Parentis area were characterized by carbonate deposits marking a transgressive period. During the Albian, pelagic shales were deposited, including locally clastic turbidites. The Pyrenean compression started during the Upper Cretaceous when the Parentis Basin continued to record a thick sequence of shaly limestones and clays (Biteau et al. 2006).

The beginning of the Cenozoic was a period of decreasing sedimentation rates within an open marine context where the continental influence was marked by the presence of numerous marls. During the Oligocene a carbonate shelf developed westwards filled with marly deposits. From the Miocene until today, the area was covered by continental sediments.

Fluid escape features in the Aquitaine Basin

An active fluid system along the Aquitaine Shelf was recently discovered based on previously acquired data collected during recurrent marine expeditions conducted by Ifremer (Pegase98, <https://doi.org/10.17600/98040070> and Pelgas2000 to 2011, <https://doi.org/10.18142/18>). Several echo soundings were recorded in the water column caused by gas bubbles located at 140-220 m water depth (Dupré et al. 2014). This fluid system has been further assessed during the GAZCOGNE1 (Loubrieu 2013) and GAZCOGNE2 surveys (Dupré 2013). It extends over 375 km² along the Aquitaine Shelf, with 2612 bubbling sites (Dupré et al. 2020) (Fig. 1).

Molecular and isotopic analysis on gases (δD and $\delta^{13}C$) revealed that these fluids are composed of almost pure biogenic methane (> 99.94% mol of the gases) generated from CO₂ reduction (Ruffine et al. 2017) without any link to the thermogenic sources from the Parentis Basin. Associated with these gas escapes, authigenic carbonate pavements are widely developed above and below the sub-seafloor over 375 km² (Pierre et al. 2017a; Dupré et al. 2020). The bubbling sites, as well as the authigenic carbonates, are located east of the continental shelf break (Fig. 1) and no such activities were observed along the slope or inside the erosional canyon where the uppermost Pleistocene layers were removed (Michel et al. 2017; Dupré et al. 2020). Plio-Pleistocene and Holocene deposits are potential candidates for the source layers from which the microbial methane is generated (Dupré et al. 2020) as they record high sediment and organic matter supply (Cremer 1983).

Several scenarios for the source rock layers were investigated by Michel (2017). Based on regional horizon geometry from seismic data, geochemical evidence from Rock-Eval analysis and potential migration pathways, the source rocks for microbial methane are most likely located within the Upper Pleistocene progradational units (Michel 2017). However, based on the regional thermal gradient (Biteau et al. 2006) and temperature ranges for microbial activity (Katz 2011), it cannot be excluded that deeper source rocks may also contribute to the microbial gas generation (Dupré et al. 2020).

The isotopic signature of the carbonate cements demonstrates that these sedimentary features are the result of Anaerobic Oxidation of Methane (AOM) (Pierre et al. 2017a). The precipitation of the methane-derived authigenic carbonates takes place within the Sulphate-Methane Transition Zone (SMTZ) which corresponds to an oxic-anoxic boundary located in most cases below the seafloor at variable depth (Boetius et al. 2000).

These shallow-water seeps in the Aquitaine Basin are very different from classical deep-sea cold water seeps. As proposed by Pierre et al. (2017a) this system could be compared with seeps found along the northern U.S. Atlantic Margin (Pierre et al., 2017b) where methane emission sites have been discovered at 50-1700 m water depth as the result of freshwater discharge to the seafloor more than 100 km away from the coast (Cohen et al. 2010; Skarke et al. 2014). Indeed, based on the oxygen isotopic signature of bulk carbonate and aragonite cements, MDAC from the Aquitaine Shelf precipitated from a mixture of seawater and freshwater as the result of submarine groundwater discharge at the seafloor (Pierre et al. 2017a). This fluid system is highly dynamic. Therefore, it is easily influenced by the depth variations of the AOM and SMTZ, and possibly by the amount of groundwater discharge at the seafloor and along the slope where the erosion within canyons partially removed the uppermost sources of the biogenic methane.

This process linked to the precipitation of MDAC could be the reason why the location and

migration of the methane seeps occur east of the shelf break. Indeed, emission sites are mainly located along a narrow band oriented N-S parallel to the Aquitaine Shelf with highly variable amount of emitted gas or MDAC deposits (Dupré et al. 2020). The fluid activity is more intense in the southern part of the basin compared with the northern part and the same differences are observed for the MDAC deposits which are widely distributed in the southern part and more localized in the northern area (Dupré et al. 2020). Note that both thickness and initial age of the MDAC are still unknown. Based on Dupré et al. (2014; 2020) gas migration pathways are mainly controlled by sedimentary processes (indicated by precipitation of MDAC) rather than by tectonic activity (faults). As MDAC pavements can have a major control on the gas migration and they represent a major sink for methane, we accounted for the AOM in our model. The study area is located in the northern part of the Aquitaine Basin where the flow rate of methane emitted into the water column is estimated to be around 35 Mg/y (Dupré et al. 2020) (Fig. 1b).

3. DATA SET

Source rock samples

The geochemical characterization of the organic matter was done through Rock-Eval analysis (Espitalié et al. 1977; Espitalié et al. 1985; Lafargue et al. 1998). Based on previous studies (Michel 2017; Dupré et al. 2020) and on the

regional geothermal gradient (Biteau et al. 2006), it is accepted that the main target zone for biogenic gas production in our system is located at shallow depths in the Plio-Pleistocene progradational systems. However, deeper source rocks may take part in the generation of microbial methane (Dupré et al. 2020). Thus, we collected samples between 595-1530 m bsf in the Plio-Pleistocene to upper Miocene sediments (Table S1). Exploration wells usually target reservoirs and not source rocks that are deeper so that samples from cores are rarely available at these depths. Nevertheless, 20 cuttings were collected from two exploration wells (Pelican-1, Pingouin-1) located at the external shelf area (Fig. 3). Cuttings are broken pieces of rocks derived from drilling processes. They are used to make a record of the investigated rock with a depth uncertainty of around ± 15 m related to recovery operation. Considering that the minimum thickness of the source rock layers defined in our model is greater than 15 m, this uncertainty was assumed acceptable for our case study. All samples were washed, desalted and prepared in accordance with the procedure applied at IFPEN (Lafargue et al. 1998; Behar et al. 2001).

Maps and well data

Interpreted seismic horizons from the top basement to Cretaceous were taken from the OROGEN project (funded by Total, BRGM, CNRS & INSU), and from base Miocene to seabed from Ortiz et al. (2020), and they were used to

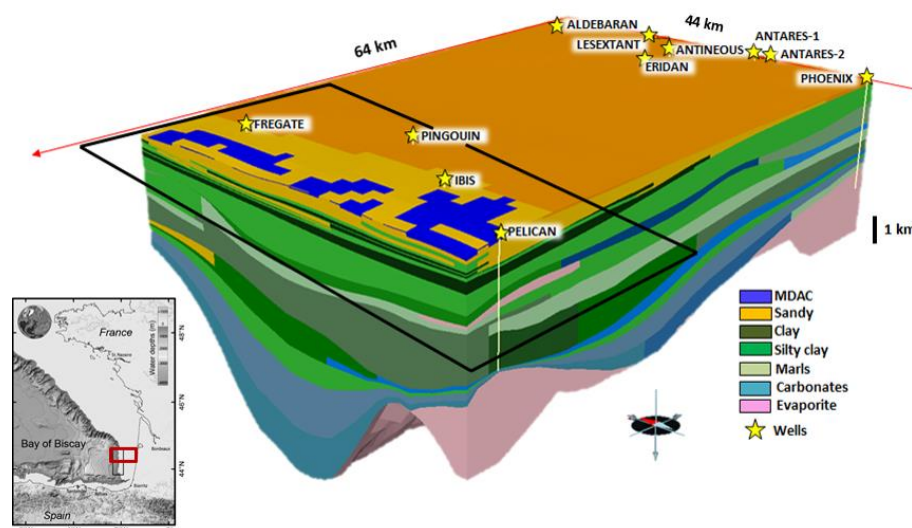


Figure 3. 3D block diagram of the study area from TemisFlow®. The model covers an area of ~2800 km² representing a shelf part of the offshore Aquitaine Basin (red rectangle) (Fig. 1a) where seeps have been mapped (black rectangle) (Fig. 1b) with in situ measurements and annual estimation of methane flow rates (Dupré et al. 2020). The black rectangle represents the extent of maps in Figs. 12, 14 and 17.

construct a 3D model of the Bay of Biscay (Table 1). The interpretation of the three main units composing the Plio-Pleistocene progradational system are given in Michel (2017) (U1, U2 and U3, Table 1). Eleven exploration wells were drilled by Elf Aquitaine in the area of interest during the 60s, 70s and 80s. They are mainly located along the coast and along the shelf-break area as shown in Fig. 3. Measurements performed at these wells provide data used to calibrate the basin model as described in the next sections: facies logs, uncorrected Bottom Hole Temperatures (BHT) for 7 wells (see Fig. 7), vitrinite reflectance for 6 wells (Fig. 8) and pressure at two wells (Fig. S1).

Correction of BHT measurements can be more than 10% above the actual measure (Deming 1989). Because no information about the mud circulation time was found in the composite logs, it was decided to correct these measurements by adding 10% of the measured value and to consider an uncertainty of $\pm 10\%$.

Vitrinite reflectance data yield information about the maximum temperature experienced by the sediments (Jones and Edison 1979; Oberlin, 1980; Carr 2000). The measurements however were reported without any description of the sample

type (e.g. dispersed organic matter, coal, extracted kerogen), therefore these measurements remain questionable. Pressure measurements indicate hydrostatic gradients which have been used to determine the average water salinity in the offshore Aquitaine Basin.

4. METHODS

Rock Eval analysis to determine biogenic gas generation potential

The Rock-Eval technique is widely used in academia and petroleum industry to determine the hydrocarbon potential, type and maturity of source rocks (Espitalié et al. 1977; Espitalié et al. 1985; Lafargue et al. 1998; Behar et al. 2001). This type of analysis is applied either on bulk rock samples (Espitalié et al. 1977) or on isolated kerogens or coals (Behar et al. 2001). The Rock-Eval technique consists in a thermal analysis of the sample through two analytical steps with specific temperature programs: a pyrolysis under inert atmosphere (N₂) followed by a combustion of the residual sample under an oxidative atmosphere (air). The hydrocarbons are detected using a Flame Ionization Detector. The CO₂ and CO released by the pyrolysis and oxidation phases are continuously swept towards an infrared detector

(Espitalié et al. 1985). A small amount of crushed source rock (about 70 mg) or isolated kerogen (5 to 30 mg) is usually exposed in the pyrolysis oven to a temperature of 300 °C for 3 minutes before applying a heating rate at 25°C/min up to 650 or 800°C respectively. But since our samples are recent sediments containing immature organic matter, we applied a lower isotherm and the samples were heated at an initial temperature of 200°C as proposed in Baudin et al. (2015). During the pyrolysis cycle, three peaks are detected. The S1 peak obtained during the pyrolysis isotherm determines the amount of free hydrocarbons in the samples (mg HC/g of rock). The S2 peak obtained during the pyrolysis heating rate corresponds to the hydrocarbons released by thermal cracking (mg HC/g of rock). This S2 peak represents the remaining hydrocarbon potential of a source rock. The S3 peaks partly correspond to the amount of CO and CO₂ released during thermal cracking (mg CO or CO₂/g of rock). The main parameters calculated from Rock-Eval data are: Total Organic Carbon (TOC%) representing the total organic carbon content, Hydrogen Index (HI) (mg HC/g TOC) and Oxygen Index (OI) (mg CO₂/g TOC). These parameters are used to determine the type (e.g. lacustrine, marine or continental) and the maturity of organic matter. Another parameter is also used as a proxy for the maturity of a source rock: Tmax (°C) that corresponds to the temperature measured at the peak of S2.

Basin modelling

Sedimentary model

The static model of the Aquitaine Basin was built based on present-day topography (Ortiz et al. 2020) and 13 subsurface horizons that were derived from seismic interpretations (Table 1) (Michel 2017; Ortiz et al. 2020; M. Roger, personal com.). The surface of the model area is around 2800 km² (Fig. 3), divided horizontally into grid blocks of 1x1 km². The model also includes the methane-derived authigenic carbonates distribution at the sub-seafloor (Dupré et al. 2020). The eleven exploration wells were used to cross-check the depth maps (Fig. 3).

Table 1. Geological layers and sub-layering for the main target area of biogenic gas generation. Interpreted seismic horizons are derived from OROGEN Project (Total) (Basement to Oligocene), Ortiz et al. (2020) (Miocene to Seabed), and Michel (2017) (Plio-Pleistocene units). The two uppermost layers are created by a lithoswitch to account for precipitation of MDACs during CH₄ upward migration.

Top Age (Ma)	Layers	Interpreted Horizons from seismic	Sub-layering
0.0	MDAC		
0.14	Seabed	x	
0.25	Plio-Pleistocene U3	x	8 sub-layers
1.76	Plio-Pleistocene U2	x	7 sub-layers
3.53	Plio-Pleistocene U1	x	
5.30	Miocene	x	6 sub-layers
13.82	Langhian-Serravallian	x	
20.24	Aquitainian		
23.03	Oligocene	x	
33.90	Upper Eocene		
41.20	Lower Eocene		
56.00	Paleocene		
66.00	Upper Cretaceous	x	
100.50	Albian	x	
113.00	Aptian	x	
125.00	Barremian		
130.00	Neocomian		
145.00	Top Jurassic	x	
175.60	Top Lias		
201.30	Top Triassic	x	
250.00	Top Basement	x	

Finally, each isopach was associated with a lithofacies map (Fig. 3). The facies distribution was obtained by well log correlation, with an additional uppermost MDAC layer for wells located within the sub-seafloor MDAC area (i.e. Pelican-1 and Fregate-1) (Figs 3, 7 and 8). The paleo-bathymetry for each horizon was defined in accordance with literature (Desegaulx and Brunet 1990; Brunet 1994). In order to more accurately model the processes of biogenic gas generation, the vertical resolution was increased in the main zone of biogenic gas production. Thus, the shallower strata from the Miocene to the Plio-Pleistocene layers were subdivided into several sub-layers (Table 1). The Miocene layer, which presents an average thickness of 600 m, was subdivided into six 100 m-thick sub-layers. The Plio-Pleistocene units U2 and U3 were also refined. The U2 unit was subdivided into seven sub-layers with an average thickness of 60 m. The

U3 unit was subdivided into eight sub-layers with a thickness of 90 m. No sub-layering was applied to the U1 unit as its thickness is only around 100 m. Finally, we applied a lithological switch at two uppermost layers in order to account for MDAC deposits, that mimics the appearance of these particular lithofacies after deposition. The final static model is composed of 39 depositional events and one litho-switch event (Fig. 3, Table 1).

Boundary Conditions

In order to model the thermal evolution through time, a lithosphere model was created with varying bottom boundary conditions. The three main elements that characterize the lithosphere (upper crust, lower crust and upper mantle) were taken from publications (Artemieva and Thybo 2013; Brunet 1994; Brunet 1997). The base of the upper mantle is assumed to be the base of the model, defined by the 1333°C mantle isotherm representing the Lithosphere-Asthenosphere Boundary (LAB) and was digitized from Artemieva and Thybo (2013). Two rifting events experienced by the Bay of Biscay (Ferrer et al. 2008; Tugend et al. 2014; Brunet 1994; Desegaulx and Brunet 1990) were defined to model heat flow variations in the geological past. The rifting is initiated from a McKenzie-type crustal model with an instantaneous (less than 20 My) stretching of the lower and upper crust (McKenzie 1978). Then, the subsidence of the basin is simulated using extension coefficients (β -factor) from Brunet (1997): $\beta = 1.2$ for the Triassic rift event and $\beta = 1.4$ for the Upper Jurassic rift event.

The upper thermal boundary is defined as a surface temperature map at the top of the model for each geological time step using the *Paleo-latitude calculator for Paleoclimate study* from van Hinsbergen et al. (2015) and the equivalent diagram from Wygrala (1989) which require paleo-latitudes of the basin over time. Since temperatures at the sea-bottom are usually much cooler compared with onshore environments at the same latitude (Dembicki 2016), the sea bottom surface temperature was corrected for paleo-bathymetry using the method described in Toole (1981). This resulted in a series of temperature

maps, one for each geological event, that were imposed at the top of the model and that account for the changing latitude and bathymetry of the basin.

Biogenic source rock definition

Biogenic gas generation of a given source rock occurs between 10 and 100°C (Katz et al. 2011) and is determined as a function of thermal gradient (°C/km) and sedimentation rate (m/My) (Schneider et al. 2016). An optimal heating rate at deposition time ranges between 7°C/My and 18°C/My (Clayton, 1992) (Fig. 4).

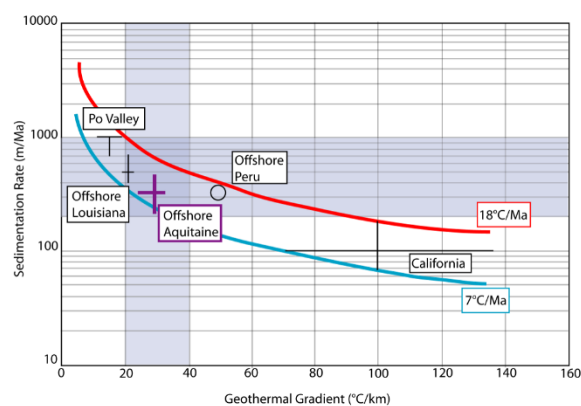


Figure 4. Biogenic gas maturity windows based on the heating rate which is determined as a function of the sedimentation rate over the geothermal gradient (modified after Clayton 1992). The highlighted area indicates the normal geothermal gradient and sedimentation rate for worldwide sedimentary basins (Clayton 1992). In the offshore Aquitaine, the Plio-Pleistocene sequences are characterized by favorable conditions for biogenic gas generation (purple lines).

The thermal gradient and sedimentation rate maps were computed by the TemisFlow® simulator and multiplied to determine the heating rate maps at deposition time for each layer (Fig. 5a-c). These maps were then converted into biogenic potential index maps that determine the areas in which any OM may be converted to microbial CH₄ (Fig. 5d).

Five potential source rock layers in the Plio-Pleistocene series and one potential source rock in the Miocene sediments presented optimal conditions for biogenic gas generation. Their input geochemical parameters (e.g. TOC and HI) were taken from the Rock-Eval analysis (Table S1).

Concepts of modelling biogenic gas generation and migration processes

Published OM degradation models (Westrich et al. 1984; Janssen 1984; Middelburg 1989; Middelburg et al. 1996; Canuel and Martens 1996; Boudreau and Ruddick 1991; Robinson and Brink 2005; Arndt et al. 2013) are the results of experimental laboratory studies, performed at human time scales and at specific thermal conditions. A basin model however needs to represent the time span of the entire geological history of a basin and its thermal evolution. A general modelling approach is needed that accounts for the main biogenic gas production processes but that can also be applied at different geological space and time scales.

Our modelling approach considers the total initial Sedimentary Organic Matter (SOM) is composed of TOClab, TOCzlab and TOCbio-ref. The labile TOClab is (Eq. 1, Fig. 2) the part of the OM that is immediately degraded at the moment of deposition according to the degradation law of Middelburg (1989) which is a function of OM reactivity (R_{bio}) and microbial activity ($\mu(T)$) (Eq. 1). This model describes an exponential decrease of the OM with depth and time and leads to a strong degradation in the first few meters of the sedimentary column. This shallow depth is challenging in basin simulators where the vertical resolution of layers is usually in the range of tens to hundreds of meters. In addition, all hydrocarbons generated or migrated in the uppermost layer are assumed lost to the surface. Under these conditions, only the fraction of TOClab at greater depth would be capable of generating biogenic gas. In order to account for a higher fraction of the biodegradable OM, a thermogenic source of labile TOC is introduced in our conceptual model (Burdige 2007; Burdige 2011). It is represented by the thermo-labile part (TOCzlab) of the initial TOC and corresponds to the OM that can be trapped and protected in the mineral matrix during the first stages of diagenesis (Burdige 2011). When temperature increases, TOCzlab can turn into labile OM which is sensitive to biodegradation. This process releases

new labile compounds later in time and results in an additional generation of biogenic gas at greater depth. The transformation of TOCzlab is modelled using a first-order kinetic cracking scheme (Eq. 2). For a continental-derived OM, composed mainly by waxes of higher plants (Largeau and Vandenbroucke 2007; Kamga 2016), the generation of methane at low temperature is mainly the result of the degradation of the aliphatic portions (*e.g.* long fatty acids) (Kamga 2016) considered as the most thermo-labile compounds with low activation energy. The third and last fraction of the initial TOC (TOCbio-ref) is bio-refractory and corresponds to the TOC fraction that is used in traditional petroleum systems analysis. TOCbio-ref is not sensitive to microbial activity and is converted into hydrocarbons by thermogenic cracking reactions only. In this study, TOCbio-ref values are derived from Rock-Eval analysis (see Table 3).

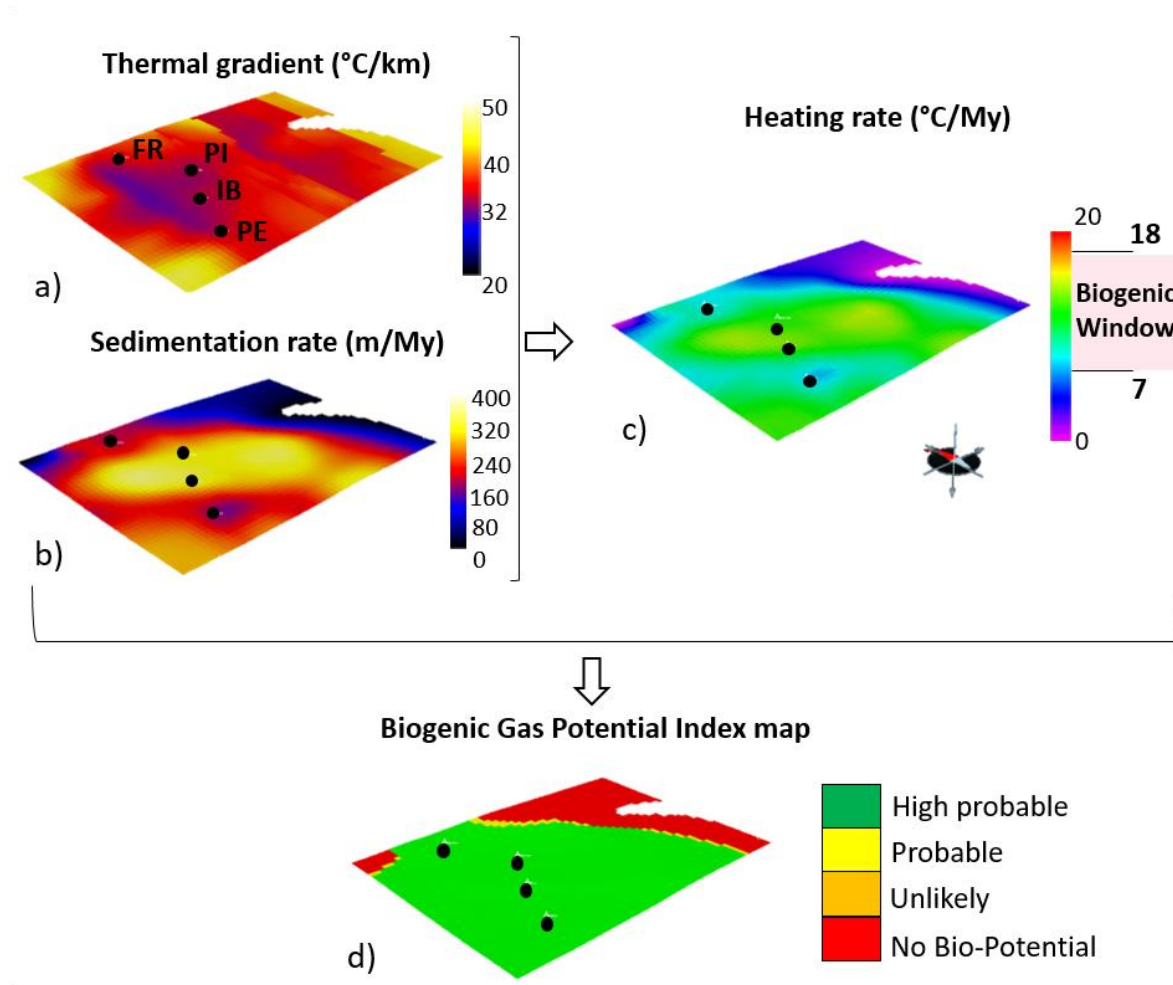


Figure 5. The thermal gradient (a) and the sedimentation rate maps (b) computed in TemisFlow® are multiplied to obtain the heating rate map (c). This map is then converted into a “Biogenic Gas Potential Index” map (d) to determine the areas entering the biogenic maturity window in which any OM may be converted into microbial methane for the upper Miocene layer. Black dots represent offshore wells (FR – Fregate-1; PI – Pingouin-1; IB – Ibis-1; PE – Pelican-1) (for well locations see Fig. 3)

Thus, the total initial SOM is defined as the sum of these three fractions (Fig. 2):

$$Total\ Initial\ SOM = TOC_{bio-ref} + TOC_{lab} + TOC_{zlab}$$

TOClab evolution through time follows a continuous degradation law (Eq. 1):

$$\frac{\partial TOClab}{\partial t} = -R_{bio} * (a_{bio} + t)^{-b} * \mu(T) * TOClab - \frac{\partial TOCzlab}{\partial t} \quad (1)$$

where R_{bio} represents a dimensionless calibration parameter linked to the sedimentary environment. A default value of 0.16 is derived from

Middelburg (1989). a_{bio} is the apparent initial age of the OM (Ma), t the time of the degradation process (Ma) and b is equal to 0.95 (Middelburg 1989). $\mu(T)$ (°C) is the temperature dependent function of microbial activity derived from Belyaev et al. (1983).

TOCzlab degradation is defined by a first order kinetic reaction (Eq. 2):

$$\frac{\partial TOCzlab}{\partial t} = -k(T) * TOCzlab \quad (2)$$

where reactivity k is defined by the Arrhenius law (Eq. 3):

$$-k(T) = A * e^{-\frac{Ea}{RT}} \quad (3)$$

T represents the temperature (K), Ea the activation energy (kJ mol^{-1}), R the universal gas constant ($8.3144621 \text{ J.mol}^{-1}.\text{K}^{-1}$) and A the frequency factor (s^{-1}).

The final generated biogenic gas is derived from the transformation of the labile organic carbon fraction whose biogenic CH_4 generation rate (τ_{bio}) (Eq. 4) is defined as:

$$\tau_{bio} = - \frac{m_{CH_4}}{m_C} * s_{bio} * \frac{\partial TOC_{lab}}{\partial t} \quad (4)$$

where m_{CH_4} = methane molar mass, m_C = carbon molar mass and s_{bio} = stoichiometric coefficient controlling the amount of organic carbon which is converted to microbial methane.

In conclusion, biogenic methane is directly generated by the labile TOC fraction following two steps (Fig. 2): first, the labile TOC fraction is transformed into methane, and then the thermo-labile TOC is transformed at greater depth into labile TOC that is afterwards converted into additional methane.

Once the biogenic gas is generated, it is subject to the following processes (in order of priority): (1) adsorption by the organic matter following the Langmuir law, which quantifies the capacity of the OM to adsorb methane as a function of temperature and pressure; (2) dissolution in formation water following an equation of state (EOS) which is a function of pressure, temperature and salinity, and subsequent advective transport in the water phase (Duan et al. 1992); (3) migration in a separate vapor phase following multi-phase Darcy's law.

Biogenic gas can also be accumulated in structural or stratigraphic traps in a vapor phase, or as a solid phase in the form of gas hydrates (Brothers et al. 2014; Johnson et al. 2015; Skarke et al. 2014). In the Aquitaine Basin, however, temperature and pressure conditions are not conducive to gas hydrate deposits (Dupré et al. 2020). The absence

of hydrates over geological time is also confirmed by our numerical simulations.

Quantitative sensitivity analysis

As mentioned in the introduction, the values of the model parameters, and especially those describing the biogenic gas generation process, are uncertain. Sensitivity analysis can be performed to estimate the impact of these parameters on the modelled processes and to determine those that are the most critical. This can help to better understand the processes involved in the biogenic gas production and migration and to simplify the calibration process by focusing on the relevant parameters.

Here we performed a variance-based global sensitivity analysis to quantify the influence of the parameters on the output of interest (Sobol' 1990). More specifically, input parameters are considered to be independent random variables with given probability distributions. Indices are then computed that quantify the impact of the parameter uncertainty on the output variance. The main (or first-order) effect measures the part of the output variance explained by the parameter alone. It ranges between 0 and 1. The total effect, as defined in Homma and Saltelli (1996), estimates the global sensitivity of the output to the parameter. The difference between the total and main effects corresponds to interactions between the studied parameter and some other parameters.

The estimation of the main and total effects requires knowing the value of the output of interest for a very large number of models. To avoid such a computational overburden, we consider here meta-models that mimic the simulator. More precisely, we generate a sample of the parameter space and perform the corresponding simulations. This provides a set of basin models, the training set, that is used to approximate the relationship between the input parameters and the output of interest, providing fast estimations of this output for any parameter values (Wendebourg 2003; Feraille and Marrel 2012). If these estimations are accurate enough, they can replace the calls to the simulator during the computation of the sensitivity indices. To

check the quality of the meta-model estimations, we consider here an additional sample of the parameter space, independent from the training set, and compare the output simulated values for these new models with those predicted by the meta-model. The resulting errors are gathered in the R2 correlation index (see Gervais et al. (2018) for more details).

This workflow has already been used in a variety of contexts. In what follows, meta-models are built by kriging interpolation, and are combined with reduced-basis decomposition to predict the spatial distribution of properties in the basin as described for instance in Gervais et al. (2018).

5. RESULTS

Organic Matter Characterization

As mentioned above, to characterize the OM we collected cuttings at depths ranging from 595 to 1530 m from the Pelican-1 and Pingouin-1 wells located in the offshore Parentis Basin. At the same depth and formation interval, the two wells showed different TOC values (Table 1S). Pingouin-1 is characterized by a very low OM content which an overall decrease with depth ranging from 0.44% in the shallower Plio-Pleistocene to 0.32% TOC in the Miocene. The Pelican-1 well shows higher OM content, with TOC values principally ranging from 0.44% to 0.47% respectively from the top Plio-Pleistocene to the base Miocene. Only one sample (PELICAN-7) is characterized by a higher TOC value of around 10.35% which is probably due to the presence of black OM in vitrinite residues already observed and described in Michel (2017). Otherwise, the samples show OI values between ~240 and 500 mgCO₂/gTOC and very low HI (≤ 55 mg HC/gTOC) suggesting an altered continental-derived OM (Fig. 6). A mean Tmax value of 420°C indicates that the OM is immature.

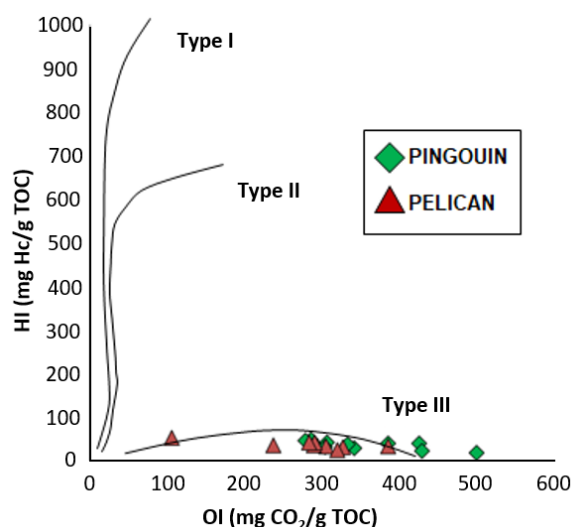


Figure 6. Rock-Eval results on cuttings collected from Pelican-1 and Pingouin-1 wells offshore Aquitaine. Well locations are displayed in Figure 3. The OM derives from continental origin (Type III). The samples are mainly characterized by poor TOC content (see Table S1) and very low HI values.

Thermal and pressure regime

Calibration of present-day temperatures was obtained by modifying thermal conductivities of lithologies in each strata in accordance with those given in Pasquale et al. (2011). Calibration results are shown in Figure 7. A lithospheric model (section 4) constrained the thermal evolution of the basin through time which was calibrated with vitrinite reflectance data from 6 wells (Fig. 8). Note that in this study, we do not model any deeper thermogenic petroleum systems as those known in the offshore Parentis Basin as we focus on Cenozoic strata within which the biogenic gas source rocks are found. According to the calibrated model, the Miocene layer reaches its maximum temperature between 32 and 45°C at the present day. These temperatures also correspond to the microbial activity peak and optimal conditions for the generation of microbial gas (Katz et al. 2011). Note also that vitrinite measurements were reported without any description of the rock samples from which they were taken adding to the uncertainty of the final paleo-temperature history. Pressure measurements indicate some overpressure in the basin: Pelican-1 encountered an overpressure of 6.28 MPa at 3125

m in a shaly horizon, Antares-1 encountered a small overpressure of 1.78 MPa at 2056 m (Figure 1S). Hydrostatic pressure gradients depend on salinity. The water composition offshore Aquitaine is highly variable, probably related to the presence of large salt accumulations and extensive diapirism. Salinities encountered in Pelican-1 show a mean value of 65 g/l ± 15 at 1823-1860 m depth (Paleocene), a mean value of 150/180 g/l at 2500 m (Aptian), and values up to 145 g/l at 2800 m (Barremian). Salinities from the Antares-1 well show lower values at similar depths (56 g/l at 2567 m). Despite such a high variability of water salinity, pressure calibration was achieved with a mean water salinity of 50 g/l.

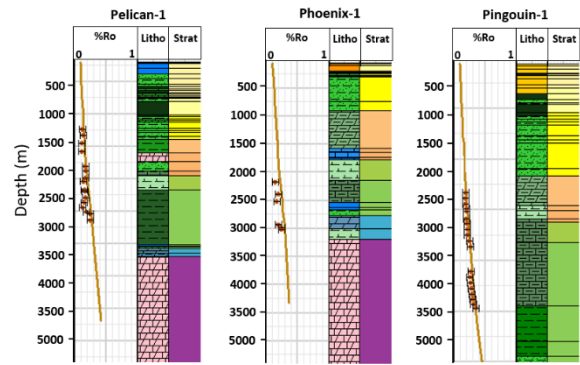


Figure 8. Paleo-thermal calibration of vitrinite reflectance data for 3 of the 6 wells of the Aquitaine Basin with corresponding stratigraphy and lithology used in the model (Fig. 7). Well locations are shown in Figure 3.

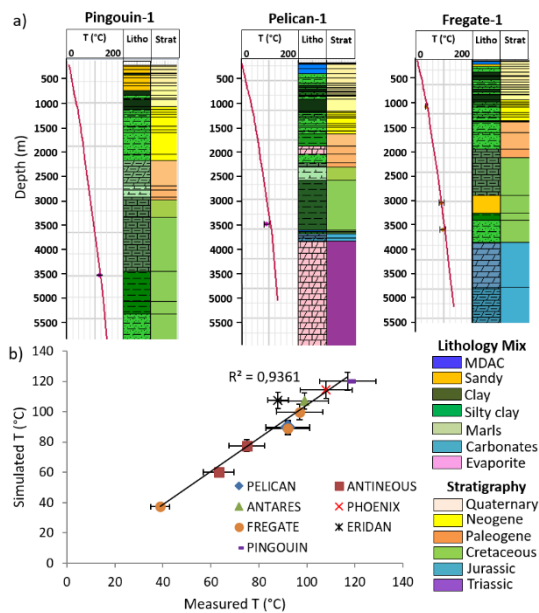


Figure 7. a) Present-day temperature calibration results for 3 wells located offshore Aquitaine with corresponding stratigraphy and lithology used in the 3D model. b) Temperature calibrations for all 7 wells are given by a cross-plot “Simulated vs Measured Temperatures”. Well locations are shown in Figure 3.

Sensitivity Analysis on biogenic gas generation

As mentioned previously, the parameters describing the biogenic gas generation are not completely known for continental-derived terrestrial type III-OM in the Aquitaine Basin. We thus performed a sensitivity analysis on 7 input parameters likely to have a significant impact on biogenic gas generation in the offshore Aquitaine: TOClab, TOCzlab, R_{bio} , E_a , $\mu(T)$, S_{bio} and water salinity.

Ranges of kinetic parameters are based on published data for a type III organic matter (Middelburg 1989; Hedges and Oades, 1997; Martens and Canuel al. 1996; Burdige 2007, 2011) and on previous modelling work of biogenic gas generation (Ducros and Wolf 2014; Ducros et al. 2015). As presented in Burdige (2011 and reference therein), the activation energy (E_a) for recent organic matter can vary between 50 to 130 kJ/mol. In our case study, biogenic gas generation is favorable when E_a is comprised between 80-110 kJ/mol. Higher or lower value prevent the biogenic gas generation. We therefore reduced the range proposed in Burdige (2011) as proposed in Table 2. Here, we did not consider the frequency factor (A) of the TOCzlab kinetics (Eq. 3) as a critical parameter. Indeed, it is well known that, for the same reactivity, variations in E_a can be compensated by A (Peters et al. 2018). In accordance with previous kinetic studies (Behar et al. 1997; Dieckmann 2005; Schenk et al. 1997) we

fixed A and varied E_a in the range of published data to find an optimal kinetic law for TOC_{zlab}. However, in order to more accurately describe the degradation of a recent type-III OM and reduce uncertainty, further research should focus on the analytical assessment of the molecular composition of a recent continental-derived organic matter.

Table 2. Range of parameters considered as uncertain in this study (Min and Max) and values selected for an optimal biogenic gas production (“This study”).

Input Parameter	Min	Max	This Study	Unit
TOC _{lab}	20	24	22	%
TOC _{zlab}	15	19	19	%
R _{bio}	0.16	9	1.7	
E _a	80	110	83	kJ/mol
S _{bio}	0.2	0.4	0.35	
Salinity	40	60	50	g/L
$\mu(T)$	30	55	32	°C

The perturbation of the $\mu(T)$ function is performed through the variation of the temperature corresponding to the peak of maximum activity instead of varying the function as presented in Table 2. Water salinity was included in the sensitivity analysis to assess its impact on methane dissolution rather than on the final amount of generated gas. The ranges of variation of all the critical input parameters are given in Table 2.

To estimate the sensitivity indices, a Latin Hypercube sample of 100 models was generated (McKay et al. 1979) and used to get first qualitative results.

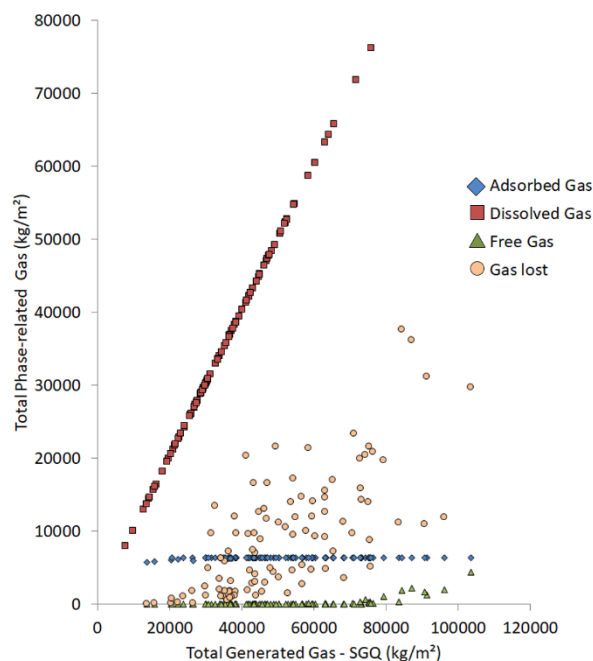


Figure 9. Microbial gas phase behavior as function of the total generated gas (SQG) based on a set of 100 simulations sampling the uncertain parameter space. The gas can be free in the system only when water becomes saturated. The total amount of gas lost at the surface increases as the cumulative generated gas increases.

Since the migration of microbial gas evolves as a function of the total amount of generated gas (SQG, Fig. 9), special attention was given to the sensitivity of SQG to the uncertain parameters. Figure 10 shows the value of SQG for the 100 models of the sample as a function of E_a , S_{bio} and R_{bio} . We can observe a negative correlation between SQG and the activation energy (E_a), as well as a positive correlation for both S_{bio} (Fig. 10a,b) and low values of R_{bio} (Fig. 10c). No clear trend can be observed for the other parameters.

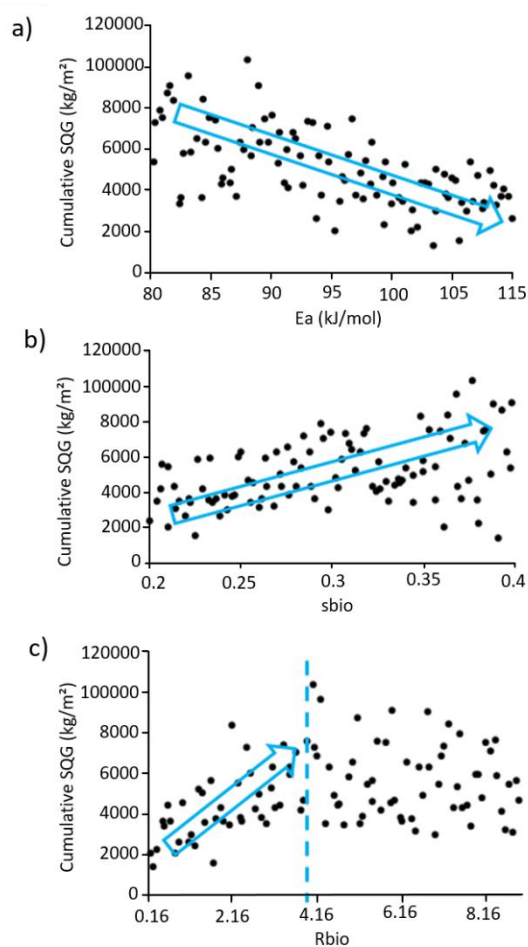


Figure 10. Total amount of generated gas (SQG) as function of three critical parameters for the 100 simulations of the training set. a) with activation energy (E_a); b) with stoichiometry coefficient (s_{bio}); c) with sedimentary environment parameter (R_{bio}).

The results of the variance-based sensitivity analysis on SQG are presented in Figure 11. The meta-models used to compute these total and main effects were derived from the 100 models and quality-checked using 50 additional models. Parameters E_a , s_{bio} and R_{bio} appear to be the most influential on SQG, while the proportion of labile versus thermo-labile compounds in the OM (TOClab and TOCzlab) seems to have only a limited impact. This may be related to the quite small range of variation chosen for these fractions.

If we now consider in more details the spatial distribution of parameters E_a , s_{bio} and R_{bio} total effect on SQG in the layers (Fig. 12), we can observe some variability depending on the source rock horizon.

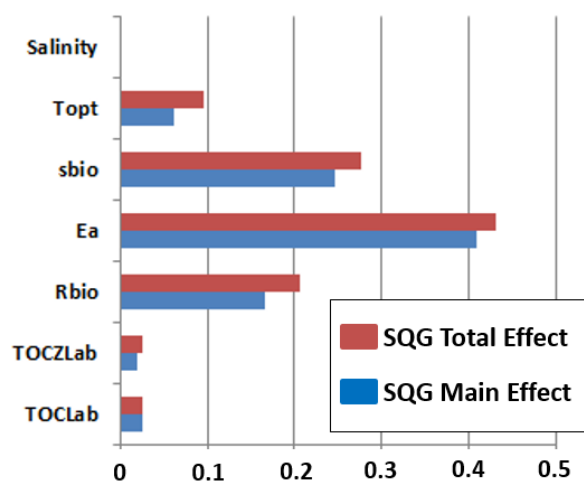


Figure 11. Total and main effects on the total generated gas (SQG) computed for the 7 uncertain parameters. The small differences between the two effects highlight that, in our case study, there are no significant interactions between the parameters that affect the generation of methane. SQG is mainly impacted by E_a , s_{bio} and R_{bio} parameters, in order of priority.

The impact of E_a is strongest in the Miocene source rock and decreases in the shallower Plio-Pleistocene layers (Fig. 12). This is probably due to degradation rates for the thermo-labile part of the OM that increase with temperature (Eq. 3) and thus with depth. As a result, the variability of E_a has more impact at greater depth. The same trend is visible for s_{bio} : the influence on SQG increases with depth, with a higher impact on the deeper Miocene source rock compared with the uppermost Plio-Pleistocene sediments (Fig. 12). This result is probably linked to the higher organic carbon availability in the deeper source rock, derived from the total transformation of both TOClab and TOCzlab, which is then converted to biogenic methane as function of s_{bio} (Eq. 4). The results for R_{bio} show the opposite behavior: the impact is strongest in the uppermost layers where TOClab is the most sensitive to degradation, and small in the deeper layers (Fig. 12).

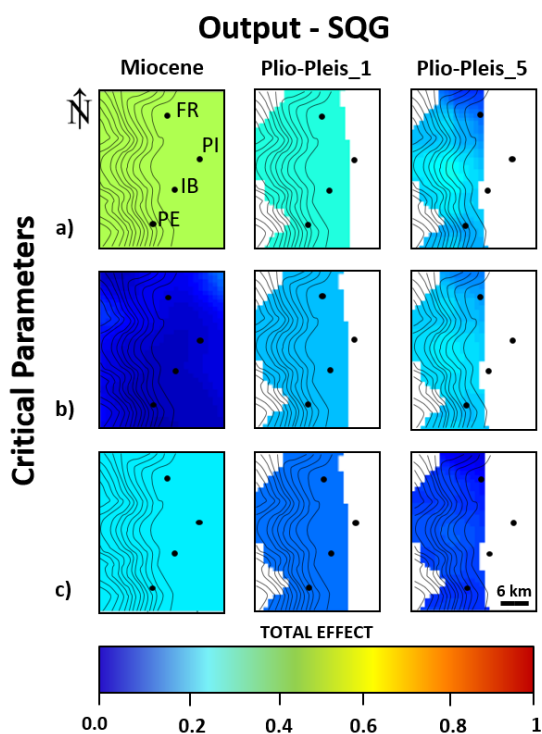


Figure 12. Total effect obtained for the three main influential parameters (Ea, sbio, Rbio) on three of the six source rock layers (Table 3) over the northern studied area (see location in Fig. 1b). Black dots represent the offshore wells (FR – Fregate-1; PI – Pingouin-1; IB – Ibis-1; PE – Pelican-1) (Figs. 1, 3 and 5). Black lines represent the seafloor bathymetry with a contour interval of 50 m.

Scenario for microbial gas generation

In our model, each source rock layer, from the deeper Miocene to the shallower Plio-Pleistocene, is defined by a constant TOC_{bio-ref} determined from Rock-Eval analysis (Table 3). The degradation laws for the labile compound and the kinetic laws for the thermo-labile fraction are identical for each source rock layer. We use the estimation of the gas flux in the northern area identified by Dupré et al. (2020) to constrain these laws. More specifically, the difference between the total mass of generated gas and the total mass of gas in place (either adsorbed, dissolved or free) provides us an estimation of the amount of gas lost at the seafloor, and thus an estimation of the gas flux which can be compared to the flux measured by Dupré et al. (2020) in the northern area. The optimal value among the set of models is obtained for the input parameters values given in Table 2

(“This study” column). We can see that it requires a low activation energy of 83 kJ/mol, which is necessary to activate the thermo-labile TOC fraction at low temperatures as in the case of the Plio-Pleistocene source rocks. This model is considered in what follows as our reference scenario.

Table 3. Source rock age, modelled temperature and thermal conductivity. TOC bio-refractory (TOC_{bio-ref}) values are defined after the Rock-Eval analysis (Table S1).

Source Rock	Top_Age	Mean Depth	Mean Temperature	Mean Thermal Conductivity	TOCbio-ref
	(Ma)	(m)	(°C)	(W/m.°C)	(%)
Plio-Pleis_5	1.76	585	14	1.60	0.49
Plio-Pleis_4	1.98	618	16	1.64	0.42
Plio-Pleis_3	2.20	670	17	1.66	0.44
Plio-Pleis_2	2.42	708	20	1.63	0.30
Plio-Pleis_1	2.87	823	22	1.61	0.29
Miocene	5.53	1100	30	1.54	0.51

With this scenario, the average per-area amount of generated gas is 78 kg/m² (Fig. 13) which amounts to 25.5 Gt/My when integrated over time along the entire area of ~1188 km² (Fig. 14). The highest microbial gas amount is generated by the upper Miocene source rock which reached its highest temperature (~ 32°C) at the present day. Methane is first generated by the initial labile fraction during early diagenesis but continues to be generated by other labile molecules derived from the transformation of TOC_{zlab} with increasing temperature. The area of maximum generation is localized along the shelf edge where the sediment thickness is the highest resulting in both higher burial and temperature. Generation decreases along the upper slope where no fluid activity has been identified (Dupré et al. 2020) (Figs. 1, 14). Part of this generated gas is adsorbed to the source rock, or dissolved in the pore water, or trapped as a free gas when saturations are high enough. As shown in Figure 13, biogenic gas is mainly present in the system as dissolved in water. Formation water is almost always under-saturated with respect to CH₄ and a free methane phase is minimal in the uppermost layers mainly at the shelf break (Fig. 13d). Dissolved gas moves driven by hydrodynamic gradients. As compaction is the main driving force, water flow is mainly vertical and therefore methane flux is also mainly vertical, from the source rock to the seafloor.

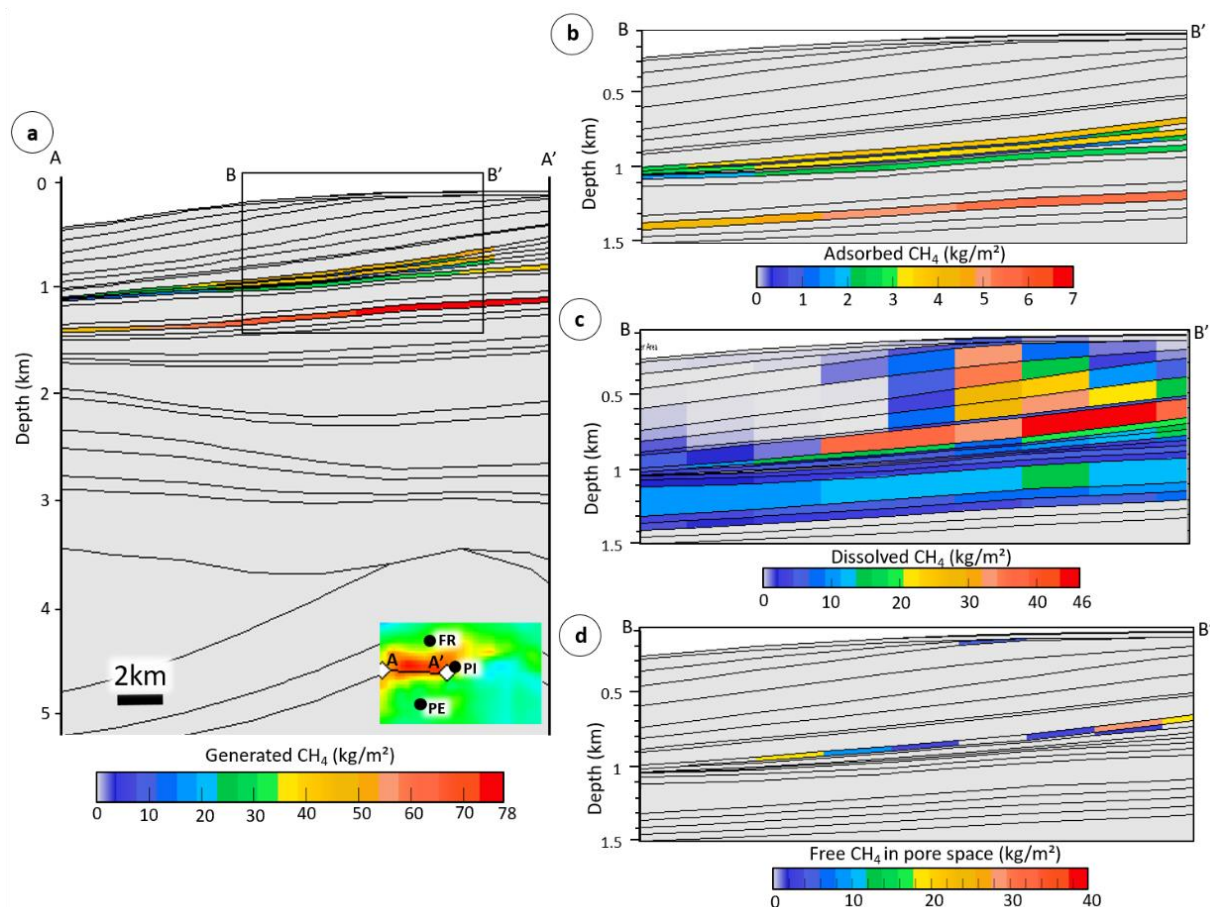


Figure 13. 2D sections across the basin model (profile AA') showing mass of a) the generated gas from biogenic production per area and b-d) mass of gas in place per area at the present day, with b) total mass of gas adsorbed in the organic matter; c) total mass of gas dissolved in formation water; and d) total mass of free gas in pore space.

However, flow in the uppermost strata is impacted by MDAC deposits which prevent gas to easily escape to the seafloor. The modelled gas migrates upwards along a narrow N-S oriented strip near and east of the shelf break (Fig.14) where gas generation rate and sediment permeability are most favorable.

Once the fluid reaches the seafloor, methane is exsolved as a free gas phase. Our results suggest that gas seeps at the seabed may be principally linked to gas diffusion close to the water/sediment interface rather than from large quantities of free gas migrating to the surface. Considering the difference between the total mass of generated and in place gas (either adsorbed, dissolved or free), we estimate that the amount of gas lost at the seafloor is 0.91 Gt/My over an area of ~107 km²

which corresponds to the gas flux in the northern area modelled after Dupré et al. (2020) (Fig. 14).

6. DISCUSSIONS

Cumulative volume of released microbial methane at the seafloor in the Aquitaine Shelf

Dupré et al. (2020) estimated an amount of emitted methane over the Aquitaine Shelf of 144 Mg/yr based on measurements from local bubbling sites (Ruffine et al. 2017) and acoustic water column signatures of escaping gas bubbles. Our study area is restricted to the northern Aquitaine Shelf (see location in Fig. 1b) and corresponds to 1.88 Tcf/My (Trillion Cubic Feet per million years) (Dupré et al. 2020).

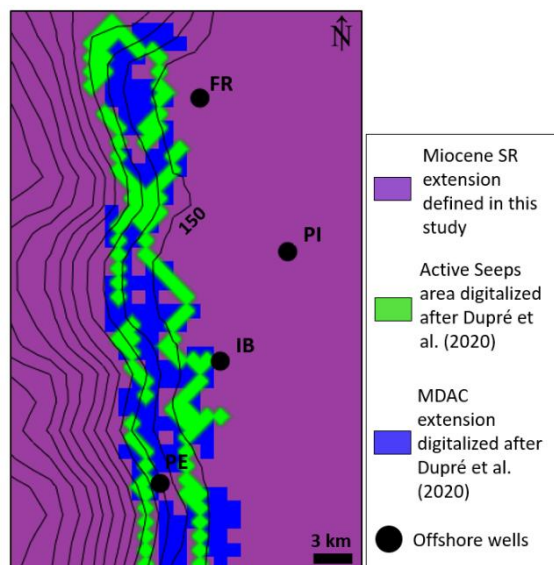


Figure 14. Map of Miocene Source Rock (SR) defined in this study with extent of seeps and MDACs digitized from Dupré et al. (2020) over the northern study area (see map location in Fig. 1b). The location of the offshore wells (FR – Fregate-1; PI – Pingouin-1; IB – Ibis-1; PE – Pelican-1) is given in Figs.1 and 3. Black lines represent the seafloor bathymetry with a contour interval of 50 m.

Our model indicates a total mass of generated microbial methane of 25.5 Gt/My over 5.53 My corresponding to the time since the beginning of the generation process. At the maximum generation depth (mean depth ~1100 m), the deeper source rock is at P-T conditions of ~ 10 MPa and ~ 35°C where CH₄ density is 72 kg/m³ using the AGA8 equation of state (ISO 12213-2 2006; Starling and Savidge 1992) (Fig. 15). Thus the total volume of generated gas is 3.55*10⁺⁵ Mm³/My (equivalent to 12.8 Tcf/My).

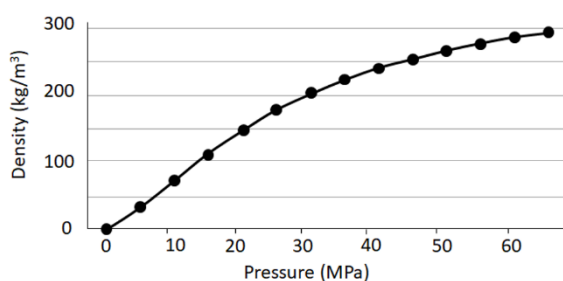
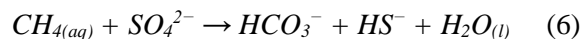


Figure 15. Methane density as function of pressure using the AGA8 equation of state (ISO 12213-2, 2006; Starling and Savidge1992).

At the water depth range of emission sites, P-T conditions are 2.6 MPa and 10°C resulting in a gas density of 19.7 kg/m³ (Fig. 15). Based on a gas loss of 0.91 Gt/My, we can estimate the cumulative volume of emitted gas as 4.63*10⁺⁴ Mm³/My (equivalent to 1.62 Tcf/My).

MDAC pavements represent a sink of CH₄. At the edge of the Aquitaine Shelf, they are associated with microbial methane seeps which are oxidized in the Anaerobic Methane Oxidation zone to CO₂ (Pierre et al. 2017a). During upward migration, the generated methane meets the SO₄²⁻ of the downward diffusing seawater in the Sulphate-Methane Transition Zone where it is consumed by the activity of methanotrophic archaea with SO₄²⁻ reducing bacteria (Boetius 2000; Conrad 2005; Thauer 2010; Lash 2015) in anoxic conditions. Note that we did not account for the sulfate-reduction of organic matter as it is one of the process less likely to induce local authigenic carbonate precipitation compared to the AOM (Paull and Ussler 2008). In addition, extensive precipitation of MDACs within the subsurface, is usually related to SMTZ occurring at shallower sub-bottom depths (e.g. < 20 mbsf) (Paull and Ussler 2008 and reference therein) which can be the case of the Bay of Biscay (Pierre et al. 2017a, Dupre et al. 2020). Here, we assume that in the Bay of Biscay the AOM is the driving process for MDAC precipitation.

The AOM redox reaction can be described as the net reaction between seawater sulfate and methane (Eq. 6):



The dissolved inorganic carbon (bicarbonate) generated in the STMZ under anaerobic conditions increases alkalinity that promotes carbonate precipitation resulting in the formation of authigenic-carbonate (Eq. 7) (Boetius 2000; Regnier et al. 2011; Lash 2015).



This process is a widespread diagenetic reaction along modern continental margins (Reeburgh 2007, Lash 2015) where part of the generated

methane is consumed before it reaches the seafloor (Regnier et al. 2001). Therefore, methane oxidation during upward migration should also be taken into account to model biogenic gas processes. However, the integration of this process in basin modelling is complicated by the fact that the AOM thickness is very small, around 2 m within the STMZ, and occurs at variable shallow depths.

Based on the current knowledge from the offshore Aquitaine (Dupré et al. 2020), we can estimate the average amount of CH₄ consumed through the AOM. Using a mass balance approach, the CO₂ “trapped” in MDAC is 43% of the total molar mass of CaCO₃. The exact thickness of the MDAC outcropping and sub-cropping is unknown but with information from seismic data (Fig. 1, Dupré et al. 2020), we can estimate a variable thickness of 2 to 10 m which is discontinuous along the shelf. Considering an extent of MDAC of 200 km² (Fig. 14), we can determine an average volume of MDAC. Assuming an average thickness of 5 m for the MDAC, we can estimate the amount of CO₂ stored in the carbonates which corresponds to the total amount of CH₄ consumed through AOM.

The total mass of consumed CH₄ (mCH_4) through the AOM can be defined as (Eq. 8):

$$mCH_4 = \rho * V * f \quad (8)$$

where ρ is the CaCO₃ density (2700 kg/m³), V is the CaCO₃ volume (m³) and f is the molar fraction of CO₂ trapped as MDAC equal to 43%. Note that we are assuming that all CO₂ both in the system and trapped in the MDAC derives from methane oxidation only.

To convert the total CH₄ mass (Eq. 8) to total gas volume, we consider that at the emission water depth the gas density is 19.7 kg/m³ (Fig. 15) resulting in 5.89*10¹⁴ Mm³ of CH₄ (2.06 Tcf) that is trapped in MDAC. This means that 23% of the uprising methane is consumed through AOM resulting in a reduced total emission rate of 1.25 Tcf/My. Note that if we consider a lower limit of MDAC thickness of 2 m, the emission rate is 1.48 Tcf/My corresponding to 9% of CH₄ consumed

through AOM. In contrast, a higher thickness of 10 m results in 0.87 Tcf/My of microbial CH₄ emitted at the seafloor, corresponding to 46% of CH₄ trapped in MDAC.

Modelled present-day flow rates of microbial methane

The modelled hydrodynamic regime of the northern Aquitaine Basin is shown in Figure 16. During compaction, porosity loss induces vertical water expulsion (Fig. 16a, b). In our model, most of the gas is dissolved in the formation water (Fig. 13) in the upper layers that are characterized by unconsolidated sediments with high porosity (modelled values between 50 and 60%) (Fig. 16a, b). Therefore, we can approximate the methane flux to the vertical water flux. We also observe that the low porosity of MDAC at the seafloor acts as a barrier preventing the water to circulate easily up to the water-sediment interface (Fig. 16a). Migration and expulsion processes are then controlled by the hydrodynamic regime of the upper part of the basin in which methane migrates to the seafloor as a function of sediment geometry, permeability and water flux.

Our model indicates methane in a free gas phase whenever gas saturation is reached in the water. This condition is sensitive to the amount of free water in the layer, P-T conditions and amount of generated gas. Basin modelling grids are limited by their spatial resolution. Layer thickness and cell size can impact the amount of free water in the system. Gas saturation is reached when gas generation or pressure conditions are high enough to exceed the solubility threshold or when layer thickness is sufficiently small which reduces the amount of free water. In our model, we observe that the majority of the gas is dissolved in water due to gas saturation that is decreasing during upward migration caused by AOM. Indeed, in the Aquitaine Shelf, MDACs represent the main sink for CH₄ and therefore imply that gas remains dissolved in water up to the seafloor where it diffuses due to changing thermodynamic conditions at the seafloor. Given the high permeability of the upper unconsolidated sediments (Fig. 16 b), we can assume that the total

gas released at the present day is proportional to the water flow through the uppermost layer. Due to the absence of capillary pressure, it is not possible to accumulate hydrocarbons in the shallowest layer.

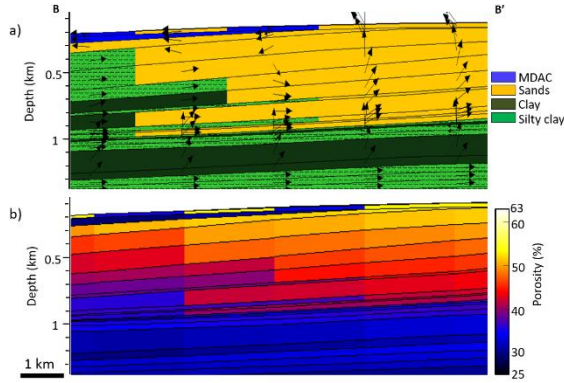


Figure 16. Modelled results along the 2D section B-B' shown in Figure 13. a) Facies distribution; b) Porosity (%). The black arrows show the water flow direction which is a function of facies and porosity.

Thus, we calculated the water flow through the second-last layer as follows (Eq. 9)

$$\text{Methane Flux} = \frac{[CH_4]_f t_f - [CH_4]_i t_i}{t_f - t_i} \quad (9)$$

where t_i corresponds to the last geological event defined in the model (0.14 Ma) and t_f to the present day. As shown in Figure 16, gas is migrating upward to the seafloor along the Aquitaine Shelf edge but no such activity is observed on the slope (Dupré et al. 2020; Michel et al. 2017). Variations of methane concentration in water have been computed for several grid cells and integrated over the northern study area (Fig. 1b) which yields an average methane flow rate of 27 Mg/y (Fig. 17). This number has the same order of magnitude as the estimated methane flow rate of 35 Mg/y from in situ flow rate measurements and acoustic data (Dupré et al. 2020).

In our model, the total mass of emitted methane yields a methane flux of 23 mgCH₄/m²/y over the northern Aquitaine surface (Fig. 1b). Present-day methane flow rates have also been compared with paleo-flow rates. We computed concentration changes of dissolved gas in water between the

deposition of the first Plio-Pleistocene source rock at 2.87 Ma and the following geological event ($\Delta t = 0.23$ My). The average amount of emitted methane in that time interval reaches 11 Mg/y corresponding to 9.8 mgCH₄/m²/y. In contrast, the deposition of the last source rock layer at 1.76 Ma and the following geological event ($\Delta t = 0.19$ My) results in a methane flow rate of 41 Mg/y corresponding to 35 mgCH₄/m²/y, which turns out to be the maximum modelled methane flux through the seafloor. Therefore, present-day flow rates are relatively smaller because all the source rocks are already deposited and the more “mature” Miocene source rock had already generated a large part of its labile potential resulting in a higher flux in the past compared to what we currently observe. This result is probably due to the absence of sediments above the Plio-Pleistocene source rocks during time of deposition (1.76 Ma), where the gas can easily escape through the seafloor compared to the present day where gas migration is controlled by an overburden and its permeability. Thus, gas migration over time along the offshore Aquitaine Shelf edge evolves as a function of variable generation and sedimentation rates. Note that in our study, we did not take into account a probable input from a Holocene source rock as proposed in Dupré et al. (2020). Indeed, in our model, the Holocene layers are too shallow (between 150 to 200 m of water depth along the shelf) to act as a probable biogenic source rock. We can also assume that its contribution to the final cumulative volume of generated/emitted gas would be low compared to any deeper source rock.

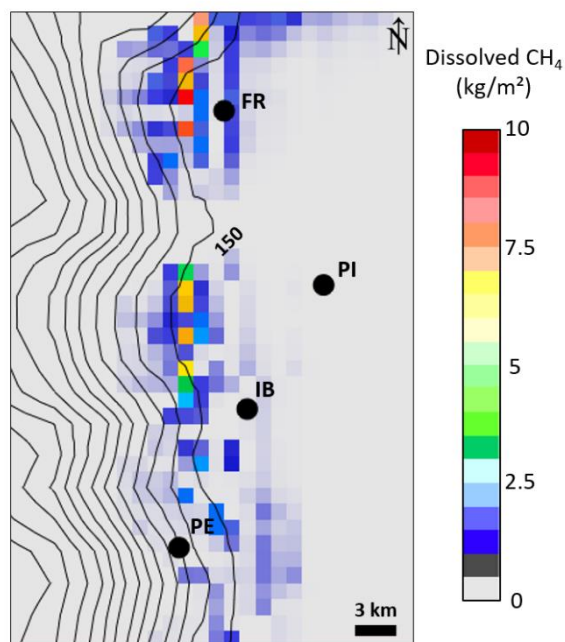


Figure 17. Present-day modelled dissolved methane (kg/m^2) in the second layer from top seafloor along the northern study area emission sites (for map location see Fig. 1b). Black dots indicate the offshore wells (FR – Fregate-1; PI – Pingouin-1; IB – Ibis-1; PE – Pelican-1) (Figs. 1, 3). Black lines represent the seafloor bathymetry with a contour interval of 50 m.

7. CONCLUSIONS

This study presents for the first time an attempt to quantify the total amount of emitted biogenic gas at the seafloor over time, applied to the Aquitaine Shelf. Along with a calibrated basin model, geochemical results from Rock-Eval and quantitative sensitivity analysis, we propose a model for the evolution of the microbial methane system in the sediments of the offshore Aquitaine Basin.

A global sensitivity analysis based on meta-models helped to identify the most critical parameters for gas generation. Given the uncertainty ranges for the input parameters, methane production appears mainly controlled by the reactivity of the OM rather than by the relative percentage of labile and thermo-labile compounds. The final amount of generated microbial methane strongly depends on the deposition age of the source rock. In our model, all source rocks depleted their thermo-labile fraction that is defined by a low activation energy. Only the shallower and more recent Plio-Pleistocene source

rocks still have a labile potential to generate biogenic gas compared to the older and deeper Miocene source rock that is totally depleted. However, a dedicated analytical assessment of the reaction kinetics and reactivity of the OM is required in order to more accurately assess OM degradation.

The generated gas is mainly present in the system as dissolved in water migrating vertically until it is finally released as a separate gas phase at the seafloor. Migration pathways are controlled by sediment permeability and by maximum generation rates along the shelf. This system seems to be active since the first source rock was deposited in the Messinian, with a mean modelled methane flow rate of 11 Mg/y until the deposition of the last source rock during the early Pleistocene where it reaches a maximum emission rate of 41 Mg/y when all source rocks were deposited without any further sedimentation and the gas was easily released at the seafloor. Modelling results also show that present-day methane flow rates (27 Mg/y) are in the same order of magnitude than flow rates estimated from in situ flow rate measurements and acoustic data (35 Mg/y) (Dupré et al. 2020). Our results confirm that the absence of a seal at the top of the system resulted in continuous methane emission over time along the offshore Aquitaine Shelf edge and CH_4 flow rate intensities evolved as function of microbial methane generation and sedimentation rates.

Our modelling approach demonstrates that a gas system originating from only microbial activity can be active over millions of years generating significant methane volumes that depend on the specific geological setting. In our 3D model, the mass of generated gas over time corresponds to 25.5 Gt/My of biogenic CH_4 . The difference between the total mass of generated methane and the total mass still in place (in either adsorbed, dissolved or free state) yields a loss of 0.91 Gt/My . However, part of this gas is not directly released at the seabed but rather oxidized into CO_2 through AOM during upward migration. Based on MDAC thickness variation of 2 - 10 m and assuming that all CO_2 present in the system is sourced by methane oxidation only, we could determine an average amount of consumed CH_4 through AOM

varying between 9% and 46% of the initial generated methane volume. Thus, the average volume of emitted gas over time along the Aquitaine Shelf ranges between 0.87 Tcf/My and 1.48 Tcf/My. This result demonstrates that if we want to better understand and estimate the total amount of emitted methane and its impact on the ocean/atmosphere carbon budget, we need to account for (1) the total amount of generated gas, (2) the total amount of trapped gas in the system and (3) the total amount of consumed gas through the AOM.

In this study, we present a new workflow to assess biogenic gas occurrences in continental shelf settings at the basin scale where microbial CH₄ is sourced from recent continental-derived OM. This new approach, applied and calibrated to the offshore Aquitaine, can help estimate the total CH₄ emitted naturally from shallow-water shelf areas that may reach the atmosphere. This subject is of particular interest for the scientific community working on the impact of global warming issues as methane is a major greenhouse gas with a negative contribution on climate and environment.

ACKNOWLEDGMENTS

The PhD thesis as well as the oceanographic expeditions Gazcogne1 (<http://dx.doi.org/10.17600/13020070>) and Gazcogne2 (<http://dx.doi.org/10.17600/13030090>) are co-funded by TOTAL, IFP Energies Nouvelles and IFREMER as part of the PAMELA (Passive Margin Exploration Laboratories) scientific project. Structural maps were provided by the OROGEN Project funded by Total, BRGM, CNRS & INSU. The author would like to thank Renaud Traby and Didier Granjeon for their constructive advices which helped to improve the basin model and Daniel Pillot for assistance during laboratory analysis. We also would like to thank Frederic Schneider and Matthieu Dubille from Beicip-Franlab for the helpful discussions and suggestions. Chris Boreham and an anonymous reviewer are also thanked for providing useful and constructive comments.

SUPPLEMENTARY MATERIALS

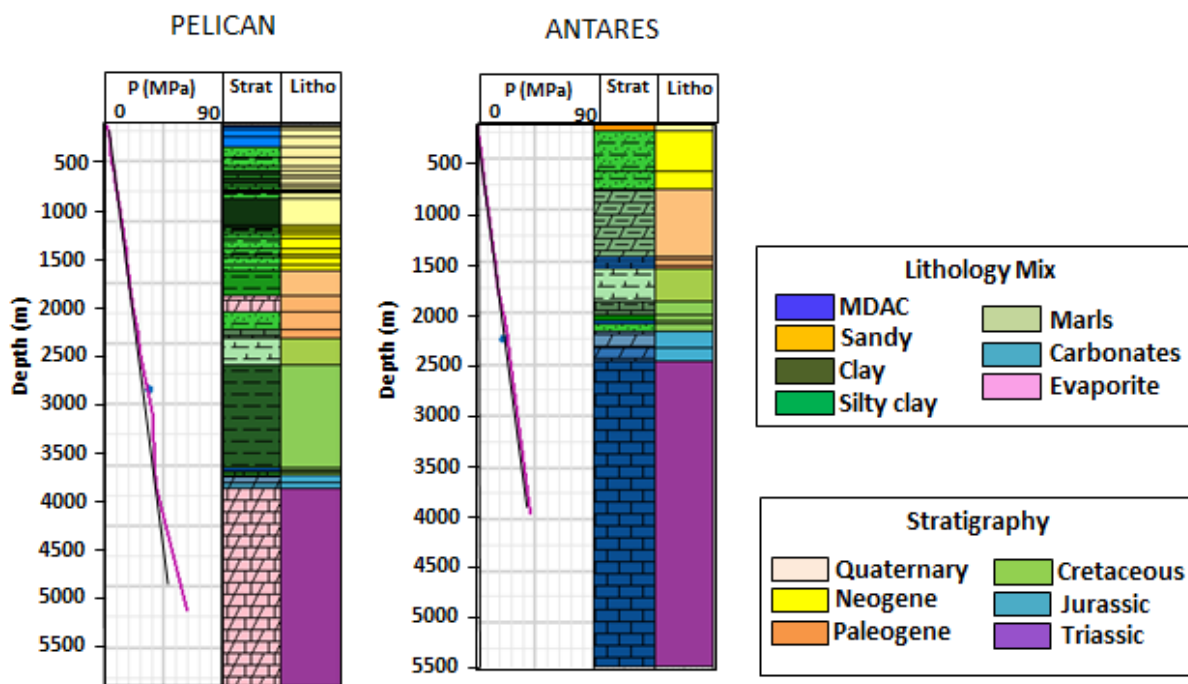


Figure S1. Pressure calibration for two wells. Well location is given in Fig. 3.

Table S1. Rock-Eval results on cuttings collected from two offshore wells (Pingouin-1 and Pelican-1). Well locations are given in Fig. 3.

Sample	Depth (m)	S2 (mgHc/g-rock)	Tmax (°C)	HI (mgHc/g TOC)	OI (mgCO₂/g TOC)	TOC (%)
PINGOUIN-1	595	0.22	424	51	286	0.44
PINGOUIN-2	715	0.12	437	41	427	0.28
PINGOUIN-3	735	0.11	423	41	387	0.26
PINGOUIN-4	875	0.04	422	21	501	0.2
PINGOUIN-5	955	0.09	421	31	343	0.29
PINGOUIN-6	1025	0.11	420	39	334	0.29
PINGOUIN-7	1125	0/05	420	25	430	0.22
PINGOUIN-8	1145	0.14	420	39	292	0.35
PINGOUIN-9	1265	0.14	422	43	307	0.32
PINGOUIN-10	1325	0.15	421	47	279	0.32
PINGOUIN-11	1425	0.1	421	33	305	0.31
PELICAN-1	740	0.14	421	32	328	0.44
PELICAN-2	860	0.15	424	34	306	0.44
PELICAN-3	960	0.19	424	38	290	0.49
PELICAN-4	1050	0.19	422	43	292	0.46
PELICAN-5	1200	0.1	422	27	321	0.36
PELICAN-6	1280	0.15	439	36	387	0.41
PELICAN-7	1493	5.67	432	55	106	10.35
PELICAN-8	1500	0.21	421	38	238	0.53
PELICAN-9	1530	0.2	420	43	284	0.47

REFERENCES

- Arndt, S.; Jørgensen, B.B.; LaRowe, D.E.; Middelburg, J.J. Pancost, R.D. Regnier, P. (2013). Quantifying the degradation of organic matter in marine sediments. A review and synthesis. *Earth-Science Reviews*, 123, 53–86. [https://DOI: 10.1016/j.earscirev.2013.02.008](https://doi.org/10.1016/j.earscirev.2013.02.008).
- Arning, E.T., van Berk, W., dos Santos Neto, E.V., Naumann, R., and Schulz, H.M. (2013). The quantification of methane formation in Amazon fan sediments (ODP leg 155, site 938) by hydrogeochemical modeling solid–aqueous solution–gas interactions. *Journal of South American Earth Sciences*, 42, 205-215.
- Artemieva, I.M.; Thybo, H. (2013): EUNaseis. A seismic model for Moho and crustal structure in Europe, Greenland, and the North Atlantic region. In: *Tectonophysics*, 609, pp. 97–153. DOI: 10.1016/j.tecto.2013.08.004.
- Baudin, F.; Disnar, J.R.; Aboussou, A.; Savignac, F. (2015): Guidelines for Rock–Eval analysis of recent marine sediments. In: *Organic Geochemistry*, 86, pp. 71–80. DOI: 10.1016/j.orggeochem.2015.06.009.
- Behar, F. Vandenbroucke, M. Tang, Y. Marquis, F. and Espitalié, J. 1997, Thermal cracking of kerogen in open and closed systems: determination of kinetic parameters and stoichiometric coefficients for oil and gas generation. *Organic Geochemistry*, 26, 321–339
- Behar, F.; Beaumont, V.; B. Penteado, H.L.D.B. (2001): Rock-Eval 6 Technology. Performances and Developments. In: *Oil and Gas Science and Technology - Rev. IFP n. 2*, 56, pp. 111–134. DOI: 10.2516/ogst:2001013.

- Belyaev, S.S.; Wolkin, R.; Kenealy, W.R.; De Niro, M.J.; Epstein S.; Zeikus, J.G. (1983): Methanogenic Bacteria from the Bondyuzhskoe Oil Field: General Characterization and Analysis of Stable-Carbon Isotopic Fractionation. In: *Applied and Environmental Microbiology* n. 2, 45, pp. 691–697.
- Biteau, J.J.; Le Marrec, A.; Le Vot, M.; Masset, J.M. (2006): The Aquitaine Basin. In: *Petroleum Geoscience* n. 12, pp. 247–273.
- Boetius, A.; Ravenschlag, K.; Schubert, C.J.; Rickert, D.; Widdel, F.; Gieseke, A. et al. (2000): A marine microbial consortium apparently mediating anaerobic oxidation of methane. In: *Nature* n. 6804, 407, pp. 623–626. DOI: 10.1038/35036572.
- Boillot, G.; Dupeuble, P.A.; Malod, J. (1979): Subduction and tectonics on the continental margin off northern Spain. In: *Marine Geology* n. 1-2, 32, pp. 53–70. DOI: 10.1016/0025-3227(79)90146-4.
- Bois, C.; Pinet, B.; Gariel, O. (1997): The sedimentary cover along the ECORS Bay of Biscay deep seismic reflection profile. A comparison between the Parentis basin and other European rifts and basins. In: *Mémoires de la Société géologique de France*, n. 171, pp. 143–165.
- Boudreau, B.P. and Ruddick, B.R. (1991): On a reactive continuum representation of organic matter diagenesis. In: *American Journal of Science* n. 5, 291, pp. 507–538. DOI: 10.2475/ajs.291.5.507.
- Brothers, D.S. Ruppel, C. Kluesner, J.W. Ten Brink, U.S. Chaytor, J.D. Hill, J. C. Andrews, B.D and Flores, C. (2014). Seabed fluid expulsion along the upper slope and outer shelf of the US Atlantic continental margin. *Geophysical Research Letters*, 41(1), 96-101.
- Brunet, M.F. (1994): Subsidence in the Parentis Basin (Aquitaine, France): Implications of the Thermal Evolution. In: *Hydrocarbon and Petroleum Geology of France*. Volume 4 ISBN : 978-3-642-78851-2
- Brunet, M-F (1997): Subsidence along the ECORS Bay of Biscay deep seismic profile. In: *Mémoires de la Société géologique de France*, 171, pp. 167–176.
- Burdige, D.J. (2007): Preservation of organic matter in marine sediments: controls, mechanisms, and an imbalance in sediment organic carbon budgets? In: *Chemical reviews* n. 2, 107, pp. 467–485. DOI: 10.1021/cr050347q.
- Burdige, D.J. (2011): Temperature dependence of organic matter remineralization in deeply-buried marine sediments. In: *Earth and Planetary Science Letters* n. 3-4, 311, pp. 396–410. DOI: 10.1016/j.epsl.2011.09.043.
- Canuel, E.A. and Martens, C.S. (1996). Reactivity of recently deposited organic matter: Degradation of lipid compounds near the sediment-water interface. *Geochimica et cosmochimica acta*, 60 (10), 1793-1806.
- Carr, A.D. (2000): Suppression and retardation of vitrinite reflectance, Part 1. Formation and significance for hydrocarbon generation. In: *Journal of Petroleum Geology* n. 23, pp. 313–343.
- Clayton, C. (1992): Source Volumetrics of Biogenic Gas Generation. In: *Bacterial Gas*, 1992, pp. 191–204.
- Cohen, D., Person, M., Wang, P., Gable, C.W., Hutchinson, D., Marksamer, A., Dugan B., Kooi, K., Groen, K., Lizarralde, D., Evans R.L., Day-Lewis, F.D., Lane, J.W.J. (2010). Origin and extent of fresh paleowaters on the Atlantic continental shelf, USA. *Ground Water*, 48(1), 143-158.
- Conrad, R. (2005). Quantification of methanogenic pathways using stable carbon signatures: a review and a proposal. *Org. Geochem.* 36, 739-572.

- Cowie, G. L., Hedges, J. I., & Calvert, S. E. (1992). Sources and relative reactivities of amino acids, neutral sugars, and lignin in an intermittently anoxic marine environment. *Geochimica et Cosmochimica Acta*, 56(5), 1963-1978.
- Cremer, M. (1983). Approches sédimentologique et géophysique des accumulations turbiditiques: l'éventail profond du Cap Ferret (Golfe de Gascogne), la série des grès d'Annot (Alpes de Haute Provence). Thèse de doctorat de l'Université Bordeaux 1, 419 pp.
- Dembicki, H. (2016): Practical petroleum geochemistry for exploration and production. 1st edition. Waltham MA: Elsevier.
- Deming, D. (1989): Application of bottom-hole temperature corrections in geothermal studies. In: *Geothermics* n. 5-6, 18, pp. 775–786. DOI: 10.1016/0375-6505(89)90106-5.
- Desegaulx, P.; Brunet, M.F. (1990): Tectonic subsidence of the Aquitaine Basin since Cretaceous times. In: *Bulletin de la Société Géologique de France* n. 2, VI, pp. 295–306. DOI: 10.2113/gssgfbull.VI.2.295.
- Dickens, G.R. (2004): Hydrocarbon-driven warming. In: *Nature* n. 429, 6991, pp. 513–515.
- Dieckmann, V. (2005): Modelling petroleum formation from heterogeneous source rocks: the influence of frequency factors on activation energy distribution and geological prediction. *Marine and Petroleum Geology*, 22, 375-390.
- Duan, Z.; Moller, N.; Weare, J.H. (1992). Prediction of methane solubilities in natural waters to high ionic strength from 0 to 250 °C and from 0 to 1600 bar. *Geochim.Cosmochim. Acta* 56, 1451–1460.
- Ducros, M. and Wolf, S. (2014): Tests des développements du modèle de génération du gaz biogénique dans Visco. IFPEN Internal Report (R161/MD-OC 14-005).
- Ducros, M.; Cacas, M.C.; Rouchon, V.; Wolf, S.; Blanchet, D.; Ravin, A.; Pujol, A. (2015): Simulation of anaerobic SOM biodegradation and biogenic methane production in the TemiFlow basin model. IMOG. Prague, 2015.
- Dupré, S. (2013) GAZCOGNE2 cruise, RV Pourquoi pas ? doi:<https://doi.org/10.17600/13030090>
- Dupré, S. Woodside, J. Foucher, J.P. de Lange, G. Mascle, J. Boetius, A. Mastalerz, V. Stadnitskaia, A. Ondréas, H. Huguen, C. Harmegnies, F. Gontharet, S. Loncke, L. Deville, E. Niemann, H. Omoregie, E. Olu-Le Roy, K. Fiala-Medioni, A. Dählmann, A. Caprais, J.C. Prinzhofer, A. Sibuet, M. Pierre, C. Sinninghe Damsté, J. NAUTINIL scientific Party (2007) Seafloor geological studies above active gas chimneys off Egypt (Central Nile Deep Sea Fan). *Deep Sea Research Part I: Oceanographic Research Papers* 54 (7):1146-1172. doi:10.1016/j.dsr.2007.03.007
- Dupré, S.; Berger, L.; Le Bouffant, N.; Scalabrin, C.; Bourillet, J.F. (2014): Fluid emissions at the Aquitaine Shelf (Bay of Biscay, France). A biogenic origin or the expression of hydrocarbon leakage? In: *Continental Shelf Research*, 88, pp. 24–33. DOI: 10.1016/j.csr.2014.07.004.
- Dupré, S. Loubrieu, B. Pierre, C. Scalabrin, C. Guérin, C. Ehrhold, A. Ogor, A. Gautier, E. Ruffine, L. Biville, R. Saout, J. Breton, C. Floodpage, J. Lescanne, M. (2020) The Aquitaine Shelf Edge (Bay of Biscay): A Primary Outlet for Microbial Methane Release. *Geophysical Research Letters* 47 (7):e2019GL084561. doi:10.1029/2019gl084561.
- Espitalié, J.; Deroo, G.; Marquis, F. (1985): Rock-Eval pyrolysis and its applications. In: *Revue De Institut Francais Du Petrole* n. 5, 40, pp. 563–579.

- Espitalié, J.; Madec, M.; Tissot, B.; Mennig, J. J.; Leplat, P. (1977): Source Rock Characterization Method for Petroleum Exploration. In: Offshore Technology Conference. OTC, 1977/1/1: Offshore Technology Conference, p. 6.
- Etiopie, G. and Klusman, R. W. (2002). Geologic emissions of methane to the atmosphere. *Chemosphere*, 49(8), 777-789.
- Etiopie, G. Lassey, K.R. Klusman, R.W. and Boschi, E. (2008). Reappraisal of the fossil methane budget and related emission from geologic sources. *Geophysical Research Letters*, 35(9).
- Etiopie, G. and Klusman, R. W. (2010). Methane microseepage in drylands: soil is not always a CH₄ sink. *Journal of Integrative Environmental Sciences*, 7(S1), 31-38.
- Etiopie, G. and Schwietzke, S. (2019). Global geological methane emissions: an update of top-down and bottom-up estimates. *Elementa-Science of the Anthropocene*.
- Feraille, Marrel, 2012. Prediction under uncertainty on a mature field. *Oil Gas Sci. Technol.* 67 (2), 193–206. <https://doi.org/10.2516/ogst/2011172>.
- Ferrer, O.; Roca, E.; Benjumea, B.; Muñoz, J. A.; Ellouz, N.; MARCONI Team (2008): The deep seismic reflection MARCONI-3 profile. Role of extensional Mesozoic structure during the Pyrenean contractional deformation at the eastern part of the Bay of Biscay. In: *Marine and Petroleum Geology* n. 8, 25, pp. 714–730. DOI: 10.1016/j.marpetgeo.2008.06.002.
- Floodgate, G.D.; Judd, A.G. (1992): The origins of shallow gas. In: *Continental Shelf Research* n. 10, 12, pp. 1145–1156. DOI: 10.1016/0278-4343(92)90075-U.
- Fujii, T., Tin Aung, T., Wada, N., Komatsu, Y., Suzuki, K., Ukita, T., Wygrala, B., Fuchs, T., Rottke, W., Egawa, K. (2016). Modeling gas hydrate petroleum systems of the Pleistocene turbiditic sedimentary sequences of the Daini-Atsumi area, eastern Nankai Trough, Japan. *Interpretation*, 4(1), SA95-SA111.
- Gervais, V.; Ducros, M.; and Granjeon, D. (2018). Probability maps of reservoir presence and sensitivity analysis in stratigraphic forward modeling. *AAPG Bulletin*, 102(4), 613-628.
- Hedges, J. I., and Oades, J. M. (1997). Comparative organic geochemistries of soils and marine sediments. *Organic geochemistry*, 27(7-8), 319-361.
- Homma, T. and Saltelli, A. (1996): Importance measures in global sensitivity analysis of model output: Reliability Engineering and System Safety, v. 52, no. 1, p. 1–17, doi: 10.1016/0951-8320(96)00002-6.
- Hornafius, J.S.; Quigley, D.; and Luyendyk, B.P. (1999). The world's most spectacular marine hydrocarbon seeps (Coal Oil Point, Santa Barbara Channel, California): Quantification of emissions. *Journal of Geophysical Research: Oceans*, 104(C9), pp. 20703-20711.
- Hovland, M.; Gardner, J.V.; Judd, A.G. (2002): The significance of pockmarks to understanding fluid flow processes and geohazards. In: *Geofluids* n. 2, 2, pp. 127–136. DOI: 10.1046/j.1468-8123.2002.00028.x.
- IPCC (2013). Climate Change 2013: The Physical Science Basis. Contribution of Working Group I to the Fifth Assessment Report of the Intergovernmental Panel on Climate Change. Cambridge, UK and New York: Cambridge University Press. doi:10.1017/CBO9781107415324
- ISO 12213-2 (2006) Natural gas - Calculation of compression factor - Part 2: Calculation using molar-composition analysis.

- Janssen, B.H. (1984): A simple method for calculating decomposition and accumulation of 'young' soil organic matter. In: *Plant and Soil*, 76, pp. 297–304.
- Jensen, P. (1992): "Bubbling reefs' in the Kattegat: submarine landscapes of carbonate- cemented rocks support a diverse ecosystem at methane seeps. In: *Mar. Ecol. Prog. Ser.* n. 83, pp. 103–112.
- Johnson, H.P. Miller, U.K. Salmi, M.S. and Solomon, E.A. (2015). Analysis of bubble plume distributions to evaluate methane hydrate decomposition on the continental slope. *Geochemistry, Geophysics, Geosystems*, 16(11), pp. 3825-3839.
- Jones, R.W. Edison, A. (1979): Microscopic observations of kerogen related to geochemical parameters with emphasis on thermal maturation. In: *Society Economic Paleontologists and Mineralogists*, pp. 1–12.
- Judd, A.G.; Hovland, M.; Dimitrov, L.I.; Garcia Gil, S.; Jukes, V. (2002): The geological methane budget at Continental Margins and its influence on climate change. In: *Geofluids* n. 2, 2, pp. 109–126. DOI: 10.1046/j.1468-8123.2002.00027.x.
- Judd, A.G. (2004). Natural seabed gas seeps as sources of atmospheric methane. *Environmental Geology*, 46(8), 988-996.
- Kamga, N. (2016). "Low-Temperature Artificial Maturation Studies of Type II and Type III Kerogens: Implications for Biogenic Gas Production". Doctor of Philosophy (PhD), Dissertation, Chemistry and Biochemistry, Old Dominion University, DOI: 10.25777/5sj5-4y45.
- Katz, B.J. (2011): Microbial Processes and Natural Gas Accumulations. In: *TOGEOJ* n. 1, 5, pp. 75–83. DOI: 10.2174/1874262901105010075.
- Khalil, M.A.K. (2013). Atmospheric methane: sources, sinks, and role in global change (Vol. 13). Springer Science and Business Media.
- Klusman, R.W.; Leopold, M.E.; LeRoy, M.P. (2000). Seasonal variation in methane fluxes from sedimentary basins to the atmosphere: Results from chamber measurements and modeling of transport from deep sources. *Journal of Geophysical Research: Atmospheres*, 105(D20), 24661-24670.
- Kvenvolden, K.A. (1993): Gas hydrates geological perspective and global change. In: *American Geophysical Union*, pp. 173–187.
- Kvenvolden, K.A.; Lorenson, T.D.; Reeburgh, W.S. (2001). Attention turns to naturally occurring methane seepage. *Eos, Transactions American Geophysical Union*, 82(40), 457-457.
- Lafargue, E.; Marquis, F.; Pillot, D. (1998): Rock-Eval 6 Applications in Hydrocarbon Exploration, Production, and Soil Contamination Studies. In: *Rev. Inst. Fr. Pét.* n. 4, 53, pp. 421–437. DOI: 10.2516/ogst:1998036.
- Lash, G.G. (2015). Pyritization induced by anaerobic oxidation of methane (AOM)—An example from the upper devonian shale succession, western New York, USA. *Marine and Petroleum Geology*, 68, 520-535. <https://doi.org/10.1016/j.marpetgeo.2015.10.002>.
- Loubrieu, B. (2013) GAZCOGNE1 cruise, RV Le Suroît. doi:<https://doi.org/10.17600/13020070>
- Martens, Canuel, 1996. Reactivity of recently deposited organic matter: Degradation of lipid compounds near the sediment-water interface. *Geochem. Cosmochim. Acta* 60 (10), 1806–1973. [https://doi.org/10.1016/0016-7037\(96\)00045-2](https://doi.org/10.1016/0016-7037(96)00045-2).

- McKay, M.D.; Beckman, R.J.; Conover, W.J. (1979): Comparison of three methods for selecting values of input variables in the analysis of output from a computer code: *Technometrics*, v. 21, no. 2, p. 239–245.
- McKenzie, D. (1978): Some remarks on the development of sedimentary basins. In: *Earth and Planetary Science Letters* n. 1, 40, pp. 25–32. DOI: 10.1016/0012-821X(78)90071-7.
- Michel G. (2017) Mise en place et pérennisation d'un vaste système fluide microbien sur le Plateau Aquitain: caractérisation et facteurs de contrôle. Thèse de doctorat de l'Université Pierre et Marie Curie, Paris, pp. 482.
- Michel, G.; Dupré, S.; Baltzer, A.; Ehrhold, A.; Imbert, P.; Pitel, M. et al. (2017): Pockmarks on the South Aquitaine Margin continental slope: the 2 seabed expression of past fluid circulation and bottom currents Corresponding Author. In: *Comptes Rendus Géoscience, Elsevier Masson* n. 8, 349, pp. 391–401.
- Middelburg, J.J. (1989): A simple rate model for organic matter decomposition in marine sediments. In: *Geochimica et Cosmochimica Acta* n. 7, 53, pp. 1577–1581. DOI: 10.1016/0016-7037(89)90239-1.
- Middelburg, J.J.; Klaver, G.; Nieuwenhuize, J.; Wielemaker, A.; de Haas, W.; Vlug, T.; van der Nat, J.F. (1996). Organic matter mineralization in intertidal sediments along an estuarine gradient. *Marine Ecology Progress Series*, 132, 157-168.
- Mitterer, R.M. (2010). Methanogenesis and sulfate reduction in marine sediments: A new model. *Earth and Planetary Science Letters*, 295(3-4), 358-366.
- Oberlin, A.; Boulmier, J.L.; Villey, M. (1980). Electron microscopic study of kerogen microtexture. In: Durand, B. (Ed.), *Selected Criteria for Determining the Evolution Path and Evolution Stage of Kerogen*. Kerogen, Editions Technip, Paris, pp. 191–242.
- Ortiz, A.; Guillocheau, F.; Lasseur, E.; Briais, J.; Robin, C.; Serrano, O.; Fillon, C. (2020). Sediment routing system and sink preservation during the post-orogenic evolution of a retro-foreland basin: The case example of the North Pyrenean (Aquitaine, Bay of Biscay) Basins. *Marine and Petroleum Geology*, vol. 112, p. 104085.
- Pasquale, V.; Gola, G.; Chiozzi, P.; Verdoya, M. (2011): Thermophysical properties of the Po Basin rocks. In: *Geophysical Journal International* n. 1, 186, pp. 69–81. DOI: 10.1111/j.1365-246X.2011.05040.x.
- Paull, C.K., and Ussler III, W. (2008, July). Re-evaluating the significance of seafloor accumulations of methane-derived carbonates: seepage or erosion indicators. In *Proceedings of the 6th International Conference on Gas Hydrates (ICGH 2008), Vancouver, British Columbia, Canada, July* (pp. 6-10).
- Peters, K.E.; Burnham, A.K.; Walters, C.C.; Schenk, O. (2018). Guidelines for kinetic input to petroleum system models from open-system pyrolysis. *Marine and Petroleum Geology*, 92, 979-986.
- Pierre, C.; Demange, J.; Blanc-Valleron, M.M.; Dupré, S. (2017a): Authigenic carbonate mounds from active methane seeps on the southern Aquitaine Shelf (Bay of Biscay, France). Evidence for anaerobic oxidation of biogenic methane and submarine groundwater discharge during formation. In: *Continental Shelf Research*, 133, pp. 13–25. DOI: 10.1016/j.csr.2016.12.003.
- Pierre C, Blanc-Valleron M-M, Boudouma O, Lofi J (2017b) Carbonate and silicate cementation of siliciclastic sediments of the New Jersey shelf (IODP Expedition 313): relation with organic matter diagenesis and submarine groundwater discharge. *Geo-Marine Letters* 37 (6):537-547. doi:10.1007/s00367-017-0506-6

- Pujol, A.; Rouchon, V.; Ravin, A.; Wolf, S.; Blanchet, D.; Ducros, M.; Maurand, N. (2016): Simulation of Anaerobic SOM Biodegradation and Biogenic Methane Production for Basin Modeling. AAPG Hedberg Conference. Santa Barbara, California, 2016.
- Reeburgh, W.S. (2007). Oceanic methane biogeochemistry. *Chem. Rev.* 107, 486-513.
- Regnier, P. Dale, A.W. Arndt, S. La Rowe, D.E. Mogollon, J. Van Cappellen, P. (2011). Quantitative analysis of anaerobic oxidation of methane (AOM) in marine sediments: a modeling perspective. *Earth-Sci. Rev.* 106, pp. 105-130.
- Rice, D.D. (1992): Controls, habitat, and resource potential of ancient bacterial gas. In: *Bacterial Gas*, 1992, pp. 91–118.
- Rice, D.D. and Claypool, G.E. (1981): Generation, Accumulation, and Resource Potential of Biogenic Gas. In: *AAPG Bulletin* n. 1, 65, pp. 5–25.
- Robinson, A.R. and Brink, K.H. (2005). The global coastal ocean: multiscale interdisciplinary processes (Vol. 13). Harvard University Press.
- Roca, E.; Muñoz, J.A.; Ferrer, O.; Ellouz, N. (2011): The role of the Bay of Biscay Mesozoic extensional structure in the configuration of the Pyrenean orogen. Constraints from the MARCONI deep seismic reflection survey. In: *Tectonics* n. 2, 30, n/a-n/a. DOI: 10.1029/2010TC002735.
- Römer, M.; Sahling, H.; Pape, T.; Bahr, A.; Feseker, T.; Wintersteller, P.; Bohrmann, G. (2012): Geological control and magnitude of methane ebullition from a high-flux seep area in the Black Sea—the Kerch seep area. In: *Marine Geology*, 319-322, pp. 57–74. DOI: 10.1016/j.margeo.2012.07.005.
- Ruffine, L.; Donval, J.P.; Croguennec, C.; Bignon, L.; Birot, D.; Battani, A. Bayon, G.; Caprais, J.C.; Lantéri, N.; Levaché, D.; Dupré, S. (2017): Gas Seepage along the Edge of the Aquitaine Shelf (France). Origin and Local Fluxes. In: *Geofluids* n. 66, 2017, pp. 1–13. DOI: 10.1155/2017/4240818.
- Saunois, M.; Bousquet, P.; Poulter, B.; Peregon, A.; Ciais, P.; Canadell, J. G.; ... and Janssens-Maenhout, G. (2016). The global methane budget 2000–2012. *Earth System Science Data*, 8(2), 697-751.
- Schenk, H.J.; Horsfield, B.; Krooss, B.; Schaefer, R.G.; Schwochau, K. (1997)b. Kinetics of petroleum formation and cracking, Petroleum and basin evolution; insights from petroleum geochemistry, geology and basin modeling. Springer, Berlin, Federal Republic of Germany
- Schneider, F.; Dubille M.; Montadert, L. (2016) Modeling of microbial gas generation: application to the eastern Mediterranean "Biogenic Play". *Geologica Acta* 14 (4), pp. 403-417. doi:10.1344/GeologicaActa2016.14.4.5
- Schulz, H.D. and Zabel, M. (2006): Marine geochemistry. 2nd rev. updated and extended ed. Berlin, New York: Springer.
- Schwietzke, S.; Sherwood, O.A.; Bruhwiler, L.M.; Miller, J.B.; Etiope, G.; Dlugokencky, E.J.; ... and Tans, P.P. (2016). Upward revision of global fossil fuel methane emissions based on isotope database. *Nature*, 538(7623), 88-91.
- Sibuet, J.C.; Monti, S.; Loubrieu, B.; Mazé, J.P.; Srivastava, S. (2004). Carte bathymétrique de l'Atlantique nord-est et du golfe de Gascogne: implications cinématiques (9 fig. 1 pl ht). *Bulletin-Société Géologique De France*, 175, 429-442.
- Skarke, A.; Ruppel, C.; Kodis, M.; Brothers, D.; Lobecker, E. (2014): Widespread methane leakage from the sea floor on the northern US Atlantic margin. In: *Nature Geosci* n. 9, 7, pp. 657–661. DOI: 10.1038/ngeo2232.

- Sobol', I.M. 1990, On sensitivity estimation for nonlinear mathematical models: *Mathematical Modeling and Computational Experiment*, v. 1, no. 4, p. 407–414.
- Starling, K.E. and Savidge, J.L. (1992). Compressibility factors of natural gas and other related hydrocarbon gases. American Gas Association, Operating Section.
- Thauer, R.K. (2010). Functionalization of methane in anaerobic microorganisms. *Angewandte Chemie International Edition*, 49(38), 6712-6713.
- Thinon, I.; Fidalgo-González, L.; Réhault, J.P.; Olivet, J.L. (2001): Déformations pyrénéennes dans le golfe de Gascogne. In: *Comptes Rendus de l'Académie des Sciences - Series IIA - Earth and Planetary Science* n. 9, 332, pp. 561–568. DOI: 10.1016/S1251-8050(01)01576-2.
- Toole, J.M. (1981): Sea ice, winter convection, and the temperature minimum layer in the Southern Ocean. In: *Journal of Geophysical Research: Oceans* n. C9, 86, pp. 8037–8047. DOI: 10.1029/JC086iC09p08037.
- Tugend, J.; Manatschal, G.; Kuszniir, N.J.; Masini, E. (2015): Characterizing and identifying structural domains at rifted continental margins. Application to the Bay of Biscay margins and its Western Pyrenean fossil remnants. In: *Geological Society, London, Special Publications* n. 1, 413, pp. 171–203. DOI: 10.1144/SP413.3.
- Tugend, J.; Manatschal, G.; Kuszniir, N. J.; Masini, E.; Mohn, G.; Thinon, I. (2014): Formation and deformation of hyperextended rift systems. Insights from rift domain mapping in the Bay of Biscay-Pyrenees. In: *Tectonics* n. 7, 33, pp. 1239–1276. DOI: 10.1002/2014TC003529.
- van Hinsbergen, D.J.J.; de Groot, L.V.; van Schaik, S.J.; Spakman, W.; Bijl, P.K.; Sluijs, A.; Langereis, C.G.; Brinkhuis, H. (2015): A Paleolatitude Calculator for Paleoclimate Studies. *PloS one* (6).
- Vandenbroucke, M., and Largeau, C. (2007). Kerogen origin, evolution and structure. *Organic Geochemistry*, 38(5), 719-833.
- Wallmann, K.; Aloisi, G.; Haeckel, M.; Obzhairov, A.; Pavlova, G.; Tishchenko, P. (2006): Kinetics of organic matter degradation, microbial methane generation, and gas hydrate formation in anoxic marine sediments. In: *Geochimica et Cosmochimica Acta* n. 15, 70, pp. 3905–3927. DOI: 10.1016/j.gca.2006.06.003.
- Wellsbury, P., Mather, I., & Parkes, R. J. (2002). Geomicrobiology of deep, low organic carbon sediments in the Woodlark Basin, Pacific Ocean. *FEMS microbiology ecology*, 42(1), 59-70.
- Wendebourg, J. (2003). Uncertainty of petroleum generation using methods of experimental design and response surface modeling: application to the Gippsland Basin, Australia. In: Düppenbecker, S. Marzi, R. (Eds.), *Multidimensional Basin Modeling*, AAPG/Datapages Discovery Series, vol. 7, pp. 295–307.
- Westrich, J.T. and Berner, R.A. (1984): The role of sedimentary organic matter in bacterial sulfate reduction: The G model tested. In: *American Society of Limnology and Oceanography*, pp. 236–249.
- Whiticar, M.J. (1994): Correlation of Natural Gases with Their Sources: Chapter 16: Part IV. Identification and Characterization.
- Whiticar, M.J.; Faber, E.; Schoell M. (1986): Biogenic methane formation in marine and freshwater environments: CO₂ reduction vs. acetate fermentation - Isotope evidence. In: *Geochimica et Cosmochimica Acta*, 50, pp. 693–709.

Whiticar, M.J. (1999): Carbon and hydrogen isotope systematics of bacterial formation and oxidation of methane. In: *Chemical Geology* n. 1-3, 161, pp. 291–314. DOI: 10.1016/S0009-2541(99)00092-3.

Wygrala, B. (1989). Integrated study of an oil field in the southern Po basin, northern Italy (No. FZJ-2014-03033). Publikationen vor 2000.

Zonneveld, K.A., Versteegh, G. J., Kasten, S., Eglinton, T.I., Emeis, K. C., Huguet, C., Koch, B.P., de Lange, G.J., de Leeuw, J.W., Middelburg, J.J., Mollenhauer, G., Prahl, F.G., Rethemeyer, J., Wakeham, S.G. (2010). Selective preservation of organic matter in marine environments; processes and impact on the sedimentary record. *Biogeosciences*, 7(2), pp. 483-511.

6. Issues with the analytical procedure to characterize recent terrestrial OM

Determining the degradation rate of a SOM is a challenging task and requires a good assessment of the molecular composition of the original deposited OM. Even if early diagenesis mechanisms and rates have been largely studied, the interaction between the microbial activity and the molecular composition of a SOM requires further investigations. Several studies have been published to reconstruct the initial molecular composition of the OM and its repartition in refractory and labile compounds (Hatcher et al. 2014a; Ravin et al. 2013; Ravin et al. 2017; Burdige 2007, 2011; Clayton 1992). However, all of these studies have been mainly applied on a type II OM, and initial fractions of molecular compounds derived from enriched lacustrine (type I OM), Sulphur-enriched (type II/S OM) or continental (type III OM) sources are still lacking.

Ravin et al. (2013) and later Hatcher et al (2014) published a workflow to calculate the initial TOC during early diagenesis. The authors reconstructed the initial molecular composition of a type II OM from samples of organic-rich sediments of the Ocean Drilling Program collected in offshore Namibia. Through Rock-Eval and Elemental Analysis, Fourier Transform Infrared Spectroscopy (FTIR) and Nuclear Magnetic Resonance Spectroscopy (^{13}C NMR) they were able to determine a quantitative repartition of the OM compounds in different classes (*e.g* aliphatic, aromatic, ester, carboxylic, amide...). Based on the ^{13}C NMR results, they deduced the initial SOM composition of main biomolecules (proteins, carbohydrates, lipids and lignin).

In our study, we tried to apply a simplified experimental strategy following the same procedure to reconstruct the initial TOC of the OM on a type III kerogen. The objective was to estimate a repartition of the initial TOC between labile and refractory fractions for the SOM collected in recent sediments of the Aquitaine Basin and the Mozambique Channel, and the degradation rate of such labile fractions (*i.e.* R_{bio} parameter - chapter 5) and the reactivity of the thermo-labile components (*i.e.* Ea parameter - chapter 5).

The geochemical characterization of the OM collected in the Aquitaine Basin was performed on cuttings collected from exploration wells since it was not possible to work on core samples. Although cuttings samples are not appropriate to study pure OM, we tentatively

characterized the evolution of the OM from the Miocene source rock layers to the shallowest layers (Plio-Pleistocene units). Previous Rock-Eval 6 analyses on bulk rocks from Miocene layers were used to select OM rich-intervals. The selection of cuttings from the shallower strata was based on well-log analysis (e.g. gamma-ray). Two wells were selected in the offshore Aquitaine: PINGOUIN and PELICAN. The wells are located along the shelf break of the basin where fluid emissions were identified (Dupré et al. 2014, 2020). All the cuttings are stored in the TOTAL scientific center (CSTJF - Pau) (Figure 27).



Figure 27. Cuttings storage at the CSTJF – Pau. 20 cuttings samples were collected from PELICAN and PINGOUIN wells.

Based on quality and quantity, we selected 20 samples from cuttings. All samples were washed and prepared in accordance with the procedure applied in Total. However, they presented an elevated salt content which can alter the Rock-Eval device (Baudin et al. 2015). Thus, the samples required to be properly desalted using distilled water. A Rock-Eval pre-screening was performed to infer an average TOC content of the set of samples.

A first Rock-Eval analysis was conducted on the entire sample-set (Table 2). The samples showed low to moderate TOC content with HI and OI values typical of a type III OM.

Table 2. Results from Rock-Eval analysis on bulk rock samples. Based on the average TOC content and the OI vs HI evolution, we selected 10 samples to extract the OM.

Analysis Bulk Rock										
Well	Sample	Depth	S1	S2	S3	Tmax	HI	OI	TOC	MIINC
		(m)	(mgHc/grock)	(mgHc/grock)	(mgCO ₂ /grock)	°C	(mgHc/gTOC)	(mgCO ₂ /gTOC)	%	%
Pelican-1	PELICAN740	740	0,01	0,14	1,46	421	32	328	0,44	2,79
	PELICAN860	860	0	0,15	1,33	424	34	306	0,44	2,1
	PELICAN960	960	0	0,19	1,42	424	38	290	0,49	1,95
	PELICAN1050	1050	0,01	0,19	1,33	422	43	292	0,46	1,7
	PELICAN1200	1200	0	0,10	1,14	422	27	321	0,36	1,81
	PELICAN1280	1280	0	0,15	1,57	439	36	387	0,41	1,45
	PELICAN1493	1493	0,01	5,67	10,96	432	55	106	10,35	2,8
	PELICAN1500	1500	0	0,21	1,27	421	38	238	0,53	4,55
PELICAN1530	1530	0	0,20	1,32	420	43	284	0,47	3,91	
Pingouin-1	PINGOUIN595	595	0,01	0,22	1,25	424	51	286	0,44	1,83
	PINGOUIN715	715	0,01	0,12	1,2	437	41	427	0,28	2,04
	PINGOUIN735	735	0,01	0,11	1,02	423	41	387	0,26	2,01
	PINGOUIN875	875	0,01	0,04	0,99	422	21	501	0,2	1,47
	PINGOUIN955	955	0,01	0,09	0,98	421	31	343	0,29	1,18
	PINGOUIN1025	1025	0,02	0,11	0,98	420	39	334	0,29	1,33
	PINGOUIN1125	1125	0,01	0,05	0,94	420	25	430	0,22	1,61
	PINGOUIN1145	1145	0,01	0,14	1,03	420	39	292	0,35	1,56
	PINGOUIN1265	1265	0	0,14	1	422	43	307	0,32	2,55
	PINGOUIN1325	1325	0,01	0,15	0,9	421	47	279	0,32	2,79
	PINGOUIN1425	1425	0	0,1	0,93	421	33	305	0,31	2,80

Based on this first screening, we selected 9 samples to isolate the OM that were further analyzed using the Rock-Eval 7S including the quantification of carbon, and sulfur (Table 3). Despite their low maturity and the fact that they only contained small amounts of OM, we applied the kerogen extraction procedure described by Durand and Nicaise (1980) and adapted for immature sediments by Ravin et al. (2013). The samples have been prepared at ambient temperature and treated with HCl followed by a mixture of HF/HC. After the first treatment, they were washed 4 times every 45' with deionized water, and after a second treatment they were re-washed 6 times every 45' and dried at room temperature nitrogen. The results are summarized in Table 3. The samples present a TOC content in the range of 1 to 3 %, with higher values (17% < TOC < 31%) for three samples (PELICAN1200, PINGOUIN595, PINGOUIN955) but still average TOC values are far lower than a typical TOC content measured for pure OM of more than 60%.

Table 3. Results from Rock-Eval 7S kerogen analysis on the selected 9 samples after extraction.

Analysis KEROGEN											
Well	Sample	Depth (m)	S1 (mgHc/grock)	S2 (mg/g) (mgHc/grock)	S3 (mg/g) (mgCO ₂ /grock)	PI	Tmax (°C)	HI (mgHc/gTOC)	OI (mgCO ₂ /TOC)	TOC (%)	Total S (%)
Pelican1	PELICAN1200	1200	0,74	17,35	16,18	0,04	407	97	90	17,88	2,67
	PELICAN1493	1493	0,4	8,37	1,71	0,05	167	251	51	3,33	2,44
	PELICAN1530	1530	0,33	6,02	2,64	0,05	414	188	82	3,21	1,84
	PELICAN860	860	0,3	5,57	1,59	0,05	736	228	65	2,44	1,7
	PELICAN960	960	0,12	3,29	1,17	0,03	418	207	74	1,59	0,91
Pingouin1	PINGOUIN1265	1265	0,15	4,68	1,15	0,03	419	205	51	2,28	1,57
	PINGOUIN595	595	3,88	74,27	21,6	0,05	410	239	70	31,06	13,1
	PINGOUIN875	875	0,06	0,81	0,4	0,06	421	126	62	0,65	0,15
	PINGOUIN955	955	3,31	60,84	16,42	0,05	414	215	58	28,32	11,21

One reason of these disappointing results could be that the cold acid treatment was not enough to destroy all the mineral matrix or that the cuttings were polluted by contaminants used in the drilling mud. Moreover, pyrite is present in the isolated OM (about 30% of the total sulfur content) contributing also partly to the dilution of carbon in OM.

The current IFPEN procedure is based on Ravin et al. (2013) which requires a cold acid treatment. However, this procedure has been validated only for immature type II-OM with high TOC content (~ 3%) from offshore Namibia. The protocol proposed in Ravin et al. (2013) was also applied on IODP samples from the Mozambique Channel. As expected, the proposed protocol was also not effective on such samples as they correspond to dispersed type-III OM with low TOC content ($0.6 < \text{TOC}\% < 1.04$). Indeed, after acid attacks, the samples showed TOC content of the order of 10%, which is unlikely considering that after the extraction procedure, samples should have pure OM containing about 60% of carbon. Associated with these low OM content was also a low pyrite content (0.5 to 2 %). Additional analysis through X-Ray Fluorescence showed that all the silicates had been destroyed during the acid attack (HF/HCl) (no traces of silica on the OM). In contrast to previous results from the offshore Aquitaine, we observed an important precipitation of minerals such as Ralstonite ($\text{Na}_x\text{Mg}_x\text{Al}_2\text{-}_x(\text{F},\text{OH})_6\cdot(\text{H}_2\text{O})$). This is probably the result of the cold acid treatment in the presence of HF resulting in the formation of complex fluoride oxides, especially when the OM is associated with fine clay and silt particles. However, such mineral precipitations were not observed from samples collected offshore Namibia (Ravin et al. 2013). Consequently, additional tests were performed to avoid the precipitation of these complex fluorides without impacting the elemental composition of the OM (*e.g.* avoid using high temperatures for the fluoric acid attack as for mature sediments).

Therefore, another test was performed to extract OM from 2 IODP samples collected offshore Zambezi, called here 27X and 1X, using a cold acid treatment (HF/HCl) but with an

additional washing procedure of 4h with HCl both at cold and higher temperature (70°C). The additional washing procedure helped to increase the final recovered TOC for the two samples. However, the two samples showed different results to the attack at higher temperature. The Elemental Analysis on the first sample (27X) showed that all the fluorides had been destroyed with the treatment at higher temperature. In contrast, the second sample (1X) showed issues related to the higher temperature resulting in abnormal oxygen values (50%) which indicates widespread oxidation.

These preliminary tests showed that a different and improved extraction procedure is required for immature continental-derived sediments with poor OM content when associated with clay minerals. An appropriate procedure should be able to concentrate OM without altering its initial OM composition or precipitation of heavy oxide minerals.

7. Conclusions

Previous results collected in the framework of the PAMELA research project (PASSive Margin Exploration LABORatories) allowed identifying several active seepage sites along the Aquitaine Shelf in the Bay of Biscay (Dupre et al. 2014, Ruffine et al. 2017, Pierre et al. 2017, Michel 2017; Dupre et al. 2020) and the Mozambique Channel (Mozambique and Madagascar margins) (Deville et al. 2018 - internal IFPEN report; Deville et al. 2020). Gas sample analyses showed an isotopic signature typical of pure biogenic gas (99.9% of CH₄) at all sites. The gas is generated from CO₂ reduction. However, gas samples present differences in terms of $\delta^{13}\text{C-CH}_4$ between the three main areas (offshore Aquitaine, offshore Zambezi and offshore Madagascar). In order to better understand the evolution of these fluid systems, we (1) characterized the Organic Matter (OM) starting from the PAMELA data set (core samples, moorings, interface cores and cuttings), and (2) developed a new modelling approach to assess biogenic gas processes and predict biogenic gas occurrences at the basin scale for continental shelf areas. From the results obtained in this PhD thesis, we can now answer several questions concerning biogenic gas systems, and in particular those found in offshore Aquitaine and in the Mozambique Basin. Here we only present global conclusions. Detailed discussions and conclusions of each of the two case studies are presented in the respective papers that are given in chapters 3 and 5.

Our work allows us to better understand the impact of the OM quality and quantity on biogenic gas which can explain the observed differences in terms of isotopic signatures. Despite the fact that biogenic gas is generated with the same biological process (Fig. 11), both the Zambezi offshore (Mozambique Margin) and the northern Majunga sector (Madagascar Margin) showed different isotopic signatures (Fig. 11). In particular, gas samples collected in the offshore Zambezi are characterized by lighter $\delta^{13}\text{C-CH}_4$ values between -95‰ and -85‰. In contrast, gas samples collected along the Majunga sector present heavier $\delta^{13}\text{C-CH}_4$ values between -80‰ and -70‰. Our results on recent OM samples collected in the Mozambique Channel suggest that these variations can be the result of different transport and preservation conditions in these two sites. The Majunga sector is characterized by a higher amount of OM ($1 < \text{TOC}\% < 2$) and by HI values of 150 mgHc/g TOC. Based on EDS-SEM analysis, O₂ profiles and SAR, we determined that the Majunga sector presents OM transport and preservation conditions compatible with a more undisturbed (and anaerobic) depositional environment compared to the Mozambique system. Indeed, the offshore Zambezi presents

lower amount of OM (TOC% < 0.8) with lower HI values (75 mgHC/g TOC). In addition, samples from recent sediments demonstrate that the OM is already oxidized and altered which is compatible with a higher sedimentation rate, and a perturbed and more aerobic depositional environment. Since both sites are characterized by an initial input of terrestrial-OM, we can assume that the lighter gas isotopic signature along the Zambezi offshore results from the decomposition of a more oxidized OM compared to the Majunga sector where OM is better preserved and less degraded.

Our new modelling approach allows us to determine the most critical factors during biogenic gas generation at the basin scale. We observe that, in the offshore Aquitaine, biogenic gas processes from generation to emission are mainly controlled by (1) the degradability of the OM labile compound (R_{bio}), (2) the reactivity of the thermo-labile fraction (E_a), (3) the OM degradation ratio into methane (S_{bio}), and (4) the couple geothermal gradient/sedimentation rate. The relative percentage of labile vs thermo-labile TOC fractions as well as the temperature for microbial activity ($\mu(T)$) show a moderate impact on the final amount of generated gas. Thanks to this new modelling approach, we can propose a geochemical characterization of immature sediments with poor terrestrial-OM. However, our approach is based on a global sensitivity analysis rather than on OM characterization, which allows to optimize and hierarchize the geochemical parameters affecting biogenic gas processes in shallow systems. Therefore, we are aware that a better characterization of terrestrial-OM through analytical methods is required in order to improve our proposed approach.

Our results allow also to conclude that the biogenic system in offshore Aquitaine is active at the present-day and sourced by Plio-Pleistocene sediments with poor terrestrial-OM content rather than by an older system that is slowly degassing. Our model confirms that the absence of a seal in the shallow system results in continuous sea-floor emissions of methane over time, and that flow rate intensities evolve as a function of microbial methane generation and sedimentation rate. The system started to generate biogenic gas during the upper Miocene (5.5 Ma), reaching a maximum emission peak during the Pleistocene (1.7 Ma). Therefore, we can determine the beginning of the biogenic gas generation process. In addition, we are able to determine the cumulative amount of emitted gas over time which yields 1.62 TCF/My. However, part of this gas is consumed during its upward migration within the anaerobic oxidation of methane (AOM) zone. Carbon is partially stored in the MDACs which are widely distributed over the Aquitaine shelf break area. Depending on carbonate thickness, we estimate

a methane sink efficiency of the AOM varying between 9% to 46%, resulting in an effective methane emission rate between 0.87 to 1.48 TCF/My that is consistent with measured data from *in situ* bubbling sites and acoustic signatures in the water column (Dupre et al. 2020). Our results demonstrate that in order to estimate the total amount of emitted methane and its impact on the ocean/atmosphere carbon budget, we need to account for the total amount of generated gas which depends on the quality and quantity of OM, for the total amount of carbon trapped in the form of carbonate, but also for the total amount of trapped gas in the form of hydrates if pressure and temperature are suitable for their formation (which is not the case at the Aquitaine Shelf).

This PhD work helps to improve our knowledge about biogenic gas systems in continental shelf areas, from the source in the deeper sediments to the seeps at the seafloor. We observe that biogenic systems mainly occur in geological settings with high input of terrigenous sediments and low geothermal gradients. In addition, microbial systems can be active over millions of years and generate large amounts of gas from microbial activity only, even in sediments with low organic carbon content ($0.3 < \text{TOC}\% < 0.6$). Microbial activity is very efficient and already active at low temperatures in sediments with dispersed-OM. Biogenic gas can remain dissolved in pore water all the way up to the seafloor where it diffuses into the ocean water column due to changing thermodynamic conditions. Migration is not focused but diffuse and very efficient, resulting in prolific methane emissions at the sea floor of continental shelf areas. The specific geological setting of a basin controls if biogenic accumulations may occur which is a function of the timing of gas generation and trap formation. For instance, the high porosity of the shallower Plio-Pleistocene sediments offshore Aquitaine and the absence of a seal at the top of the system are not favorable for trapping of any generated gas, and large amounts of gas (144 Mg/y of microbial methane) are continuously emitted directly into the ocean (Dupre et al. 2014; 2020).

In addition, our work points to the importance of the AOM when estimating the amount of gas that can either be emitted or trapped in a basin. The Methane Derived-Authigenic Carbonates (MDAC) represent one of the main carbon sinks for biogenic gas, and it is important to assess their distribution and the amount of carbon that can be stored in such features for two reasons:

1. MDAC can have a major control on biogenic gas migration/accumulation as they alter the permeability structure of the sediments

2. By neglecting MDAC, we can over-estimate the amount of biogenic gas that can be emitted or trapped in a system.

In our work, we show how basin modelling integrated with geochemical analysis can help to assess the biogenic methane budget which can be useful to predict biogenic gas occurrences. In addition, our workflow is also useful to estimate present and past flux of methane through the seafloor and therefore helps to assess the methane budget from geological sources. The most important aspect that is still lacking for a general budget calculation concerns the large amount of methane that can be stored as hydrates, and therefore it is important to analyze and assess their role in biogenic systems. Further analysis to address this point is discussed in chapter 8.

8. Future research on biogenic gas generation and migration

8.1 Hydrate stability zones as paleo-gas migration indicators

As previously discussed, basin modelling integrated with microbial processes can be used to quantify biogenic methane accumulations/emissions at the large scale. This PhD study has demonstrated that in order to better assess the methane budget in continental shelf areas, it is required to account for the main processes affecting methane once it is generated, including oxidation through the AOM. What is still missing in this study is an analysis of the solid phase of methane (*i.e.* hydrates). The Mozambique Channel, and in particular the offshore Zambezi, shows evidence of an active fluid system including seeps (water and gas), MDACs and pockmarks (Deville et al. 2020). Therefore, we investigated the conditions for hydrate occurrence in the offshore Zambezi along a 2D dip-section (Fig. 28). A corresponding 2D basin model (Fig. 29) was taken from Yabre et al. (2020 – TOTAL Internal Report) which is based on a reflection seismic profile, used to define the sedimentary cover (Ponte et al. 2019), and a refraction seismic profile used to describe the crustal geometry (Etheve et al. 2020) which also includes information concerning the present-day crustal model, thermal calibration and sedimentation rates.

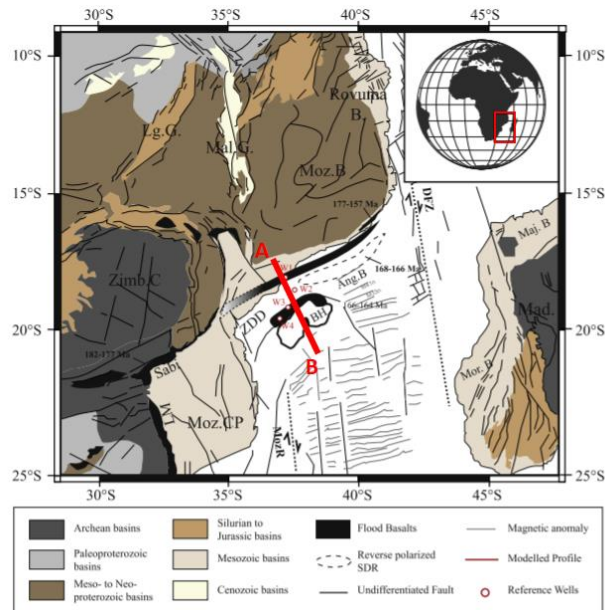


Figure 28. Geological and tectonic map of the Mozambique Margin (modified after Etheve et al. 2020). The red line shown the location of the 2D profile of the offshore Zambezi oriented NW-SE (A-B). ZDD: Zambezi Delta Depression; BH: Beira High. The reader can refer to Etheve et al. (2020) for a better comprehension of the tectonic setting of the Mozambique Basin.

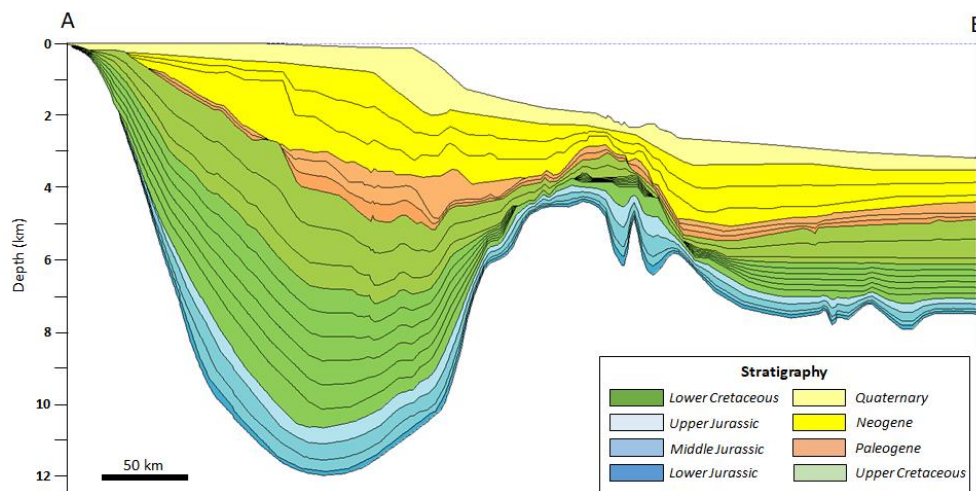


Figure 29. Stratigraphy section of 2D TemisFlow basin model of the offshore Zambezi (extracted from Yabre et al. 2020 – TOTAL Internal Report). The location of the section is shown in Figure 28. The dashed blue line indicates the water/atmosphere interface.

As presented in chapter 4.4, it is possible with the TemisFlow simulator to determine the evolution of the hydrates stability zone (HSZ) during the geological history of a basin as a function of pressure and temperature, even in the absence of methane. A first run was tested to verify the probability of HSZ at present-day. Hydrates are stable in the eastern part of the Beira High (BH) (Fig. 30). If these hydrates represent clathrates of biogenic methane, they could indicate the presence of a biogenic gas system.

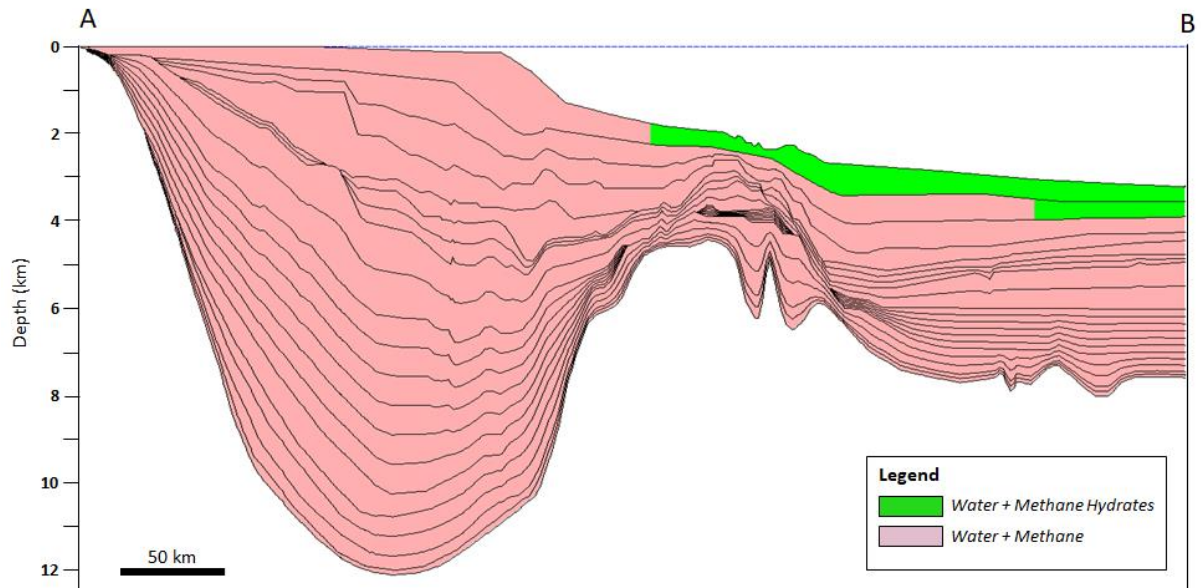


Figure 30. 2D section of the offshore Zambezi in Temis Flow showing the stability area of methane hydrates at the present-day (extracted from Yabre et al. 2020 – TOTAL Internal Report). The location of the dip-profile is shown in Figure 28. The dashed blue line indicates the water/atmosphere interface.

Figure 31 shows that at the deposition time, several layers in the basin saw favorable conditions for biogenic gas generation. In particular, Cretaceous sediments (aged from 123 to 93 Ma) and the uppermost Neogene and Quaternary sequences of the basin indicate that along the shelf break and in some areas of the deep-water domain, conditions were favorable for biogenic methane generation if methanogens and dispersed SOM are present (Fig. 31).

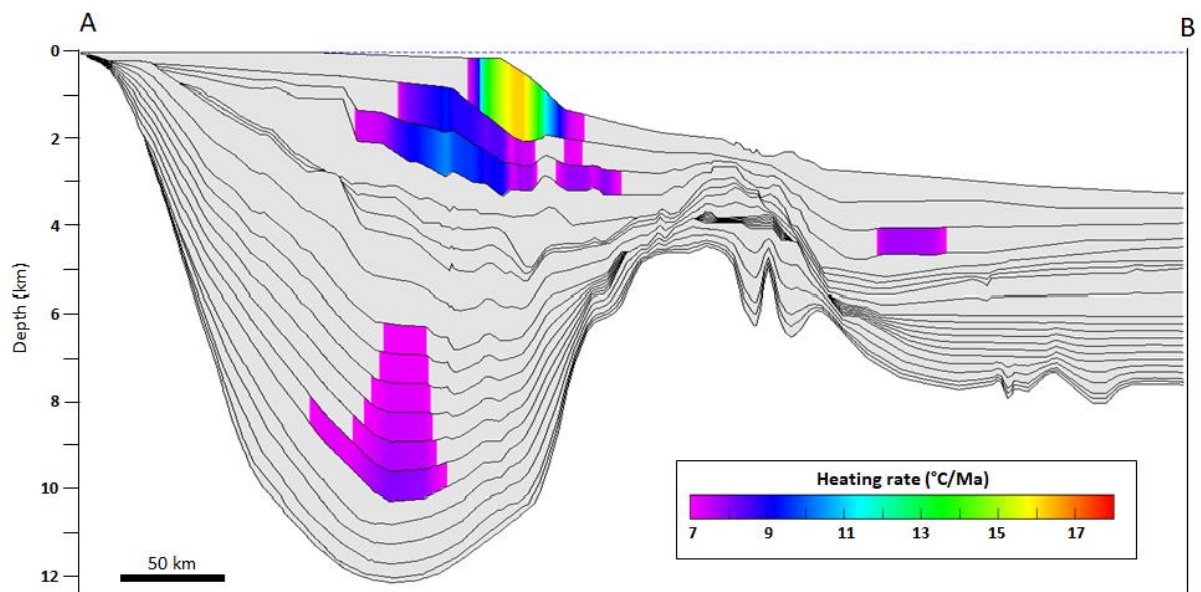


Figure 31. 2D section of the offshore Zambezi in Temis Flow (extracted from Yabre et al. 2020 – TOTAL Internal Report) showing the heating rate °C/Ma of each layer at the deposition time (Clayton 1992). The location of the dip-profile is shown in Figure 28. The dashed blue line indicates the water/atmosphere interface.

Despite favorable conditions for both a biogenic gas system and HSZ, the analysis of several seismic dip- and strike-lines did not show any bottom surface reflectors (BSR) along the western or eastern flank of the BH (TOTAL internal communication). Their absence on seismic profiles could also be related to the flat geometry of the sedimentary layers in the eastern areas of the Beira High.

Despite the absence of BSRs in the deep-water domain, the Zambezi Delta presents some evidence of collapsed paleo-pockmarks along the western flank of the BH (Imbert 2016 – TOTAL Internal Report). These features were already identified by Sultan et al. (2010) in the Niger Delta and Imbert and Ho (2012) in the Northwest shelf of Australia (Carnarvon Basin). Such hydrate-related pockmarks can be identified on seismic cross-sections as sub-circular geometries similar to canyon features widely distributed over several square kilometers. They can be active (chapter 1.3.1) or fossilized, indicating an ancient focused-fluid system where they represent collapsed hydrates that can be used to determine the age of an ancient fluid systems and to estimate the amount of emitted gas as a function of their geometry. As the stability of such hydrates varies with temperature and pressure conditions, it can also give insights into the type of the escaped fluids (e.g. biogenic methane vs. heavier thermogenic gas or CO₂).

Hydrate-related pockmarks can be generated from a focused column of gas migrating upward. As shown in Figure 32, the growth of the former hydrates at the base of the GHSZ induces a conical fracture along which the gas migrates and diffuses upward, generating hydrate-bearing sediments. A change in pressure and temperature conditions results in a rise of the GHSZ followed by the melting and expulsion of hydrates and sediments (Imbert and Ho 2012).

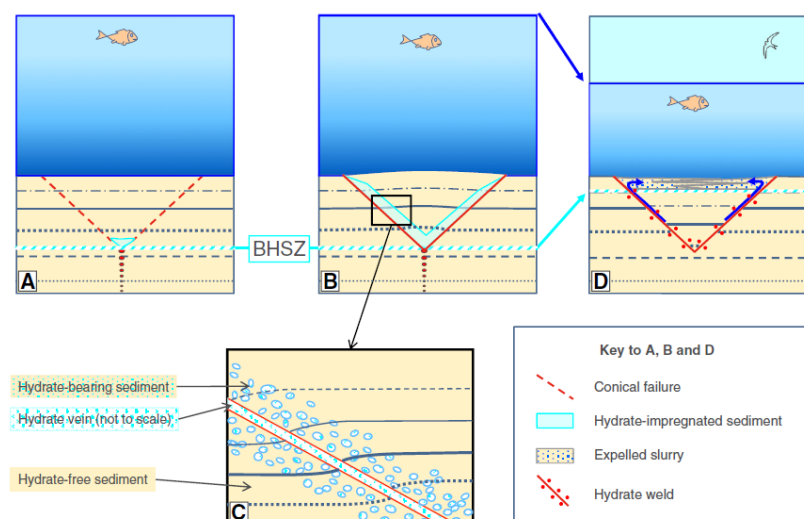


Figure 32. Interpreted generation process for a single hydrate paleo-pockmark (Imbert and Ho, 2012). A: Hydrates form at the base of the GHSZ triggering a conical fracture along the dotted red line. B: Increase of hydrate-bearing sediment volume due to gas migration and diffusion along the fracture zone. C: zoom on the fracture which may be filled with a stronger vein of hydrate surrounded by hydrates-bearing sediments and a free-gas phase in the lower area. D. Final stage of hydrate dissociation due to a change in P-T conditions, expulsion of the hydrates-bearing sediment along the fracture.

Hydrate-related pockmarks can be recognized on 3D-seismic data and can be used to determine the amount of hydrate-bearing sediments that have been expelled during collapse. For further information, the readers are referred to Imbert and Ho (2012). According to the authors, observations in the Carnarvon Basin allow to identify paleo-pockmark hydrates over an area of 5000 km². As mentioned in the introduction, estimates of the total amount of gas released during the collapse can be determined geometrically, considering that 1 m³ of pure methane-hydrate contains 164 m³ of methane (Kvenvolden 1988). The volume of hydrates contained in a volume of sediments varies from 10% to 30%. Therefore, with an average hydrate amount of 15%, 25 m³ of methane have been expelled for each m³ of sediments. In the Carnarvon Basin, the authors speculate that the destabilization of hydrates may have been triggered by the Paleocene-Eocene Thermal Maximum (PETM) with an estimated global warming of 4 °C (Imbert and Ho 2012).

Features as the ones in the Carnarvon Basin (Imbert and Ho 2012) have been identified also along the western flank of the Beira High and Zambezi Delta (Fig. 33) of which interpreted seismic lines and paleo-pockmark analyses are presented in an internal report of TOTAL -R&D (Imbert 2016). Numerical modelling experiments can be used to estimate the amount of accumulated/emitted gas as the consequence of hydrate melting, but it can also be helpful to identify the origin of the gas (thermogenic, biogenic or CO₂). By extracting P-T conditions present and past from the model, and depending on the gas composition (*e.g.* CO₂, CH₄, C₂H₆,

C₃H₈...), an analysis of the thermodynamic behavior of the gas can be used to better constrain and verify modelling results and to identify the stable gas phase at that time.

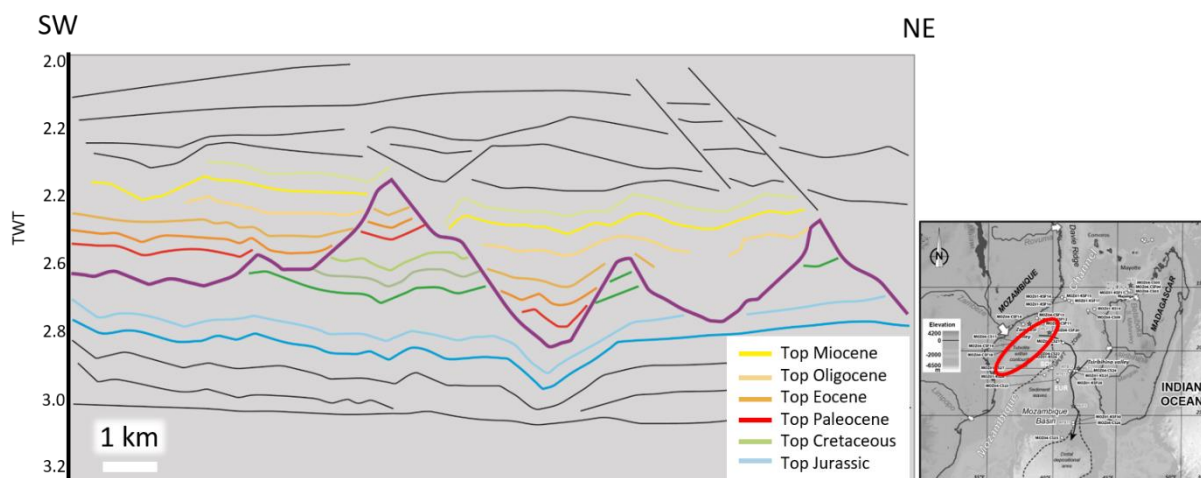


Figure 33. Sketch of an interpreted strike-seismic line along the western flank of the Beira High (Imbert 2016 – TOTAL Internal Report). The purple line on the interpreted profile represents the base of the collapsed hydrates which is similar to an erosional surface. Black lines represent the uninterpreted markers. The insert map shows the location of the profile inside the red circle.

In Figure 33, the orange reflector can be followed above and below the purple line which should represent the base of the collapsed hydrate paleo-pockmark. The purple reflector is similar to an erosional surface that can be followed for over 10,000 km². As in the Carnarvon Basin, these features in the Zambezi Delta have been observed at the Paleocene/Eocene boundary (PETM) corresponding to a global warming period of 4 °C which started at around 59 to 53 Ma (Frieling et al. 2018 and reference therein).

First results from the 2D model have shown that the Zambezi Delta experienced favorable conditions for hydrate formation already between 66 and 50 Ma at the western flank of the Beira High (Fig. 34). Based on these results, we tried to determine a possible origin of the gas. According to modelling results presented in Figure 31, sediments deposited from the lower Cretaceous (123 Ma) to the early upper Cretaceous (93 Ma) experienced favorable conditions for biogenic gas generation. Therefore, we can assume that the biogenic gas generated during the Cretaceous was first trapped in the sediments and then migrated during the Maastrichtian (66 Ma) when P-T conditions also allowed hydrate formation (Fig. 34). It is also possible that hydrates were already formed at 93 Ma, as shown in small areas along the western flank of the Beira High. However, a thermogenic origin of the gas cannot be excluded.

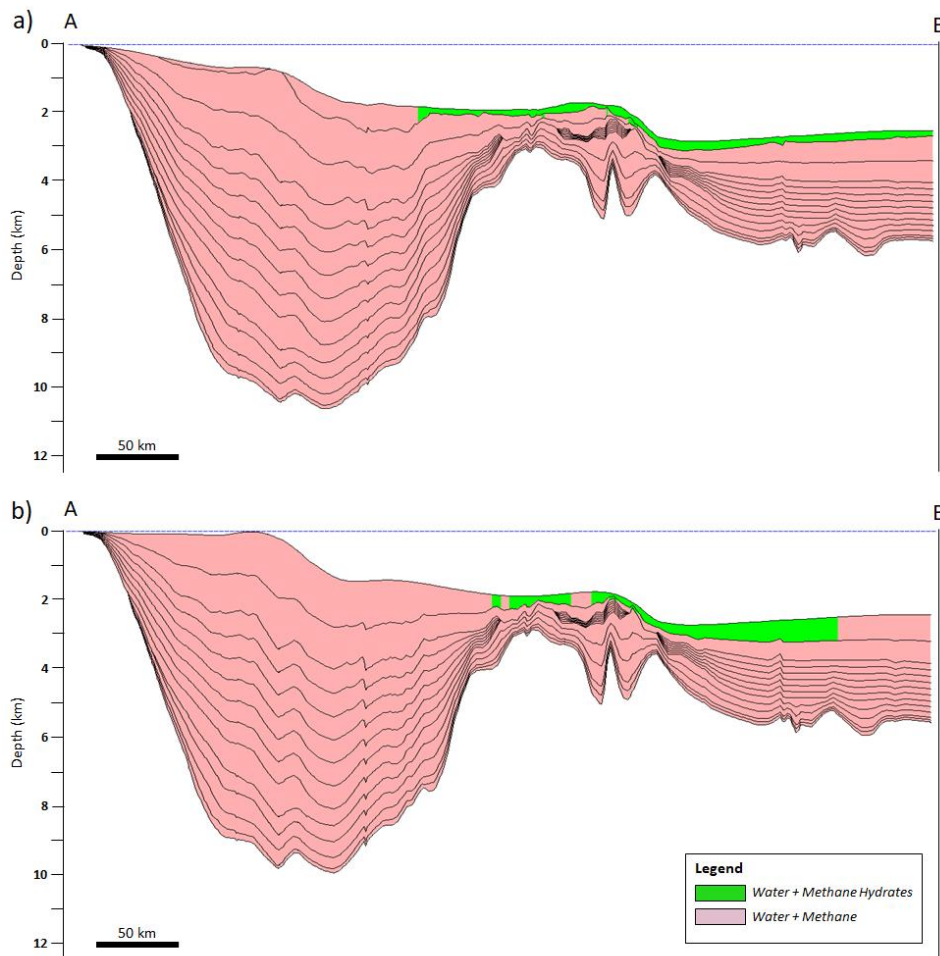


Figure 34. 2D section of the offshore Zambezi showing the modeled stability areas of methane hydrates at 50 Ma (a) and 66 Ma (b) (extracted from Yabre et al. 2020 – TOTAL Internal Report). The location of the dip-profile is shown in Figure 28. The dashed blue line indicates the water/atmosphere interface.

In accordance with Mahanjane et al. (2014 and reference therein), the Zambezi Delta contains several potential source rocks (Fig. 35): (1) the Lower Domo Shale of Albian age (TOC ~ 0.8%; HI of 52 mgHC/gTOC); (2) a Valanginian (132 Ma) oil-prone Type II marine source rock (TOC ~ 9.8%; HI of 432 mgHC/gTOC); (3) more speculative Late Jurassic (152 Ma) and Middle Jurassic (170 Ma) Type-I or Type-II source rocks (TOC ~ 8%, HI of 500 mgHC/gTOC). Other source rocks have also been proposed for the Zambezi Delta Basin (Kihle 1983; Nairn et al. 1990) such as the Paleogene Grudja and Cheringoma shales that are both gas prone source rocks (Fig. 35). The organic carbon content is not specified for these shales.

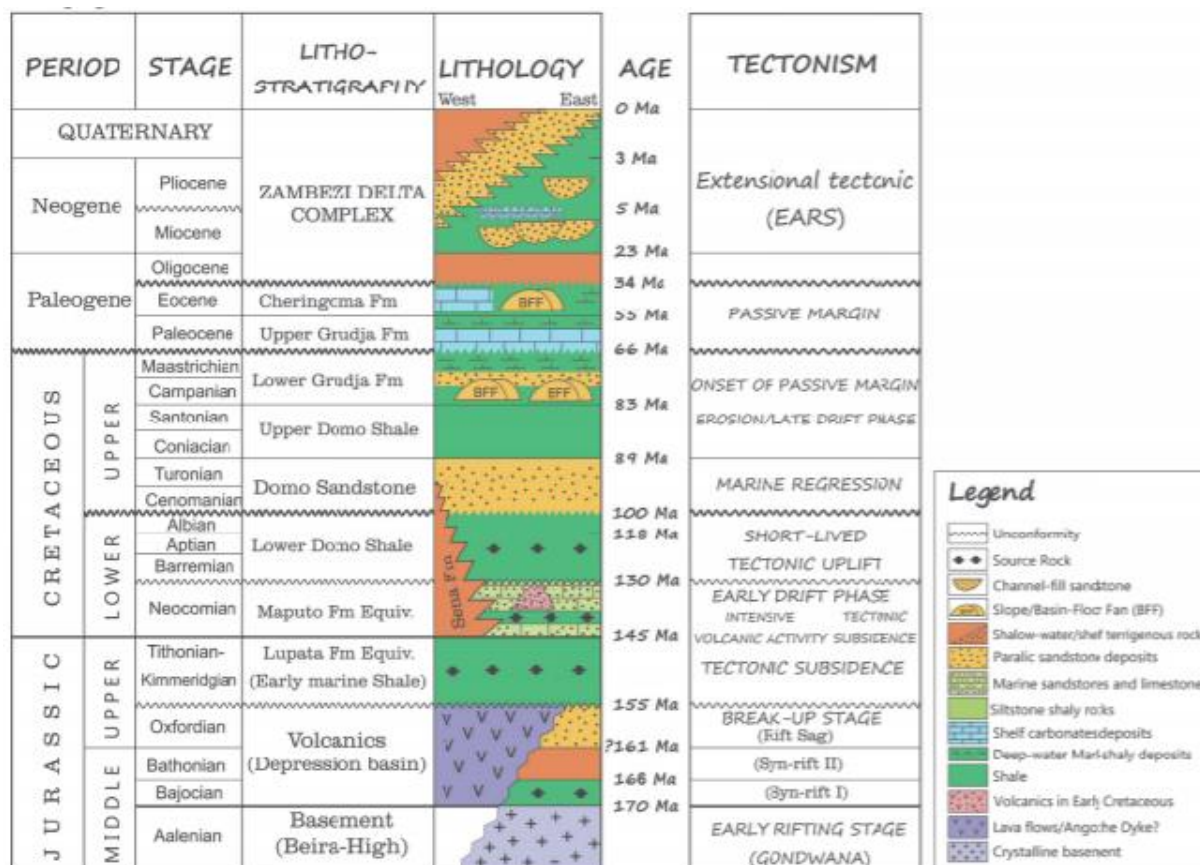


Figure 35. Stratigraphic charts for the offshore Zambezi Delta basin (Mahanjane et al. 2014).

The maturity of these Jurassic, Cretaceous and Paleogene source rocks tells us whether these layers have entered the gas window and when gas generation started (Fig. 36). This information can be used in a first time to determine if hydrates can have a thermogenic origin. Figure 36 shows the maturity evolution of the sediments through time, with accelerated burial between 93 Ma and 50 Ma representing the critical moment for hydrates occurrences.

First modelling results show that the speculative middle Jurassic source rocks entered the gas/oil window at 111 Ma (1.31 %Ro_{eq}). The vitrinite equivalent values correspond to the gas window at 99 Ma (1.9 %Ro_{eq}). The speculative upper Jurassic source rock entered the gas window at 93 Ma (1.75 %Ro_{eq}) (Fig. 36 c). At 66 Ma, the two speculative Jurassic source rocks are already overmature (Fig. 36 b). At the same time, the Valanginian source rock is in the gas window (2.25 %Ro_{eq}) (Fig. 36 b) and stayed there until 50 Ma (2.72 %Ro_{eq}) (Fig. 36 a). The Albian source rock is immature during the last stage of hydrate stability (Fig. 36 a).

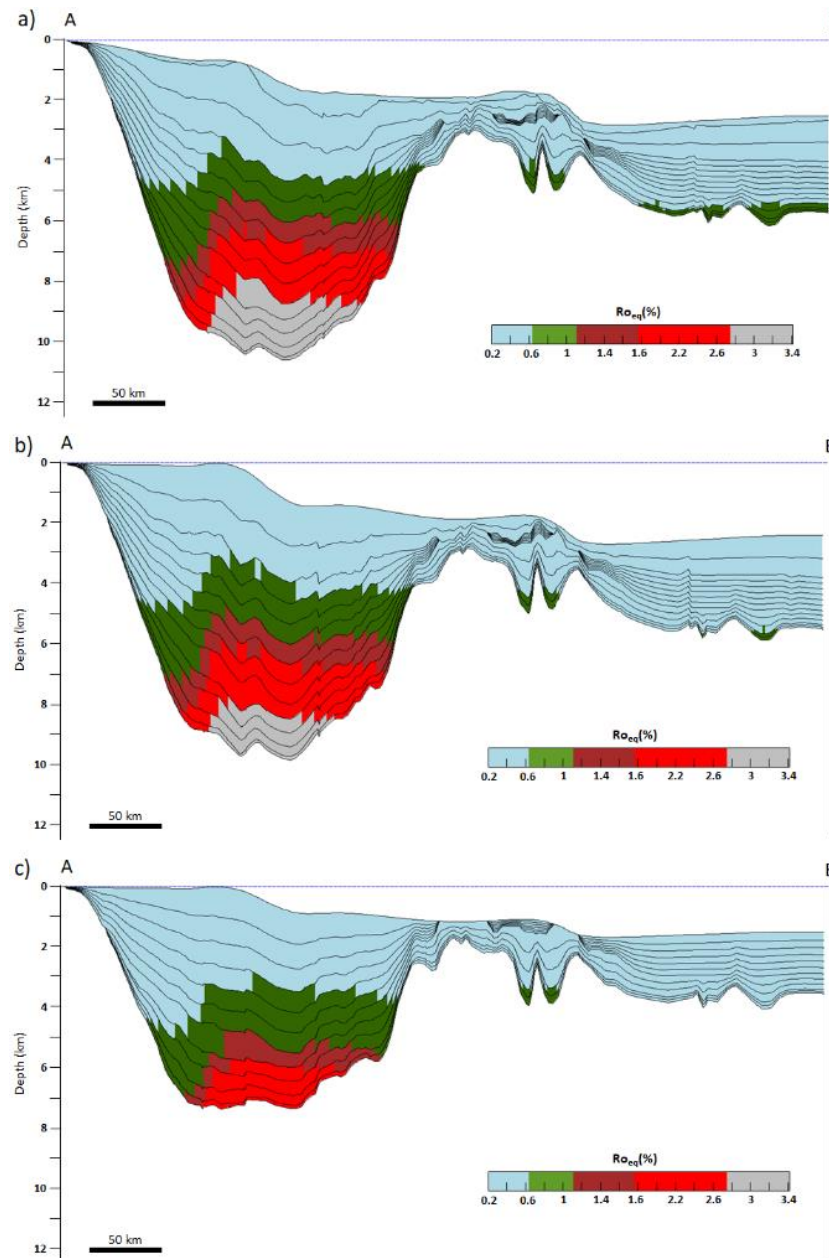


Figure 36. Modeled sediment maturity over time expressed as vitrinite equivalent values (% Ro_{eq}) along the 2D section of the offshore Zambezi (extracted from Yabre et al. 2020 – TOTAL Internal Report). a) 50 Ma; b) 66 Ma; c) 93 Ma. Immature oil (light blue), oil (green), oil and gas (dark red), gas (red) and over mature (grey).

This preliminary analysis of both the biogenic and the thermogenic systems of the Zambezi Delta demonstrates that paleo-hydrates could have been generated by pure biogenic methane or by thermogenic gas. Further analysis is required to better discriminate and describe both systems, such as the timing of generation/expulsion and migration and accumulation. According to 1D modelling results in the Zambezi Delta published by Mahanjane et al. (2014), the Late Jurassic petroleum system presents an unfavorable timing for the accumulation of

hydrocarbons. However, the critical moments of the middle Jurassic and Valanginian petroleum systems indicate a more favorable timing for hydrocarbon accumulations.

We cannot discriminate if paleo-hydrates of the Zambezi Delta have a biogenic or thermogenic origin without a more in-depth petroleum system analysis and further modelling. This includes a quantification of the amount of generated HCs from either a biogenic or a thermogenic source. For instance, it could be tested if the amount of generated biogenic gas is sufficient to justify the volumes estimated from the hydrates collapse. If this is not the case, a thermogenic contribution must be considered. Further analysis is required to assess the paleo-fluid system of the offshore Zambezi which may have contributed to large methane emissions at the seafloor during the PETM.

8.2 Additional research questions

Our work opens several perspectives regarding the study of biogenic gas processes, with combined analytical geochemical and numerical modelling approaches. However, based on our results, we recognize that further research is required to better assess the fate of organic carbon and the methane budget, and we identified the following future research topics:

- 1) A dedicated effort for a geochemical characterization of a type III OM, to determine more accurately its reactivity and degradation laws.**

In our case study presented in chapter 5, it was possible to determine a degradation rate and reactivity for labile and thermo-labile compounds of a type-III OM. However, these values are based on modelling results, because the analytical procedure used in IFPEN encountered several issues when applied to poor and dispersed terrestrial OM associated with clay particles (chapter 6). In order to more accurately describe the degradation of recent type-III OM and reduce uncertainties during modelling, further research should focus on the analytical assessment of the molecular composition of recent continental-derived OM.

In the framework of this PhD study, we have already tested a new analytical workflow on poor type III OM sediments (chapter 6). However, these different procedures were inappropriate for samples with high clay content. Therefore, we propose to test the same analytical workflow on samples enriched in type III OM to verify if its inefficiency is due to the total initial TOC or to the OM quality (*e.g.* type II vs type III). If not, the same procedure

could also be tested with a larger sample size in order to increase the probability to extract a larger quantity of pure OM.

2) A new extraction technique for type III OM from recent sediments.

As presented in chapter 6, the current analytical workflow to extract OM from immature sediments was calibrated on a marine SOM from organic-rich sediments (TOC ~ 3%) (Ravin et al. 2013). When the same workflow is applied to poor terrestrial OM (TOC ~ 0.5%) from the Mozambique Channel, the extraction technique did not allow to separate the OM from the mineral matrix and/or new minerals were generated which altered the initial composition of the samples. In order to characterize the molecular composition of terrestrial-OM when bounded to clay minerals, (which is also the most likely source of biogenic gas in recent shallow marine system), we need to propose an improved extraction technique. Once the OM can be correctly extracted, then the analytical procedure proposed by Ravin et al. (2013) and Hatcher et al. (2014) (*e.g.* Rock-Eval, Elemental Analysis and Solid-state ^{13}C NMR) can be tested on such samples to (1) determine the TOC amount, type and maturity of source rocks, (2) quantify the atomic proportions (C, H, O, N, S and Fe) and (3) quantify the distribution of carbon among the various functional groups, with their specific labile/refractory character. This approach could help to improve our understanding of the reactivity of these components. Eventually, it can allow to propose a degradation law for this poor terrestrial-OM that can be used as proxy in continental shelf areas.

3) A reactivity model for biogenic gas generation with a continuous activation energy distribution or a multi-layered source rock.

In the current version of the simulator, each biogenic source rock is defined by (1) an identical ratio of TOC labile vs. TOC thermo-labile, (2) the same degradation law for the labile fraction (R_{bio}), and (3) the same activation energy for the thermo-labile fraction (Ea). Alternatively, and more accurately, the source rock should be described by a continuous distribution of energy with a scheme similar to thermogenic source rocks by a distribution of activation energies (Fig. 37a). Such an implementation, linked with the molecular characterization of the OM, could help to better define the kinetics of the thermo-labile fraction. Indeed, the main difficulty encountered with the current approach was how to model the transformation of the thermo-labile fraction of the shallower horizons where temperature is low. In our model, we assume that each source rock, from the shallow to the deeper layers, is

characterized by the same terrestrial-OM with the same degradation laws and reactivity for labile and thermo-labile components. Reactivity of thermo-labile compounds can vary between 50 and 130 kJ/mol (Burdige 2011). In the offshore Aquitaine, biogenic gas generation is favourable when activation energy is comprised between 80-110 kJ/mol. Higher or lower values prevent biogenic gas generation. Therefore, we reduced the range from Burdige (2011) by using a sensitivity analysis that found a most likely value of an activation energy of 83 kJ/mol which is calibrated to the amount of gas emissions (chapter 5). However, in this case the thermo-labile fraction is already activated at shallow depths which creates new labile compounds that result in additional biogenic gas. But in reality, OM reactivity decreases with time and depth which results in higher activation energies for deeper source rock layers. As an alternative to a continuous distribution of activation energies, we could also represent the biogenic source rock by a multi-layer system (Fig. 37b). This can be achieved using a different reactivity for each source rock layer that is defined by a separate activation energy (Ea) and a separate frequency factor (A).

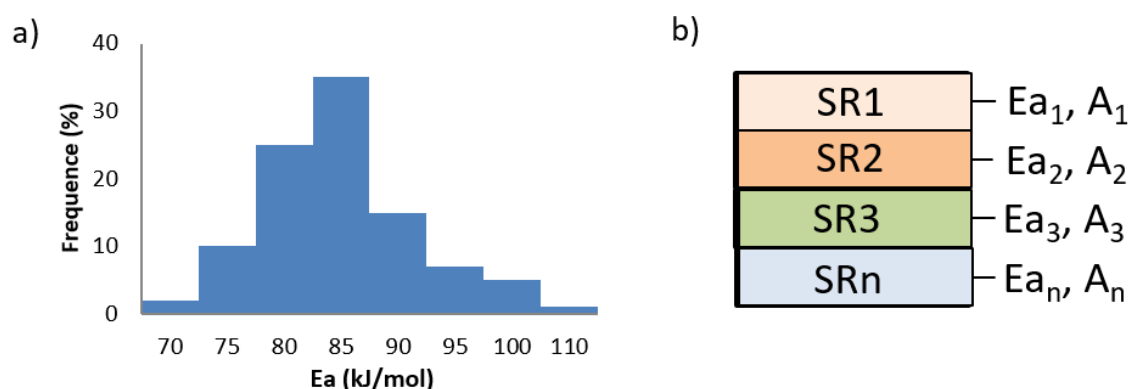


Figure 37. a) Continuous distribution of activation energy in which each Source Rock (SR) is defined by the same frequency factor (A) but with different activation energy (Ea); b) Multi-layer scheme in which each SR is defined by a different kerogen with different activation energy and frequency factor values.

4) A dedicated model that specifically integrates the consumption of CH_4 and subsequent generation of CO_2 through the AOM.

We observed in both case studies of the Mozambique Basin and the offshore Aquitaine that biogenic systems are associated with the precipitation of methane derived-authigenic carbonates (MDACs) that result from the anaerobic oxidation of methane (AOM) during upward migration of the generated methane. A large part of the gas is therefore consumed in

the system before it becomes trapped or reaches the seafloor. The amount of gas consumed by AOM varies according to AOM efficiency. In the Aquitaine Basin, we showed that the consumed gas volume in the AOM can be estimated as function of the MDACs thickness. Starting from a total amount of “emitted” gas, we determined that a large part of it is consumed before it reaches the seafloor (estimated range between 9% and 46%). For a more accurate biogenic gas budget it is required to assess the efficiency of this major methane sink to avoid an overestimation of trapped or emitted gas volumes. However, we did not model this process explicitly, leading to an overestimation of the amount of gas in the system. In addition, as observed in offshore Aquitaine, the precipitation of MDACs has a major impact on biogenic gas migration as carbonates may prevent the gas to easily escape to the surface. Such features can also be observed in seismic data suggesting the presence of an active or paleo system, as in the offshore Aquitaine (Dupre et al. 2020). In addition, MDACs can be also associated with BSRs (bottom simulating reflectors) or paleo-BSRs indicating the presence of a paleo-fluid system, as in the case of the Krishna-Godavari Basin (Kundu et al. 2008).

We suggest therefore to account for the AOM process in the basin model as AOM is a major methane sink in marine environments, and because it creates flow barriers, it also affects gas migration pathways. We need to account for the biogeochemical processes involving MDAC precipitation in our models. For instance, we need to address the competition between sulphate-reducing bacteria and methanotrophic archaea, which results in the reduction of sulphate to sulphide and in the oxidation of methane to bicarbonate (Boetius et al. 2000) which increases the amount of Dissolved Inorganic Carbon (DIC) in pore water. When pore water reaches carbonate saturation, precipitation of MDAC takes place (Boetius 2000; Regnier et al. 2011; Lash 2015).

5) A modelling procedure that accounts for methane trapped in the form of hydrates.

In the TemisFlow basin simulator, it is possible to determine P-T conditions favorable for the occurrence of gas hydrates. However, it is not possible to directly simulate the formation of hydrates and then make an estimate of the total amount of biogenic gas stored in form of hydrates. According to Ketzer et al. (2019), hydrates found in the Rio Grande Cone (SW Brazil) and in the Amazon deep-sea fan (NE Brazil) store about 780 and 430 TCF of methane respectively. When destabilized, these hydrates can lead to large amounts of released gas directly into the ocean, part of which may reach the atmosphere. Hydrates and paleo-hydrates

can also be indicators of present-day or paleo-fluid accumulations. For example, hydrates have been observed in Plio-Pleistocene sediments of the Bay of Bengal and several TCF of biogenic methane have been discovered there that are associated with hydrates, as published by Kundu et al. (2008 and references therein). The authors propose a scenario in which the deposition of new sediments destabilized paleo-hydrates during burial. This in turn led to hydrates melting and release of biogenic gas which migrated laterally into the porous reservoirs. The amount of gas that can be trapped in these reservoirs is a function of hydrate thickness and the timing of the gas release (*i.e.* timing of trap formation). Therefore, it is important to account for the formation of hydrates in a biogenic gas model, as hydrates represent a major methane storage agent. Such storage behavior in the geologic past may lead to important accumulations today. Based on such observations in the offshore Zambezi, we analyzed its paleo-hydrate stability zone which can be used as an indicator of a paleo-fluid systems.

9. References

Ahuva, A. L.; Amos, B.; Sass, E. (1993): Late Cretaceous upwelling system along the Southern Tethys Margin Israel Interrelationship between productivity, bottom water environments, and organic matter preservation. In *Paleoceanography* 8 (5), pp. 671–690.

Allen, A. and Allen, J.R. (2013): Basin Analysis; Principles and Application to Petroleum Play Assessment, 3rd Edition. (pp 632). Wiley-Blackwell.

Andresen, K. J., Huuse, M., & Clausen, O. R. (2008). Morphology and distribution of Oligocene and Miocene pockmarks in the Danish North Sea—implications for bottom current activity and fluid migration. *Basin Research*, 20(3), 445-466.

Archer, D. (2007): Methane hydrate stability and anthropogenic climate change. In *Biogeosciences Discuss.* 4 (2), pp. 993–1057. DOI: 10.5194/bgd-4-993-2007.

Arndt, Sandra; Jørgensen, B. B.; LaRowe, D. E.; Middelburg, J. J.; Pancost, R. D.; Regnier, P. (2013): Quantifying the degradation of organic matter in marine sediments. A review and synthesis. In *Earth-Science Reviews* 123, pp. 53–86. DOI: 10.1016/j.earscirev.2013.02.008.

Arning, E.T., van Berk, W., dos Santos Neto, E.V., Naumann, R., and Schulz, H.M. (2013). The quantification of methane formation in Amazon fan sediments (ODP leg 155, site 938) by hydrogeochemical modeling solid–aqueous solution–gas interactions. *Journal of South American Earth Sciences*, 42, 205-215

Artemieva, Irina M.; Thybo, Hans (2013): EUNaseis. A seismic model for Moho and crustal structure in Europe, Greenland, and the North Atlantic region. In *Tectonophysics* 609, pp. 97–153. DOI: 10.1016/j.tecto.2013.08.004.

Arthur, Michael A.; Dean, Walter E.; Pollastro, Richard M.; Scholle, Peter A. (1985): Comparative Geochemical and Mineralogical Studies of two Cyclic Transgressive Pelagic Limestone Units, Cretaceous Western Interior Basin, U.S: Special Publications of SEPM. Available online at http://archives.datapages.com/data/sepm_sp/fg4/Comparative_Geochemical.pdf.

Baudin, François; Disnar, Jean-Robert; Aboussou, Anabel; Savignac, Florence (2015): Guidelines for Rock–Eval analysis of recent marine sediments. In *Organic Geochemistry* 86, pp. 71–80. DOI: 10.1016/j.orggeochem.2015.06.009.

Baudin, François; Disnar, Jean-Robert; Martinez, Philippe; Dennielou, Bernard (2010): Distribution of the organic matter in the channel-levees systems of the Congo mud-rich deep-sea fan (West Africa). Implication for deep offshore petroleum source rocks and global carbon cycle. In *Marine and Petroleum Geology* 27 (5), pp. 995–1010. DOI: 10.1016/j.marpetgeo.2010.02.006.

Baudin, François; Stetten, Elsa; Schnyder, Johann; Charlier, Karine; Martinez, Philippe; Dennielou, Bernard; Droz, Laurence (2017): Origin and distribution of the organic matter in

the distal lobe of the Congo deep-sea fan – A Rock-Eval survey. In *Deep Sea Research Part II: Topical Studies in Oceanography* 142, pp. 75–90. DOI: 10.1016/j.dsr2.2017.01.008.

Beaumont, Christopher; Muñoz, Josep Anton; Hamilton, Juliet; Fullsack, Philippe (2000): Factors controlling the Alpine evolution of the central Pyrenees inferred from a comparison of observations and geodynamical models. In *J. Geophys. Res.* 105 (B4), pp. 8121–8145. DOI: 10.1029/1999JB900390.

Behar, F.; Beaumont, V.; B. Penteadó, H. L. de (2001): Rock-Eval 6 Technology. Performances and Developments. In *Oil & Gas Science and Technology - Rev. IFP* 56 (2), pp. 111–134. DOI: 10.2516/ogst:2001013.

Belyaev, S. S.; Wolkin, R., Kenealy, W.R., DeNiro, M.J., Epstein S., Zeikus, J.G. (1983): Methanogenic Bacteria from the Bondyuzhskoe Oil Field: General Characterization and Analysis of Stable-Carbon Isotopic Fractionation. In *Applied and Environmental Microbiology* 45 (2), pp. 691–697.

Bernard, B. B.; Brooks, J. M.; Sackett, W. M. (1976): Natural gas seepage in the Gulf of Mexico. In *Earth and Planetary Science Letters* 31 (1), pp. 48–54. DOI: 10.1016/0012-821X(76)90095-9.

Biteau, J. J.; Le Marrec, A.; Le Vot, M.; Masset, J. M. (2006): The Aquitaine Basin. In *Petroleum Geoscience* (12), pp. 247–273.

Blair, Neal E.; Aller, Robert C. (2012): The fate of terrestrial organic carbon in the marine environment. In *Annual review of marine science* 4, pp. 401–423. DOI: 10.1146/annurev-marine-120709-142717.

Boetius, A.; Ravensschlag, K.; Schubert, C. J.; Rickert, D.; Widdel, F.; Gieseke, A. et al. (2000): A marine microbial consortium apparently mediating anaerobic oxidation of methane. In *Nature* 407 (6804), pp. 623–626. DOI: 10.1038/35036572.

Bois, C.; Pinet, B.; Gariel, O. (1997): The sedimentary cover along the ECORS Bay of Biscay deep seismic reflection profile. A comparison between the Parentis basin and other European rifts and basins. In *Mémoires de la Société géologique de France*, 1997 (171), pp. 143–165.

Boudreau, B. P.; Ruddick, B. R. (1991): On a reactive continuum representation of organic matter diagenesis. In *American Journal of Science* 291 (5), pp. 507–538. DOI: 10.2475/ajs.291.5.507.

Bruneau, B.; Villié, M.; Ducros, M.; Chauveau, B.; Baudin, F.; Moretti, I. (2018): 3D Numerical Modelling and Sensitivity Analysis of the Processes Controlling Organic Matter Distribution and Heterogeneity—A Case Study from the Toarcian of the Paris Basin. In *Geosciences* 8 (11), p. 405. DOI: 10.3390/geosciences8110405.

Brunet, M. F. (1994): Subsidence in the Parentis Basin (Aquitaine, France): Implications of the Thermal Evolution. In *Hydrocarbon and Petroleum Geology of France*, checked on 4/3/2018.

Brunet, M-F (1997): Subsidence along the ECORS Bay of Biscay deep seismic profile. In *Mémoires de la Société géologique de France* 171, pp. 167–176.

Burdige, D. J. (2007): Preservation of organic matter in marine sediments: controls, mechanisms, and an imbalance in sediment organic carbon budgets? In *Chemical reviews* 107 (2), pp. 467–485. DOI: 10.1021/cr050347q.

Burdige, David J. (2006): *Geochemistry of Marine Sediments*: Princeton University Press.

Burdige, David J. (2011): Temperature dependence of organic matter remineralization in deeply-buried marine sediments. In *Earth and Planetary Science Letters* 311 (3-4), pp. 396–410. DOI: 10.1016/j.epsl.2011.09.043.

Calvert, S. E.; Pedersen, T. F. (1992): Organic carbon accumulation and preservation in marine sediments: how important is anoxia. Productivity, accumulation and preservation of organic matter in recent and ancient sediments, 1992, pp. 231–263.

Canuel, E. A., & Martens, C. S. (1996). Reactivity of recently deposited organic matter: Degradation of lipid compounds near the sediment-water interface. *Geochimica et cosmochimica acta*, 60(10), 1793-1806.

Chapelle, F. H.; Lovley, D. R. (1990): Rates of Microbial Metabolism in Deep Coastal Plain Aquifers. In *Applied and Environmental Microbiology* 56 (6), pp. 1865–1874.

Charlou, J. L., Donval, J. P., Fouquet, Y., Jean-Baptiste, P., & Holm, N. (2002). Geochemistry of high H₂ and CH₄ vent fluids issuing from ultramafic rocks at the Rainbow hydrothermal field (36° 14' N, MAR). *Chemical geology*, 191(4), 345-359.

Chenrai, P., & Huuse, M. (2017). Pockmark formation by porewater expulsion during rapid progradation in the offshore Taranaki Basin, New Zealand. *Marine and Petroleum Geology*, 82, 399-413.

Ciais, P., Sabine, C., Bala, G., Bopp, L., Brovkin, V., Canadell, J., ... & Jones, C. (2014). Carbon and other biogeochemical cycles. In *Climate change 2013: the physical science basis. Contribution of Working Group I to the Fifth Assessment Report of the Intergovernmental Panel on Climate Change* (pp. 465-570). Cambridge University Press.

Clayton, C. (1992): Source Volumetrics of Biogenic Gas Generation. In *Bacterial Gas*, 1992, pp. 191–204.

Clayton, C., J., Hay, S., J. (1994): Gas migration mechanisms from accumulation to surface. In *Bulletin of the Geological Society of Denmark* (41/1), pp. 12–23. Available online at <https://2dggf.dk/xpdf/bull41-01-12-23.pdf>, checked on 7/25/2018.

Conrad, R. (2005). Quantification of methanogenic pathways using stable carbon signatures: a review and a proposal. *Org. Geochem.* 36, 739-572.

Conrad, R. (2009). The global methane cycle: Recent advances in understanding the microbial processes involved. *Environmental Microbiology Reports*, 1, 285–292. <https://doi.org/10.1111/j.1758-2229.2009.00038.x>.

Cowie, G. L., Hedges, J. I., & Calvert, S. E. (1992). Sources and relative reactivities of amino acids, neutral sugars, and lignin in an intermittently anoxic marine environment. *Geochimica et Cosmochimica Acta*, 56(5), 1963-1978

Cowie, G. L.; Hedges, J. I. (1994): Biochemical indicators of diagenetic alteration in natural organic matter mixtures. In *Nature* 369 (6478), pp. 304–307. DOI: 10.1038/369304a0.

Dardel, R. A.; Rosset, R. (1971): Histoire géologique et structurale du bassin de Parentis et de son prolongement en mer. In *Histoire structurale du Golfe de Gascogne 2* (2.28).

Davy, B., Pecher, I., Wood, R., Carter, L., & Gohl, K. (2010). Gas escape features off New Zealand: Evidence of massive release of methane from hydrates. *Geophysical Research Letters*, 37(21).

de Almeida, J.C., Velásquez, J.A., and Barbieri, R. (2014). A methodology for calculating the natural gas compressibility factor for a distribution network. *Petroleum science and technology*, 32(21), 2616-2624.

Debyser, J., Le Pichon, X.; Montadert, L. (1971): Histoire structurale du Golfe de Gascogne, in 291 Technip.(éd). In *Publication de l'Institut Français du Pétrole, Paris, I & II* 292.

Dembicki, Harry (Ed.) (2016): Practical petroleum geochemistry for exploration and production. 1st edition. Waltham MA: Elsevier.

Deming, David (1989): Application of bottom-hole temperature corrections in geothermal studies. In *Geothermics* 18 (5-6), pp. 775–786. DOI: 10.1016/0375-6505(89)90106-5.

Deroo, G.; Herbin, J. P.; Roucaché, J. (1983): Organic geochemistry of upper Jurassic Cretaceous sediments from site-511, leg-71, western south-atlantic. In *Initial Reports of the Deep Sea Drilling Project, 71(SEP)*, 1983, pp. 1001–1013.

Desegaulx, P.; Brunet, M. F. (1990): Tectonic subsidence of the Aquitaine Basin since Cretaceous times. In *Bulletin de la Societe Geologique de France VI* (2), pp. 295–306. DOI: 10.2113/gssgfbull.VI.2.295.

Davidson, D.W., EI-Defrawy, M.K., Fuglem, M.O. and Judge, A.S., 1978. Natural gas hydrates in northern Canada. In: National Research Council of Canada. Proc. 3rd Int. Conf. on Permafrost, 1978, 1: 938-943.

Deville, E.; Mascle, A.; Callec, Y.; Huyghe, P.; Lallemand, S.; Lerat, O. et al. (2015): Tectonics and sedimentation interactions in the east Caribbean subduction zone. An overview from the Orinoco delta and the Barbados accretionary prism. In *Marine and Petroleum Geology* 64, pp. 76–103. DOI: 10.1016/j.marpetgeo.2014.12.015.

Deville, Eric; Marsset, Tania; Courgeon, Simon; Jatiault, Romain; Ponte, Jean-Pierre; Thereau, Estelle et al. (2018): Active fault system across the oceanic lithosphere of the Mozambique Channel. Implications for the Nubia–Somalia southern plate boundary. In *Earth and Planetary Science Letters* 502, pp. 210–220. DOI: 10.1016/j.epsl.2018.08.052.

Deville E., Scalabrin C., Jouet G., Cattaneo A., Battani A., Noirez S., Vermesse H., Olu K., Corbari L., Boulard M., Marsset T., Dall’Asta M., Torelli M., Pastor L., Pierre D., Loubrieu B. (2020) "Fluid seepage associated with slope destabilization along the Zambezi Margin (Mozambique)". *Marine Geology*. <https://doi.org/10.1016/j.margeo.2020.106275>

Dimitrov, L., & Woodside, J. (2003). Deep sea pockmark environments in the eastern Mediterranean. *Marine Geology*, 195(1-4), 263-276.

Doré, A. G., Augustson, J. H., Hermanrud, C., Stewart, D. J., & Sylta, Ø. (1993). Basin modelling: advances and applications. Norwegian Petroleum Society (NPF), Special Publication, v. 3

Douwe J. J. van Hinsbergen; Lennart V. de Groot; Sebastiaan J. van Schaik; Wim Spakman; Peter K. Bijl; Appy Sluijs et al. (2015): A Paleolatitude Calculator for Paleoclimate Studies. *PloS one* (6), checked on 3/23/2018.

Duan, Z., Møller, N., & Weare, J. H. (1992). An equation of state for the CH₄-CO₂-H₂O system: I. Pure systems from 0 to 1000 C and 0 to 8000 bar. *Geochimica et Cosmochimica acta*, 56(7), 2605-2617.

Duan, Z., Møller, N., & Weare, J. H. (1992). An equation of state for the CH₄-CO₂-H₂O system: II. Mixtures from 50 to 1000 C and 0 to 1000 bar. *Geochimica et Cosmochimica Acta*, 56(7), 2619-2631.

Duan Z., Moller N., Weare J.H., 1992. Prediction of methane solubilities in natural waters to high ionic strength from 0 to 250 °C and from 0 to 1600 bar. *Geochim. Cosmochim. Acta* 56, 1451–1460.

Ducros, M.; Cacas, M. C.; Rouchon, V.; Wolf, S.; Blanchet, D.; Ravin, A.; Pujol, A. (2015): Simulation of anaerobic SOM biodegradation and biogenic methane production in the TemiFlow basin model. Prague, 2015.

Ducros, M.; Wolf, S. (2014): Tests des développements du modèle de génération du gaz biogénique dans Visco. IFPEN Internal Report (R161/MD-OC 14-005).

Dudley D. Rice, George E. Claypool (1981): Generation, Accumulation, and Resource Potential of Biogenic Gas. In *AAPG Bulletin* 65 (1), pp. 5–25. Available online at <http://archives.datapages.com/data/bulletns/1980-81/images/pg/00650001/0000/00050.pdf>.

Dupré, S. Woodside, J. Foucher, J.P. de Lange, G. Mascle, J. Boetius, A. Mastalerz, V. Stadnitskaia, A. Ondréas, H. Huguen, C. Harmegnies, F. Gontharet, S. Loncke, L. Deville, E. Niemann, H. Omorigie, E. Olu-Le Roy, K. Fiala-Medioni, A. Dählmann, A. Caprais, J.C. Prinzhofer, A. Sibuet, M. Pierre, C. Sinninghe Damsté, J. NAUTINIL scientific Party (2007) Seafloor geological studies above active gas chimneys off Egypt (Central Nile Deep Sea Fan).

Deep Sea Research Part I: Oceanographic Research Papers 54 (7):1146-1172.
doi:10.1016/j.dsr.2007.03.007

Dupré, Stéphanie; Berger, Laurent; Le Bouffant, Naig; Scalabrin, Carla; Bourillet, Jean-François (2014): Fluid emissions at the Aquitaine Shelf (Bay of Biscay, France). A biogenic origin or the expression of hydrocarbon leakage? In *Continental Shelf Research* 88, pp. 24–33. DOI: 10.1016/j.csr.2014.07.004.

Durand, B., Nicaise, G. (1980): Procedures of kerogen isolation. in Durand, B. (Ed.), Kerogen, Insoluble Organic Matter from Sedimentary Rocks. In *Éditions Technip*, 1980, pp. 35–53.

Emerson; S.; Fischer, K.; Reimers, C.; Heggie, D. (1985): Organic carbon dynamics and preservation in deep-sea sediments. In *Deep Sea Research* 32 (1), pp. 1–21.

Espitalie, J.; Deroo, G.; Marquis, F. (1985): Rock-Eval pyrolysis and its applications. In *Revue De L Institut Francais Du Petrole* 40 (5), pp. 563–579.

Espitalie, J.; Madec, M.; Tissot, B.; Mennig, J. J.; Leplat, P. (1977): Source Rock Characterization Method for Petroleum Exploration. In. Offshore Technology Conference. OTC, 1977/1/1: Offshore Technology Conference, p. 6.

Espitalié, J.; Senga Makadi, K.; Trichet, J. (1984): Role of the mineral matrix during kerogen pyrolysis. In *Organic Geochemistry* 6, pp. 365–382.

Etheve, N., Jeannot, L., Cornu, T., & Callot, J. P. (2021). Kinematic modelling of the Mozambique rifted margin and associated thermal histories. *Marine and Petroleum Geology*, 123, 104712.

Etiopie, G. and Klusman, R. W. (2002). Geologic emissions of methane to the atmosphere. *Chemosphere*, 49(8), 777-789.

Etiopie, G. (2005). Mud volcanoes and microseepage: The forgotten geophysical components of atmospheric methane budget. *Annals of Geophysics*, 48(1).

Etiopie, G. Lassey, K.R. Klusman, R.W. and Boschi, E. (2008). Reappraisal of the fossil methane budget and related emission from geologic sources. *Geophysical Research Letters*, 35(9).

Etiopie, G. and Klusman, R. W. (2010). Methane microseepage in drylands: soil is not always a CH₄ sink. *Journal of Integrative Environmental Sciences*, 7(S1), 31-38.

Etiopie, G., Schoell, M., & Hosgörmez, H. (2011). Abiotic methane flux from the Chimaera seep and Tekirova ophiolites (Turkey): understanding gas exhalation from low temperature serpentinization and implications for Mars. *Earth and Planetary Science Letters*, 310(1-2), 96-104. Etiopie, G. and Schwietzke, S. (2019). Global geological methane emissions: an update of top-down and bottom-up estimates. *Elementa-Science of the Anthropocene*.

Etiopé, G., Ciotoli, G., Schwietzke, S., & Schoell, M. (2019). Gridded maps of geological methane emissions and their isotopic signature. *Earth System Science Data*.

Fernández-Viejo, Gabriela; Gallart, Josep; Pulgar, Javier A.; Córdoba, Diego; Dañobeitia, Juan José (2000): Seismic signature of Variscan and Alpine tectonics in NW Iberia. Crustal structure of the Cantabrian Mountains and Duero basin. In *J. Geophys. Res.* 105 (B2), pp. 3001–3018. DOI: 10.1029/1999JB900321.

Fernández-Viejo, Gabriela; Gallastegui, Jorge; Pulgar, Javier A.; Gallart, Josep (2011): The MARCONI reflection seismic data. A view into the eastern part of the Bay of Biscay. In *Tectonophysics* 508 (1-4), pp. 34–41. DOI: 10.1016/j.tecto.2010.06.020.

Ferrer, O.; Roca, E.; Benjumea, B.; Muñoz, J. A.; Ellouz, N.; MARCONI Team (2008): The deep seismic reflection MARCONI-3 profile. Role of extensional Mesozoic structure during the Pyrenean contractional deformation at the eastern part of the Bay of Biscay. In *Marine and Petroleum Geology* 25 (8), pp. 714–730. DOI: 10.1016/j.marpetgeo.2008.06.002.

Fierens, Ruth; Droz, Laurence; Toucanne, Samuel; Raison, François; Jouet, Gwenael; Babonneau, Nathalie et al. (2019): Late Quaternary geomorphology and sedimentary processes in the Zambezi turbidite system (Mozambique Channel). In *Geomorphology* 334, pp. 1–28. DOI: 10.1016/j.geomorph.2019.02.033.

Floodgate, G. D.; Judd, A. G. (1992): The origins of shallow gas. In *Continental Shelf Research* 12 (10), pp. 1145–1156. DOI: 10.1016/0278-4343(92)90075-U.

Forja, J. M., Ortega, T., DelValls, T. A., & Gómez-Parra, A. (2004). Benthic fluxes of inorganic carbon in shallow coastal ecosystems of the Iberian Peninsula. *Marine Chemistry*, 85(3-4), 141-156.

Fujii, T., Tin Aung, T., Wada, N., Komatsu, Y., Suzuki, K., Ukita, T., Wygrala, B., Fuchs, T., Rottke, W., Egawa, K. (2016). Modeling gas hydrate petroleum systems of the Pleistocene turbiditic sedimentary sequences of the Daini-Atsumi area, eastern Nankai Trough, Japan. *Interpretation*, 4(1), SA95-SA111.

Gallart, J.; Pulgar, J. A.; Muñoz, J. A. (2004): Integrated studies on the lithospheric structure and geodynamics of the North Iberian Continental Margin: the Marconi Project. In *Geophysical Research Abstracts*, 2004, p. 4196.

Gallastegui, J.; Pulgar, J. A.; Gallart, J. (2002): Initiation of an active margin at the North Iberian continent-ocean transition. In *Tectonics* 21 (4), 15-1-15-14. DOI: 10.1029/2001TC901046.

Ganesan, A. L., Schwietzke, S., Poulter, B., Arnold, T., Lan, X., Rigby, M., ... & Pandey, S. (2019). Advancing scientific understanding of the global methane budget in support of the Paris Agreement. *Global Biogeochemical Cycles*, 33(12), 1475-1512.

Gervais, V.; Ducros, M.; Granjeon, D. (2018): Probability maps of reservoir presence and sensitivity analysis in stratigraphic forward modeling. In *Bulletin* 102 (04), pp. 613–628. DOI: 10.1306/0913171611517242.

Grauls, D. (2001). Gas hydrates: importance and applications in petroleum exploration. *Marine and Petroleum Geology*, 18(4), 519-523.

Guichet, X. (2015): Lois de solubilisation du Méthane dans les saumures pour la modélisation de bassin. IFPEN Internal Report n.65608. 54 pp.

Hare, A. A.; Kuzyk, Z. Z. A.; Macdonald, R. W.; Sanei, H.; Barber, D.; Stern, G. A.; Wang, F. (2014): Characterization of sedimentary organic matter in recent marine sediments from Hudson Bay, Canada, by Rock-Eval pyrolysis | Elsevier Enhanced Reader. In *Organic Geochemistry*, 2014, pp. 52–60.

Hatcher, Patrick G.; Ravin, Azdine; Behar, Françoise; Baudin, François (2014a): Diagenesis of organic matter in a 400 m organic rich sediment core from offshore Namibia using solid state ¹³C NMR and FTIR. In *Organic Geochemistry* 75, pp. 8–23. DOI: 10.1016/j.orggeochem.2014.05.016.

Hatcher, Patrick G.; Ravin, Azdine; Behar, Françoise; Baudin, François (2014b): Diagenesis of organic matter in a 400 m organic rich sediment core from offshore Namibia using solid state ¹³C NMR and FTIR. In *Organic Geochemistry* 75, pp. 8–23. DOI: 10.1016/j.orggeochem.2014.05.016.

Hedges; I. J.; Clark, W.A., Come, G.L. (1988): Organic Matter Sources to the Water Column and surficial sediments of a marine bay. In *Limnol. Oceanogr.*, 1988, pp. 1116–1136.

Hedges; I. J.; Oades, M. J. (1997a): Comparative organic geochemistries of soils and marine sediments. In *Organic Geochemistry* 27 (7/8), pp. 319–361.

Hedges, John I.; Keil, R. G.; Benner, R. (1997b): What Happens to Terrestrial Organic Matter in the Ocean? In *Organic Geochemistry* 27 (5/6), pp. 195–212.

Hedges, John I.; Mayorga, Emilio; Tsamakis, Elizabeth; McClain, Michael E.; Aufdenkampe, Anthony; Quay, Paul et al. (2000): Organic matter in Bolivian tributaries of the Amazon River. A comparison to the lower mainstream. In *Limnology and Oceanography* 45 (7), pp. 1449–1466.

Henrichs, S. M.; Farrington, J. W. (1984): Peru upwelling region sediments near 15S. 1. Remineralization and accumulation of organic matter. In *Limnology and Oceanography* 29, pp. 1–19.

Hoehler, Tori M.; Albert, Daniel B.; Alperin, Marc J.; Martens, Christopher S. (1999): Acetogenesis from CO₂ in an anoxic marine sediment. In *Limnol. Oceanogr.* 44 (3), pp. 662–667. DOI: 10.4319/lo.1999.44.3.0662.

Hovland, M., Judd, A. G., & King, L. H. (1984). Characteristic features of pockmarks on the North Sea Floor and Scotian Shelf. *Sedimentology*, 31(4), 471-480.

Hovland, M., & Judd, A. G. (1988). *Seabed pockmarks and seepages: impact on geology, biology and the marine environment*. Graham & Trotman.

Hovland, M. (1989). The formation of pockmarks and their potential influence on offshore construction. *Quarterly Journal of Engineering Geology and Hydrogeology*, 22(2), 131-138.

Hovland, M. (2005). Pockmark-associated coral reefs at the Kristin field off Mid-Norway. In *Cold-water corals and Ecosystems* (pp. 623-632). Springer, Berlin, Heidelberg.

Hornafius, J.S.; Quigley, D.; and Luyendyk, B.P. (1999). The world's most spectacular marine hydrocarbon seeps (Coal Oil Point, Santa Barbara Channel, California): Quantification of emissions. *Journal of Geophysical Research: Oceans*, 104(C9), pp. 20703-20711.

Imbert, P., & Ho, S. (2012). Seismic-scale funnel-shaped collapse features from the Paleocene–Eocene of the North West Shelf of Australia. *Marine Geology*, 332, 198-221.

Imbert P. (2016): Hydrate pockmarks / Collapsed hydrate pockmarks: A quantifiable morphological indicator of present and past gas escape. Rapport Interne TOTAL, R&D Results for Exploration #6, EP/SCR/RD/PRG-FTE-2016-219.

Ishiwatari, R. (1992): Macromolecular material (humic substance) in the water column and sediments. In *Marine Chemistry* 39, pp. 151–166.

Jackson, R. B., Saunio, M., Bousquet, P., Canadell, J. G., Poulter, B., Stavert, A. R., ... & Tsuruta, A. (2020). Increasing anthropogenic methane emissions arise equally from agricultural and fossil fuel sources. *Environmental Research Letters*, 15(7), 071002.

Janssen, B. H. (1984): A simple method for calculating decomposition and accumulation of 'young' soil organic matter. In *Plant and Soil* 76, pp. 297–304.

Jay Katz, Barry (2011): Microbial Processes and Natural Gas Accumulations. In *TOGEOJ* 5 (1), pp. 75–83. DOI: 10.2174/1874262901105010075.

Jensen, P. (1992): "Bubbling reefs" in the Kattgat: submarine landscapes of carbonate-cemented rocks support a diverse ecosystem at methane seeps. In *Mar. Ecol. Prog. Ser* (83), pp. 103–112.

Jørgensen, N. O. (1976). Recent high magnesian calcite/aragonite cementation of beach and submarine sediments from Denmark. *Journal of Sedimentary Research*, 46(4), 940-951.

Judd, A. G.; Hovland, M.; Dimitrov, L. I.; Garcia Gil, S.; Jukes, V. (2002): The geological methane budget at Continental Margins and its influence on climate change. In *Geofluids* 2 (2), pp. 109–126. DOI: 10.1046/j.1468-8123.2002.00027.x.

Judd, A.G. (2004). Natural seabed gas seeps as sources of atmospheric methane. *Environmental Geology*, 46(8), 988-996.

Judd, A., Croker, P., Tizzard, L., & Voisey, C. (2007). Extensive methane-derived authigenic carbonates in the Irish Sea. *Geo-Marine Letters*, 27(2-4), 259.

Kamga, N. (2016). "Low-Temperature Artificial Maturation Studies of Type II and Type III Kerogens: Implications for Biogenic Gas Production". Doctor of Philosophy (PhD), Dissertation, Chemistry and Biochemistry, Old Dominion University, DOI: 10.25777/5sj5-4y45.

Katz, B. J. (1983): Limitations of Rock-Eval pyrolysis for typing organic matter. In *Organic Geochemistry*, pp. 195–199.

Katz, B., & Williams, K. (2003). Biogenic gas potential offshore Guajira peninsula, Colombia.

Kearns, H. (2018): Using BSRs to derive geothermal gradients & de-risk frontier margins. *Biogenic Gas and Gas Hydrates: New Opportunities and Future Challenges*. Milan, 2018.

Keil, R. G.; Montluçon, D. B.; Prahl, F. G.; Hedges, J. I. (1994): Sorptive preservation of labile organic matter in marine sediments. In *Nature* (6490), p. 549.

Ketzer, M., Praeg, D., Pivel, M. A., Augustin, A. H., Rodrigues, L. F., Viana, A. R., & Cupertino, J. A. (2019). Gas seeps at the edge of the gas hydrate stability zone on Brazil's continental margin. *Geosciences*, 9(5), 193.

Ketzer, M., Praeg, D., Rodrigues, L. F., Augustin, A., Pivel, M. A., Rahmati-Abkenar, M., Miller, D.J., Viana, A.R., Cupertino, J. A. (2020). Gas hydrate dissociation linked to contemporary ocean warming in the southern hemisphere. *Nature communications*, 11(1), 1-9.

Khalil, M. A. K.; Shearer, M. J.; Rasmussen, R. A. (1993): Methane Sinks Distribution. In M. A. K. Khalil (Ed.): *Atmospheric methane. Sources, sinks, and role in global change*. Berlin, New York: Springer-Verlag (NATO ASI series. Series I, Global environmental change, vol. 13), pp. 168–179.

King, L. H., & MacLEAN, B. R. I. A. N. (1970). Pockmarks on the Scotian shelf. *Geological Society of America Bulletin*, 81(10), 3141-3148.

Kirschke, S., Bousquet, P., Ciais, P., Saunoy, M., Canadell, J. G., Dlugokencky, E. J., ... & Cameron-Smith, P. (2013). Three decades of global methane sources and sinks. *Nature geoscience*, 6(10), 813-823.

Klusman, R.W.; Leopold, M.E.; LeRoy, M.P. (2000). Seasonal variation in methane fluxes from sedimentary basins to the atmosphere: Results from chamber measurements and modeling of transport from deep sources. *Journal of Geophysical Research: Atmospheres*, 105(D20), 24661-24670.

Kundu, N.; Pal, N.; Sinha, N.; Budhiraja, I.L. (2008). Paleo Hydrates and its Role in Deep Water Plio-Pleistocene Gas Reservoirs in Krishna-Godavari Basin, India. Proceedings of the –th International Conference on Gas Hydrates. Vancouver, British Columbia, Canada, July 6-10.

Kvenvolden, K. A. (1988). Methane hydrates and global climate. *Global biogeochemical cycles*, 2(3), 221-229.

Kvenvolden, Keith A. (1993): Gas hydrates geological perspective and global change. In *American Geophysical Union*, pp. 173–187.

Kvenvolden, K. A. (1998). A primer on the geological occurrence of gas hydrate. *Geological Society, London, Special Publications*, 137(1), 9-30.

Kvenvolden, K.A.; Lorenson, T.D.; Reeburgh, W.S. (2001). Attention turns to naturally occurring methane seepage. *Eos, Transactions American Geophysical Union*, 82(40), 457-457.

Lafargue, E.; Marquis, F.; Pillot, D. (1998): Rock-Eval 6 Applications in Hydrocarbon Exploration, Production, and Soil Contamination Studies. In *Rev. Inst. Fr. Pét.* 53 (4), pp. 421–437. DOI: 10.2516/ogst:1998036.

Lamoureux-Var, V.; Espitalié, J.; Pillot, D.; Bouton, N.; Garcia, B.; Antonas, R. et al. (2019): Rock-Eval 7S: Technology, Performance and Applications. In *European Association of Organic Geochemists*, 2019.

Lash, G.G. (2015). Pyritization induced by anaerobic oxidation of methane (AOM)—An example from the upper devonian shale succession, western New York, USA. *Marine and Petroleum Geology*, 68, 520-535. <https://doi.org/10.1016/j.marpetgeo.2015.10.002>.

Lazure P., Jégou A.M., Kerdreux M. (2006): Analysis of salinity measurements near islands on the French continental shelf of the Bay of Biscay. In *Scientia Marina*.

Luff, R., & Wallmann, K. (2003). Fluid flow, methane fluxes, carbonate precipitation and biogeochemical turnover in gas hydrate-bearing sediments at Hydrate Ridge, Cascadia Margin: numerical modeling and mass balances. *Geochimica et Cosmochimica Acta*, 67(18), 3403-3421.

Mackin, J. E., & Swider, K. T. (1989). Organic matter decomposition pathways and oxygen consumption in coastal marine sediments. *Journal of Marine Research*, 47(3), 681-716.

Mahanjane, E. S., Franke, D., Lutz, R., Winsemann, J., Ehrhardt, A., Berglar, K., & Reichert, C. (2014). Maturity and petroleum systems modelling in the offshore Zambezi Delta depression and Angoche Basin, northern Mozambique. *Journal of Petroleum Geology*, 37(4), 329-348.

Marié L, Loubrieu B, Dupré S (2019) Seawater temperature, conductivity, pressure and salinity data offshore the Aquitaine Basin (XBT profiles and near-bottom moorings). SEANO database. doi:<https://doi.org/10.17882/61855>

Mathieu, C. (1986): Geological history of the Parentis sub-Basin. In *Bulletin du Centre de recherches de Pau* 10, pp. 33–47.

Mayer, L., M. (1995): Sedimentary organic matter preservation: an assessment and speculative synthesis - a comment. In *Marine Chemistry* 49, pp. 123–126, checked on 7/27/2018.

McKenzie, D. (1978): Some remarks on the development of sedimentary basins. In *Earth and Planetary Science Letters* 40 (1), pp. 25–32. DOI: 10.1016/0012-821X(78)90071-7.

McGee, K. A., N. J. Susak, A. J., Sutton, J. L. Haas Jr. (1981). The solubility of methane in sodium chloride brines, USGS Open-File Report 81-1294. <https://doi.org/10.3133/ofr811294>.

Michel, G. (2017): Mise en place et pérennisation d'un vaste système fluide microbien sur le plateau aquitain. Caractérisation et facteurs de contrôle. Paris 6.

Michel, G.; Dupré, S.; Baltzer, A.; Ehrhold, A.; Imbert, P.; Pitel, M. et al. (2017): Pockmarks on the South Aquitaine Margin continental slope: the 2 seabed expression of past fluid circulation and bottom currents Corresponding Author. In: *Comptes Rendus Géoscience, Elsevier Masson* n. 8, 349, pp. 391–401.

Middelburg, Jack J. (1989): A simple rate model for organic matter decomposition in marine sediments. In *Geochimica et Cosmochimica Acta* 53 (7), pp. 1577–1581. DOI: 10.1016/0016-7037(89)90239-1.

Milkov, A. V., & Dzou, L. (2007). Geochemical evidence of secondary microbial methane from very slight biodegradation of undersaturated oils in a deep hot reservoir. *Geology*, 35(5), 455-458.

Milkov, A. V. (2010). Methanogenic biodegradation of petroleum in the West Siberian Basin (Russia): Significance for formation of giant Cenomanian gas pools. *AAPG bulletin*, 94(10), 1485-1541.

Milkov, A. V. (2011). Worldwide distribution and significance of secondary microbial methane formed during petroleum biodegradation in conventional reservoirs. *Organic Geochemistry*, 42(2), 184-207.

Milkov, A. V., & Etiope, G. (2018). Revised genetic diagrams for natural gases based on a global dataset of > 20,000 samples. *Organic Geochemistry*, 125, 109-120.

Miramontes, Elda; Jorry, Stephan J.; Jouet, Gwenaël; Counts, John W.; Courgeon, Simon; Le Roy, Pascal et al. (2019a): Deep-water dunes on drowned isolated carbonate terraces (Mozambique Channel, south-west Indian Ocean). In *Sedimentology* 66 (4), pp. 1222–1242. DOI: 10.1111/sed.12572.

Miramontes, Elda; Penven, Pierrick; Fierens, Ruth; Droz, Laurence; Toucanne, Samuel; Jorry, Stephan J. et al. (2019b): The influence of bottom currents on the Zambezi Valley morphology (Mozambique Channel, SW Indian Ocean). In situ current observations and hydrodynamic modelling. In *Marine Geology* 410, pp. 42–55. DOI: 10.1016/j.margeo.2019.01.002.

Mitterer, R.M. (2010). Methanogenesis and sulfate reduction in marine sediments: A new model. *Earth and Planetary Science Letters*, 295(3-4), 358-366.

Mueller, C. O.; Jokat, W. (2019): The initial Gondwana break-up_ A synthesis based on new potential field data of the Africa-Antarctica Corridor | Elsevier Enhanced Reader. In *Tectonophysics*, 2019 (750), pp. 301–328.

Muller, P. J.; Suess, E. (1979): Productivity, sedimentation rate, and sedimentary organic matter in the oceans - I. Organic carbon preservation. In *Deep Sea Research*, pp. 1347–1362.

Muñoz, J. A. (2002): The pyrenees. In *The geology of Spain*, pp. 370–385.

Muñoz, Josep Anton (1992): Evolution of a continental collision belt: ECORS-Pyrenees crustal balanced cross-section. In K. R. McClay (Ed.): *Thrust Tectonics*. Dordrecht: Springer Netherlands, pp. 235–246.

Nieto-Cid, M.; Alvarez-Salgado, A.; Pérez, F. F. (2006): Microbial and Photochemical reactivity of fluorescent dissolved organic matter in a coastal upwelling system. In *Limnology and Oceanography* 51 (3), pp. 1391–1400.

Nisbet, E. G., Manning, M. R., Dlugokencky, E. J., Fisher, R. E., Lowry, D., Michel, S. E., ... & Brownlow, R. (2019). Very strong atmospheric methane growth in the 4 years 2014–2017: Implications for the Paris Agreement. *Global Biogeochemical Cycles*, 33(3), 318-342.

Noble-James, T., Judd, A., Diesing, M., Clare, D., Eggett, A., Silburn, B., & Duncan, G. (2020). Monitoring shallow methane-derived authigenic carbonate: Insights from a UK Marine Protected Area. *Aquatic Conservation: Marine and Freshwater Ecosystems*, 30(5), 959-976.

Odobel, C. (2017). Dynamique spatiale et temporelle des communautés Archaea et Bacteria dans les sédiments marins profonds du canal du Mozambique. Doctorat de l'Université de Bretagne Occidentale, École Doctorale des Sciences de la Mer.

Omodeo-Salé, S., Eruteya, O. E., Cassola, T., Baniasad, A., & Moscariello, A. (2020). A basin thermal modelling approach to mitigate geothermal energy exploration risks: The St. Gallen case study (eastern Switzerland). *Geothermics*, 87, 101876.

Ortiz, Alexandre (2019): Géométries et bilan érosion-sédimentation d'un rétro-bassin d'avant-pays durant son évolution finie-orogénique et post-orogénique :le cas du système Pyrénées / bassin d'Aquitaine / golfe de Gascogne de 38 à 0 Ma. PhD Thesis. Université de Rennes.

Pasquale, V.; Gola, G.; Chiozzi, P.; Verdoya, M. (2011): Thermophysical properties of the Po Basin rocks. In *Geophysical Journal International* 186 (1), pp. 69–81. DOI: 10.1111/j.1365-246X.2011.05040.x.

Parkes, R. J., Wellsbury, P., Mather, I. D., Cobb, S. J., Cragg, B. A., Hornibrook, E. R., & Horsfield, B. (2007). Temperature activation of organic matter and minerals during burial

has the potential to sustain the deep biosphere over geological timescales. *Organic Geochemistry*, 38(6), 845-852.

Paull, C. K., & Ussler III, W. (2008). Re-evaluating the significance of seafloor accumulations of methane-derived carbonates: seepage or erosion indicators. In Proceedings of the 6th International Conference on Gas Hydrates (ICGH 2008), Vancouver, British Columbia, Canada, July (pp. 6-10).

Pedersen, T. F.; Calvert, S. E. (1990): Anoxia vs. Productivity. What Controls the Formation of Organic-Carbon-Rich Sediments and Sedimentary Rocks? (1). In *AAPG Bulletin* 74 (4), pp. 454–466. Available online at <http://archives.datapages.com/data/bulletns/1990-91/images/pg/00740004/0000/04540.pdf>.

Pedreira, D.; Pulgar, J. A.; Gallart, J.; Díaz, J. (2003): Seismic evidence of Alpine crustal thickening and wedging from the western Pyrenees to the Cantabrian Mountains (north Iberia). In *J. Geophys. Res.* 108 (B4), p. 681. DOI: 10.1029/2001JB001667.

Pelegrí, J. L.; Arístegui, J.; Cana, L.; González-Dávila, M.; Hernández-Guerra, A.; Hernández-León, S. et al. (2005): Coupling between the open ocean and the coastal upwelling region off northwest Africa. Water recirculation and offshore pumping of organic matter. In *Journal of Marine Systems* 54 (1-4), pp. 3–37. DOI: 10.1016/j.jmarsys.2004.07.003.

Peters, K. E. (1986): Guidelines for Evaluating Petroleum Source Rock Using Programmed Pyrolysis. In *The American Association of Petroleum Geologist Bulletin* 70 (3), pp. 318–329.

Peters, K. E., & Cassa, M. R. (1994). Applied source rock geochemistry: Chapter 5: Part II. Essential elements.

Pierre, Catherine; Demange, Jérôme; Blanc-Valleron, Marie-Madeleine; Dupré, Stéphanie (2017): Authigenic carbonate mounds from active methane seeps on the southern Aquitaine Shelf (Bay of Biscay, France). Evidence for anaerobic oxidation of biogenic methane and submarine groundwater discharge during formation. In *Continental Shelf Research* 133, pp. 13–25. DOI: 10.1016/j.csr.2016.12.003.

Pillot, D.; Deville, E.; Prinzhofer, A. (2014a): Identification and Quantification of Carbonate Species Using Rock-Eval Pyrolysis. In *Oil Gas Sci. Technol. – Rev. IFP Energies nouvelles* 69 (2), pp. 341–349. DOI: 10.2516/ogst/2012036.

Pillot, D.; Deville, E.; Prinzhofer, A. (2014b): Identification and Quantification of Carbonate Species Using Rock-Eval Pyrolysis. In *Oil Gas Sci. Technol. – Rev. IFP Energies nouvelles* 69 (2), pp. 341–349. DOI: 10.2516/ogst/2012036.

Pinet, B.; MONTADERT, L.; Curnelle, R.; Cazes, M.; Marillier, F.; Rolet, J. et al. (1987): Crustal thinning on the Aquitaine shelf, Bay of Biscay, from deep seismic data. In *Nature* 325 (6104), p. 513. DOI: 10.1038/325513a0.

Ponte, J. P., Robin, C., Guillocheau, F., Popescu, S., Suc, J. P., Dall’Asta, M., Melinte-Dobrinescu, M.C., Bubik, M., Dupont, G., Gaillot, J. (2019). The Zambezi delta (Mozambique

Channel, East Africa): High resolution dating combining bio-orbital and seismic stratigraphies to determine climate (palaeoprecipitation) and tectonic controls on a passive margin. *Marine and Petroleum Geology*, 105, 293-312.

Popescu, B. M. (1995). Romania's petroleum systems and their remaining potential. *Petroleum Geoscience*, 1(4), 337-350.

Price, L.C.; Blount, C.W.; Gowan, D.M.; Wenger, L.; Bebout, D.G.; and Bachman, A.L. (1981). *Methane solubility in brines with application to the geopressured resource* (No. CONF-811026-43).

Prather, M. J., Holmes, C. D., & Hsu, J. (2012). Reactive greenhouse gas scenarios: Systematic exploration of uncertainties and the role of atmospheric chemistry. *Geophysical Research Letters*, 39(9).

Proskurowski, G.; Lilley, M. D.; Seewald, J. S.; Früh-Green, G. L.; Olson, E. J.; Lupton, J. E.; Sylva, S.P.; Kelley, D.S. (2008). Abiogenic hydrocarbon production at Lost City hydrothermal field. *Science*, 319(5863), 604-607.

Pujol, A.; Rouchon, V.; Ravin, A.; Wolf, S.; Blanchet, D.; Ducros, M.; Maurand, N. (2016): Simulation of Anaerobic SOM Biodegradation and Biogenic Methane Production for Basin Modeling. AAPG Hedberg Conference. Santa Barbara, California, 2016.

Pulgar, J. A.; Gallart, J.; Fernández-Viejo, G.; Pérez-Estaún, A.; Álvarez-Marrón, J. (1996): Seismic image of the Cantabrian Mountains in the western extension of the Pyrenees from integrated ESCIN reflection and refraction data. In *Tectonophysics* 264 (1-4), pp. 1–19. DOI: 10.1016/S0040-1951(96)00114-X.

RABINOWITZ, PHILIP D.; COFFIN, MILLARD F.; FALVEY, DAVID (1983): The Separation of Madagascar and Africa. In *Science* 220 (4592), pp. 67–69. DOI: 10.1126/science.220.4592.67.

A. Rangela, B. Katz, V. Ramirez, E. Vaz dos Santos Neto Alternative interpretations as to the origin of the hydrocarbons of the Guajira Basin, Colombia *Marine and Petroleum Geology*, 20 (2003), pp. 129-139.

Ravin, A.; Behar, F., Hatcher, P., Baudin, F. (2013): Sedimentary Marine Organic Matter Diagenesis under Methanogenic Conditions: A New Model for Biogenic Gas. Extended Abstract. In *AAPG Bulletin*.

Ravin, Azdine; Rouchon, Virgile; Blanchet, Denis (2017): Determination of organic degradation rates in 100 My old sediments. Application to Cretaceous black shale intervals from Demerara Rise, ODP Leg 207. In *Organic Geochemistry* 113, pp. 128–140. DOI: 10.1016/j.orggeochem.2017.07.019.

Reeburgh, W.S. (2007). Oceanic methane biogeochemistry. *Chem. Rev.* 107, 486-513.

Regnier, P. Dale, A.W. Arndt, S. La Rowe, D.E. Mogollon, J. Van Cappellen, P. (2011). Quantitative analysis of anaerobic oxidation of methane (AOM) in marine sediments: a modeling perspective. *Earth-Sci. Rev.* 106, pp. 105-130.

Riboulot, V., Sultan, N., Imbert, P., & Ker, S. (2016). Initiation of gas-hydrate pockmark in deep-water Nigeria: Geo-mechanical analysis and modelling. *Earth and Planetary Science Letters*, 434, 252-263.

Rice, D. D. (1992): Controls, habitat, and resource potential of ancient bacterial gas. In *Bacterial Gas*, 1992, pp. 91–118.

Rice, D. D. (1993): Biogenic gas: Controls, habitats, and resource potential. Edited by United States Geological Survey, Professional Paper. United States (1570). Available online at <https://www.osti.gov/biblio/6814498>.

Rise, L., Bellec, V. K., Chand, S., & Bøe, R. (2014). Pockmarks in the southwestern Barents Sea and Finnmark fjords. *Norwegian Journal of Geology/Norsk Geologisk Forening*, 94(4).

Robinson, A. R.; Brink, K. H. (2005): The Global Coastal Ocean. Multiscale Interdisciplinary Processes: Harvard University Press.

Roca, Eduard; Muñoz, Josep Anton; Ferrer, Oriol; Ellouz, Nadine (2011): The role of the Bay of Biscay Mesozoic extensional structure in the configuration of the Pyrenean orogen. Constraints from the MARCONI deep seismic reflection survey. In *Tectonics* 30 (2), n/a-n/a. DOI: 10.1029/2010TC002735.

Roger, Matthieu: Tectono-sedimentary evolution of a hypert-thinned domain during plate convergence : study of the Landes Plateau. PhD thesis, Rennes University. Geoscience.

Roger, Matthieu: Tectono-sedimentary evolution of a hypert-thinned domain during plate convergence : study of the Landes Plateau. PhD Thesis. Université de Rennes.

Romankevich, E. A. (1984). Organic Carbon in Late Quarternary Sediments of Seas and Oceans. In *Geochemistry of Organic Matter in the Ocean* (pp. 105-160). Springer, Berlin, Heidelberg.

Romankevich, E.A., Vetrov, A.A., Peresyphkin, V.I., 2009. Organic matter of the world ocean. *Russ. Geol. Geophys.* 50, 299e307. <http://dx.doi.org/10.1016/j.rgg.2009.03.013>.

Römer, Miriam; Sahling, Heiko; Pape, Thomas; Bahr, André; Feseker, Tomas; Wintersteller, Paul; Bohrmann, Gerhard (2012): Geological control and magnitude of methane ebullition from a high-flux seep area in the Black Sea—the Kerch seep area. In *Marine Geology* 319-322, pp. 57–74. DOI: 10.1016/j.margeo.2012.07.005.

Rouchon, V.; Blanchet, D.; Azdine, R.; Yves, B. (2016): Réactivité de la matière organique sédimentaire : approches expérimentales et notions de modélisations pour la prédiction du gaz biogénique dans TemisFlow. IFPEN Internal Report, 005-2018-R16.

Ruffine, Livio; Donval, Jean-Pierre; Croguennec, Claire; Bignon, Laurent; Birot, Dominique; Battani, Anne et al. (2017): Gas Seepage along the Edge of the Aquitaine Shelf (France). Origin and Local Fluxes. In *Geofluids* 2017 (66), pp. 1–13. DOI: 10.1155/2017/4240818.

Saunoy, M., Jackson, R. B., Bousquet, P., Poulter, B., & Canadell, J. G. (2016). The growing role of methane in anthropogenic climate change. *Environmental Research Letters*, *11*(12), 120207.

Saunoy, M., Stavert, A. R., Poulter, B., Bousquet, P., Canadell, J. G., Jackson, R. B., ... & Ciais, P. (2020). The global methane budget 2000–2017. *Earth System Science Data*, *12*(3), 1561-1623.

Saunoy, M., Bousquet, P., Poulter, B., Pregon, A., Ciais, P., Canadell, J. G., ... & Janssens-Maenhout, G. (2016). The global methane budget 2000–2012. *Earth System Science Data*, *8*(2), 697-751.

Schneider, F., Wolf, S., Faille, I., & Pot, D. (2000). A 3D basin model for hydrocarbon potential evaluation: application to Congo offshore. *Oil & Gas Science and Technology*, *55*(1), 3-13.

Schneider, F. J. S., Noya, J. A. and Magnier, C. (2012). Model of low-maturity generation of hydrocarbons applied to the Carupano Basin, Offshore Venezuela, in K. E. Peters, D. J. Curry, and M. Kacwicz, eds., *Basin Modeling: New Horizons in Research and Applications: AAPG Hedberg Series*, no. 4, p. 51 – 69.

Schneider, F.; Dubille, M.; Montadert, L. (2016): Redalyc. Modeling of microbial gas generation: application to the eastern Mediterranean “Biogenic Play”. Available online at <http://www.redalyc.org/pdf/505/50548851004.pdf>, checked on 7/4/2018.

Schoell, Martin (1980): The hydrogen and carbon isotopic composition of methane from natural gases of various origins. In *Geochimica et Cosmochimica Acta* *44* (5), pp. 649–661. DOI: 10.1016/0016-7037(80)90155-6.

Schulz, H.D.; Zabel, M. (2006): *Marine geochemistry*. 2nd rev., updated and extended ed. Berlin, New York: Springer, checked on 8/1/2018.

Schwietzke, S.; Sherwood, O.A.; Bruhwiler, L.M.; Miller, J.B.; Etiope, G.; Dlugokencky, E.J.; ... and Tans, P.P. (2016). Upward revision of global fossil fuel methane emissions based on isotope database. *Nature*, *538*(7623), 88-91.

Sibuet, Jean-Claude; Srivastava, Shiri P.; Spakman, Wim (2004): Pyrenean orogeny and plate kinematics. In *Journal of Geophysical Research: Solid Earth* *109* (B8). DOI: 10.1029/2003JB002514.

Skarke, A.; Ruppel, C.; Kodis, M.; Brothers, D.; Lobecker, E. (2014): Widespread methane leakage from the sea floor on the northern US Atlantic margin. In *Nature Geosci* *7* (9), pp. 657–661. DOI: 10.1038/ngeo2232.

Spivey, J.P.; McCain, W.D.; and North, R. (2004). Estimating density, formation volume factor, compressibility, methane solubility, and viscosity for oilfield brines at temperatures from 0 to 275 C, pressures to 200 MPa, and salinities to 5.7 mole/kg. *Journal of Canadian Petroleum Technology*, *43*(7), 52-61.

Stow, D.A.V.; Huc, A. Y.; Bertrand, P. (2001): Depositional Processes of Black Shales in Deep Water. In *Marine and Petroleum Geology* 18, pp. 491–498.

Suess, Erwin (1980): Particulate organic carbon flux in the oceans—surface productivity and oxygen utilization. In *Nature* 288 (5788), p. 260. DOI: 10.1038/288260a0.

Sultan, N., Marsset, B., Ker, S., Marsset, T., Voisset, M., Vernant, A. M., ... & Drapeau, D. (2010). Hydrate dissolution as a potential mechanism for pockmark formation in the Niger delta. *Journal of Geophysical Research: Solid Earth*, 115(B8).

Sultan, N., Bohrmann, G., Ruffine, L., Pape, T., Riboulot, V., Colliat, J. L., ... & Marsset, T. (2014). Pockmark formation and evolution in deep water Nigeria: Rapid hydrate growth versus slow hydrate dissolution. *Journal of Geophysical Research: Solid Earth*, 119(4), 2679-2694.

Tegelaar, E. W.; Leeuw, J. W. de; Derenne, S.; Largeau, C. (1989): A reappraisal of kerogen formation. In *Geochimica et Cosmochimica Acta* 53, pp. 3103–3106.

Teles, V., Fornel, A., Houel, P., Delmas, J., Mengus, J. M., Michel, A., & Maurand, N. (2014). Coupling basin and reservoir simulators for an improved CO₂ injection flow model. *Energy Procedia*, 63, 3665-3675.

Thauer, R.K. (2010). Functionalization of methane in anaerobic microorganisms. *Angewandte Chemie International Edition*, 49(38), 6712-6713.

Thinon, I.; Matias, L.; RÉhault, J. P.; Hirn, A.; Fidalgo-González, L.; Avedik, F. (2003): Deep structure of the Armorican Basin (Bay of Biscay). A review of Norgasis seismic reflection and refraction data. In *Journal of the Geological Society* 160 (1), pp. 99–116. DOI: 10.1144/0016-764901-103.

Thinon, I.; Fidalgo-González, L.; RÉhault, J.P.; Olivet, J.L. (2001): Déformations pyrénéennes dans le golfe de Gascogne. In *Comptes Rendus de l'Académie des Sciences - Series IIA - Earth and Planetary Science* 332 (9), pp. 561–568. DOI: 10.1016/S1251-8050(01)01576-2.

Thompson, J. O.; Moulin, M., Aslanian, D., de Clarens, P., Guillocheau, F. (2019): New starting point for the Indian Ocean : Second phase of breakup for Gondwana. In *Earth-Science Reviews*, 2019 (191), pp. 26–56.

Tissot, B.P., and Welte, D.H. (1984). *Petroleum formation and occurrence* (pp. 702). Springer-Verlag Berlin, Heidelberg. DOI: 10.1007/978-3-642-87813-8

Toole, John M. (1981): Sea ice, winter convection, and the temperature minimum layer in the Southern Ocean. In *Journal of Geophysical Research: Oceans* 86 (C9), pp. 8037–8047. DOI: 10.1029/JC086iC09p08037.

Torelli, M.; Traby, R.; Teles, V.; Ducros, M. (2020). Thermal evolution of the intracratonic Paris Basin: Insights from 3D basin modelling. *Marine and Petroleum Geology*, 119, p. 104487.

Tugend, J.; Manatschal, G.; Kuszniir, N. J.; Masini, E. (2015): Characterizing and identifying structural domains at rifted continental margins. Application to the Bay of Biscay margins and its Western Pyrenean fossil remnants. In *Geological Society, London, Special Publications* 413 (1), pp. 171–203. DOI: 10.1144/SP413.3.

Tugend, J.; Manatschal, G.; Kuszniir, N. J.; Masini, E.; Mohn, G.; Thion, I. (2014): Formation and deformation of hyperextended rift systems. Insights from rift domain mapping in the Bay of Biscay-Pyrenees. In *Tectonics* 33 (7), pp. 1239–1276. DOI: 10.1002/2014TC003529.

Ungerer, P., Burrus, J., Doligez, B. P. Y. C., Chenet, P. Y., & Bessis, F. (1990). Basin evaluation by integrated two-dimensional modeling of heat transfer, fluid flow, hydrocarbon generation, and migration. *AAPG bulletin*, 74(3), 309-335.

van Krevelen, D. W. (1950): Graphical-statistical method for the study of structure and reaction processes of coal. In *Fuel* 29, pp. 269–284.

Vaughn, T. L., Bell, C. S., Pickering, C. K., Schwietzke, S., Heath, G. A., Pétron, G., Zimmerle, D.J., Schnell, R.C. and Nummedal, D. (2018). Temporal variability largely explains top-down/bottom-up difference in methane emission estimates from a natural gas production region. *Proceedings of the National Academy of Sciences*, 115(46), 11712-11717.

Verweij, J. M., Nelskamp, S. N., Ten Veen, J. H., De Bruin, G., Geel, K., & Donders, T. H. (2018). Generation, migration, entrapment and leakage of microbial gas in the Dutch part of the Southern North Sea Delta. *Marine and Petroleum Geology*, 97, 493-516.

Vu, T.T.A.; Horsfield, B.; Mahlstedt, N.; Schenk, H. J.; Kelemen, S. R.; Walters, C. C. et al. (2013): The structural evolution of organic matter during maturation of coals and its impact on petroleum potential and feedstock for the deep biosphere. In *Organic Geochemistry* 62, pp. 17–27. DOI: 10.1016/j.orggeochem.2013.06.011.

Wakeham, Stuart G.; Lee, Cindy; Hedges, John I.; Hernes, Peter J.; Peterson, Michael J. (1997): Molecular indicators of diagenetic status in marine organic matter. In *Geochimica et Cosmochimica Acta* 61 (24), pp. 5363–5369. DOI: 10.1016/S0016-7037(97)00312-8.

Waldron, Patricia J.; Petsch, Steven T.; Martini, Anna M.; Nüsslein, Klaus; Nüslein, Klaus (2007): Salinity constraints on subsurface archaeal diversity and methanogenesis in sedimentary rock rich in organic matter. In *Applied and Environmental Microbiology* 73 (13), pp. 4171–4179. DOI: 10.1128/AEM.02810-06.

Wallmann, K.; Aloisi, G.; Haeckel, M.; Obzhairov, A.; Pavlova, G.; Tishchenko, P. (2006): Kinetics of organic matter degradation, microbial methane generation, and gas hydrate formation in anoxic marine sediments. In *Geochimica et Cosmochimica Acta* 70 (15), pp. 3905–3927. DOI: 10.1016/j.gca.2006.06.003.

Wang, X. C.; Druffel, E.R.M.; Griffin, S.; Lee, C.; Kashgarian, M. (1998): Radiocarbon Studies of Organic Compound Classes in Plankton and Sediment of the Northeastern Pacific Ocean. In *Geochimica et Cosmochimica Acta* 62 (8), pp. 1365–1378.

Welhan, J.A. and Craig, H. (1983). Methane, hydrogen and helium in hydrothermal fluids at 21 N on the East Pacific Rise. In *Hydrothermal processes at seafloor spreading centers* (pp. 391-409). Springer, Boston, MA.

Welte, D. H. (1970). Organic carbon and the evolution of photosynthesis on earth. *Die Naturwissenschaften*, 57(1), 17.

Wellsbury, P., Mather, I., & Parkes, R. J. (2002). Geomicrobiology of deep, low organic carbon sediments in the Woodlark Basin, Pacific Ocean. *FEMS microbiology ecology*, 42(1), 59-70.

Wendebourg, J. (2003). Uncertainty of petroleum generation using methods of experimental design and response surface modeling: application to the Gippsland Basin, Australia. In: Düppenbecker, S. Marzi, R. (Eds.), *Multidimensional Basin Modeling*, AAPG/Datapages Discovery Series, vol. 7, pp. 295–307.

Westrich, J.T. and Berner, R.A. (1984): The role of sedimentary organic matter in bacterial sulfate reduction: The G model tested1. In *American Society of Limnology and Oceanography*, pp. 236–249, checked on 7/25/2018.

Whiticar, Michael J. (1999): Carbon and hydrogen isotope systematics of bacterial formation and oxidation of methane. In *Chemical Geology* 161 (1-3), pp. 291–314. DOI: 10.1016/S0009-2541(99)00092-3.

Whiticar, Michael J.; Elvert, M.; Suess, E. (1999): Anerobic methane oxidation associated with marine gas hydrates: superlight C-isotopes from saturated and unsaturated C20 and C25 irregular isoprenoids. In *Naturwissenschaften* 86, 1999, pp. 295–300.

Whiticar, M., J. (1994): Correlation of Natural Gases with Their Sources: Chapter 16: Part IV. Identification and Characterization. With assistance of Michael J. Whiticar. Available online at <http://archives.datapages.com/data/specpubs/methodo2/data/a077/a077/0001/0250/0261.htm>.

Whiticar, M., J., Faber, E., Schoell M. (1986): Biogenic methane formation in marine and freshwater environments: CO₂ reduction vs. acetate fermentation - Isotope evidence. In *Geochimica et Cosmochimica Acta* 50, pp. 693–709, checked on 8/2/2018.

Wygrala, Björn (1989): Integrated Study of an Oil field in the Southern Po Basin, Northern Italy. Forschungszentrum Jülich GmbH (Publikationen vor 2000, Juel-2313).

Yabre A., Gout C., Cretu, M. (2020): Etude des incertitudes thermiques sur la position de la limite lithosphère asthénosphère et son impact sur la maturité des roches mères dans la marge passive du Mozambique. Rapport de stage TOTAL

Young D.M. and Crowell A.D. (1962): *Physical Adsorption of Gases*, Butterworth, London, book.

Zeikus, J. G. (1997): The Biology of Methanogenic Bacteria. In *American Society for Microbiology* 2, pp. 514–541. DOI: 10.1016/B978-0-408-70918-7.50005-3.

Zeikus, J. G., Winfrey, M.R. (1976): Temperature Limitation of Methanogenesis in Aquatic Sediments. In *Applied and Environmental Microbiology* (1), pp. 99–107.

Zhang, X., and Lin, C. M. (2017). Characteristics and accumulation model of the late Quaternary shallow biogenic gas in the modern Changjiang delta area, eastern China. *Petroleum Science*, 14(2), 261-275.

Zindler SH (1993): Physiological ecology of methanogens. In: Ferry JG, Ed. *Methanogenesis: Ecology, Physiology, Biochemistry and Genesis*, pp. 128–206.

10. Figures Table

Figure 1. Main elements of carbon circulation in the biosphere (modified after Tissot and Welte 1984). Most of the carbon is fixed in sediments (82% and 18% of the total inorganic and organic carbon in sedimentary rocks respectively). The organic carbon produced by living organism is rapidly oxidized in CO ₂ and recycled in the biosphere. A small amount of carbon can escape the carbon cycle through burial in sediments which subsequently generate hydrocarbons (Allen and Allen 2013).	12
Figure 2. The two main organic carbon cycles on earth (Schulz and Zabel 2006; Tissot and Welte 1984).....	13
Figure 3. Distribution of the main elements along the sedimentary column (modified after Clayton and Hay 1994).....	18
Figure 4. OM degradation pathways (acetate fermentation vs CO ₂ reduction) in freshwater and marine settings (Whiticar et al.;1986; Whiticar 1999).	19
Figure 5. Evolution of the bacterial activity levels as a function of increasing temperature (Katz 2011).	19
Figure 6. Sedimentation rate vs geothermal gradient converted to heating rate for methanogenesis (Clayton 1992). The microbial gas production is likely when the curve is comprised between 18°C/Ma and 7°C/ Ma.	20
Figure 7. Pore-fluid pressures vs depth for Plio-Pleistocene and Paleogene sequences in the Southern North Sea delta (modified after Verweij et al. 2018). Pore-fluid pressures are hydrostatic or close to hydrostatic in the first 1000 m of depth.....	21
Figure 8. Morphological and geometrical characterization of the two different types of pockmarks (Riboulot et al. 2016). a) Type-I pockmark with gas chimney association; b) Type-II pockmark with an irregular shape associated to hydrates occurrence.	22
Figure 9. Examples of methane-derived authigenic carbonate structures Offshore Zambezi (A) (Deville et al. 2020) and Offshore Aquitaine (B) (Pierre et al. 2017).....	24
Figure 10. Pressure-temperature equilibrium diagram for hydrate stability (Grauls 2001).	25
Figure 11. Geochemical results on gas samples collected in the offshore Mozambique (MOZ04 – CSF19 and CSF04) and in the Bay of Biscay (Gazcogne2 Pegaz samples) (Deville et al. 2018 Internal Report IFPEN; Ruffine et al. 2017). The isotopic composition of the collected gas shows that for all the studied areas the gas is purely of biogenic origin. However, the comparison between the two study sites highlighted differences in terms of	

$\delta^{13}\text{C}\text{-CH}_4$ signature. It could be related to the presence of different OM sources, as well as different geodynamic conditions or differences in terms of microbial activities.....27

Figure 12. (1) Location of the study area offshore Zambezi. (2) Location of the pockmarks in the study area: (A) authigenic carbonates occurrences; (B,C) vertical seismic anomalies interpreted as gas escape pathway (modified after Deville et al. 2020).29

Figure 13. Location map of the collected cores during the PAMELA missions (MOZ01 and MOZ-04) (Deville et al. 2018, IFPEN Internal Report). The red stars represent the position of the particle traps installed during the MOZ-01 mission (December 2014) and the red dots represent the positions of the collected cores during the missions MOZ-01 and MOZ-04.....30

Figure 14. a) Bathymetric map of the Bay of Biscay (Southwestern France) and modelled area (red rectangle) of Fig. 3 modified after Sibuet et al. (2004) and Dupré et al. (2020); b) Detailed shaded bathymetric map offshore Aquitaine (Loubrieu 2013, Gazcogne1) with gas emission site distribution and localization of the sub-bottom profile (red line) shown in Fig. 1c and the modelled offshore area in Fig. 1b (black rectangle) (modified after Dupré et al. 2020); c) Sub-bottom profile acquired in the emission site showing the presence of sub-cropping MDACs from Dupré et al. (2020).32

Figure 15. Upper left: synthetic 3D block of the central part of the Parentis basin representing the main geometry and stratigraphy (Michel 2017). In the first scenario (upper right), methane is generated from a deep source located in the Cretaceous. In the second scenario (lower left), the methane is generated from a Paleogene source. In the third scenario (lower right), methane is generated from a Miocene source. In all three scenarios, methane can migrate 1) from the bottom of the shelf break through the Plio-Pleistocene clinoforms; 2) vertically through the sedimentary column; 3) from the eastern side to the shelf break with a westward migration imposed by the presence of the aquifer.34

Figure 16. Evolution of the OM and different OM compounds with depth (Arndt et al. 2013). The OM degradability evolves in accordance with the degradability of its different components. The depth profiles of the relative contributions of each compound shows a dominance of the refractory compounds at depth.40

Figure 17. General scheme of the main stages of the evolution of the OM and the relative hydrocarbon generated (modified after Tissot and Welte 1984). The composition of the fresh OM is based on published data for general coastal sediments (Tissot and Welte 1984; Cowie and Hedges 1992; Hedges and Oades 1997; Burdige 2007). AA – Amino Acids; CH – Carbohydrates; FA – Fatty Acids (Lipids); LI - Lignin.43

Figure 18. Reactivity (k) of Organic Carbon as function of time (t) in oxic plankton decomposition experiment presented by Westrich and Berner (1984).	81
Figure 19. Reactivity of OC vs time (Middelburg 1989 and reference within). First order degradation parameters are calculated starting from Equation 6. The compilation of field work results and laboratory data covers a large range of natural environment.	82
Figure 20. The main concept accounted in the biogenic gas simulator. The Total Initial Organic Carbon is composed by a refractory TOC and a biodegradable TOC which is prone to generation of CH ₄ . Only this last one is accounted by the simulator during biogenic CH ₄ generation.....	84
Figure 21. Example of methane mass production evolution over time (Pujol et al. 2016).	86
Figure 22. Main steps required to construct a basin model and examples from the Paris Basin case study (modified after Torelli et al. 2020). a) 3D sedimentary model of the Paris Basin; b) Facies map distribution including facies variations in the same horizon; c) erosion event map for the main Cretaceous erosion event; d) Basal Heat Flow carried out through a lithospheric model of the Paris Basin.	88
Figure 23. Compressibility factor for methane as function of temperature (K) and pressure (bar) (de Almeida et al. 2014). The ideal gas model could be used to represent the behavior of methane assuming values highlighted between the blue lines.	90
Figure 24. Evolution of the generated biogenic CH ₄ in TemisFlow. 1) The generated biogenic methane is firstly adsorbed onto the OM. 2) Once the sorption capacity is reached, the biogenic methane is dissolved in the water. 3) Once the water is saturated in gas, the biogenic methane can migrate in the vapor phase.	91
Figure 25. Langmuir isotherms defined in TemisFlow to account for the gas adsorption on the OM during methanogenesis.	92
Figure 26. The presence of gas hydrates is linked to pressure and temperature conditions at given depths shown in the diagram on the left (modified after Kearns 2018). In the diagram, the Aquitaine Shelf (yellow dot) falls outside the methane hydrate window (temperature of 12°C at 150 m of water depth) (Marié et al. 2019; Dupré et al. 2020). When the property of hydrate formation in the TemisFlow simulator is activated (right figure), there are no P-T conditions to accumulate methane in the solid phase.	95
Figure 27. Cuttings storage at the CSTJF – Pau. 20 cuttings samples were collected from PELICAN and PINGOUIN wells.....	131
Figure 28. Geological and tectonic map of the Mozambique Margin (modified after Etheve et al. 2020). The red line shown the location of the 2D profile of the offshore Zambezi oriented	

NW-SE (A-B). ZDD: Zambezi Delta Depression; BH: Beira High. The reader can refer to Etheve et al. (2020) for a better comprehension of the tectonic setting of the Mozambique Basin. 140

Figure 29. Stratigraphy section of 2D TemisFlow basin model of the offshore Zambezi (extracted from Yabre et al. 2020 – TOTAL Internal Report). The location of the section is shown in Figure 28. The dashed blue line indicates the water/atmosphere interface. 140

Figure 30. 2D section of the offshore Zambezi in Temis Flow showing the stability area of methane hydrates at the present-day (extracted from Yabre et al. 2020 – TOTAL Internal Report). The location of the dip-profile is shown in Figure 28. The dashed blue line indicates the water/atmosphere interface. 141

Figure 31. 2D section of the offshore Zambezi in Temis Flow (extracted from Yabre et al. 2020 – TOTAL Internal Report) showing the heating rate °C/Ma of each layer at the deposition time (Clayton 1992). The location of the dip-profile is shown in Figure 28. The dashed blue line indicates the water/atmosphere interface. 141

Figure 32. Interpreted generation process for a single hydrate paleo-pockmark (Imbert and Ho, 2012). A: Hydrates form at the base of the GHSZ triggering a conical fracture along the dotted red line. B: Increase of hydrate-bearing sediment volume due to gas migration and diffusion along the fracture zone. C: zoom on the fracture which may be filled with a stronger vein of hydrate surrounded by hydrates-bearing sediments and a free-gas phase in the lower area. D. Final stage of hydrate dissociation due to a change in P-T conditions, expulsion of the hydrates-bearing sediment along the fracture. 143

Figure 33. Sketch of an interpreted strike-seismic line along the western flank of the Beira High (Imbert 2016 – TOTAL Internal Report). The purple line on the interpreted profile represents the base of the collapsed hydrates which is similar to an erosional surface. Black lines represent the uninterpreted markers. The insert map shows the location of the profile inside the red circle. 144

Figure 34. 2D section of the offshore Zambezi showing the modeled stability areas of methane hydrates at 50 Ma (a) and 66 Ma (b) (extracted from Yabre et al. 2020 – TOTAL Internal Report). The location of the dip-profile is shown in Figure 28. The dashed blue line indicates the water/atmosphere interface. 145

Figure 35. Stratigraphic charts for the offshore Zambezi Delta basin (Mahanjane et al. 2014). 146

Figure 36. Modeled sediment maturity over time expressed as vitrinite equivalent values (%Ro_{eq}) along the 2D section of the offshore Zambezi (extracted from Yabre et al. 2020 –

TOTAL Internal Report). a) 50 Ma; b) 66 Ma; c) 93 Ma. Immature oil (light blue), oil (green), oil and gas (dark red), gas (red) and over mature (grey). 147

Figure 37. a) Continuous distribution of activation energy in which each Source Rock (SR) is defined by the same frequency factor (A) but with different activation energy (Ea); b) Multi-layer scheme in which each SR is defined by a different kerogen with different activation energy and frequency factor values. 150

11. Tables Table

Table 1. Global CH ₄ emissions and sinks by main source type summarized after Saunois et al. (2020) (left column) for bottom-up and top-down approaches in Tg CH ₄ yr ⁻¹ (second and third column respectively) and the relative fraction of BU and TP approaches (fourth and fifth column respectively). The difference between emissions and sinks result in a negative methane budget mainly due to anthropogenic emissions. Here, we are giving only the average estimate for each methane source and sink. Range of values associated with uncertainties and presented in this thesis, are given in Saunois et al. (2020).	11
Table 2. Results from Rock-Eval analysis on bulk rock samples. Based on the average TOC content and the OI vs HI evolution, we selected 10 samples to extract the OM.	132
Table 3. Results from Rock-Eval 7S kerogen analysis on the selected 9 samples after extraction.....	133

12. Appendices

12.1 Publications

- Torelli M., Battani A., Pillot D., Kohler E., Lopes De Azevedo J., Kowalewski I., Pastor L., Brandily C., Schmidt S., Jouet G., Deville E. "Organic matter distribution in modern sediments of the Mozambique Channel: Evidence for widespread oxidation processes in the deep-water domains". *Marine Geology* (to be submitted)
- Torelli M., Gervais V., Kowalewski I., Wendebourg J., Dupré S., Wolf S., Gout C., Deville E. (2021) "Quantification of natural microbial methane from generation to emission in the offshore Aquitaine: A basin modelling approach". *Marine and Petroleum Geology*, 127, 04949. <https://doi.org/10.1016/j.marpetgeo.2021.104949>
- Torelli M. and Wendebourg J. (2021) "Biogenic gas generation and migration in the Offshore Aquitaine: a basin modeling approach to quantify the budget of methane in continental shelf areas" In: *Processes of clastic sedimentation: Source Rocks*, TOTAL internal R&D publication
- Torelli, M., Traby, R., Teles, V., & Ducros, M. (2020). Thermal evolution of the intracratonic Paris Basin: Insights from 3D basin modelling. *Marine and Petroleum Geology*, 119, 104487. <https://doi.org/10.1016/j.marpetgeo.2020.104487>
- Deville E., Scalabrin C., Jouet G., Cattaneo A., Battani A., Noirez S., Vermesse H., Olu K., Corbari L., Boulard M., Marsset T., Dall'Asta M., Torelli M., Pastor L., Pierre D., Loubrieu B. (2020) "Fluid seepage associated with slope destabilization along the Zambezi Margin (Mozambique)". *Marine Geology*. <https://doi.org/10.1016/j.margeo.2020.106275>

12.2 International Conferences

- Torelli M., Kowalewski I., Gervais V., Wendebourg J., Wolf S., Dupré S., Gout C., Deville E. (2021) "Modeling Biogenic Gas Processes in Marine Environments: A Case Study from the Bay of Biscay" – AAPG Annual Convention & Exhibition, May 24th – 26th 2021, Denver (Colorado). Accepted Abstract – Oral Presentation

ABSTRACT

Biogenic gas has received increasing attention in the last few decades as a major and cleaner fossil energy source. Despite the growing interest for biogenic methane gas, its generation mechanisms are still not well understood. The efficiency of the production process is largely determined by biogeochemical mechanisms at the sea bottom that depend on the quality and quantity of the Sedimentary Organic Matter (SOM). Numerical modeling experiments are a relevant means to study the interaction of the various processes leading up to biogenic gas generation and accumulation. In the framework of the PAMELA research project, we apply a new numerical approach to simulate biogenic methane production at the basin scale to the Aquitaine Basin (Bay of Biscay, southwestern coast of France) where a few thousand methane seeps have been recorded in the water column at water depth of 140-220 m (Dupré et al 2020). The carbon isotope signature of methane indicates that the system is charged by biogenic gas generated from CO₂ reduction (Ruffine et al 2017). The new prototype accounts for three different SOM fractions: a labile-SOM which is degraded into methane following the model of Middelburg (1989), (2) a thermo-labile-SOM which is transformed into labile-SOM at greater temperature as function of a first order kinetics and (3) a bio-refractory-SOM which is unreactive and constant during biogenic gas simulations. Finally, the generated gas is distributed in the basin as either adsorbed in the organic matter, dissolved in water, or as free gas in a vapor phase. In order to better describe the organic matter deposited in the study area, Rock-Eval analyses were performed on cuttings collected from two different offshore wells. The system is charged by gas from a type III continental-derived SOM which is very immature ($T_{max} < 425^{\circ}\text{C}$). The model includes the deposition of methane derived-authigenic carbonates in the uppermost layers which result from the Anaerobic Oxidation of Methane (AOM) during its upward migration (Pierre et al 2017). A sensitivity analysis was also performed on the model input critical parameters to discriminate and quantify their impact on the final biogenic gas production and expulsion/migration processes. Our results show that the generated methane is mainly transported as dissolved phase in water formation and released as free gas phase at the water-sediment interface. Migration pathways are mainly sub-vertical, from the Plio-Pleistocene source rocks directly to the seafloor controlled mainly by sediment permeability. The model can reproduce observed natural processes such as gas migration along the seepage area. The origins of the biogenic methane,

which is alimented by a present-day active system sourced by Miocene to Plio-Pleistocene sediments are discussed and a first quantification of the total amount of emitted gas into the water column over time is assessed.

- Torelli M., Battani A., Pillot D., Kohler E., Lopes De Azevedo J., Kowalewski I., Brandily C., Pastor L., Jouet G., Deville E. (2019) "Organic matter distribution in the modern sediments of the Mozambique Channel: Evidence for a widespread oxidation processes in the deep water domains" - IAS conference, September 10th-13th, Rome (IT). Oral Presentation

ABSTRACT

The geochemical study of Organic Matter (OM) sampled in piston cores, in moorings and in interface cores collected within the recent sediments of the Mozambique Channel, has shown heterogeneous organic matter contents (mainly of continental origin). Core samples show Total Organic Carbon (TOC) contents ranging between 1 and 2% in the Majunga continental slope (offshore northern margin of Madagascar) and in the Zambezi continental slope (offshore Southern margin of Mozambique). This OM is largely oxidized (Oxygen Index > 300 mg CO₂ / g TOC). Away from these margin areas, within the deep basin in the Mozambique Channel, the study of samples collected in moorings, within particles traps, shows that OM is transported either by surface currents or turbidite and/or contour currents. The collected water-borne OM shows higher Total Organic Carbon (TOC between 1.5 and 3%) compared to the deposited OM samples by core and only small amount of TOC is preserved within the distal areas of the Zambezi turbidite system at water depth below 3000 m (Total Organic Carbon < 0.5%). The samples collected at the sea bottom (by the interface cores) show intermediate TOC values between those collected in the particle traps and those taken from the piston cores. This result suggests that the degradation of the organic matter is mainly active in the first centimeters below the sea bottom. This is consistent with the relatively high O₂ contents measured in the first centimeters of the sediments of the deep water areas suggesting higher oxidation processes compared to the shallower waters of the continental margins. Preliminary results from SEM analysis highlighted mineralogical differences between the depositional systems along the Majunga and the Zambezi margins. First measurements on cores samples from the Zambezi offshore present a mineral matrix which include iron oxides typical of higher oxygen content

compared to the Majunga sector. The process of oxidation and degradation of OM in the deeper waters of the Mozambique Basin is probably related to the activity of important bottom currents that allow a mobilization of the OM particles at the sea bottom resulting in an important oxidation of these particles at the seabed and in the first centimeters of the sediments. Lower sedimentation rates in the deep sea areas contribute also to higher oxidation processes.

Key words: organic matter, transport, sedimentation, oxidation, Mozambique Channel

- Torelli M., I. Kowalewski, R. Traby, M. Roger, S. Dupré, M. Cretu, E. Deville (2019) “Biogenic gas generation process: Application to the Bay of Biscay. Data integration and basin modelling” AAPG Annual Convention & Exhibition, May 19th–22th, San Antonio (TX). Poster Presentation

ABSTRACT

Sub seafloor sediments near continental margins are known to be enriched in biogenic CH₄. The microbial production of methane is the result of complex digestion processes of the Organic Matter (OM) that take place at different diagenesis stages. The efficiency of methane production depending on OM degradability potential, is largely determined by the biogeochemical processes at the sea bottom linked to the quality and quantity of the OM. In offshore environment, the accumulation and production of biogenic gas is likely and of commercial interest since it starts under the oxygenation zone of organic compounds from the reduction of sulphate in sea water. The rates of OM degradation and burial play a crucial role in the production of microbial gas. Therefore, the knowledge of OM spatial distribution in sediments and the temperature is a prerequisite for estimating the biogenic CH₄-generating potential of marine sediments. The objective of this study is a better understanding of the microbial gas generation/migration process by a sensitivity analysis on the key controlling factors, using a 3D basin modelling approach. The numerical approach to describe biogenic CH₄ production and implemented into TemisFlow™ takes into account the TOC distribution, the sedimentation rate and degradability law.

The macroscopic post processing model of microbial CH₄ generation, was applied to the Bay of Biscay. In 2013, several fluid emissions were found in the offshore of the

Aquitaine shelf, east of the shelf break, at a water depth around 140 to 185 m. The gas is primarily composed by CH₄ and secondarily by CO₂. The ¹³C isotopic signatures concludes to a purely biogenic origin derived from CO₂ reduction. However, the isotopic signature of the C1 is slightly heterogeneous as well as the amount of the gas emitted along the different sites of the shelf break. These differences could be explained by several factors such as the quality of the substratum, the temperature at which the methane is produced, the oxidation of the hydrocarbon, the mixing with different gas sources and mixture of hydrocarbon transport/migration process. All of these factors were analyzed and tested in order to obtain a generation/migration biogenic gas model calibrated on real data. The OM potential of the Bay of Biscay was analyzed using a 3D basin modelling approach. After the model calibration, several scenario of C1 generation and migration were tested, compared to observed data and discussed.

12.3 Internal PAMELA seminars

- Torelli, M. “Modeling Microbial Methane Processes in Marine Environments: from Source to Seeps”. Seminar to EXPLO/ EVAPET – TOTAL. February, 5th 2021.
- Torelli, M., Kowalewski I., Traby, R., Dupré, S. Cretu, M., Roger, M., Ortis, A., Gout, C., Deville, E. “Modeling microbial gas generation process: Application to the Bay of Biscay”. PAMELA Séminaire de clôture – CST Total November, 21th-22th, 2019. Oral presentation and Poster session

EXTENDED ABSTRACT

Introduction

Marine sediments near continental margins are known to be enriched in biogenic CH₄. The microbial production of methane is the result of complex digestion processes of the Organic Matter (OM) that take place at different diagenesis stages. The efficiency of methane production depending on OM degradability potential, is largely determined by biogeochemical processes at the sea bottom linked to the quality and quantity of the OM. In offshore environment, the accumulation and production of biogenic gas is likely and of commercial interest since it starts under the oxygenation zone of organic

compounds from the reduction of sulphate in sea water. The rates of OM degradation and burial play a crucial role in the production of microbial gas. Therefore, the knowledge of OM spatial distribution in sediments and the temperature is a prerequisite for estimating the biogenic CH₄-generating potential of marine sediments. Amino acids, carbohydrates, proteins and lipids are the primary compounds degraded by microbial activity. The preserved OM constitutes the kerogen and represents the refractory part of the initial SOM (Burdige 2007). The initial OM can be divided into a refractory part (TOC_{ref}), which can turn in hydrocarbons by thermogenic reaction and a biodegradable part prone to generate of methane. Within the biodegradable compound, we can find other two types of TOC. According to Wallman et al. (2006), the biodegradable part of the initial TOC is usually composed by a sensitive TOC, called “Labile” (TOC_{lab}) which accounts for about 30-40% of the initial OM for a type II kerogen. This labile compound is easily altered once the OM is deposited. However, a part of the labile TOC can act as refractory in the first diagenesis states, but it becomes labile when a temperature increase occurs, enriching the labile pool. This part is called “Thermo-labilizable” (TOC_{zlab}) and accounts for the 8-15% of the initial TOC for a type II OM (Burgige et al. 2011).

Objective

The objective of our study is a better understanding of the microbial gas generation/migration process by a sensitivity analysis on the key controlling factors, using a 3D basin modelling approach. A numerical approach to describe biogenic CH₄ production, at a basin scale, was developed and implemented into the IFPEN basin modeling software TemisFlow™ (Pujol et al. 2016). This methodology was applied to the Bay of Biscay where biogenic CH₄ active seepages have been discovered recently (Dupré et al. 2014). Results from simulated scenarios are compared with geological models proposed by Michel G. (2017) to determine the possible CH₄ generation and migration pathways.

Method

This numerical approach accounts for:

- An initial TOC composed of 3 portions: Refractory, Labilizable (8-15% of the TOC_{tot} for a type II OM - Burdige et al. 2011) and Labile (30-40% of the TOC_{tot} for type II OM - Wallman et al. 2006)
- The decrease of organic matter reactivity with time using published models
- The temperature during the calculation of degradation rates during burial
- The preservation of the refractory fraction (constant during degradation process)

$$TOC_{tot} = TOC_{ref} + TOC_{zlab} + TOC_{lab}$$

$$\frac{\partial TOC_{zlab}}{\partial t} = -k(T) * TOC_{zlab}$$

• $-k(T) = A * e^{-\frac{E_a}{RT}}$ (kinetic equation)

$$\frac{\partial TOC_{lab}}{\partial t} = -r_{bio} * \mu(T) * TOC_{lab} - \frac{\partial TOC_{lab}}{\partial t}$$

- $\mu(T)$ = Temperature dependence function for microbial activity
- r_{bio} = Adjustment parameter (Ma^{-1})

Preliminary results

The macroscopic post processing model of microbial CH_4 generation, was applied to the Bay of Biscay. In 2013, several fluid emissions were found in the offshore of the Aquitaine shelf, east of the shelf break, at a water depth around 140 to 185 m. The isotopic signature of the $C1$ is slightly heterogeneous as well as the amount of the gas emitted along the different sites of the shelf break. These differences could be explained by several factors such as the quality of the substratum, the temperature at which the methane is produced, the oxidation of the hydrocarbon, the mixing with different gas sources and mixture of hydrocarbon transport/migration process. All of these factors can be analyzed and tested using a modeling approach to obtain a generation/migration biogenic gas model calibrated on real data. The OM potential of the Bay of Biscay was analyzed using a 3D basin modelling approach. The model covers an area of about 2800 km^2 . The horizontal resolution is set to $1 \times 1 km^2$. It is composed by 29 main horizons created from well log and seismic interpretation. The thermal calibration was made applying a lithospheric model at the base of the sedimentary basin. Based on the seismic interpretation and the geological scenarios proposed by Michel (2017) we tested the biogenic gas module in the 3D basin model simulator TemisFlow. A first approach was based on reproducing the free gas accumulation below the subsurface where several acoustic blanking were already observed. In our scenario the source rocks are represented by 3 Miocene layers with different Initial TOC but the same repartition of the TOC compounds, r_{bio} and microbial activity curve. First results highlighted that the production of biogenic gas and the presence of free gas accumulation is strongly linked

to the initial amount of the TOC as well as to the source rock thickness, the sedimentation rate and the temperature distribution.

Perspectives

The repartition of the different TOC fractions available in literature was based on a fine characterization of a type II OM (Wallman et al. 2006; Burdige et al. 2007). In our case study, the OM is mainly continental which can result in a higher refractory kerogen content. In order to better define the distribution of the different TOC fractions we planned a geochemical characterization of the OM by Rock-Eval analysis, EA and Solid State ^{13}C NMR. In the meanwhile, also a sensitivity analysis will be done. Starting from the main variables accounted in the module, such as the TOC_{lab} , the TOC_{zlab} , the rbio , the microbial activity curve, the salinity and the activation energy for the thermolabile compound, we will try to determine the parameters which have a major impact on our case study.

References

- Biteau, et al., 2006.; The Aquitaine Basin. *Petroleum Geoscience* ; 12 (3): 247–273.
- Burdige, David J. (2011): Temperature dependence of organic matter remineralization in deeply-buried marine sediments. In *Earth and Planetary Science Letters* 311 (3-4), pp. 396–410. DOI: 10.1016/j.epsl.2011.09.043.
- Dupré et al., (2014). Fluid emissions at the Aquitaine Shelf (Bay of Biscay, France): A biogenic origin or the expression of hydrocarbon leakage?. *Continental Shelf Research*, 88, 24-33.
- Jammes et al., (2010). Extreme crustal thinning in the Bay of Biscay and the Western Pyrenees: From observations to modeling. *Geochemistry, Geophysics, Geosystems*, 11(10).
- Michel, G. (2017): Mise en place et pérennisation d'un vaste système fluide microbien sur le plateau aquitain. *Caractérisation et facteurs de contrôle*. Paris 6.
- Pujol et al., (2016): Abstract: Simulation of Anaerobic SOM Biodegradation and Biogenic Methane Production for Basin Modeling. Hedberg Conference 2016, Santa Barbara, Ca
- Wallmann, K.; Aloisi, G.; Haeckel, M.; Obzhairov, A.; Pavlova, G.; Tishchenko, P. (2006): Kinetics of organic matter degradation, microbial methane generation, and gas hydrate formation in anoxic marine sediments. In *Geochimica et Cosmochimica Acta*

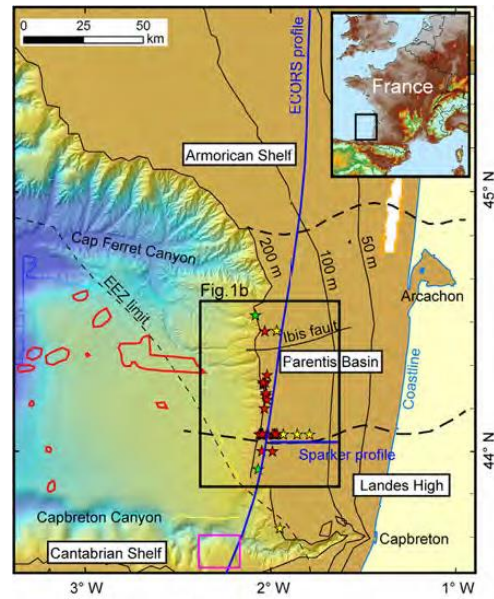


Fig. 1. Bathymetry map of the Aquitaine margin (Bay of Biscay) and location of the gas seeps analyzed (black square) (Dupré et al., 2014). The location of the 3D geological model is shown in the red rectangle.

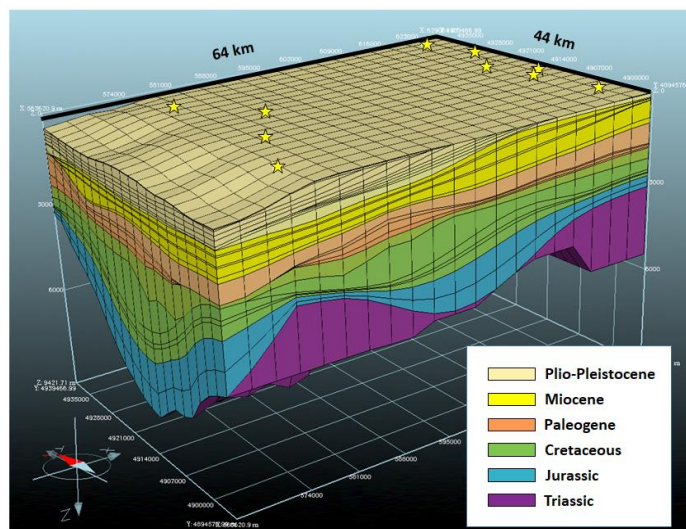


Fig. 2. The 3D geological model is located in the Parentis basin offshore (red rectangle). It was carried out with TemisFlow™ and calibrated on 10 wells (yellow stars); The location of the model is shown in Figure 1

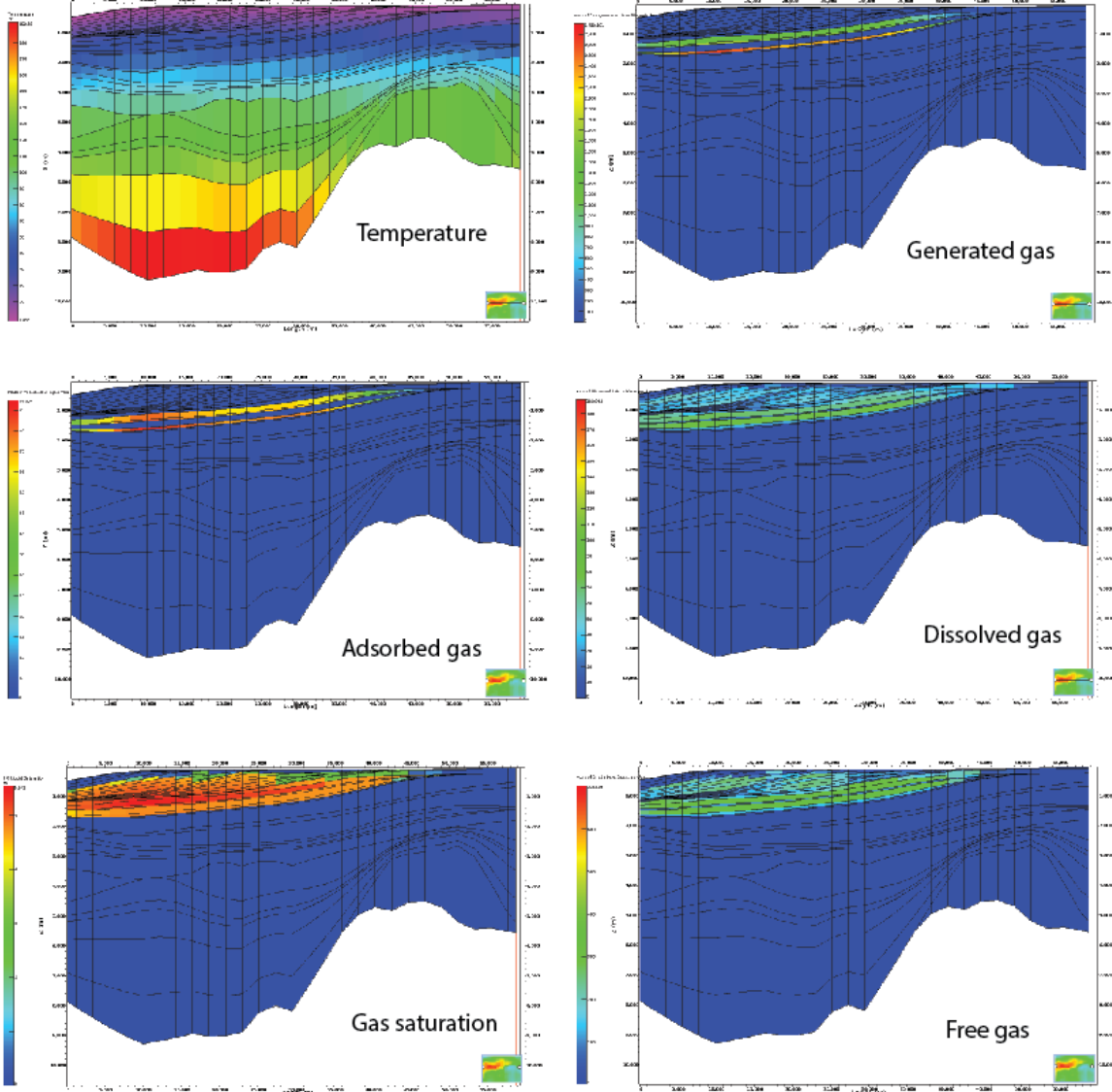


Fig. 3. Preliminary results showing some 2D sections derived from the 3D simulation. The temperature distribution, the generated gas, the adsorbed gas, the dissolved gas, the gas saturation and the free gas accumulation at the present-day.

- Torelli M., Battani A., Pillot D., Kohler E., Lopes De Azevedo J., Kowalewski I., Pastor L., Brandily C., Schmidt S., Jouet G., Deville E. “Organic matter distribution in modern sediments of the Mozambique Channel: Evidence for widespread oxidation processes in the deep-water domains”. PAMELA Séminaire de clôture – CST Total November, 21th-22th, 2019. Poster presentation

ABSTRACT

The characterization of the sedimentary Organic Matter (OM) sampled from recent sediments in the Mozambique Channel, has shown heterogeneities in terms of quality and quantity. Results from Rock-Eval analysis on core samples have shown that the Majunga offshore, the northern sector of the Madagascar and the Zambezi continental slope present the highest Total Organic Carbon (TOC) contents (between 1 and 2%). Far from the marginal areas, within the Mozambique Basin, the OM characterization on samples collected in moorings, within particles traps, has shown higher TOC contents (between 1.5 and 3%). The sediments are transported in the distal areas either by surface, turbidite and/or contour currents resulting in largely oxidized OM close to the water-sediment interface (Oxygen Index values around 300 mg CO₂ / g TOC). Only small amount of TOC is preserved within the distal areas of the Zambezi turbidite system at water depth below 3000 m (Total Organic Carbon < 0.5%). Samples collected at the sea bottom (interface cores) show intermediate TOC values between those collected in the particle traps and those taken from the piston cores. This result suggests that the degradation of the organic matter is mainly active at the sea bottom and in the first centimeters below the sea bottom. This oxidation and degradation process of OM in the Mozambique Basin deep-water is probably related to the activity of important bottom currents that allow remobilization of the OM particles at the sea bottom and thus important oxidation of these particles. Results from Scanning Electron Microscopy (SEM) analysis have shown different composition of the mineral matrix between the depositional systems along the Majunga and the Zambezi margins. The Zambezi offshore presents mineral matrix which include iron oxides typical of higher oxygen content compared to the Majunga sector. These results give new insight to discuss the role of the mineral matrix on the final OM preservation.

Key words: organic matter, transport, sedimentation, oxidation, Mozambique Channel

12.4 PhD thesis pitch

- Torelli, M. (2021). Pitch-5'. Journées des Doctorants - Atelier « Partager les données et les informations marines ». Ifremer 27 Janvier 2021

Modeling Microbial Gas Processes in Marine Environments: from Source to Seep
Insights from Basin Analysis

Martina Torelli
PhD candidate

Director : E. Deville (IFPEN)
Co-Director: S. Dupré (IFREMER)
Advisors: I. Kowalewski (IFPEN), C. Gout and J. Wendebourg (TOTAL)

1

PAMELA PROJECT - PASSIVE MARGIN EXPLORATION LABORATORIES

UNDERSTANDING THE EVOLUTION OF FLUID SYSTEMS ALONG TRANSFORM AND PASSIVE MARGINS

PAMELA Target Areas:
a) MOZAMBIQUE CHANNEL (Madagascar and Mozambique)
b) BAY OF BISCAY (Offshore Aquitaine)

2

UNDERSTANDING BIOGENIC GAS OCCURRENCES - WORKFLOW STRATEGY

1 (a) The Mozambique Channel
Organic Matter Characterization
GEOCHEMICAL ANALYSIS
• Screening of Organic Matter evolution

2 (b) The Bay of Biscay
3D Basin model
NUMERICAL MODELING
• understanding biogenic gas processes at basin scale

3 (a) Offshore Mozambique
PREDICTING BIOGENIC GAS SYSTEMS
• 2D modeling - Hydrates Analysis

3

1. THE MOZAMBIQUE CHANNEL

Rock-Eval Analysis
SEM Analysis
OPD Analysis

4

2. THE BAY OF BISCAY

What are the main processes leading up to biogenic gas accumulations at basin scale?

Basin Model
Test the IFPEN Prototype for microbial CH₄ processes
Microbial processes
CH₄ Gas
Offshore Aquitaine

Source Rock Characterization
Global Sens Analysis
Quantification of natural microbial methane from generation to emission in the offshore Aquitaine: A basin modelling approach

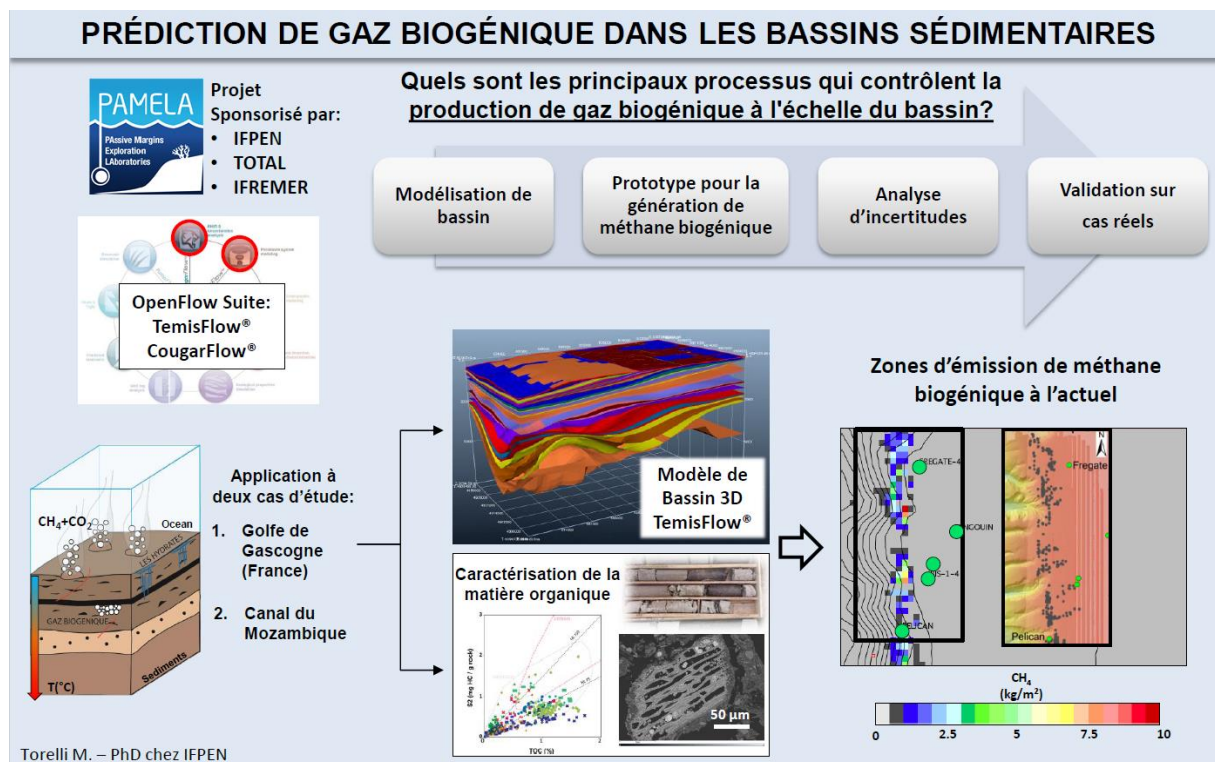
5

THANK YOU FOR YOUR ATTENTION

Martina TORELLI
IFP Energies nouvelles
Email address: martina.torelli@ifpen.fr

6


- Torelli, M. (2020). Pitch-3' à la Directrice générale adjointe Recherche et Innovation - IFPEN. 6 Juillet 2020



12.5 International Training and School

- Torelli, M., Kowalewski, I., Traby, R., Dupré, S., Deville, E. “Biogenic gas generation process: Application to the Bay of Biscay and Mozambique Channel”. Materials for Energy and Sustainability VII - International School of Materials for Sustainable Development and Energy - Erice (IT), July, 2018. Poster Presentation

Renewable energies | Eco-friendly production | Innovative transport | Eco-efficient processes | Sustainable resources




PAMELA
Passive Margins Exploration Laboratories

Biogenic gas generation process: Application to the Bay of Biscay and Mozambique channel

Integration and basin modelling

Martina Torelli¹, Isabelle Kowalewski¹, Renaud Traby¹, Stéphanie Dupré², Eric Deville¹

¹IFPEN Energies Nouvelles, Geosciences Division, 1 & 4 Av. de Bois-Préau, 92852 Rueil-Malmaison Cedex, France
²IFREMER, Unité Géosciences Marines, 29280 Plouzané Cedex, France



International State of Materials for Energy and Sustainability (ISEM) (2017-2018)

INTRODUCTION

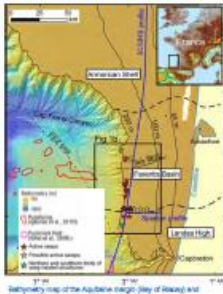
The PAMELA research project (PAssive Margins Exploration Laboratories) is a collaborative study between IFPEN, TOTAL, IFREMER, Universities of Brest, Rennes and Paris 6. Numerous results were obtained concerning the gas systems on the studied margins, in particular in the Bay of Biscay and in the Mozambique Channel. The gas systems highlighted in those areas are linked to microbial activity. Firstly, the present Ph.D. study will focus on better characterizing the organic matter (OM) with associated gas emissions. Additional geochemical analyzes on OM (RE6S, MEB, fluid inclusions, $\delta^{13}C$), gas fraction (fluid inclusions, gas crushing, $\delta^{13}C$) and authigenic carbonates (DRX, MEB, $\delta^{13}C$, clumped isotopes) will be performed. Secondly, thanks to these new results, the numerical biogenic gas generation model will be validated with TemiFlow™.

OBJECTIVES

- Synthesize of the previous studies in the framework of the PAMELA project
- Characterize and quantify the organic matter to better understanding the generation process of the biogenic gas
- Validate with basin modelling, using the numerical approach implemented in TemiFlow™ for the biogenic gas generation

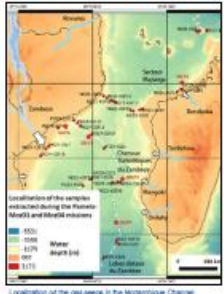
GEOLOGICAL SETTING

THE BAY OF BISCAKY



- The studied area is located in the Aquitaine shelf (Bay of Biscay - France) (Biteau et al., 2006)
- Main tectonic events (Jammes et al., 2010):
 - Rifting phase oriented W-E along the Ibis fault (Berriasian - Albian)
 - The Pyrenean compression phase (Senonian - Lutetian)
- Gas seeps were identified in the Parents Basin and in the Landes High (Dupré et al., 2014)

THE MOZAMBIQUE CHANNEL



- The Mozambique Channel is a narrow gateway between Mozambique and Madagascar
- Main events (Bassias, 1992):
 - Drifting of Madagascar southward (Late Jurassic - Early Cretaceous)
 - Deposition of thick flysch sediments (Cretaceous to Pliocene)
- Gas seeps were identified along the Zambezi and Madagascar coasts

METHODS

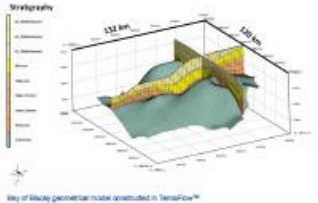
1. GEOCHEMISTRY

Characterization of the OM, gas fraction and authigenic carbonates:

- Rock-Eval 6S
- Petrographic analysis
- Isotopic analysis ($\delta^{13}C$)
- Fluid inclusion

2. BASIN MODELLING

- Construction of the geological framework
- Thermal calibration of the models using measured data
- Fine tuning of the biogenic numerical gas model

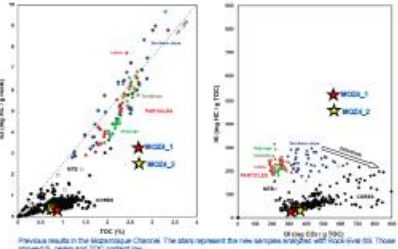


Bay of Biscay geometrical model constructed in TemiFlow™

RESULTS

Previous results obtained in the framework of the PAMELA project highlighted:

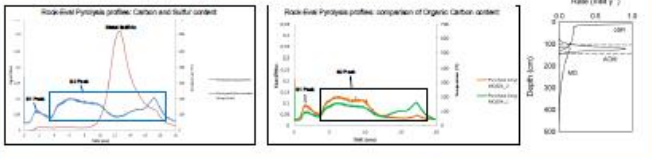
- Different OM concentration along the Zambezi shelf compared to Madagascar shelf
- Increasing of the OM oxidation at the water/sediment interface along the Zambezi slope



Previous results in the Mozambique Channel. The stars represent the new samples analyzed with Rock-Eval 6S. Those obtained by petro and TOC content use.

PERSPECTIVES

Evolution of the organic and mineral sulfur in the OM samples using Rock-Eval 6S in order to better constrain the Anaerobic Oxidation of Methane (AOM) zone.



13. Summary

Marine sediments in continental margins are known to be enriched in **Sedimentary Organic Matter** (SOM) which can yield methane by microbial activity. Previous results collected in the framework of the **PAMELA** research project (PAssive Margin Exploration Laboratories) allowed to identify several seepages of **microbial methane** offshore Aquitaine (Bay of Biscay) and along the Mozambique and Madagascar continental margins. The generation of microbial methane is a bio-geochemical process, called methanogenesis, that occurs in anaerobic conditions and at microscopic scales. Microbial methane generation is a complex process which implies biochemical redox reactions that are heterogeneous laterally and vertically as function of SOM availability and environmental conditions. In order to better understand the impact of the Organic Matter (OM) on such fluid systems, we (1) characterized the OM collected from cores, sediment-trap moorings and cuttings from exploration wells, and (2) proposed a new modelling approach to predict methane cycle at the basin scale from its generation to migration and release.

The OM in the **Mozambique Channel** shows heterogeneities at large scale in quality and quantity between the Mozambique and the Madagascar margins. We concluded that isotopic signature variations can be the result of different transport and preservation conditions between the two sites. In addition, we observed that sediments are transported in the distal areas either by surface, turbidite and/or contour currents resulting in largely oxidized OM close to the water-sediment interface (Oxygen Index values around 300 mg CO₂ / g TOC). Our results indicated that the degradation of the OM is mainly active at the sea bottom and in the uppermost centimeters of sediments. This oxidation and degradation processes of OM in the Mozambique Channel are probably related to the activity of important bottom currents leading to oxic conditions and higher oxygen exposure time near the sediment-water interface.

In the second part, we propose a new modelling approach to reproduce biogenic gas processes at the basin scale, accounting for the geological evolution of the basin and the OM composition and degradation by bacterial activity through time and space. This new approach was applied to the **offshore Aquitaine** (Bay of Biscay) biogenic fluid system. It consists of a basin modelling workflow of microbial gas generation and migration process at the basin scale and accounts for OM biodegradation processes and the main biogenic gas sink. The geochemical

characterization of the OM by Rock-Eval analyses can be used to define its biogenic gas potential. A sensitivity analysis was performed on the main model input parameters to quantify their impact on the biogenic gas production and expulsion/migration processes which resulted in a reference scenario for microbial gas production in offshore Aquitaine that is compared with measured data from *in situ* bubbling sites and acoustic water column signatures. The model reproduces natural processes such as gas migration at emission points (gas seeps). The microbial generation process is estimated to have started in the early Pliocene (5.5 Ma). The biogenic system appears to be sourced by biogenic gas system found in the Plio-Pleistocene sediments that is still active, with a mean flow rate estimated between 0.87 Tcf/My and 1.48 Tcf/My. This new workflow allows to better assess biogenic gas occurrences in offshore Aquitaine. More generally, this workflow can help to improve estimates of the amount of biogenic methane emitted naturally in continental shelf areas to the oceans that may reach the atmosphere.

Keywords: Biogenic methane, Basin Modelling, TemisFlow, Geochemistry, offshore Aquitaine, Mozambique Channel, Organic Matter, Methane Derived-Authigenic Carbonates, Methane Budget

14. Résumé

Les sédiments marins des marges continentales sont enrichis en **Matière Organique Sédimentaire** (MOS) qui peut être transformée en méthane par l'activité microbienne. Les précédents résultats obtenus dans le cadre du projet de recherche **PAMELA** (PAssive Margin Exploration Laboratories) ont permis d'identifier plusieurs points d'émissions de **méthane biogénique** sur le plateau continental aquitain (Golfe de Gascogne) et le long des marges du Mozambique et de Madagascar. La génération de gaz biogénique est un processus biochimique, appelé méthanogenèse, qui se produit dans des conditions anaérobies à échelle microscopique. La génération de gaz par activité microbienne est un processus complexe qui implique des réactions biochimiques redox hétérogènes latéralement et verticalement en fonction de la disponibilité de la MOS et des conditions environnementales. Afin de mieux comprendre l'impact de la nature de la Matière Organique (MO) sur ces systèmes fluides, nous avons (1) caractérisé la MO collectée à partir de carottes, de mouillages et de carottes d'interface et de déblais, et (2) proposé une nouvelle approche de modélisation pour estimer la présence de gaz biogénique à l'échelle du bassin.

Les premiers résultats concernant l'évolution du matériel organique à grande échelle dans le **Canal du Mozambique**, ont montré des hétérogénéités en termes de qualité et de quantité de MO entre les marges du Mozambique et de Madagascar. Nous avons conclu que les variations des signatures isotopiques peuvent être le résultat des conditions de transport et de préservation différentes entre les deux sites. Nous avons aussi observé que les sédiments sont transportés dans les zones distales soit par des courants de surface, de turbidité et/ou de contour entraînant une MO largement oxydée à proximité de l'interface eau-sédiment (valeurs d'indice d'oxygène autour de 300 mg CO₂ / g TOC). Les résultats de cette étude indiquent que la dégradation de la MO est principalement active au fond de la mer et dans les premiers centimètres des sédiments très récents. Ces processus d'oxydation et de dégradation de la MO dans les eaux profondes du Canal du Mozambique sont probablement liés à l'activité d'importante des courants de fond favorisant des conditions oxiqes et des temps d'exposition à l'oxygène plus élevés dans les premiers centimètres des sédiments.

Nous avons également proposé une nouvelle approche de modélisation numérique de bassin pour reproduire les processus de génération du gaz biogénique à grande échelle. Le modèle intègre l'évolution géologique du bassin, la composition de la MO et sa dégradation par l'activité

bactérienne dans le temps et dans l'espace. Cette nouvelle approche a été appliquée au système biogénique localisé sur le rebord du plateau aquitain (Golfe de Gascogne). L'approche de la modélisation numérique des processus de génération et de migration de méthane microbien à l'échelle du bassin tient compte des paramètres de biodégradation de la MO actuellement disponible, ainsi que des principaux processus de consommation de ce méthane biogénique. De ce fait, nous avons aussi inclus dans notre approche la caractérisation géochimique de la MO, par des analyses Rock-Eval, pour mieux définir son potentiel en gaz biogénique. La modélisation intègre une analyse de sensibilité appliquée aux principaux paramètres d'entrée du modèle pour quantifier leur impact sur la production de méthane biogénique et les processus de migration et d'expulsion. Les résultats ont conduit à un scénario de référence pour la production de méthane microbien dans le Bassin Aquitain offshore qui est cohérent avec les quantités de méthane émis au fond de la mer. Le modèle peut reproduire des processus naturels tels que la migration du gaz aux points d'émissions (« seeps »). Grâce à cette approche, nous pouvons estimer le début du processus de la génération du gaz microbien au début du Pliocène (5,5 Ma). Le gaz biogénique est généré actuellement dans les sédiments du Plio-Pléistocène, avec une quantité moyenne de gaz émis au fond de la mer estimée entre 0,87 Tcf / My et 1,48 Tcf / My. Cette nouvelle approche de modélisation nous a permis d'évaluer les processus d'un système de méthane biogénique, depuis sa génération jusqu'aux émissions en fond de mer sur le rebord du plateau aquitain. Cette approche permet d'améliorer les estimations du budget total de méthane biogénique émis naturellement dans les zones de plateaux continentaux où le méthane peut potentiellement atteindre l'atmosphère, avec un impact négatif sur le climat et l'environnement.

Mots clés : Méthane Biogénique, Modélisation de bassin, TemisFlow, Géochimie, Bassin Aquitain offshore, Canal du Mozambique, Matière Organique, Carbonates Authigènes Dérivés du Méthane, Budget de méthane